UNIVERSITAT POLITÈCNICA DE VALÈNCIA

Departamento de Ingeniería Química y Nuclear

Institut de Seguretat Industrial, Radiofísica i Mediambiental

A thesis submitted for the degree of Doctor of Philosophy

Impact of Nuclear Parameters Processing Techniques on BWR Dynamic Calculations

Ph.D. Thesis

Submitted by:

María Desamparados Soler Martínez

Supervised by:

Dr. D. Rafael Miró Herrero

Dr. D. Gumersindo Jesús Verdú Martín

Valencia, July 2024

A mis padres.

A mis sobrinas,
Emily y Valeria.

Y a todas las personas que encuentran su vocación y persiguen sus sueños.

AGRADECIMIENTOS

Quisiera expresar mi más sincero agradecimiento a mis tutores de la tesis doctoral, el Dr. Rafael Miró y el Dr. Gumersindo Verdú, por su inestimable apoyo y orientación a lo largo de este proceso. Su profundo conocimiento y experiencia en el campo de la ingeniería nuclear han sido una fuente constante de inspiración y guía.

Esta tesis industrial no habría sido posible sin el apoyo a lo largo de todos estos años del Dr. Alberto Concejal, director del Departamento de Combustible Nuclear de Iberdrola Generación Nuclear. Muchas gracias por la generosidad en proporcionarme todos los recursos necesarios, especialmente los datos de planta, para poder llevar a cabo una investigación detallada y con valor para la industria. Estoy muy agradecida por su confianza y apoyo.

Asimismo, deseo extender mi más sincera gratitud a Don Pablo Julio García Sedano, por la revisión de esta tesis en un tiempo récord y por todo lo que he aprendido sobre combustible nuclear a su lado. Sin duda, es un referente en la industria nuclear, especialmente en el comportamiento del combustible en reactores BWR, y tener la oportunidad de haber trabajado unos años junto a él ha sido un verdadero privilegio.

Además, esta tesis no habría sido posible sin el apoyo constante e incondicional de mi empresa, Nfoque Advisory Services, y de todo mi equipo en el departamento nuclear. Su aliento en los momentos de flaqueza y su ayuda inestimable para compaginar la tesis con las tareas diarias como consultores nucleares han sido un pilar fundamental en este camino. Quiero mencionar de manera especial y con gran cariño a la Dra. María José Rebollo y al Dr. Emilio Castro, por su desinteresado apoyo cada vez que he requerido su ayuda, especialmente en la revisión del ATWS y en la creación de los scripts de graficación en Python que han permitido que este documento cuente con gráficos excepcionales. Su dedicación y profesionalismo me han hecho sentir afortunada por tenerlos como compañeros y amigos en esta apasionante, aunque a veces muy dura y frustrante, aventura.

I would also like to extend my sincerest thanks to Dr. Andrew Ward and Dr. José March-Leuba, who have accompanied me throughout this exciting journey. Their unwavering support, dedication, and generosity in sharing their extensive experience in the field of nuclear engineering have been a fundamental pillar in my growth as a researcher. I feel deeply honored to count on their friendship and to have learned from two such extraordinary figures in the nuclear field.

I would like to express my gratitude to Dr. Tomas Downar and Dr. Nathaniel Hudson (from the U.S. NRC) for their support during my time at the University of Michigan. Their insights and assistance significantly enriched my research experience.

Muchas gracias a los profesores de la Universidad Politécnica de Valencia, Dr. César Queral y la Dra. Nuria García Herranz, por todas las veces que he ido a consultarles cuestiones referentes a las secciones eficaces o a las secuencias del ATWS, dedicándome todo el tiempo necesario y siempre con una sonrisa.

A lo largo de todos estos largos 7 años de tesis, me he encontrado a muchas personas, especialmente en el ámbito profesional de la SNE (Sociedad Nuclear Española) y de WiN (Women in Nuclear), que siempre han tenido una palabra de apoyo, de ánimo y de cariño cuando les hablaba sobre la tesis, cuando me faltaban ideas para seguir, cuando no sabía cómo enfocar algunos puntos o simplemente cuando sentía que era demasiado duro compaginar una tesis doctoral con el trabajo. A todos, que sabéis perfectamente quiénes sois, muchas gracias por todas las veces que me habéis transmitido fuerza para continuar.

Y para el final, he dejado lo más importante para mí. Hay un dicho que dice: "si quieres llegar rápido, ve solo; si quieres llegar lejos, ve acompañado." Por ello, alcanzar la meta de esta carrera de fondo no habría sido posible sin la ayuda y la compañía de muchas personas.

A mis amigos desperdigados por el mundo, por su constante apoyo y cariño que trascienden distancias.

A mis queridas amigas de toda la vida, Eva y Araceli, por hacer lo imposible para vernos cada vez que visito Valencia. Vuestra amistad es un tesoro que valoro profundamente.

A mis amigas de Algar, María José y Mónica, por los almuerzos, las risas y las confidencias.

A mis caramelitos, Iván, Ramón y mi BFF Sandra, por los viajes, los conciertos, los festivales y la alegría. Vuestras palabras de ánimo constantes han sido esenciales en este camino. Soy verdaderamente afortunada de teneros en mi vida.

A mis Loles Queen, Maita y Claudia, por ser las amigas que todo el mundo querría tener. No tengo suficientes palabras ni de agradecimiento ni de cariño para explicar todo lo que ambas suponen para mí. Son el mejor regalo que la vida me ha hecho en los últimos años. Maita, millones de gracias por todo el trabajo que has hecho en esta tesis, tanto el real con el formato, poniendo en orden los capítulos o ayudándome en las correcciones, como en el apoyo incondicional a lo largo de cada paso de esta tesis. Este doctorado es un poco tuyo también.

A toda mi familia, materna y paterna, por su amor incondicional y por estar siempre a mi lado en cada paso de este camino.

A mi hermana Carmen, por darme una de las mejores alegrías de mi vida, ser tía por partida doble. Tu apoyo y entusiasmo tienen un valor incalculable para mí.

A mi madre, la persona que siempre ha creído en mí y en mi potencial. Gracias por comprender mi vocación desde pequeña y por animarme a perseguir mis sueños sin reservas. Tu amor y fe en mí me han impulsado a seguir adelante, incluso en los momentos más desafiantes

Y, por último, agradecerle a mi padre que, aunque ya no esté físicamente entre nosotros y no pueda ver cómo acabo la tesis, siempre me inculcara el amor por el esfuerzo, la constancia y el trabajo bien hecho. Te echo de menos cada día. Estarías orgulloso de la mujer en la que me he convertido.

ABSTRACT

The analysis of fuel depletion is essential for understanding the long-term changes in reactor fuel composition due to burnup. As fuel undergoes burnup, its isotopic composition alters, significantly influencing the reactor's operational life, stability, and control mechanisms. To address these complexities, the employment of a meticulously selected set of cross-sections and nuclear parameters is crucial. This approach not only ensures accurate predictions of reactor behavior under both steady-state and transient conditions but also optimizes the fuel cycle and enhances overall reactor performance.

Cross-section libraries form the backbone of any three-dimensional code used in core calculations. However, a significant challenge in neutron transport calculations arises from the necessity for each method to utilize cross-sections structured with varying methodologies, formats, and contents. This thesis undertakes a comprehensive exploration of reactor physics, focusing on these critical issues. It seeks to unravel how reactor phenomena are captured and represented through an in-depth analysis of cross-section libraries. By investigating the sources of cross-sections and kinetic data, and understanding the detailed requirements for solving various problems, this work advances robust safety assessments and ensures an accurate representation of reactor behavior.

A central focus of the research is the evaluation of the accuracy of the CASMO-4/GenPMAXS/PARCS computational sequence in analyzing modern Boiling Water Reactor (BWR) operations with current fuels. This entails rigorous verification of cross-section libraries through code-to-code comparisons, ensuring consistency and accuracy in steady-state performance parameters and two-group energy cross-sections. The predictions of the nodal code PARCS are meticulously assessed against the plant core simulator SIMULATE-3, which serves as a benchmark for each simulated case.

Furthermore, the validation of the created cross-section libraries is conducted through comparisons with real plant data utilizing the In-Core Traveling Probe (TIP) system equipped with high-resolution gamma detectors. Simulating the TIP response is a critical element for core simulators, enabling the reliable use of TIP measurements to validate predictions and assess the accuracy of calculated radial and axial power distributions by comparing them with measured in-core instrument reaction rates. This study leverages TIP measurements to validate the capability of PARCS in modeling advanced BWR fuel designs and calculating 3D power distributions under actual reactor operating conditions. The utilization of real plant data not only enhances the reliability of the models but also significantly elevates the practical value of this research within the field of nuclear reactor physics.

The impact of cross-section libraries on safety analyses is further examined by applying them to Main Steam Isolation Valve Closure (MSIVC) transients without SCRAM (ATWS) through the coupled code TRAC-BF1/PARCS. In an MSIVC ATWS event, core responses are influenced by the interplay between void reactivity feedback, driven by void collapse, and negative Doppler reactivity feedback. Consequently, the

severity of the transient hinges on both system behavior and the accuracy of cross-section libraries in predicting nuclear parameters. Given these considerations, the MSIVC ATWS scenario serves as an exemplary context for assessing the efficacy of cross-section libraries in predicting the evolution of critical parameters under demanding transient conditions. This assessment enhances the modeling capabilities for such events and allows for the simulation of complex thermal-hydraulic and feedback phenomena over extended durations.

A significant contribution of this thesis is the identification of limitations within the NUREG/CR-7164 recommendations for modeling cross-sections for BWR analysis. These recommendations fall short of encompassing the full operational range of BWR/6 reactors, particularly concerning fuel history under Extended Power Uprate (EPU) and MELLLA+ operational conditions. This conclusion holds substantial relevance for the development and validation of tools necessary for 1D/3D analysis of operational and accident transients beyond the design basis.

The results of this thesis yield new insights into the accuracy required for simulations to produce better estimates, introducing innovative strategies to enhance precision in coupled simulations. While the work primarily targets BWRs, its findings have broader implications for all types of Light Water Reactors (LWRs). Thus, this research represents a noteworthy advancement in reactor safety and reliability, contributing significantly to the field of nuclear reactor physics.

RESUMEN

El análisis del decaimiento de combustible es fundamental para comprender los cambios a largo plazo en la composición del combustible del reactor debido al quemado del mismo. A medida que se consume el combustible, su composición isotópica cambia y eso afecta significativamente la vida útil operativa del reactor, su estabilidad y sus mecanismos de control. Para abordar estas complejidades, es crucial emplear un conjunto meticulosamente seleccionado de secciones eficaces y parámetros nucleares. Este enfoque no solo garantiza predicciones precisas del comportamiento del reactor tanto en condiciones estacionarias y transitorias, sino que también optimiza el ciclo del combustible y mejora el rendimiento global del reactor.

Las librerías de secciones eficaces son la columna vertebral de cualquier código tridimensional utilizado en los cálculos del núcleo. Sin embargo, uno de los principales retos que plantea el cálculo del transporte de neutrones es la necesidad de que cada método empleado haga uso de secciones eficaces estructuradas con metodologías, formatos y contenidos distintos.

Esta tesis lleva a cabo una exploración exhaustiva de la física de reactores, centrándose en estos problemas críticos. Su objetivo es desentrañar cómo se capturan y representan los fenómenos de los reactores mediante un análisis en profundidad de las librerías de secciones eficaces. Mediante la investigación de las fuentes de secciones eficaces y datos cinéticos, y la comprensión de los requisitos detallados para resolver diversos problemas, la tesis contribuye a avanzar en las evaluaciones de seguridad robustas y garantizar una representación precisa del comportamiento del reactor.

Uno de los aspectos centrales de la tesis es la evaluación de la secuencia computacional CASMO-4/GenPMAXS/PARCS en el análisis de la operación de Reactores de Agua en Ebullición (BWR) con combustibles actuales. Esta evaluación implica una rigurosa verificación de las librerías de secciones eficaces a través de comparativas código a código, lo que garantiza consistencia y precisión en la predicción de la potencia radial y axial del reactor a lo largo del ciclo, mediante librerías de secciones eficaces colapsadas en dos grupos de energía. Además, se realiza un análisis de las predicciones del código nodal PARCS, que se compara con el simulador del núcleo de la planta, SIMULATE-3, utilizado como referencia en cada simulación.

Adicionalmente, se incluye la validación de las librerías de secciones eficaces creadas y la comparación del modelo neutrónico del código de núcleo 3D PARCS con datos reales de planta utilizando el sistema detector In-Core Traveling Probe (TIP) con detectores gamma de alta resolución. La simulación de la respuesta del TIP es de importancia crucial para los simuladores del núcleo, ya que permite el uso fiable de las mediciones proporcionadas por este sistema para validar las predicciones y evaluar la precisión de las distribuciones de potencia radiales y axiales calculadas, contrastándolas con las tasas de reacción medidas por los instrumentos in-core. Este estudio emplea las mediciones del TIP para validar la capacidad del código PARCS en la modelización de diseños avanzados de combustible BWR y en el cálculo de

distribuciones de potencia tridimensionales bajo condiciones operativas reales. La utilización de datos de planta no solo incrementa la fiabilidad de los modelos, sino que también refuerza el valor práctico de esta investigación dentro del campo de la física de los reactores nucleares. El impacto de las librerías de secciones eficaces en los análisis de seguridad se examina aplicándolas a los transitorios de cierre de la válvula de aislamiento de vapor principal (MSIVC) sin SCRAM (ATWS) mediante el código acoplado TRAC-BF1/PARCS. En un evento de MSIVC ATWS, las respuestas del núcleo se ven afectadas por la interacción entre la retroalimentación de reactividad debida al vacío, impulsada por el colapso del vacío, y la retroalimentación de reactividad Doppler negativa. Así, la severidad del transitorio depende tanto del comportamiento del sistema como de la precisión de las librerías de secciones eficaces en la predicción de los parámetros nucleares. Considerando estas variables, el escenario de MSIVC ATWS se presenta como un contexto ideal para evaluar la eficacia de las librerías de secciones eficaces en la predicción de la evolución de parámetros críticos bajo condiciones transitorias exigentes, mejorando las capacidades de modelado para tales eventos y permitiendo la simulación de fenómenos termohidráulicos y de realimentación complejos a lo largo de períodos prolongados.

Una de las contribuciones más destacables de esta tesis es la identificación de limitaciones en las recomendaciones NUREG/CR-7164 para el modelado de secciones eficaces en el análisis de BWR. Estas recomendaciones no abarcaban completamente el rango operativo de los reactores BWR/6, especialmente en lo que respecta a la historia del combustible en condiciones de Aumento de Potencia Extendida (EPU) y MELLLA+. Esta conclusión tiene una relevancia considerable para el desarrollo y la validación de herramientas necesarias para el análisis 1D/3D de transitorios operacionales y accidentes más allá de la base de diseño.

En definitiva, los resultados de esta tesis proporcionan nuevos conocimientos sobre la precisión requerida para que las simulaciones generen estimaciones más exactas, introduciendo estrategias innovadoras para mejorar la precisión en las simulaciones acopladas. Aunque el trabajo se enfoca principalmente en BWR, sus hallazgos tienen implicaciones para todos los tipos de reactores de agua ligera (LWR). Por lo tanto, este trabajo representa un avance significativo en la seguridad y confiabilidad de los reactores, contribuyendo de manera sustancial al campo de la física de los reactores nucleares.

RESUM

L'anàlisi del decaïment del combustible és fonamental per a comprendre els canvis a llarg termini en la composició del combustible del reactor deguts al seu cremat. A mesura que el combustible es consumeix, la seua composició isotòpica es modifica, la qual cosa afecta significativament la vida útil operativa del reactor, la seua estabilitat i els mecanismes de control associats. Per a abordar aquestes complexitats, resulta crucial emprar un conjunt meticulosament seleccionat de seccions eficaces i paràmetres nuclears. Aquest enfocament no sols garanteix prediccions precises sobre el comportament del reactor, tant en condicions estacionàries com transitòries, sinó que també optimitza el cicle del combustible i millora el rendiment global del reactor.

Les llibreries de seccions eficaces constitueixen l'eix fonamental de qualsevol codi tridimensional utilitzat en els càlculs del nucli del reactor. No obstant això, un dels principals reptes que presenta el càlcul del transport de neutrons radica en la necessitat que cada mètode aplicat utilitze seccions eficaces estructurades conforme a diferents metodologies, formats i continguts.

Aquesta tesi aborda una exploració exhaustiva de la física de reactors, centrant-se en aquestes qüestions crítiques. L'objectiu és desentranyar com es capten i es representen els fenòmens característics dels reactors mitjançant una anàlisi profunda de les llibreries de seccions eficaces. Mitjançant la investigació de les fonts de seccions eficaces i dels paràmetres cinètics, així com la comprensió detallada dels requisits necessaris per a resoldre diverses problemàtiques, aquest treball contribueix a avançar en la robustesa de les avaluacions de seguretat i a garantir una representació precisa del comportament del reactor.

Un dels aspectes centrals d'aquesta investigació és l'avaluació de la seqüència computacional CASMO-4/GenPMAXS/PARCS en l'anàlisi de l'operació de reactors d'aigua en ebullició (BWR) amb combustibles contemporanis. Aquesta avaluació implica una rigorosa verificació de les llibreries de seccions eficaces mitjançant comparatives codi a codi, la qual cosa garanteix consistència i precisió en la predicció de la potència radial i axial del reactor al llarg del cicle, emprant llibreries de seccions eficaces col·lapsades en dos grups d'energia. A més, es realitza una anàlisi de les prediccions del codi nodal PARCS, comparant-les amb el simulador del nucli de la planta, SIMULATE-3, utilitzat com a referència en cada simulació.

A més, s'inclou la validació de les llibreries de seccions eficaces generades i la comparació del model neutrònic tridimensional del codi PARCS amb dades reals de la planta, obtingudes a través del sistema detector In-Core Traveling Probe (TIP), equipat amb detectors gamma d'alta resolució. La simulació de la resposta del TIP és d'importància crucial per als simuladors del nucli, ja que permet l'ús fiable de les mesures proporcionades per aquest sistema per a validar les prediccions i avaluar la precisió de les distribucions de potència radials i axials calculades, contrastant-les amb les taxes de reacció mesurades pels instruments in-core.

Aquest estudi empra les mesures del TIP amb l'objectiu de validar la capacitat del codi PARCS en la modelització de dissenys avançats de combustible BWR i en el càlcul de distribucions de potència tridimensionals sota condicions operatives reals. La utilització de dades de planta no sols augmenta la fiabilitat dels models, sinó que també reforça de manera significativa el valor pràctic d'aquesta investigació en l'àmbit de la física de reactors nuclears.

L'impacte de les llibreries de seccions eficaces sobre els anàlisis de seguretat s'avalua a través de la seua aplicació en transitoris de tancament de la vàlvula principal d'aïllament de vapor (MSIVC) sense SCRAM (ATWS), emprant el codi acoblat TRAC-BF1/PARCS. En un escenari de MSIVC ATWS, la resposta del nucli es veu condicionada per la interacció entre la retroalimentació de reactivitat deguda al col·lapse del buit i la retroalimentació negativa de reactivitat Doppler. La gravetat del transitori depén, per tant, del comportament del sistema i de la precisió de les llibreries de seccions eficaces a l'hora de predir els paràmetres nuclears. Sota aquestes consideracions, l'escenari MSIVC ATWS esdevé un context exemplar per a avaluar l'eficàcia de les llibreries de seccions eficaces en la predicció de l'evolució de paràmetres crítics en condicions transitàries exigents. Aquesta avaluació millora les capacitats de modelatge per a esdeveniments d'aquest tipus i facilita la simulació de fenòmens termohidràulics complexos i de retroalimentació al llarg de períodes prolongats.

Una de les contribucions més notables d'aquesta tesi és la identificació de les limitacions presents en les recomanacions NUREG/CR-7164 per al modelatge de seccions eficaces en l'anàlisi de BWR. Aquestes recomanacions no abasten plenament el rang operatiu complet dels reactors BWR/6, especialment pel que fa a l'historial del combustible en condicions d'Aument de Potència Extesa (EPU) i en els escenaris operatius MELLLA+. Aquesta conclusió té una rellevància considerable per al desenvolupament i validació de les eines necessàries per a l'anàlisi unidimensional (1D) i tridimensional (3D) de transitoris operacionals i d'accidents més enllà de la base de disseny.

Els resultats obtinguts en aquesta tesi proporcionen nous coneixements sobre el grau de precisió necessari en les simulacions per a que aquestes produïsquen estimacions més exactes, introduint estratègies innovadores orientades a millorar la precisió en simulacions acoblades. Encara que el treball se centra principalment en els BWR, les seues conclusions tenen implicacions significatives per a tot tipus de reactors d'aigua lleugera (LWR). En definitiva, aquesta investigació representa un avanç important en la seguretat i fiabilitat dels reactors nuclears, contribuint de manera substancial al camp de la física de reactors nuclears.

.

TABLE OF CONTENTS

LIST OF FIGURES

LIST OF TABLES

ACRONYMS

ABWR	Advanced Boiling Water Reactor
ADF	Assembly Discontinuity Factor
ADS	Automatic Depressurization System
ANM	Analityc Nodal Method
AOO	Anticipated Operational Occurrence
APRM	Average Power Range Monitor
ARO	All Rods Out
ARI	All Rods In
ATWS	Anticipated Transient Without Scram
BDBA	Beyond Design Basis Accidents
BOC	Beginning-of-Cycle
BOP	Balance of Plant
BP	Burnable Poison
BWR	Boiling Water Reactor
CBP	Condensate Booster Pump
CD	Core Damage
CDF	Corner-point Discontinuity Factors
CE	Continuos Energy
CFR	Code Federal Regulations
CHAN	Channel Component in TRAC-BF1 Input
CMFD	Course-Mesh Finite-Difference
CP	Condensate Pump
CPM	Collision Probability Method
CPR	Critical Power Ratio
CR	Control Rod
CRDS	Control Rod Drive System
CSS	Coupled Steady-State Calculation Mode
CTR	Coupled Transient Calculation Mode
CZP	Cold Zero Power
DBA	Design Basis Accidents
DC	Density Coolant
DEC	Design Extension Conditions
DOM	Discrete Ordinates Method
DSA	Deterministic Safety Analysis

EAF	European Activation File
ECCS	Emergency Core Cooling System
ED	Emergency Depressurization
ENDF	Evaluated Nuclear Data File
EOC	End of Cycle
EOP	Emergency Operating Procedures
EPG	Emergency Procedure Guidelines
EPU	Extended Power Uprate
ET	Event Tree
FA	Fuel Assembly
FW	Feedwater
FWRT	FeedWater Reduced Temperature
Gd	Gadolinium
GDC	General Design Criterion
GE	General Electric Company
HCR	History Control Rod
HCTL	Heat Capacity Temperature Limit
HDC	History Density Coolant
HFP	Hot Full Power
HPCS	High-pressure Core Spray
HZP	Hot Zero Power
IAEA	The International Atomic Energy Agency
ICMS	In-Core Monitoring System
IORV	Inadverted Opening of a Relief Valve
IRM	Intermediate Range Monitor
JEF	Joint Evaluated File of NEA Countries
JENDL	Japanese Evaluated Nuclear Data Library
LHGR	Linear Heat Generation Rate
LOCA	Loss-of-Coolant Accident
LOOP	Loss-of-Offsite Power
LPCI	Low-Pressure Core Injection
LPCS	Low-Pressure Core Spray
LPRM	Local Power Range Monitor
LWR	Light Water Reactor
MAPLHGR	Maximum Average Planar Linear Heat Generation
MCPR	Minimum Critical Power Ratio
MELLL	Maximum Extended Load Line Limit
MELLLA	Maximum Extended Load Line Limit Analysis

MELLLA+	Maximum Extended Load Line Limit Analysis Plus
MG	Multi Group
MLHGR	Maximum Linear Heat Generation Rate
MOC	Middle of Cycle
MOC	Method of Characteristics
MSCP	Minimum Steam Cooling Pressure
MSCWL	Minimum Steam Cooling Water Level
MSIV	Main Steam Isolation Valve
MSIVC	Main Steam Isolation Valve Closure
MSLB	Main Steam Line Break
NEA	Nuclear Energy Agency
NEM	Nodal Expansion Method
NEMTAB	Nuclear Energy-dependent Multi-Group Table
NFY	Neutron-induced Fission Product Yields
NK	Neutron Kinetics
NRC	United States Nuclear Regulatory Commision
NPP	Nuclear Power Plant
ODE	Ordinary Differential Equation
OLTP	Originally Licensed Thermal Power
PARCS	Purdue Advanced Reactor Core Simulator
PCT	Peak Cladding Temperature
PDF	Probability Density Function
PhD	Doctor of Philosophy
PIE	Postulated Initiated Event
PMAXS	Purdue Macroscopic Cross-section
PPM	Parts per Million by Weight of Boron Concentration Diluted in the Moderator
PRFO	Pressure Regulator Failure - Open
PRM	Power Range Monitor
PSA	Probabilistic Safety Analysis
PWR	Pressurized Water Reactor
RC	Recirculation Flow
RCIC	Reactor Core Isolating Cooling
RCF	Rated Core Flow
RDD	Radioactive Decay Data
REA	Rod Ejection Accident
RHR	Residual Heat Removal
RMS	Root-Mean-Square
RPF	Relative Power Fraction

RPS	Reactor Protection System
RPT	Recirculation Pump Trip
RPV	Reactor Pressure Vessel
RWL	Reactor Water Level
SAFDL	Specified Acceptable Fuel Design Limits
SC	Success Criteria
SCRAM	Safety Control Rods Activator/Actuator Mechanism
SLCS	Stand-by Liquid Control System
SMR	Small Modular Reactor
SRM	Source Range Monitor
SRP	Standard Review Plan (NUREG-0800)
SRV	Safety Relief Valve
SSA	Steady-State Stand-Alone Calculation Mode
SP	Suppression Pool
SPT	Suppression Pool Temperature
TAF	Top-of-Active Fuel
TH	Thermal-hydraulics
TIP	Traversing In-core Probe
TM	Moderator Temperature
TMI	Three Mile Island
TF	Fuel Temperature
TSL	Thermal Scattering Law Data
TTWB	Turbine Trip With Bypass
UPV	Universitat Politècnica de València
XS	Cross-section

Chapter 1
Introduction

1.1 Foreword.

Nuclear power plants produced about 10% of the electricity in the world in 2023. In Spain specifically, nuclear power accounted for an impressive 20.34% of the country's electricity production. This energy was generated by seven Light Water Reactors (LWRs), collectively producing a staggering 28.16% of Spain's CO_2-free electricity.

Six of the seven reactors in operation belong to the widely adopted Pressurized Water Reactor (PWR) design, while the remaining one utilizes a Boiling Water Reactor (BWR) configuration.

Over the years, nuclear power generation has experienced remarkable advancements since its inception in the 1950s. In the pursuit of generating cleaner electricity, nuclear power plants have embraced more aggressive operational strategies. Indeed, the operational approach to BWRs has undergone significant transformations since the 1960s when these reactors first entered service.

This evolution has paved the way for vendors to develop innovative fuel solutions to enhance the economics of BWR operations. With an emphasis on improving efficiency and performance, these advancements have presented new challenges. Plant management and engineering teams must rise to the occasion by implementing robust measures to guarantee the plant's continued safe and optimal functioning.

More than fifteen years ago, the Maximum Extended Load Line Limit Plus Analysis (MELLLA+) domain was proposed for BWRs that had already implemented Extended Power Uprates (EPU). The MELLLA+ domain would allow operation at the EPU reactor thermal power, i.e., up to 120% of Originally Licensed Thermal Power (OLTP), but at reduced reactor core flow as low as 80% of Rated Core Flow (RCF).

The reduced flow capability creates an operating window that allows reactivity changes to compensate for the burnup of fissile and burnable absorber material during normal operation without the need for control rod motion.

Regardless of operational strategy, all commercial LWRs must operate within prescribed limits based upon this information to assure fuel integrity and thus protect the public's safety. Similarly, this information is used to evaluate reactor control actions and track the performance of the fuel under regular operation, anticipated operational transients, and accidental scenarios.

In recent years, regulations and safety analysis have transitioned their focus from highly unlikely severe accidents to less severe but more likely operational accidents. Thus, accurately predicting BWR core behavior (mostly eigenvalue, reactivity, and thermal limits) is essential in more demanding operational domains.

Margin improvement in new operating strategies such as 24-month cycle extensions, power increases, operating map extensions, or further licensing requirements demands the use of the so-called best-estimate codes and 3D methodologies with proper treatment of uncertainties.

Cross-section libraries are fundamental to any 3D code used for core calculation. Yet, the main weakness of all neutronics calculations is that each method, i.e., diffusion vs. transport, nodal/homogeneous vs. heterogeneous, deterministic vs. Monte Carlo, Point Kinetics vs. 1D vs. 3D, static vs. transient, feedback type, burnup conditions, require cross-sections prepared in a different way, methodology, format, and content.

This thesis provides a study of basic fundamental questions like the sources of the cross-sections and kinetic data, understanding the detail necessary to solve the pertinent, and which features could vary depending on the problem.

By navigating these challenges and seizing opportunities for improvement, the nuclear power industry continues to make significant strides in providing sustainable and clean energy solutions. As the demand for electricity grows, it becomes increasingly important to optimize the operation of nuclear power plants, leveraging technological advancements to meet the world's energy needs while minimizing environmental impact.

1.2 Statement of Objectives.

Fuel depletion analysis plays a crucial role in assessing the long-term changes in reactor fuel composition resulting from fuel burnup during reactor operation. These changes have a profound impact on the reactor's operational lifespan, stability, and control. Thus, it is imperative to utilize an appropriate set of cross-sections and nuclear parameters to ensure the accurate prediction of reactor behavior under both steady-state and transient conditions because it enables the optimization of the fuel cycle and enhances overall reactor performance.

Having this in mind, this dissertation aims to:

- understand how reactor physics phenomena are captured and represented through a thorough analysis of cross-section libraries;
- contribute to robust safety assessments by ensuring that the cross-section libraries accurately represent the behavior of the reactor;
- evaluate the accuracy of the CASMO-4/GenPMAXS/PARCS computational sequence when analyzing modern Boiling Water Reactor operation using currently available BWR fuels;
- verify the cross-section libraries through code-to-code benchmarks to ensure consistency and accuracy in providing reliable results. This code-to-code comparison is intended for steady-state performance parameters and two-group nuclear cross-sections for BWR fuel assemblies;
- compare the predictions of the nodal code PARCS against the plant core-follow computer SIMULATE-3, which serves as the reference for every simulated case;
- validate the selected cross-section sets and benchmark the PARCS model against measured power distributions, i.e., real plant data, using the In-core Traveling Probe (TIP) detector system, which utilizes high-resolution gamma detectors;
- assess the impact of cross-section libraries on safety analyses by applying them to an Anticipated Transient Without Scram (ATWS) Main Steam Isolation Valve Closure (MSIVC) transients and to study the effectiveness of the libraries in predicting the evolution of the main figures of merit facing demanding transient scenarios;
- improve the ability to model such events with coupled codes, i.e., TRAC-BF1/PARCS, mainly focused on covering good enough the expected range for the independent variables of the transient;
- simulate complicated thermal-hydraulic problems for a sufficiently long time to understand the response of critical components and, most specifically, the core response;
- enhance the development of effective accident management strategies through the analysis of cross-section sets.

All our analyses involve an exhaustive examination of historic and instantaneous variables, and burnup points within the cross-section libraries. By undertaking these comprehensive studies, the behavior and significance of cross-section libraries in nuclear safety analysis will be fully explored, leading to conclusions and recommendations on improving the accuracy of reactor physics simulations.

This dissertation includes new research into the accuracy needed for best-estimate simulations. New strategies were developed to achieve increased accuracy in coupled simulations. The findings presented here are mainly focused on BWRs but could be extended to any LWR type of reactor.

The knowledge gained through this research contributes to the improvement of reactor safety and ensures the reliable operation of LWRs.

1.3 Thesis Outline.

The thesis is comprised of nine chapters and is organized as follows:

Chapter 2 covers the most common neutronics topics, such as the neutronics governing equations, including the nuclear data needed to solve them. Special attention is paid to diffusion theory, with significant emphasis on cross-section libraries and lattice calculations, crucial for generating accurate multigroup cross-sections and modeling reactor behavior under various conditions.

The chapter also discusses the importance of nuclear data, including energy group representations, and the impact of lattice transport code precision on reactor core estimation. Finally, it explores reactivity feedback mechanisms, explaining how changes in core conditions affect reactor reactivity, which is vital for safety and stability assessments. This chapter's main theoretical discussions aim to serve as a basis to establish contexts for all the work developed during this dissertation; thus, they are included for that purpose.

Chapter 3 explores advanced methodologies and tools essential for nuclear data processing and their crucial impact on reactor safety and performance. It highlights the importance of integrating thermal-hydraulic and neutronic calculations to provide a comprehensive view of reactor core behavior across various operational scenarios. This integration enhances the accuracy and reliability of reactor analyses. The chapter emphasizes the role of transient analysis in managing both anticipated operational occurrences and beyond design basis accidents. It also addresses the significance of Anticipated Transient Without Scram (ATWS) scenarios.

The chapter concludes with an in-depth review of common reactor core analysis codes, CASMO-4, SIMULATE-3, GenPMAXS, PARCS, and TRAC-BF1, showing their contributions to more precise and reliable reactor core understanding, thereby advancing nuclear reactor safety.

On the grounds that a significant variation of the core parameters is expected over the length of the cycle, an accurate set of cross-sections would be needed to predict reactor behavior correctly in steady-state and transient conditions. Thus, **Chapter 4** provides a more in-depth discussion of cross-section generation & modeling for BWRs, paying particular attention to the cross-section variations and its impact on core simulator results due to the instantaneous and history effects.

This chapter also reviews the conclusions from NUREG/CR-7164, *"NRC Guidelines for BWR"*. The NUREG/CR-7164 guidelines were established by comparing several cross-section sets calculated using different methodologies and codes and were intended to apply to all BWR designs. However, some limitations in the methodology were found are addressed and discussed throughout the dissertation.

An overview of the PARCS cross-section model and a detailed description of the PMAXS files, the most common cross-section files used by PARCS for core simulation and depletion analysis purposes, are likewise included.

Chapter 5 presents the results of a code-to-code benchmark intended for steady-state performance parameters and two-group nuclear cross-sections for BWR

fuel lattices. The code-to-code benchmark compares steady-state 3D power distributions of two different cycles at several depletion steps provided by the plant core-follow computer SIMULATE-3 and predicted by the nodal code PARCS. Assorted conclusions drawn from the results provide insights to cross-section library generation and modeling.

Building upon these comparisons, **Chapter 6** contains benchmarks of PARCS results against measured TIP plant data at various burnup steps. TIPs measurements are used to validate the capability of PARCS to model advanced BWR fuel designs and to calculate 3D power distributions for actual reactor operating conditions using the different cross-section sets modeled in Chapter 5.

The calculation sequence CASMO-4/GenPMAXS/PARCS has been used and assessed in all simulated cases in Chapters 5 and 6.

Chapter 7 is devoted to simulating a postulated Anticipated Transient Without SCRAM (ATWS) initiated by Main Steam Line Isolation Valve Closure (MSIVC). Two operator action scenarios are used to study the plant behavior and the impact of the cross-section library on the overall core response under demanding transient scenarios like ATWS.

All ATWS simulations are performed using TRAC-BF1/PARCS coupled code system in the time domain employing the cross-section modeling guidelines concluded in Chapter 5. The TRAC-BF1 model incorporates features that facilitate the simulation of ATWS events in a BWR/6 housed in a Mark III containment.

The simulation results reinforce the importance of cross-section modeling and confirm the coupled code applicability to analyze complex transients such as ATWS.

Chapter 8 summarizes the work carried out in this study, the findings and the concluding remarks. This chapter also includes recommendations for future work that might add value to the work undertaken here.

Chapter 9 contains references to publications and data that support this research.

Chapter 2
Introduction to Neutronics Methods and Techniques

2.1 Introduction.

Neutronics, as a discipline dedicated to the transport of neutrons through matter and the characterization of their interactions, plays a fundamental role in nuclear reactor physics. Specifically, neutronics focuses on determining the spatial and temporal distributions of neutrons within the reactor and the evolution of isotopes in reactor materials.

The intrinsic characteristics of BWRs give rise to significant spatial variations within the operating core, as highlighted in (Bozzola, S., 1982). Additionally, core parameters such as neutron flux, fission power, moderator density, control rods, coolant inlet temperature and flow, Xenon/Samarium concentrations, and fuel temperatures are intricately interrelated. This interdependence leads to strong feedback mechanisms that influence the core's behavior under varying operating conditions. Thus, accurate analysis and prediction of neutronic behavior in nuclear systems require the application of robust theory methodologies and advanced computational tools that strike a balance between accuracy, speed, and robustness.

2.2 Neutronics Governing Equations.

Since one of the primary quantities involved in neutronics is the neutron distributions and their travelling through matter, the need to study the behavior of the neutron population and its interplays with the constituent reactor materials is evident. Thus, understanding neutron transport is essential for accurately determining the neutron distribution within the reactor.

Neutronics is characterized by its utilization of microscopic data, derived from the quantum realm (such as microscopic cross-sections), to compute macroscopic quantities (such as reactor power density). Therefore, it can be viewed primarily as a science of the macroscopic.

2.2.1 Neutron Transport Equation.

According to (Duderstadt, J. J. & Hamilton, L. J., 1976), and quoting verbatim;

> To determine the distribution of neutrons in the nuclear reactor, we must investigate the process of neutron transport, that is, the motion of the neutrons as they stream about the reactor core, frequently scattering off of atomic nuclei and eventually either being absorbed or leaking out of the reactor.

Rewriting the last paragraph in a far easier way, the neutron transport equation provides the fundamental and exact description of the neutron population within the reactor. Accounting for the fact that there will surely be neutron gains and losses throughout the reactor, the challenge here is to convert the Balance-the-neutrons game into mathematical words.

Considering any arbitrary volume V, the number of neutrons in V with energy E in dE and traveling in a direction $\hat{\boldsymbol{\Omega}}$ in $d\hat{\boldsymbol{\Omega}}$ within this volume is

$$\left[\int_V n\left(\vec{\boldsymbol{r}}, E, \hat{\boldsymbol{\Omega}}, t\right) d\left(\vec{\boldsymbol{r}}\right)\right] dE\, d\hat{\boldsymbol{\Omega}}$$

Then, the change rate of the number of neutrons by time will be given by a balanced equation as follows:

$$\frac{\partial}{\partial t}\left[\int_V n\left(\vec{\boldsymbol{r}}, E, \hat{\boldsymbol{\Omega}}, t\right) d\left(\vec{\boldsymbol{r}}\right)\right] dE\, d\hat{\boldsymbol{\Omega}} = gain\ in\ V - loss\ from\ V \qquad \textbf{Equation 2.1}$$

Assuming that the arbitrary volume V does not depend on time, the last equation can be transformed into

$$\frac{\partial}{\partial t}\left[\int_V n\left(\vec{r},E,\widehat{\boldsymbol{\Omega}},t\right)d(\vec{r})\right]dE\,d\widehat{\boldsymbol{\Omega}}=\left[\int_V \frac{\partial n}{\partial t}d(\vec{r})\right]dE\,d\widehat{\boldsymbol{\Omega}} \qquad \textbf{Equation 2.2}$$

Now, if we then consider all the reactions by which the gain or loss of neutrons can be produced in the given volume V, the ensuing classification can be contemplated:

Gain mechanisms:

1) Any neutron sources in V,
2) Neutrons streaming into V through the surface S, and
3) Neutrons of different E' and $\widehat{\boldsymbol{\Omega}}'$, suffering a scattering collision in V, that changes E' and $\widehat{\boldsymbol{\Omega}}'$ into the E and $\widehat{\boldsymbol{\Omega}}$ of interest.

Loss mechanisms:

4) Neutrons leaking out through the surface S, and
5) Neutrons in V suffering a collision.

Note that,

$$Neutron\ balance\ in\ V = 1+2+3-4-5 \qquad \textbf{Equation 2.3}$$

Then, writing every one of these contributions into mathematical expressions in terms of the angular density $n\left(\vec{r},E',\widehat{\boldsymbol{\Omega}'},t\right)$, we find

$$\int_V d(\vec{r})\left[\frac{\partial n}{\partial t}+v\,\widehat{\boldsymbol{\Omega}}\cdot\boldsymbol{\nabla}\,n+v\Sigma_t\,n\left(\vec{r},E,\widehat{\boldsymbol{\Omega}},t\right)-\int_0^{\infty}dE'\int_{4\pi}d\widehat{\boldsymbol{\Omega}}'\,v'\Sigma_s\left(E'\to E,\widehat{\boldsymbol{\Omega}}'\to\widehat{\boldsymbol{\Omega}}\right)n\left(\vec{r},E',\widehat{\boldsymbol{\Omega}'},t\right)-s\left(\vec{r},E,\widehat{\boldsymbol{\Omega}},t\right)\right]dE\,d\widehat{\boldsymbol{\Omega}}=0 \qquad \textbf{Equation 2.4}$$

Yet, because the volume V was arbitrarily chosen, the integral for any V can vanish as follows:

$$\int_{any\ V} d(\vec{r})\,f(\vec{r})=0\ \rightarrow f(\vec{r})\equiv 0 \qquad \textbf{Equation 2.5}$$

Hence, we arrive at a balance equation as

$$\frac{\partial n}{\partial t} + v\,\hat{\boldsymbol{\Omega}}\cdot\boldsymbol{\nabla}\,n + v\Sigma_t\,n\left(\vec{\boldsymbol{r}},E,\hat{\boldsymbol{\Omega}},t\right) = \\ = \int_{4\pi} d\hat{\boldsymbol{\Omega}}' \int_0^{\infty} dE'\,v'\Sigma_s\left(E'\to E,\hat{\boldsymbol{\Omega}}'\to\hat{\boldsymbol{\Omega}}\right) n\left(\vec{\boldsymbol{r}},E',\hat{\boldsymbol{\Omega}}',t\right) \\ + s\left(\vec{\boldsymbol{r}},E',\hat{\boldsymbol{\Omega}}',t\right)$$

Equation 2.6

Which is known as the ***Boltzmann Transport Equation.*** Bold formatting is utilized for all equations to emphasize vector components.

The Boltzmann Transport Equation is an integro-differential equation that describes the transport of neutrons in a medium and calculates the balance of the neutron population in each region of the reactor core.

As seen, Equation 2.6 is linear in the unknown dependent variable $n\,(\vec{\boldsymbol{r}}, E, \hat{\boldsymbol{\Omega}}, t)$ with seven independent variables ($\vec{\boldsymbol{r}} = x, y, z; E; \hat{\boldsymbol{\Omega}} = \theta, \varphi; t$). However, due to the derivatives, initial and boundary conditions for the angular density will be needed and properly specified.

As outlined in (Duderstadt, J. J. & Hamilton, L. J., 1976), Equation 2.6 involves only a single time derivative. Therefore, we can straightforwardly select the initial condition by specifying the initial value of the angular density for all positions, energies, and directions. Additionally, the boundary conditions will vary depending on the specific problem under consideration.

The neutron transport equation offers an essentially exact description of the neutron distribution within the reactor and its solution contains all the information required concerning the nuclear behavior of the reactor. Indeed, the neutron transport equation has been the cornerstone of several approximate methods used in nuclear reactor analysis.

However, in practice, solving the neutron transport equation directly is not always straightforward due to the complexities involved. Consequently, most analyses rely on assumptions and approximations to address the equation effectively.

2.2.2 Diffusion Equation.

The Boltzmann equation serves as the fundamental framework for describing neutron transport in nuclear reactors, accounting for neutron interactions with materials and their transport across spatial and energy domains. Its comprehensive nature enables precise predictions of neutron flux distributions and reaction rates, critical for reactor design and safety assessments. However, the computational demands of solving the Boltzmann transport equation for complex reactor geometries and operational conditions necessitate pragmatic approximations.

Quoting from (Stacey, W. M., 2018);

> The simplest and most widely used mathematical description of the neutron distribution in nuclear reactors is provided by Neutron Diffusion Theory. For simplicity of explication, the neutrons are treated as if they are all of one effective speed, and effects associated with changes in neutron energy are suppressed.

Therefore, it is apparent that solving the Boltzmann transport equation for full-core calculations involves high computational and memory storage costs, necessitating the use of approximations.

As a result, *Neutron Diffusion Theory* arises as a simplified yet effective approximation of the Boltzmann equation under certain conditions. Widely adopted in reactor physics, the diffusion equation offers computational efficiency and ease of implementation compared to the Boltzmann transport equation. It assumes negligible angular dependence of neutron flux and provides accurate solutions for many reactor configurations.

Other approximations, such as the P1, (Duderstadt, J. J. & Hamilton, L. J., 1976), and SP3 methods (Lewis, E. E. & Miller, W. F., 1984), extend the diffusion theory by incorporating higher-order angular moments to capture more nuanced neutron behaviors. These approaches strike a balance between computational feasibility and accuracy, catering to diverse reactor scenarios and analysis requirements. Ultimately, the diffusion equation and its variants remain indispensable tools in the nuclear industry, supporting efficient reactor design, operational optimization, and safety evaluation processes.

However, it is important to emphasize that while diffusion and two-group approximations are well-suited for LWRs, this applicability cannot be generalized to all reactor types. Each reactor design has unique characteristics and operating conditions that may necessitate different neutron transport methodologies. Thus, while diffusion theory may yield accurate results for conventional LWRs, it may not be equally effective for other reactor types such as Small Modular Reactors (SMRs) or advanced reactors such as Generation III+ and IV designs.

The simplicity of the diffusion theory model allows for scientific insight and quantitative understanding of many reactor features, making it a suitable computational method in nuclear physics. In essence, the neutron diffusion theory simplifies the transport equation by eliminating flux angular dependence, effectively homogenizing the spatial distribution of neutron flux.

As pointed out while discussing the diffusion approximation in (Silvennoinen, P., 1976), the separation of $\hat{\boldsymbol{\Omega}}$ from the velocity necessitates the notation $\phi(\vec{r}, E)$ for the scalar flux. Therefore, the cross-sections and the angular scattering distribution function are viewed as functions of energy and direction separately.

The Diffusion Equation, which is known as ***Fick's Law,*** is written as follows:

$$\boldsymbol{J}(\vec{r}, t) = -D(\vec{r}, t)\nabla\phi(\vec{r}, t) \qquad \textbf{Equation 2.7}$$

Where $\boldsymbol{J}$ is known as the *Neutron Current Density* and D is the so-called *Diffusion Coefficient*, which is obtained from the relationship:

$$D(\vec{r},t)=\frac{1}{3\Sigma_{tr}(\vec{r},t)} \qquad \textbf{Equation 2.8}$$

where Σ_{tr} is called the *Macroscopic Transport Cross-Section*.

Thus, the neutron diffusion theory is used to describe mathematically the distribution of neutrons in a nuclear reactor under different approximations as (Duderstadt, J. J. & Hamilton, L. J., 1976):

1) The angular flux is only weakly dependent on angle.
2) The neutron source term is isotropic.
3) The neutron current density changes slowly on a time scale compared to the mean collision time.

Actually, only the first of these approximations is really crucial and points the way to the validity of the diffusion equation. In fact, strong angular dependence can be associated with neutron fluxes having a strong spatial variation.

However, the assumption of weak angular dependence is violated in the following cases:

1) Near boundaries or where material properties change dramatically from point to point over distances comparable to a mean free path.
2) Near localized sources.
3) In strongly absorbing media, such as a fuel rod or a control element.
4) If the sources are not isotropic.

Despite that, industrial reactors are often computed, with satisfactory results, with few-energy group diffusion theory. For the case in which the neutron energy dependence is retained, the diffusion equation in two-energy groups and six delayed neutron precursor groups is expressed, using standard notation, as (Downar, T. et al., 2012):

$$\frac{1}{v_1}\frac{\partial\phi_1(\vec{r},t)}{\partial t}=-\nabla\left(-D_1(\vec{r},t)\nabla\phi_1(\vec{r},t)\right)-\left(\Sigma_{a1}(\vec{r},t)+\Sigma_{12}(\vec{r},t)\right)\phi_1(\vec{r},t)+(1-\beta)\upsilon\Sigma_{f1}(\vec{r},t)\phi_1(\vec{r},t)+(1-\beta)\upsilon\Sigma_{f2}(\vec{r},t)\phi_2(\vec{r},t)+\sum_{k=1}^{6}\lambda_k C_k(\vec{r},t)\chi \qquad \textbf{Equation 2.9}$$

$$\frac{1}{v_2}\frac{\partial\phi_2(\vec{r},t)}{\partial t}=-\nabla\left(-D_2(\vec{r},t)\nabla\phi_2(\vec{r},t)\right)-\Sigma_{a2}(\vec{r},t)\phi_2(\vec{r},t)+\Sigma_{12}(\vec{r},t)\phi_1(\vec{r},t) \qquad \textbf{Equation 2.10}$$

$$\frac{\partial C_k(\vec{r},t)}{\partial t}=\beta_k\upsilon\Sigma_{f1}\phi_1(\vec{r},t)+\beta_k\upsilon\Sigma_{f2}\phi_2(\vec{r},t)-\lambda_k C_k(\vec{r},t);\quad(k=\ 1,\dots,6) \qquad \textbf{Equation 2.11}$$

The set of parameters and variables, including cross-sections, fast and thermal flows, and the concentration of the six groups of precursors, are dependent solely on time and space, without angular dependence. The selected nomenclature aligns with traditional conventions found in relevant literature.

2.2.3 Numerical Methods.

Two methods exist for simulating and modeling the neutronic governing equations: *Deterministic* and *Stochastic* methods. The data requirements and methods of cross-section preparation - continuous energy or multigroup - depend on the method that will subsequently be used to solve the Boltzmann equation or an approximation to it.

2.2.3.1 Deterministic.

Deterministic methods solve the Boltzmann Transport Equation in a numerically approximated manner everywhere throughout a modeled system.

Deterministic methods are based on discretizing and linearizing the Boltzmann Transport Equation in each of its independent variables, resulting in a vast algebraic system of equations and unknowns that must be solved afterward, demanding a considerable number of computational resources.

This massive number of unknowns is a direct consequence of that steady-state 3D transport problems require a 6D phase space (three space dimensions plus three motion angles). Computer codes have been written for 3D problems with 1D or 2D spatial symmetry to minimize the number of unknowns. This reduces the number of independent spatial and angular variables. However, it is necessary to use iterative methods to calculate solutions for most practical problems.

In the earlier era of neutronics, the deterministic approach was the primary consideration. Even today, despite significant technological advancements, it remains the most commonly used method due to its favorable cost-to-accuracy ratio. Thus, improved energy discretization techniques are crucial for achieving predictability and estimating uncertainty in deterministic modeling.

The computational cost associated with fast industrial calculations remains a major obstacle for the deterministic resolution of the transport equation, especially when applied to heterogeneous 3D cores. This underscores why reactor core analyses generally rely on nodal coarse-mesh two-group diffusion methods, particularly for current low-heterogeneous LWR cores.

2.2.3.2 Monte Carlo.

Stochastic (or Monte Carlo) methods are based on a probabilistic interpretation of the transport process, which models the nuclear system almost exactly and then solve the exact model statistically (approximately) anywhere in the modeled system.

In this approach, the random histories of individual particles are calculated using pseudorandom number sequences, and the results are averaged over a large number of histories. This can be done in such a way because, typically in the physical process of

particle transport, many particles undergo random and independent histories (Cacuci, D. G. (Ed.)., 2010).

Stochastic methods rely on the detailed physics of individual neutrons and nuclei interactions. Therefore, the spatial, angular, or energy discretization are not required and allow the use of the most detailed treatment possible of cross-sections (continuous energy libraries).

When it is impractical to describe a physical phenomenon via deterministic equations (balance equations, distribution functions, differential equations), the Monte Carlo method becomes the preferred option. Actually, in many applications, the physical process is simulated directly characterized by its Probability Density Functions (PDFs). If the geometry of the system and its cross-sections are known, then the results of the Monte Carlo simulation contain only statistical errors. Moreover, processing a sufficient number of particles makes it possible to reduce this statistical error below any specified level.

Monte Carlo methods are widely used because of their relative ease of implementation, their ability to treat complex geometries with excellent fidelity, and their ability to solve problems accurately with cross-section data that can have highly complex energy dependence.

Currently, the Monte Carlo method, known for its high accuracy, is not commonly used for large-scale industrial calculations due to its computational requirements. However, as we look ahead to the future of nuclear technology, particularly with the advent of Small Modular Reactors (SMRs), there is a growing need to employ stochastic solutions to tackle the complex physics associated with their innovative fuel designs and flexible operational modes.

Although this thesis focuses on industrial applications, and therefore a deterministic approach has been chosen as the primary calculation method for the comprehensive analysis of the topic at hand, it is important to acknowledge the potential of the Monte Carlo method for future developments. As we continue to refine algorithms and enhance computing resources, the Monte Carlo method may eventually become a viable option for industrial-scale calculations.

2.2.4 Nuclide Depletion Calculations.

Nuclear reactions influence the neutron population and induce variations in the population of atomic nuclei. Therefore, the evolution in concentrations of the various nuclides, considering atomic nuclei generations and disappearances through nuclear reactions and the radioactive decay process, must be assessed.

As the reactor operates, the fuel composition changes and affects the core's reactivity. In other words, *"the composition of each fuel element varies significantly according to their initial state and current irradiation status"*, as stated in (Silvennoinen, P., 1976).

Hence, to understand the behavior of a reactor's core over its operating lifetime, it is necessary to predict the changes in the isotopic composition of the core as a function

of both time and space. The analysis of these changes is complicated because the time and spatial variation in the isotopic composition will depend on the neutron flux distribution, which itself depends on core composition.

Fuel depletion calculations aim to track and determine the evolution of all isotopes of interest within each assembly, including fissile, fertile, burnable poison, and fission products, as a function of burnup.

Burnup is defined as the amount of energy released per unit mass of fuel, typically measured in megawatt-days per metric ton (1000 kg) of uranium (MWd/MTU). Alternatively, burnup can also be expressed as megawatt days per short ton (2000 pounds) of uranium (MWd/st), with the conversion factor between both units typically around 0.907.

In essence, burnup serves as a measure of the fuel's utilization and depletion over time. It allows us to assess how much energy has been extracted from the fuel and how the composition of isotopes changes because of nuclear reactions. Then, the balance of the concentration of nuclides of the system can be determined accordingly:

TIME VARIATION = **PRODUCTION AS A RESULT OF DECAY OF PARENT NUCLIDE**
+ PRODUCTION AS A RESULT OF NUCLEAR REACTIONS INVOLVING OTHER NUCLIDES
– LOSS AS A RESULT OF ITS OWN DECAY
– LOSS AS A RESULT OF A NUCLEAR REACTIONS INVOLVING NUCLIDE 'A' ITSELF

Turning these expressions into mathematical form yields to Equation 2.12, which are known as the ***Bateman Equations***:

$$\frac{dN_A(t)}{dt} = \lambda_B N_B(t) + \sum \sigma_C^{\gamma} \phi N_C(t) - \lambda_A N_A(t) - \sum \sigma_A^{a} \phi N_A(t) \qquad \textbf{Equation 2.12}$$

The Bateman equations form a stiff Ordinary Differential Equation (ODE) system with constant coefficients that can be solved by numerical methods that evaluate the solution in a discrete sequence of time steps. Solving the Bateman equations provides the concentrations of the various nuclides present in the reactor (also needed among the data of the Boltzmann equation), as well as related activities.

As extensively discussed in (Cacuci, D. G. (Ed.)., 2010), assuming that the isotopes' spatial movement from their place of origination does not occur, the spatial dependence of the isotopic number densities can be suppressed. Therefore, the Bateman balance equations solely need to describe the time dependency of the isotopic number densities.

It is worth mentioning that the Boltzmann and Bateman equations form a coupled system, see Figure 2.1, since reaction rates depend on the neutron flux and vice versa, which implies that a coupled problem must be solved.

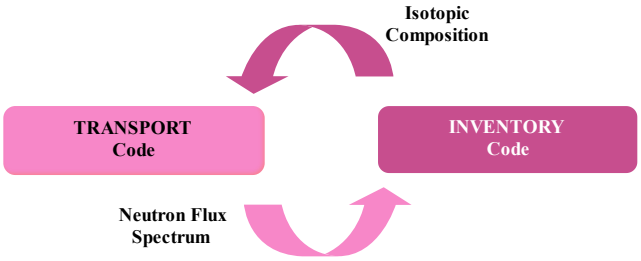

Figure 2.1. Boltzmann – Bateman Coupling Scheme.

In practice, however, these equations can be decoupled by solving them separately over successive time intervals, short enough to neglect variations in isotopic composition in the Boltzmann equation and variations in flux in the Bateman equations over each of these intervals. The length of the interval - *step* Δt_{burn} - is usually given in terms of burnup since it is the burnup that causes changes in the fuel.

For the decoupled solution calculations, the *middle-of-step predictor-corrector* algorithm, see Figure 2.2, is the most widely used and works as follows:

1) Transport calculation using the known initial isotopic composition,
2) Inventory calculation - *predictor* - to determine the interval midpoint isotopic composition,
3) Transport calculation employing the interval midpoint isotopic composition,
4) Inventory recalculation - *corrector* - through the whole interval.

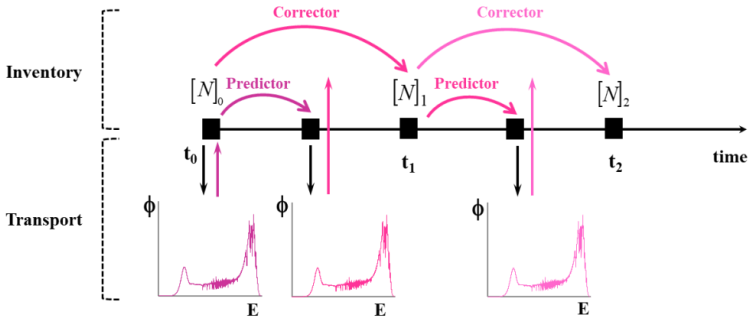

Figure 2.2. Predictor-Corrector Boltzmann – Bateman Coupling Scheme.

Saying that the cell composition changes with burnup, as well as the conditions in the fuel and the moderator, is tantamount to affirm that the neutron spectrum changes. Change in the neutron spectrum in turn means that the average macroscopic

cross-sections may have to be recalculated in every step. Thereby, the cross-sections are certainly calculated for every step and for every region of the core necessarily by the lattice physics codes.

2.3 Nuclear Data for the Solution of the Neutronics Calculations.

Primary nuclear data (cross-sections, resonance parameters, fission-product yields, spectra of emitted particles, et cetera) encompasses continuous energy libraries based on evaluated and depletion data files for a considerable large amount of fission products and actinides.

All the above data are available in evaluated nuclear reaction data libraries for general and special purposes as the ENDF/B (United States Evaluated Nuclear Data File), JEF (Joint Evaluated File of NEA Countries), or JENDL (Japanese Evaluated Nuclear Data Library), among others.

To solve the neutronic equations, the nuclear data detailed in Table 2.1 are required:

Table 2.1. Nuclear Data Libraries.

	Evaluated Libraries	Format	Content
General Purposes	Incident Neutron Library (N)	ENDF-6	Neutron Data
	Thermal Scattering Law Data (TSL)	ENDF-6	Neutron Data
	Radioactive Decay Data (RDD)	ENDF-6	Decay Data
	Neutron-induced Fission Product Yields (NFY)	ENDF-6	Fission Product Yields
Special Purposes	Neutron Activation Transmutation Library	ENDF-6 or EAF	Neutron Activation Data (including branching ratios)

The nuclear data library formats EAF (European Activation File) and ENDF-6 are widely used in the nuclear industry for the representation and exchange of important nuclear data as seen in Table 2.1. These libraries employ comprehensive formats to store and distribute evaluated nuclear data for a wide array of isotopes and reactions. Their well-defined structures facilitate the exchange, comparison, and integration of nuclear data from various sources.

Before inclusion in the evaluated libraries, nuclear data undergo thorough evaluation processes, derived from experimental measurements and/or theoretical

models. Despite the vast amount of data contained in these libraries, not all are directly applicable to neutronics calculations; hence, they require pre-processing.

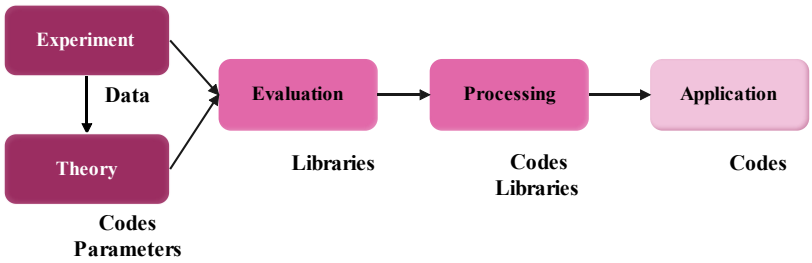

Source: (Oblozinsky & Schwerer, 1998).

Figure 2.3. Nuclear Data Libraries Collection Process.

Processing Codes play a pivotal role in converting evaluated nuclear data into a more user-friendly format. Figure 2.3 illustrates that evaluated neutron cross-section data form the cornerstone of information essential for nuclear technology applications.

The cross-sections are represented as a combination of cross-sections and resonance parameters in the evaluated libraries. The processing codes reconstruct the cross-sections from the data contained in the evaluated libraries, modify their values to consider the Doppler effect, address the treatment of the resonances in the unresolved range, and write the data in a format suitable for the neutronics codes to be used.

As a result, two basic approaches are obtained: a Continuous Energy (CE) library or the Multigroup (MG) library. The multigroup approximation is the basis of nearly all reactor physics codes, making it one of most widely used approximations of neutron transport and the only approximation for the diffusion theory.

2.3.1 Continuous Energy.

Continuous Energy methods in nuclear engineering are pivotal for accurately modeling neutron transport across a wide range of energies, crucial for understanding reactor physics and performance. The primary challenge lies in the intricate energy dependence of material cross-sections, which necessitates detailed characterization across the entire energy spectrum.

As noted by (Cochran, R. G. & Tsoulfanidis, N., 1999), the energy variable (E) in the transport equation introduces significant complexity due to the diverse interactions of neutrons with materials at different energies. Cross-sections must therefore be defined across a continuous range of energies to capture these interactions accurately. This requirement leads to extensive data sets that specify how neutrons interact with various isotopes under different energy conditions.

Processing CE cross-sections involves addressing several technical hurdles. These include accurately reconstructing energy-dependent cross-sections, managing

unresolved resonance regions, and accounting for Doppler broadening effects caused by temperature variations, as discussed by (Cacuci, D. G. (Ed.)., 2010). These challenges are critical in ensuring that computational models accurately reflect real-world reactor conditions and behavior.

2.3.2 *Energy Collapsing.*

Energy collapsing represents a strategic approach to managing the computational burden associated with CE methods. In this approach, the continuous energy spectrum is discretized into discrete energy groups.

As illustrated in Figure 2.4, the multigroup approximation to Boltzmann equation is initiated by partitioning the total continuous energy range of interest into discrete energy groups. At this point, the energy group structure is an intermediate-group level called *Fine-group* data and contains around ~1000 or more groups.

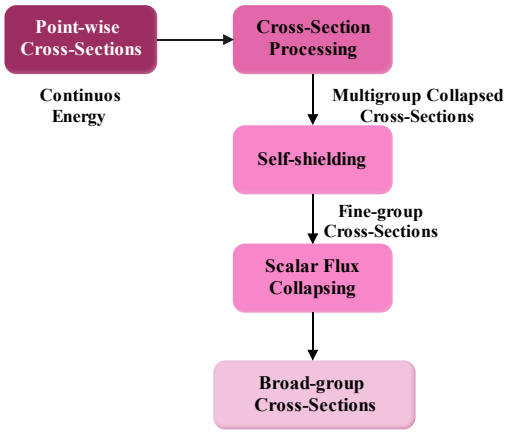

Figure 2.4. Standard Procedure for Generation Broad-group Libraries.

It is important that the intermediate-group assembly transport calculation uses enough groups to represent the spectral interactions among fuel pins of different composition, control rods, water channels, as well as different operating temperatures, depletion steps, or void fractions.

Therefore, the issue raised next is how to determine these multigroup cross-sections so that the multigroup reaction rates preserve the reaction rates predicted by the continuous-energy equation. This process, known as *Cross-section Collapsing*, results in the creation of a new group called *Broad-group*, as depicted in Figure 2.5.

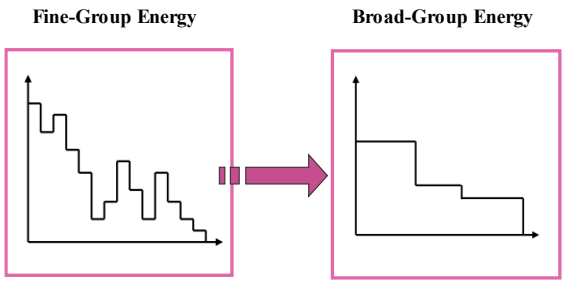

Source: (Fujita, T., 2015).

Figure 2.5. Energy Collapsing Illustration.

The broad group sets, typically consisting of ~200 groups based on an LWR average composition, serve as an intermediate level depending on the specific objectives of reactor core calculations. For most reactor calculations there is no need for such large number of energy groups; thus, a smaller library might be considered, such as ~50 groups. Nevertheless, the *Two-group Approximation* remains the most widely employed method in the nuclear industry for its balance of simplicity and effectiveness in capturing neutron behavior.

The two-group approximation simplifies the neutron diffusion equation, allowing for rapid computation of reactor kinetics parameters such as reactivity feedback coefficients, effective multiplication factor (k_{eff}), and power distributions during transient conditions.

In safety analysis scenarios such as reactor transients, the two-group model provides insights into the neutron behavior under abnormal operating conditions, aiding in the assessment of reactor safety margins and the design of safety features.

Two-group models are also used in fuel cycle analysis to evaluate the burnup of nuclear fuel, predict isotopic composition changes, and optimize fuel management strategies over the operational lifetime of reactors. This capability allows nuclear engineers to forecast fuel performance, manage nuclear waste, and plan refueling operations efficiently.

2.4 Lattice Calculations.

Nuclear data are essential for understanding and quantifying engineering processes in nuclear fission reactors, such as neutron fields, reaction rates, nuclide inventories, activation, decay heat, and safety margins (e.g., criticality, reactivity coefficients, power distributions, and burnup). Cross-sections are a key parameter in nuclear physics that describe the probability of specific nuclear reactions occurring by representing the effective area that a target nucleus presents to an incoming particle.

All cross-section data are generated from *Lattice Physics Assembly Calculations*. These lattice physics codes are a crucial part of reactor analysis, and the quality of the generated cross-section sets is integral to the accuracy of core simulation results.

Reactor Lattice Physics Codes are computer programs used to calculate the neutron flux distribution and the infinite medium multiplication factor (k_∞). It takes a multigroup library of isotopic nuclear data and a detailed description of the reactor lattice as inputs, solving the neutron transport equation over a specified region within the lattice. This region can be a unit cell or a macrocell. Consequently, lattice codes incorporate methods for solving the relevant equations for neutron flux and k_∞ across discrete energy groups and spatial points (Kulikowska, T., 2001).

The computed neutron flux is then used to generate sets of macroscopic cross-sections, homogenized over selected subregions and within a chosen broad energy group structure, as depicted in Figure 2.6.

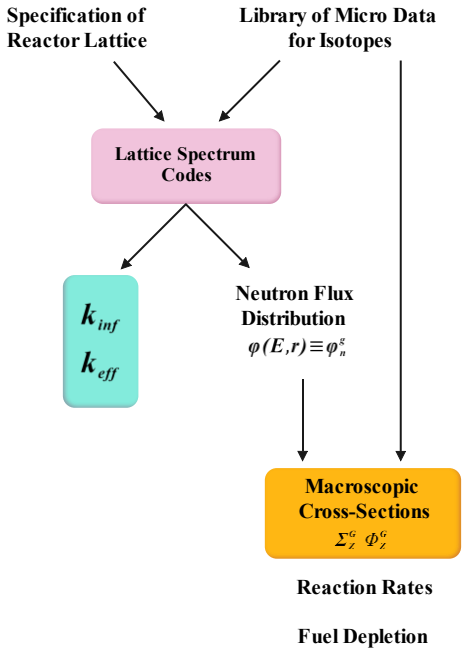

Source: (Kulikowska, T., 2001).

Figure 2.6. General Diagram of the Input and Output of a Reactor Lattice Code.

Typically, lattice codes employ one of several established transport methodologies, which may encompass the Collision Probability Method (CPM), the Method of Characteristics (MOC), or the Discrete Ordinates Method (DOM). These methods are invariably coupled with two-dimensional geometric modeling to produce cross-sections as a function of burnup, fuel history, and state core variables.

Notably, the realm of cross-section generation draws upon a suite of sophisticated computational tools such as CASMO-4 (Edenius, M. et al., 1995), PHOENIX (Vondy, D. R., et al., 1973), HELIOS (Peterson, L., 2003), PARAGON (Alcouffe, R. E., et al., 1991), CPM-3 (Lucius, R., 1980), APOLLO2 (Gruel, J., et al., 2011), TransLAT (Trkov, A., et al., 2010), SCALE6.1 (Rearden, B. T., 2018), SERPENT (Leppänen, J., et al., 2014), and WIMS (Muir, D., et al., 1982), to name a few prominent instances.

The macroscopic cross-section sets (also sometimes known as nodal cross-sections) are subsequently utilized as material data inputs for various codes that solve the neutron transport or diffusion equations for the entire reactor or specific sections of it. The nodal cross-sections are parametrized as function of instantaneous operating conditions and the history of operation, as will be discussed in detail in Chapter 4. Additionally, the calculated neutron flux can be employed for reaction rate calculations and fuel depletion analyses.

According to (Kulikowska, T., 2001), lattice codes are applied in three principal areas, as illustrated in Figure 2.7. These areas are:

1) **Analysis of Experimental Data**: This involves studying critical lattices and measuring parameters such as buckling and reaction rates in specific nuclides.
2) **Criticality Determination**: Lattice codes are employed to ascertain the criticality of reactor systems, which is essential for ensuring safe and efficient operation.
3) **Power Reactor Design, Assessment, and Operation**: This is the domain where deterministic methods, such as lattice codes, prove most effective. In this context, lattice codes are used to compute fuel depletion and assess reactivity feedback effects due to burnup, fuel temperature, and density variations. They facilitate the creation of libraries of homogenized cross-sections, which are then integrated into whole reactor codes for fuel management and simulation studies.

The utilization of lattice codes in reactor design and operation underscores their importance in developing accurate and reliable models for nuclear reactors. Their role in generating cross-section libraries and analyzing complex reactor behavior contributes significantly to the optimization of reactor performance and safety.

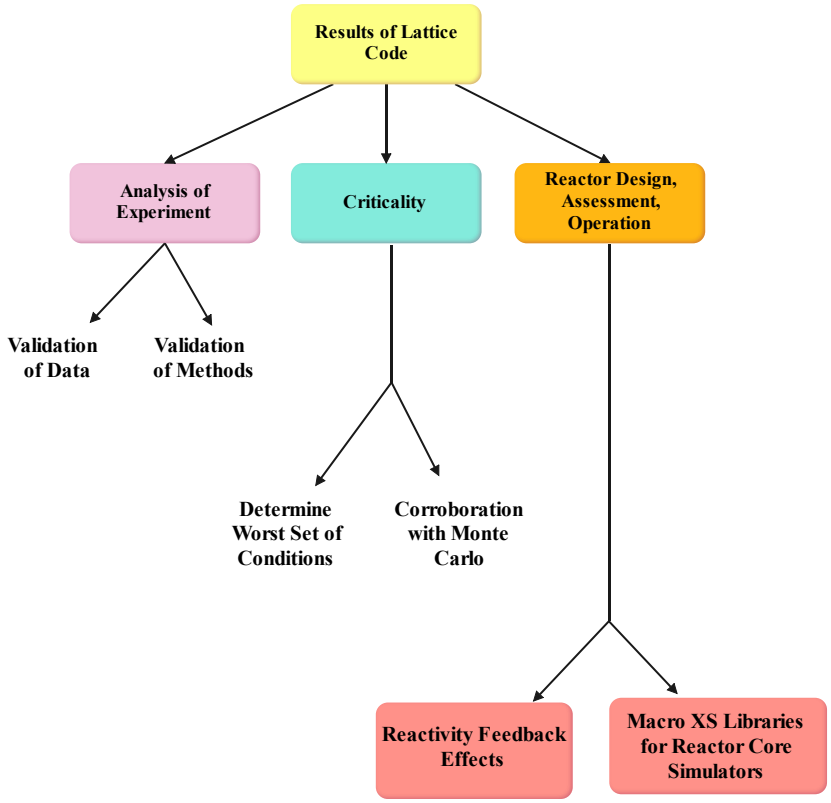

Source: (Kulikowska, T., 2001).

Figure 2.7. Areas of Application of the Lattice Code Results.

Lattice physics codes are used to generate few-group cross-section data for nodal codes, which are used to model the coupled neutronics and thermal-hydraulics behavior of the entire reactor core during steady-state and transient operation.

The nodal code models the entire reactor core as a collection of homogeneous prisms, referred to as nodes. A model of a full-sized reactor core will use anywhere from 5k to 30k nodes. Core simulators are normally advanced 3D two-group nodal codes and fundamental in BWR core design because they provide for a variety of design and operational analyses involving different fuel loading patterns, fuel management, or multi-cycle design studies.

The precision of the lattice transport code significantly impacts the accuracy of the reactor core estimation. Therefore, it is important to develop advanced neutronics methodologies to ensure that the nuclear data used in the diffusion codes are as accurate as possible. This involves improving the modeling of physical phenomena such as fuel depletion, resonance self-shielding, and thermal feedback effects, as well as the use of more advanced numerical methods for solving the transport equation.

2.4.1 Homogenization of Cross-Sections.

According to the U.S. NRC's glossary, (*US-NRC Library - Glosary*, 2021):

> ….During normal reactor operations, nuclear fuel sustains a fission chain reaction or criticality. A reactor achieves criticality (and is said to be critical) when each fission event releases a sufficient number of neutrons to sustain an ongoing series of reactions.

The criticality of the reactor is expressed by the condition $k_{eff} = 1$, meaning that the reactor is in a self-sustaining state with a constant neutron population, and the excess reactivity relative to criticality of the system, ρ, is given by:

$$\rho = \frac{k_{eff} - 1}{k_{eff}} \qquad \textbf{Equation 2.13}$$

where k_{eff} is the neutron multiplication factor. Thus, the neutron multiplication factor indicates whether a nuclear reactor is critical, subcritical, or supercritical. Values of k_{eff} greater than 1 denote supercritical conditions, where the neutron population increases exponentially over time. Conversely, values of k_{eff} less than 1 indicate subcritical conditions, where the neutron population decreases over time.

In operating conditions, the reactor is kept critical by means of balancing the different reactivity components which separately cause positive or negative changes in the system (Silvennoinen, P., 1976).

To predict criticality and other reactor characteristics accurately, it is essential to assess the fine-structure flux distribution resulting from the heterogeneous composition of reactor components, such as fuel elements and control rods. However, the predominant methods for calculating criticality and global flux distributions, mainly relying on diffusion calculations, are traditionally based on the assumption of homogeneous regions. The techniques utilized to substitute a heterogeneous region with equivalent homogeneous ones are denoted as *Homogenization Theory*.

As discussed in (Stacey, W. M., 2018), homogenization of a heterogeneous assembly usually proceeds in two steps: a transport calculation to obtain the detailed heterogeneous flux distribution within a unit cell or fuel assembly, followed by using this detailed flux distribution to calculate average homogeneous cross-sections for the unit cell or assembly.

Besides, the homogenization of the material sets is done using a straightforward flux and volume weighting of the heterogeneous material sets (Cacuci, D. G. (Ed.)., 2010). This concept is illustrated in Figure 2.8.

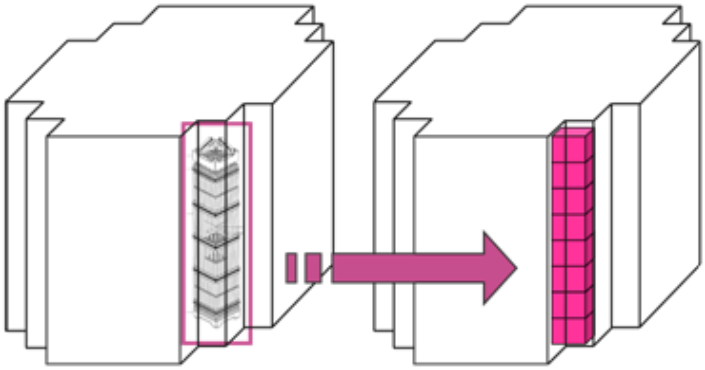

Figure 2.8. Core Homogenization's Concept.

Thus, since many core simulators solve the neutron problem using diffusion theory in homogenized zones with few energy groups, homogenized parameters in each zone as input data are hence required.

For the diffusion solution to be equivalent to the transport solution, these parameters must include cross-sections and correction factors. In addition, the parameters must be generated following a homogenization technique and must be known as a function of the state variables that modify the neutron properties during reactor operation.

The accurate calculation of the diffusion coefficient or transport cross-section is a challenging task in neutronics analysis. While the same type of definition characterizes the cell-average fission and scattering cross-sections, defining the diffusion coefficient correctly is less straightforward. This is because the diffusion coefficient must represent the net leakage from the cell, which in turn depends on the specific calculation method employed for that purpose.

The practical difficulty is that the exact solution of the global transport equation is not known, and the homogenized solution of the global diffusion equation requires the homogenized group constants as input. Furthermore, the solution to the homogenized problem cannot preserve in detail the solution to the initial heterogeneous problem since the homogenization process is accompanied with information loss, and only the mean values of the solution can be maintained.

This is when the basic concept of *Equivalence* comes into play, which specifies the requirement to preserve reaction rates when going from the nuclear reactor's actual configuration to its modeled configuration, reference (CEA, 2015).

The most important quantities to be preserved are the multiplication constant, k_{eff}, the group flux and reaction rates averaged over the homogenization region, and the group currents averaged over the surface of the homogenization region.

In order to conserve the neutron reaction rate in each node and the current at the interface between nodes, it is necessary to provide both the effective macroscopic

cross-sections of the homogeneous node and the *Assembly Discontinuity Factors* (ADFs). The ADFs are defined as ratios of heterogeneous flux and the homogenous flux,

$$f_{s,g} = \frac{\phi_{s,g}^{Het}}{\phi_{s,g}^{Hom}}, \quad g = 1,2,\dots G, \qquad s = surfaces \qquad \textbf{Equation 2.14}$$

The heterogeneous flux can be obtained directly from lattice calculation. If the lattice calculation is for a single assembly with reflective or white boundary conditions on all surfaces, then the homogenous fluxes of all surfaces are equal to assembly average fluxes. In this case,

$$f_{s,g} = \frac{\phi_{s,g}^{Het}}{\bar{\phi}_{a,g}^{Het}}, \quad g = 1,2,\dots G, \qquad s = surfaces \qquad \textbf{Equation 2.15}$$

These homogenization procedures result in homogenized cross-sections that can be used for an entire fuel assembly or collections of fuel assemblies in a full core calculation. As stated by (Smith, 1986), the use of ADFs reduces typical homogenization errors by about a factor of three (in BWRs, from 10% errors reduced to ~ 2.0 - 3.0%).

Then, the nodal code pieces the various lattices together to construct the several fuel assemblies in the reactor core as shown in Figure 2.9. For a typical BWR fuel assembly, heterogeneity is larger than in PWR due to the channel box, the water rods, the non-uniform axial enrichment, and the control rod insertion.

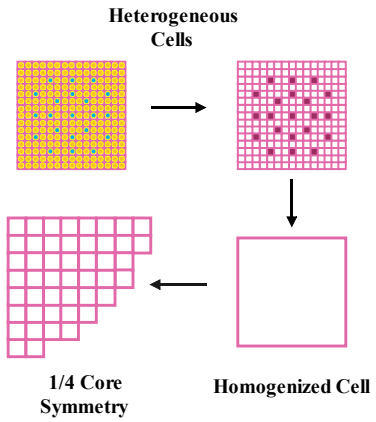

Figure 2.9. Fuel Assembly Homogenization for Core Calculations.

Finally, when performing a nodal or a pin-by-pin steady-state calculations, the homogenized parameters indicated in Table 2.2 will be required by the diffusion code for solving the diffusion equation.

Table 2.2. Base Macroscopic Cross-Section Coefficients.

	Parameter	Symbol	Units
1	Diffusion Coefficients	D^g	cm
2	Absorption	Σ_a^g	cm^{-1}
3	Nu-Fission	$\nu\Sigma_f^g$	cm^{-1}
4	Kappa-Fission	K	W·S
5	Scattering	$\Sigma_s^{g\to g'}$	cm^{-1}
6	Discontinuity Factors	f^g	-
7	Fission Spectrum	χ^g	-

These parameters must be generated using appropriate homogenization techniques to ensure that the diffusion solution yields to an equivalent result to the related transport solution with all the spatial detail without the homogenization.

The choice of diffusion coefficient significantly influences the solution for the homogeneous flux in the calculation. However, bear in mind that the results obtained by code simulations cannot be better than the original data.

2.4.2 Cross-section Libraries.

Cross-section libraries support numerous applications, including reactor core design, safety analysis, fuel cycle analysis, and operational strategy development. By encapsulating the dynamic characteristics of nuclear fuel and moderator materials with respect to the fundamental variables governing neutronics, these libraries provide essential data for the analysis, simulation, and optimization of nuclear reactors.

The neutronic model requires the fuel temperature distribution since the neutron interactions depend explicitly on material temperatures and densities. So, modeling cross-section libraries requires a deep understanding of the fuel assembly behavior in the reactor core.

A typical nuclear cross-section library contains data on, reference (Duderstadt, J. J. & Hamilton, L. J., 1976):

1) **Reaction Types**: Including absorption, fission, scattering (elastic and inelastic), and radiative capture.

2) **Energy Dependence**: Cross-sections are often provided for a range of energy groups to account for the energy-dependent nature of neutron interactions.
3) **Isotopic Data**: Detailed information for a wide array of isotopes present in reactor materials.
4) **Temperature Dependence**: Data adjusted for various temperatures, reflecting the changes in reaction probabilities due to thermal motion of nuclei.
5) **Angular Distributions**: Information on the angular dependence of scattering reactions.

Cross-section data can vary significantly based on instantaneous operational conditions and historical factors (cumulative effects of past operations). Instantaneous variations are influenced by parameters such as fuel temperature, moderator density, and neutron flux. These factors are dynamic and can change rapidly during reactor operation, necessitating real-time adjustments to the cross-section data.

Historical variations are driven by fuel burnup and the cumulative exposure of reactor materials to neutron flux over time. As fuel undergoes burnup, its isotopic composition changes, altering the associated cross-sections. To address these variations, cross-section libraries include burnup-dependent data and depletion chains that track the evolution of isotopic concentrations and their impact on reaction probabilities. Instantaneous and historical effects will be widely discussed in Chapter 4.

Cross-section libraries are structured to accommodate both instantaneous and historical variations of the cross-sections. This structure is crucial for accurately modeling the reactor's dynamic behavior over time, as described in (Fujita et al., 2014). Since the variations of the cross-sections need to be properly captured by the lattice code calculations, the creation of a cross-section set entails the execution of two distinct lattice physics computations, namely, depletion and branch calculations, reference (Fujita, T., 2015).

In depletion calculations, specific state parameters remain constant throughout the burnup process, encompassing variables such as void fraction, fuel temperature, moderator temperature, and control rod configurations. However, the neutron fluxes and number densities are computed at discrete burnup intervals. In contrast, the branch calculations do not entail the computation of number densities; instead, they rely upon the values obtained from the preceding depletion calculations. Within each burnup iteration, alterations are introduced to select state parameters, deviating partially from the conditions established in the depletion calculations and necessitating the recalculation of neutron flux distributions.

During the core calculation, each node will be identified by a specific combination of instantaneous values (*State Values*) and history (*Depletion*) variables, determining the selection and reconstruction of the macroscopic cross-sections from a particular set.

Feedback parameters, including their interdependence when two or more parameters are varied simultaneously (i.e., cross-terms), are a critical aspect of cross-section libraries. These parameters, such as reactivity coefficients and control rod worth, describe how the reactor responds to changes in operational conditions. For instance, reactivity coefficients indicate how reactor reactivity is affected by variations in fuel temperature (Doppler effect) or moderator density (void coefficient). These dependencies must be accounted for in core analysis because they are crucial for accurate transient simulations.

Previous studies, including sensitivity studies on spatial mesh overlays for PWR Rod Ejection Accident (REA) analysis (Todorova, N. & Ivanov, K., 2001), have shown that local and global predictions are very sensitive to thermal-hydraulic feedback parameters due to non-linear interactions among them. This finding is reinforced by the analysis of PWR Main Steam Line Break (MSLB) with 3D core thermal-hydraulic models (Ivanov, K. et al., 2001). Additional research has concluded that cross-section dependencies on fuel temperature, moderator temperature, and pressure are also non-linear.

As noted by (Watson & Ivanov, 2002), significant thermal-hydraulic feedback variables include local fuel temperature, pressure, moderator temperature, void fraction, and boron concentration. In a BWR, the axial void fraction distribution is of fundamental importance. At low exposure, the reactivity effect due to instantaneous void formation is apparent, while at higher exposure, the void history effect becomes particularly relevant because of its impact on burnup and the resulting isotopic composition (Bozzola, S., 1982).

Lattice codes must accurately model these feedback effects to ensure that the derived cross-sections reflect realistic reactor conditions. This involves integrating feedback parameters into the calculations, allowing cross-sections to adjust based on the reactor's current state. Properly accounting for feedback effects enhances the predictive capability of reactor simulations and supports effective reactor control and safety measures.

Upon selecting appropriate feedback parameters, two additional critical considerations warrant attention: defining the domain range for these feedback parameters and determining the number of mesh points to be deployed within the designated domain. Properly defining the mesh points is crucial for lattice code calculations, as the accuracy of interpolations is intrinsically tied to the precise specification of the parameter range. These important points will be broadly discussed in Chapter 4 and Chapter 5.

It is important to acknowledge that the utilization of 3D kinetics entails additional computational costs and augments the complexity of requisite calculations because it is important to generate cross-sections that cover of the expected operating conditions for the transients to be modeled and treat the relevant physics and co-dependencies (Watson & Ivanov, 2002; Sánchez-Cervera, et.al., 2014b). Consequently, the magnitude of neutron data and associated computations hinges upon the requisite number of neutron compositions and the minimal necessary data points needed to

adequately characterize the reactor core. This particular aspect is exhaustively examined and elaborated upon throughout the dissertation.

Such comprehensive characterization is indispensable for modeling the core kinetics across the entirety of the spectrum of transient scenarios subject to scrutiny.

Typically, lattice physics depletion calculations are performed at core-average conditions for each type of assembly. The resultant data serves as a basis for constructing cross-sectional tables as functions of assembly exposure. Dependencies on the history variables are determined by performing separate lattice physics assembly depletion calculations for each of the history effects. History variables account for the fact that the prior value of some variables influences the cross-sections.

Equally crucial is the incorporation of cross-sectional modeling, which accounts for all instantaneous properties of the fuel assembly, encompassing variables such as water density, fuel temperature, boron concentration, among others. The dependencies of cross-sections on these state variables are elucidated by conducting instantaneous branch calculations using lattice physics codes, involving deviations from the core-averaged depletion calculations to simulate off-nominal values of the state parameters.

An accurate method for modeling cross-section variations for off-nominal core conditions is essential for coupled simulations. A thorough explication of this concept is provided within the confines of Chapter 4 and Chapter 5.

Conventionally, most researchers are granted access to cross-section libraries that are either provided by vendors or universities. In most cases, the original purpose of these libraries is to analyze different reload fuel configurations for core management during normal cycle reloads and benchmarking. These libraries are optimized to operate under typical pressure, power, and moderator temperature operating conditions. However, they may not be well-suited for specific off-nominal plant applications or transients where conditions may differ significantly.

As a result, the recommendations put forth in this doctoral thesis regarding the modeling of cross-section libraries are intended for applications beyond reload and nominal conditions. It is worth noting that most lattice codes are typically proprietary and not accessible to researchers; therefore, they cannot generate problem-specific libraries, which would be more suitable to their studies.

2.4.3 Representation of Cross-section Libraries.

As broadly discussed in the literature, there are mainly two types of cross-section data libraries: multi-dimensional tabulated libraries and parameterized, reference (Sánchez-Cervera, et al., 2014a). Each type has its own advantages and disadvantages, as described by (Zimin, V. G. & Semenov, A. A., 2005; Bokov, P. M., 2009), and various nuclear codes utilize these libraries in different ways. Besides, the construction of the libraries significantly impacts the core simulations afterward, as outlined by (Ferroukhi, H. et al., 2009).

Multi-dimensional tabulated libraries represent the most straightforward method of compiling cross-section. These libraries, which store cross-section as functions of multiple state variables, such as fuel temperature, moderator temperature, and neutron spectrum, are often represented as tables or matrices where each entry corresponds to a specific combination of state variables.

This approach usually employs piece-wise linear interpolation to account for the cross-term effects between variables and can be extended to include historical information. By using this method, there is no need to approximate cross-section dependencies through functional forms, thus eliminating the effort required to derive accurate polynomials.

Some of the advantages of multi-dimensional tabulated libraries are:

- **High Accuracy**: Multi-dimensional libraries provide high-fidelity data because they explicitly account for the interactions between different state variables.
- **Detailed Modeling**: They enable detailed modeling of complex reactor phenomena, such as thermal-hydraulic feedback effects and spatial variations in reactor conditions.

However, the disadvantages are:

- **Large Data Volume**: The primary drawback is the large volume of data required to cover all possible combinations of state variables, which can lead to significant storage and computational overhead.
- **Complex Interpolation**: Accessing the required data during simulations often involves complex interpolation methods, which can increase computational time and complexity.

Parameterized cross-section libraries use mathematical functions to describe the dependencies of cross-sections on state variables. Instead of storing data for each possible combination of state variables, these libraries store coefficients for the mathematical functions that approximate the cross-sections.

Some of the advantages of parameterized libraries are:

- **Reduced Data Volume**: Parameterized libraries significantly reduce the amount of data needed, as the functional forms require fewer coefficients than multi-dimensional tables.
- **Faster Access**: During simulations, cross-section values can be quickly computed using the stored parameters, reducing the need for complex interpolation.
- **Added Flexibility**: To incorporate corrections for spectral effects.

And, the disadvantages are:

- **Potential Loss of Accuracy**: The main disadvantage is the potential loss of accuracy if the chosen parameterization does not capture all the nuances of the cross-section dependencies.
- **Complex Parameterization Process**: Developing accurate parameterizations can be complex and requires extensive validation against experimental or high-fidelity simulation data.

In the contemporary landscape of core simulators, both multi-dimensional tabulated and parameterized cross-section libraries find their place. For instance, CORETRAN (Eisenhart, L.D. et al., 2000), predominantly leans towards the utilization of parameterized libraries, providing efficient computational performance through functional approximations of cross-section dependencies.

Conversely, simulators like SIMULATE-3K (Grandi, G. M., 2005), CRONOS (Lautard, J. J. et al., 1990), and DYN3D (Grundmann, U. et al., 2005) are configured to utilize tabulated libraries for their calculations. These simulators benefit from the high accuracy and detailed modeling capabilities that tabulated libraries offer, especially in capturing complex interactions between state variables.

The choice between multidimensional and parameterized cross-section libraries depends on the specific requirements of the reactor analysis. Multi-dimensional libraries are preferred when high accuracy is paramount and storage resources are not a limiting factor. They are particularly useful in detailed core simulations where spatial and temporal variations need to be captured with high fidelity. Conversely, parameterized libraries are favored in scenarios where computational efficiency and reduced data volume are critical, such as real-time reactor monitoring and control systems.

Regarding the most employed nodal cross-section library format files, NEMTAB and PMAXS files represent two distinct approaches to managing cross-section libraries in nuclear reactor simulations.

Some of the comparative advantages and disadvantages of these both formats have been included in (Mesado, C., 2017). Overall, NEMTAB (Nuclear Energy-dependent Multigroup Table) files store cross-sections as multi-dimensional tables. This approach allows for accurate representation of cross-section behaviors across a wide range of operational scenarios, facilitating detailed neutron transport and reactor physics calculations. However, these files require significant storage space and computational resources due to the large volume of data needed to cover all possible combinations of variables. Complex interpolation methods are also necessary to access data efficiently during simulations, which can increase computational time.

On the other hand, PMAXS (Purdue Macroscopic Cross-section) files employ mathematical functions to approximate cross-section dependencies on state variables. Instead of storing actual cross-section values, PMAXS files store coefficients for these mathematical functions, enabling efficient storage and rapid access during simulations.

This approach reduces computational overhead compared to NEMTAB files while maintaining sufficient accuracy for reactor simulations. PMAXS files are advantageous for applications where computational efficiency is paramount, such as real-time monitoring and transient analyses. However, they may introduce slight inaccuracies compared to NEMTAB files in scenarios requiring precise modeling of cross-section behaviors under extreme conditions.

Both NEMTAB and PMAXS files are extensively employed in the nuclear industry, particularly within advanced reactor physics codes such as PARCS, (Downar, T. et al., 2012). PARCS utilizes NEMTAB files for detailed reactor physics analyses requiring high fidelity in cross-section data representation across multiple variables. PMAXS files are employed in PARCS for efficient computations in scenarios where rapid simulations or parameter sensitivity studies are conducted.

For the pursuit of this doctoral thesis, the utilization of cross-sections in the PMAXS format has been purposefully selected as will be discussed in Chapter 4.

2.5 Reactivity Feedback.

During operation, a nuclear reactor should behave in such a way that design safety limits are not violated. The parameters related to core safety can be classified into three categories as:

1) core reactivity parameters,
2) control rod worth parameters, and
3) other neutronic parameters as core power peaking factors or boron dilution effect.

In addition, the following must be known as a function of burnup:

- radial and axial power distribution,
- fission neutron poison worth (mostly Xenon), and
- control rod position (for BWRs) and boron concentration (for PWRs).

As aforesaid while discussing the Bateman equations, fuel burnup and depletion affects the reactivity of the core as the reactor operates. Hence, when talking about fuel depletion calculations, the essential aspects to take specific note of include:

- relationship between fuel burnup and reactivity loss,
- expected energy produced during a given cycle,
- fuel composition and core power distribution changes, and
- reactivity control during operation and its effect on core power distribution.

As explained in (Bozzola, S., 1982), there are three primary reactivity coefficients which characterize the dynamic behavior of the BWR over the operating states: the moderator void reactivity coefficient, the Doppler reactivity coefficient, and the moderator temperature coefficient.

The void reactivity coefficient, $\frac{1}{k}\frac{dk}{d\alpha}$, is the most important among BWR reactivity coefficients and determines the BWR unique features. The void coefficient is the partial derivative of the multiplication factor, neutron leakage and control system worth with respect to the void content with reactor near critical.

In the power operating range, boiling is the primary mechanism for moderator density variations and the void coefficient is the most important as input to stability and transient response calculations.

The Doppler reactivity coefficient, $\frac{1}{k}\frac{dk}{dT}$, is the change in reactivity due to a change in the temperature of the fuel. As well known, this change results from the broadening of the resonance absorption cross-sections as the temperature increases.

At beginning of life, the Doppler contribution is primarily due to ^{238}U as the exposure increases the ^{240}Pu build-up contributes to the Doppler coefficient. The Doppler reactivity coefficient provides instantaneous reactivity feedback to any rise in fuel temperature and is determined by performing lattice calculations at several fuel temperatures, while maintaining all other input parameters constant.

The reactivity change caused by Doppler coefficient is small compared to the other power related reactivity changes during normal operation; it becomes very important during postulated rapid power excursions in which large fuel temperature changes occur.

In BWRs, the moderator temperature coefficient is the least important of the reactivity coefficients since it affects core operation in a very small portion of the reactor operating range. Once the reactor reaches the power producing range, boiling begins and the moderator temperature remains essentially constant.

The power reactivity coefficient is a combination of the void and the Doppler reactivity coefficients. For safe reactor operation, this coefficient must have a negative value all over the cycle.

As one can imagine, all essential reactor parameters are closely interrelated so that strong feedback mechanisms effectively determine the core behavior under any given operating condition variations. The most relevant reactivity components for BWRs, according to (Cochran, R. G. & Tsoulfanidis, N., 1999), and their associated reactivities are shown in Table 2.3.

Table 2.3. Reactivity Balance in BWRs.

Source: (Cochran, R. G. & Tsoulfanidis, N., 1999).

Changes in the Core	Associated Reactivity (%)
Cold Zer Power (CZP) to Hot Full Power (HFP) Fuel Temperature Defect	1.5
Moderator Temperature & Void	2.0
Equilibrium Fission Product Poisoning	3.3
Burnup Compensation	6.5
Control Margin & Xenon Override	1.0
Shutdown Margin	1.0
Total	**15.3**

The initial conditions and the postulated event of a given simulation determine which of the above coefficients are significant in evaluating the response of the reactor during transient calculations and, therefore, be considered while performing core simulations and modeling cross-section libraries.

2.6 Summary.

This chapter provides a comprehensive introduction to the mathematical formulations, computational methods, and data prerequisites essential for simulating neutron behavior and analyzing reactor performance. It provides a detailed exposition of the governing equations in neutronics, with a particular emphasis on the Boltzmann Neutron Transport Equation as the fundamental framework for describing neutron dynamics within a reactor core.

This fundamental understanding extends to neutron transport calculations, essential for elucidating neutron flux distribution and reaction rates. Subsequently, the Diffusion Approximation is explored as a practical, yet robust method derived from the neutron transport equation, widely adopted in reactor core analyses for its computational efficiency while capturing essential neutron diffusion phenomena.

The chapter further investigates two primary neutronics solving methodologies: Deterministic methods, leveraging discretization techniques for efficient solution of the neutron transport equation, and Monte Carlo methods, providing stochastic solutions by simulating neutron histories and interactions within the reactor core.

Nuclide depletion calculations are highlighted for their pivotal role in forecasting changes in fuel composition throughout operational cycles, encompassing nuclide depletion due to fission and decay processes.

The critical role of nuclear data is then underscored, encompassing continuous energy representations and the consolidation of energy groups to optimize

computational efficiency without compromising accuracy. Lattice calculations, integral to reactor core analysis, are explored with a focus on cross-section libraries crucial for generating multigroup cross-sections, thereby facilitating precise modeling of reactor behavior under diverse operational conditions.

The chapter also emphasizes the critical impact of lattice transport code precision on reactor core estimation accuracy, emphasizing the need for advanced neutronics methodologies to ensure optimal utilization of nuclear data in diffusion codes. This includes enhancing models for physical phenomena like fuel depletion, resonance self-shielding, and thermal-hydraulic feedback effects, alongside employing advanced numerical techniques for solving the transport equation.

Finally, the chapter addresses reactivity feedback mechanisms, elucidating how changes in core conditions such as temperature and moderator density influence reactor reactivity. These feedback effects are essential for comprehensive reactor safety and stability analyses, highlighting their crucial role in operational and safety assessments.

Chapter 3
Impact of Nuclear Data Processing – State-of-the-Art

3.1 Introduction.

In the realm of Light Water Reactors (LWRs), the efficacy of fuel management strategies has long relied on sophisticated nodal core physics methodologies. These methodologies incorporate detailed 3D core neutronics models, complemented by simplified thermal-hydraulic feedback models that aggregate similar thermal-hydraulic channels, albeit with approximations rather than individual feedback to each 3D neutronic node.

Simulating nuclear reactor behavior using these methodologies enables engineers to achieve heightened accuracy and fidelity. This capability supports informed decision-making in reactor design, operation, and safety analysis. Enhanced operational flexibility in LWR plants becomes achievable through advanced 3D coupled thermal-hydraulic/neutronics calculations. These calculations not only evaluate safety margins but also predict reactor phenomena with precision.

State-of-the-art safety analyses methodologies rely now heavily on best-estimate coupled code multi-physics simulations, particularly for transients characterized by localized reactivity changes, asymmetric thermal-hydraulic conditions at the core inlet, and intricate 3D power distribution conditions. Research by (Perin, Y. et al., 2012;

Perin & Escalante, 2017; Ivanov, K. & Avramova, M., 2007; Perin, 2016) underscores the importance of such simulations in comprehensively assessing safety margins and understanding complex reactor behavior during operational transients.

Continual advancements in nuclear engineering are driven by enhanced computational power, refined numerical methods, and sophisticated physical models. These developments have fostered the evolution of multifaceted multi-physics simulation tools. By integrating domains such as neutronics, thermal-hydraulics, and structural mechanics, these tools offer unprecedented insight into coupled effects and interactions within nuclear reactor systems.

3.2 Reactor Core Analysis.

Predicting the state of a nuclear reactor, characterized by numerous heterogeneities and continuous changes over time, presents significant challenges that necessitate a deep understanding of *Nuclear Reactor Physics*.

Reactor core analysis plays a pivotal role in ensuring the safe and efficient operation of nuclear reactors. Key objectives include predicting neutron flux distribution, power density, and temperature profiles within the core. These predictions are crucial for core design, optimizing fuel utilization, and maintaining safety margins during operation.

3.2.1 Standard Industrial Reactor Core Analysis.

At the heart of reactor core analysis are neutronic models, which describe neutron behavior using fundamental equations such as the neutron transport and diffusion equations, supported by accurate cross-section data, as discussed in Chapter 2.

Customarily, 3D reactor core calculations are approached through three hierarchical levels of detail:

1) pin cell level,
2) fuel element level (due to cell staggering), and
3) whole core level itself (due to fuel-element staggering).

It is possible to approach the 3D calculation of the reactor core through a series of successive steps in which the initial heterogeneous problem is transformed into a more straightforward but neutronics-wise equivalent. Then, the transport equation or the diffusion equation, whichever is the case, is solved at each of these levels to obtain the representative flux that is used to average the cross-sections needed in the corresponding next one.

This approach is known as *Industry Scheme or Standard Approximation* for reactor calculations, see Figure 3.1, and it will be discussed herein next.

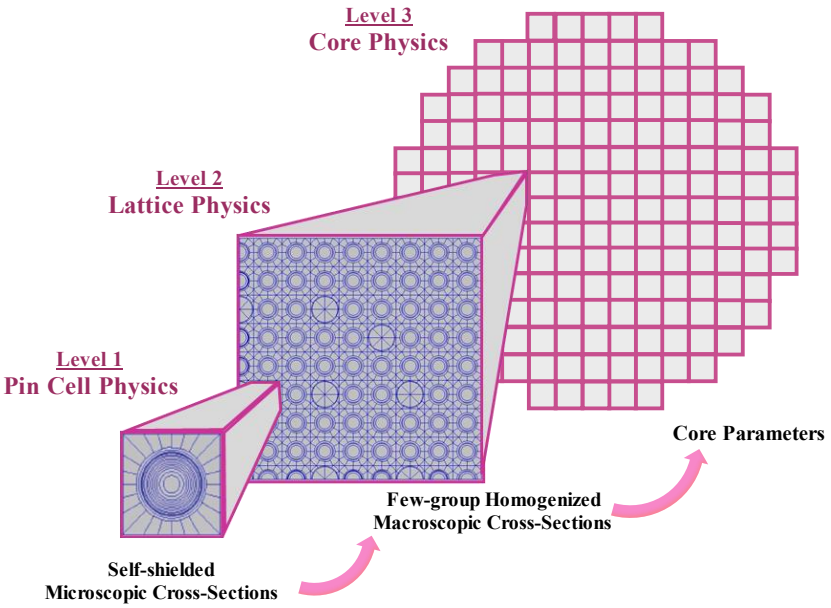

Figure 3.1. Standard Industry Scheme Calculation.

Level 1. Pin Cell calculation (cell physics).

At the pin cell level, a 1D transport equation solution is computed within each cell. This level captures significant flux variations, influenced notably by resonance self-shielding effects from fissile materials and burnable absorbers like Gadolinium (Gd). The solution, typically in continuous or multigroup energy formats depending on the chosen method, serves as a weighting factor for microscopic cross-sections. This process adjusts problem-specific multigroup libraries to account for resonance self-shielding, using pre-existing, problem-independent libraries.

Level 2. Fuel Element calculation (lattice physics).

At the fuel element level, a 2D transport equation is solved (typically with 56, 172, 238, or 252 energy groups) across each representative core element. This calculation employs an infinite regular mesh in the radial direction (with full reflective boundary conditions at bundle boundaries) and a homogeneous infinitely high geometry in the axial direction (a 2D approximation). The resulting flux homogenizes spatially and collapses energetically to derive macroscopic cross-sections in a reduced number of groups (usually two: fast and thermal). Different homogenization strategies may encompass elements, quarter-elements (nodes), or pin cells, depending on industry practices and deterministic lattice code capabilities.

Level 3. Core calculation (core physics).

The highest-level calculation involves a 3D diffusion equation (or equivalent approximation to the full transport formulation) solved across the entire core, subdivided into the previously defined homogeneous domains. This step, known as pin-by-pin or fine-mesh when discretized at the pin cell level, or nodal or coarse-mesh at the element or node level, integrates coupled neutronics and thermal-hydraulics calculations. This approach optimizes accuracy and computational efficiency in modeling reactor core behavior under diverse operational conditions.

The industry standard method, illustrated in Figure 3.1, employs a *Two-step Procedure*, (Stamm'ler, R.J. & Abbate, M.J., 1983), depicted in Figure 3.2. The first step involves *Lattice Calculation* (combining Levels 1 and 2), (Knott, D. & Yamamoto, A., 2010), which meticulously accounts for spatial and energetic variations of the elements that compose the core pattern. This initial stage yields homogenized coefficients and group parameters that are crucial for subsequent core calculations. In the second step, *Core Calculation* (Level 3), this approach is refined by replacing detailed core assemblies with simplified descriptions, striking a balance between computational feasibility and precision.

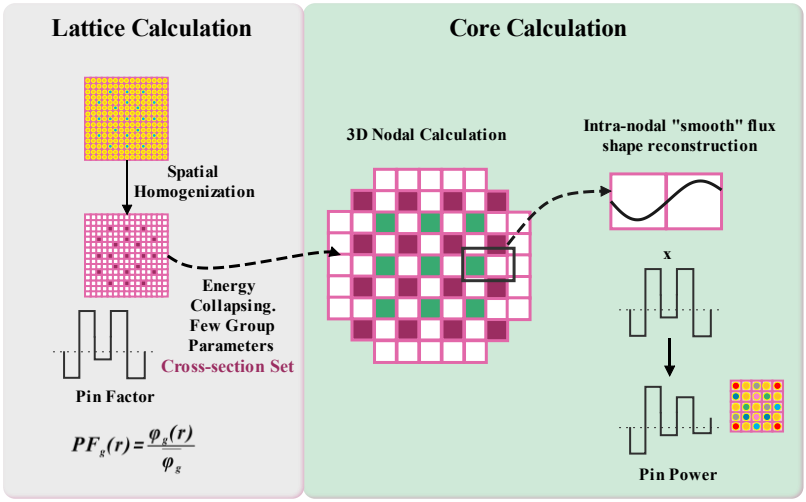

Figure 3.2. Two-Step Procedure. Overview of Standard BWR Core Analysis.

This approach is widely adopted across the industry due to its optimal balance between computational burden and accuracy. Therefore, this calculation constitutes the basis for the nuclear analyst to determine which models, codes, and assumptions will be the most suitable for an efficient, accurate solution to the problem to be tackled.

As expected, the nuclear industry demands computational codes capable of managing the intricate heterogeneities inherent in LWRs. These codes are pivotal for

generating group constants essential for simulating reactor core physics, as depicted in Figure 3.3, and conducting fuel depletion calculations efficiently and affordably.

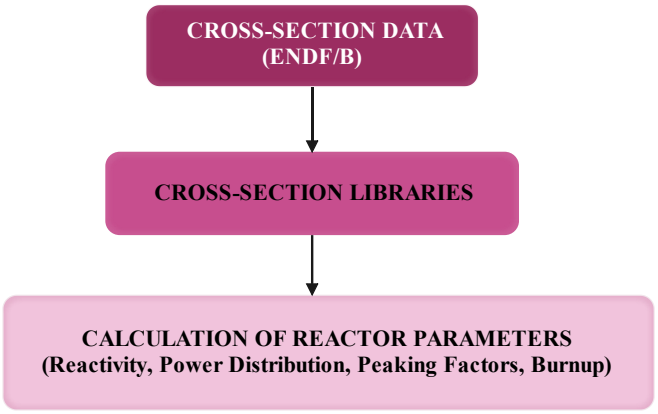

Source: (Cochran, R. G. & Tsoulfanidis, N., 1999).

Figure 3.3. Reactor Physics Calculations.

Nodal diffusion codes represent the predominant choice for 3D industrial core analyses in LWRs. These codes operate on the principles of few-energy-group diffusion theory, utilizing pre-calculated homogenized macroscopic cross-sections stored in libraries as input data. Known for their "best estimate" capabilities, these simulators provide highly accurate and detailed results compared to traditional point kinetics methods.

Economic considerations within the industry necessitate high accuracy from these reactor codes, often benchmarked against real plant parameters. A significant challenge lies in developing lattice physics schemes that can effectively condense continuous energy raw cross-section data from highly heterogeneous fuel assemblies into a unified, homogenized material represented in two characteristic energy groups. This condensed data is then utilized by nodal codes to achieve precise simulation outcomes.

Various computer codes are available for reactor physics calculations, tailored to utility-specific requirements. Despite inherent model weaknesses stemming from assumptions and simplifications (Giust et al., 2004), results of modern core calculation programs are quite accurate and typically maintain low deviation from measured data throughout operational cycles.

Table 3.1 provides an overview of widely used neutronic codes and their respective applications.

Table 3.1. Overview of the Most Common Neutronics Codes.

Spatial Scale	Features	Code	Application
Reactor Core	Monte Carlo Neutron Transport Calculation	MCNP SERPENT KENO-VI TRIPOLI4	Reference - Transport Calculations
Reactor Core	Deterministic Neutron Transport Calculation	APOLLO3 WIMS	Reference - Transport Calculations
Reactor Core	Diffusion Calculation	PARCS **SIMULATE-3** CRONOS VALKIN COBAYA DYN3D	**Industry – Reactor Core Calculations**
Fuel Element (or cluster)	Lattice Calculation Deterministic Transport Calculation	NEWT POLARIS **CASMO-4** APOLLO2 WIMS HELIOS	**Cross-section Libraries Generation**
--	Inventory and Source-term Calculation	ORIGEN ACAB FISPACT	Isotopic Evolutions

Notably, the CASMO-4/SIMULATE-3 (Edenius, M. et al., 1995), commercial code package stands out in the nuclear industry for its capability in lattice calculations and core simulations. Backed by a robust validation framework spanning diverse industrial applications, CASMO-4/SIMULATE-3 commands a high level of reliability. This underscores the value of employing code-to-code comparisons as a reliable analytical tool, a practice elaborated further in Chapter 5 and Chapter 6.

3.2.2 Thermal-Hydraulics and Neutronics Coupled Calculations.

Complementary to stand-alone neutronic models are thermal-hydraulic models, which are essential for predicting coolant flow and heat transfer within the core. These models determine temperature distributions in both fuel and coolant, directly influencing reactor safety and performance. Feedback mechanisms, such as changes in coolant

density and temperature, significantly impact neutron flux distribution and overall reactor stability.

Nuclear codes are extensively employed to simulate LWRs, assess safety margins, train operators, optimize plant design, and develop Emergency Operating Procedures (EOPs). Originally developed individually, these codes have increasingly been integrated to account for the interdependencies between neutronics and thermal-hydraulics, aiming for more precise and comprehensive reactor analyses (Mylonakis et al., 2014).

Code coupling is a technique used to integrate three-dimensional and multidisciplinary models, where multiple codes run simultaneously, exchanging relevant variables to minimize errors and enhance accuracy. This coupling can involve either running separate codes communicating periodically or integrating both neutronic and thermal-hydraulic equations into a single code for simultaneous solution.

Given the multidisciplinary nature and complex interfaces of reactor physics, effective code coupling is essential to address the broad scope of reactor core analysis. This approach finds applications across nuclear engineering, particularly in areas where interactions between neutron flux and temperature distributions play a crucial role in reactor behavior.

The integration of neutronic and thermal-hydraulic models through coupled calculations provides a comprehensive understanding of reactor dynamics, supporting diverse studies such as licensing new Nuclear Power Plants (NPPs), safety upgrades for existing plants, and the development of accident management programs (D'Auria, F. et al., 2006). This integration is particularly valuable during transient conditions, where rapid changes in reactor power and coolant flow require immediate and accurate analysis.

However, the development and utilization of coupled codes for reactor core analysis must address several challenges, including adequate computational resources, effective coupling procedures, code validation, uncertainty assessment, and overall applicability for safety analyses. These considerations are crucial for ensuring reliable and insightful predictions in nuclear reactor operations.

Advancements in computational power and refinement of numerical methods have driven continuous improvements in multi-physics simulation tools, enhancing their capability to tackle complex challenges in nuclear engineering. Nowadays, nuclear codes not only estimate transient responses in LWRs under non-standard conditions but also support safety assessments, operator training, plant design optimization, and emergency preparedness.

Thus, coupled-code simulations offer a comprehensive approach to evaluate transient impacts, identify risks, and enhance predictive capabilities for nuclear reactors, ensuring effective safety measures are in place to mitigate potential consequences. While Loss-of-Coolant Accident (LOCA) transients tend to be the more challenging with respect to safety limits and are typically the focus in reactor safety analysis, events such as Main Steam Line Break (Ivanov, K.N. et al., 1999) and Rod Ejection Accident (Kozlowski, T. & Downar, T.J., 2003) scenarios are also challenging

and require coupled neutronics and thermal-hydraulics calculations using advanced 3D kinetics methods to accurately predict neutron flux redistribution.

Figure 3.4 illustrates various applications of coupled codes highlighting their versatility in addressing complex reactor dynamics. In BWRs, specific transients of interest include Overpressurization events, Turbine Trip, Core Inlet Temperature and Flow disturbances, Rod Drop accidents, Instrumentation response, Stability Analysis, and Anticipated Transients Without Scram (ATWS).

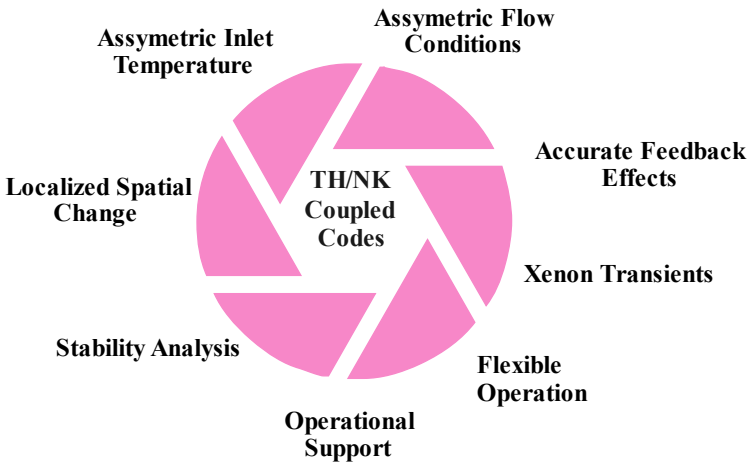

Figure 3.4. Examples of Applications of Coupled-Codes in NPPs.

A precise analysis of the reactor core requires incorporating three spatial dimensions and establishing a robust coupling mechanism between neutronics and thermal-hydraulics models. However, this coupling process is complex and challenging.

Furthermore, a thorough understanding of the underlying physics and careful evaluation of various methods, correlations, and closure models are essential prerequisites for achieving accurate results, as highlighted by (Smith, K. & Forget, B., 2013).

Inherent to this intricate interplay between thermal-hydraulics and neutronics is the recognition that changes in plant conditions lead to corresponding adjustments in operating variables. These fluctuations propagate changes in core nuclear parameters, as depicted in Figure 3.5.

Hence, it is crucial to acknowledge that core characteristics, fuel parameters, and overall plant features - critical factors in assessing and optimizing BWRs - must align appropriately to ensure the safety and efficiency of plant operations.

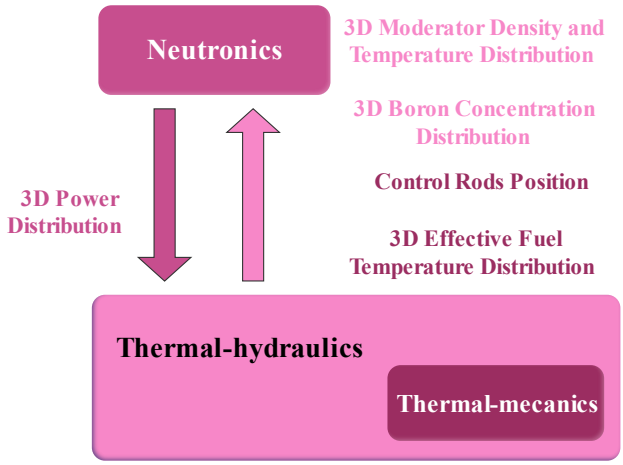

Figure 3.5. General Coupling Approach.

For effective coupling, each fuel/fluid/neutronic model plays a distinct role with specific requirements:

The thermal-hydraulic code:

- computes new moderator/fuel properties,
- provides moderator's temperature, vapor & liquid densities, void fraction, boron concentration, control rod positions, average, centerline, and surface fuel temperatures to the neutronics model, and
- uses neutronics power as a heat source for conduction in the fuel.

The neutronic code:

- uses moderator and fuel properties for local node conditions,
- updates macroscopic cross-sections based on history and local node conditions including control rod contributions, and
- provides node-wise power distribution to the fuel/fluid model.

Traditionally, assessing primary responses and in-vessel conditions during simulated transients has relied on thermal-hydraulic system analysis codes such as TRAC-PF1 (Schnurr, N.M. et al, 1992), TRAC-BF1 (Borkowski, J. et al., 1992), and RELAP5 (Allison, C. et al., 1990), often employing Point Kinetics or 1D neutron kinetics approximations (Ivanov, K. & Avramova, M., 2007).

Examples of coupled thermal-hydraulic/neutronic codes commonly used in multi-physics and multiscale simulations include TRACE/PARCS, RELAP/PARCS, ATHLET/DYN3D, TRAC-PF1/NEM, and TRAC-BF1/NEM, each with specific applications and challenges detailed in (Mylonakis et al., 2014).

TRACE/PARCS is currently considered state-of-the-art for coupled regulatory analysis in the United States, demonstrating proficiency in analyzing large/small break LOCAs and system transients across both PWRs and Boiling Water Reactors BWRs.

The study of nuclear reactor dynamics encompasses a broad spectrum of analyses, crucial for both operational safety and efficiency. Having delved into reactor core analysis, where intricate neutron flux distributions and temperature profiles dictate reactor performance, we now shift our focus to transient analysis. Transients, characterized by rapid changes in reactor conditions due to operational anomalies or emergency scenarios, necessitate a deeper examination facilitated by coupled thermal-hydraulics and neutronics simulations.

3.3 Transient Analysis.

In the intricate world of nuclear reactor safety, transient analysis stands as a fundamental pillar, ensuring that reactors operate reliably and safely under a spectrum of operational scenarios. This process, embedded deeply within the regulatory framework, is crucial for validating the reactor's ability to handle deviations from normal operations and unforeseen anomalies. Thus, transient analysis is not only fundamental to reactor design but also indispensable for both safety licensing and assurance that operating goals are achievable.

At the heart of reactor safety assessments in the United States is the Code of Federal Regulations (CFR). Specifically, 10 CFR Part 50 governs existing reactors, which operate under licenses granted based on a final design tailored to specific sites. For new reactor designs, 10 CFR Part 52 is also applicable, enabling future reactors to adopt certified generic designs for their operating licenses. The U.S. NRC is currently developing 10 CFR Part 53, which will focus on advanced reactors using a risk-informed approach.

Central to the licensing process is Chapter 15 of the Final Safety Analysis Report (FSAR). This chapter is the cornerstone for evaluating how reactors respond to various design basis disturbances and equipment malfunctions, termed initiating events. Before a reactor license is granted, a thorough analysis of these events is mandatory, with designers required to provide compelling evidence that their designs can withstand these scenarios and maintain safety.

Meeting regulatory safety standards requires comprehensive transient analysis and documentation. Regulatory bodies review safety analyses to approve reactor designs, operational procedures, and emergency response plans.

Thus, analyzing transients serves multiple essential functions:

1) **Safety Assessment**: Transient events like LOCA, control rod ejections, or turbine trips can challenge safety systems. Understanding how a reactor responds to these events ensures that safety margins are maintained and that safety protocols are robust.
2) **Operational Flexibility**: Reactors must be able to respond to changes in power demand and grid requirements. Transient analysis helps optimize reactor operations under varying conditions without compromising safety.
3) **Design Verification**: During the design phase of a reactor, transient analysis validates the effectiveness of safety features and control systems

under different scenarios. It ensures that the reactor design meets regulatory safety standards.

4) **Accident Management**: Detailed transient analysis provides insights into accident progression and guides the development of emergency response procedures. Operators can simulate accident scenarios to prepare for potential emergencies effectively.

Transient analysis typically involves sophisticated computational models that integrate thermal-hydraulic and neutronic calculations. These models simulate the complex interactions between core physics and coolant behavior during transient conditions. Validating these models against experimental data and operational experience is crucial for accuracy and reliability.

Thermal-hydraulic and neutronic simulations during transients help operators and engineers predict reactor responses, optimize control strategies, and enhance safety margins. These insights contribute to continuous improvements in reactor design, operation procedures, and regulatory standards.

3.3.1 Transient Analysis in the Context of Chapter 15 of the U.S. NRC Standard Review Plan.

NUREG-0800, "*Standard Review Plan (SRP) for the Review of Safety Analysis Reports for Nuclear Power Plants*," contains guidelines for the review of license requests (both initial and modifications).

Chapter 15 of the SRP serves as a cornerstone for understanding and managing transient and accident scenarios. It provides detailed guidance on the types of analyses required to ensure reactor safety across a spectrum of operational and accident conditions (US NRC, 2007).

At the heart of SRP Chapter 15 is the rigorous examination of how reactors respond to a variety of disturbances and equipment malfunctions, collectively termed initiating events. This analysis is crucial for licensing purposes, requiring plant designers to present a thorough assessment that demonstrates their reactor's resilience under these challenging scenarios.

Transient analysis, as outlined in SRP Chapter 15, is categorized into three primary types: Anticipated Operational Occurrences (AOOs), Design Basis Accidents (DBAs), and Beyond Design Basis Accidents (BDBAs).

Anticipated Operational Occurrences (AOOs) are events expected to occur periodically throughout the reactor's operational life. These events, which represent minor deviations from normal operating conditions, are managed by the reactor's automatic safety systems without posing significant risks. AOOs are fundamental to transient analysis as they assess the reactor's capability to handle routine operational challenges while maintaining safety margins.

Examples of AOOs include:

1) **Turbine Trips**: Sudden shutdowns of the turbine due to operational or mechanical issues.
2) **Feedwater Flow Interruptions**: Disruptions in the flow of water used to maintain the reactor core's temperature.
3) **Reactor Coolant Pump Failures**: Malfunctions in the pumps that circulate coolant through the reactor core.

Design Basis Accidents (DBAs) represent hypothetical but plausible scenarios that the reactor must be designed to withstand. These scenarios are more severe than AOOs and necessitate the activation of multiple safety systems to ensure public and environmental protection. DBAs form the foundation of nuclear safety design, confirming that reactors can effectively manage severe accidents and prevent the release of radioactive materials.

Notable examples of DBAs include:

1) **Loss-of-Coolant Accidents (LOCAs)**: Large and small breaks in the reactor coolant system that could lead to a significant loss of coolant.
2) **Main Steam Line Breaks**: Ruptures in the main steam lines that carry steam from the reactor to the turbines.
3) **Reactivity Insertion Accidents**: Unintended increases in reactor power due to control rod withdrawal or other causes.

Beyond Design Basis Accidents (BDBAs) encompass scenarios of extreme severity that exceed the scope of DBAs. These accidents involve conditions not explicitly addressed in the reactor's design basis. Analyzing BDBAs is essential for understanding potential consequences and developing strategies for mitigating their impacts.

Examples of BDBAs include:

1) **Anticipated Transients Without Scram (ATWS)**: Situations where an anticipated transient occurs but the reactor scram system fails to activate, posing a significant challenge to reactor safety systems.
2) **Station Blackout (SBO)**: Complete loss-of -offsite power, challenging the reactor's ability to maintain safety without external electrical support.

In recent years, the International Atomic Energy Agency (IAEA) has introduced a new classification system known as Design Extension Conditions (DEC). This system aims to provide a more comprehensive framework for analyzing severe accident scenarios.

As illustrated in Figure 3.6, DEC is divided into two categories: DEC without core melt (DEC-A), which aligns with the former BDBA concept, and DEC with core melt (DEC-B), representing scenarios of severe accident severity. Despite the IAEA's proposal, the U.S. NRC has not yet fully adopted the DEC nomenclature. Although the

U.S. NRC has yet to fully incorporate DEC terminology, the framework is gaining traction globally for its comprehensive approach to reactor safety.

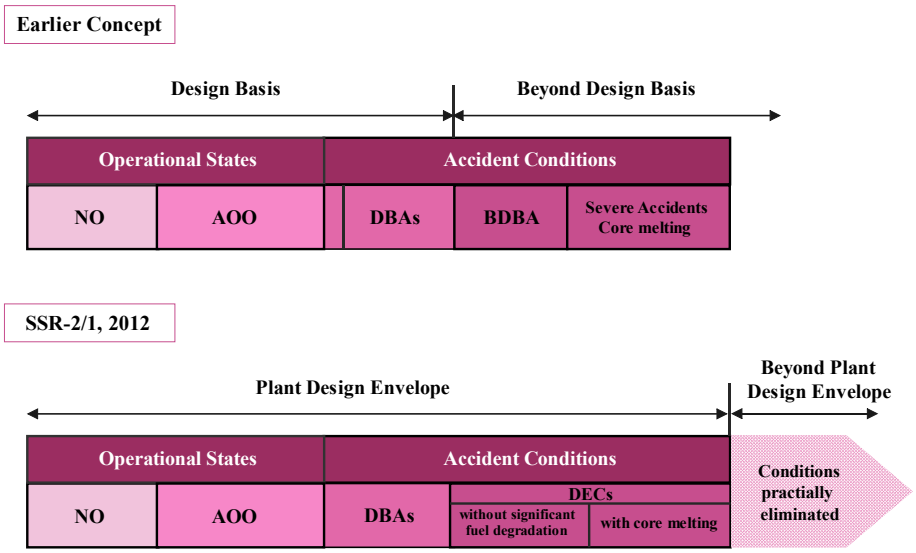

Source: (IAEA, 2016).

Figure 3.6. Evolution of DBAs an BDBAs according to the IAEA.

3.3.1.1 Relevance to Boiling Water Reactors.

The selection of a particular transient significantly influences the sequence of events, the implicated systems, and the range of variations in feedback parameters. The severity of each transient is determined by a complex interplay of nuclear parameters and system performance. It is crucial to demonstrate compliance with both design basis and regulatory requirements for each scenario, as each presents a unique sequence of events that can lead to different types of phenomena over time.

In BWRs, several specific transient scenarios are critical to safety analysis. These include loss of feedwater flow, turbine trips, and MSIVC. Among these, ATWS are particularly significant due to their potential to severely impact reactor safety and operational stability.

Nuclear power plants are equipped with control systems designed to keep system parameters within normal limits. While these control systems are effective within a specific operational range, additional protective measures are in place to safeguard the plant when event parameters exceed normal limits. This protection system primarily relies on control rods to maintain acceptable conditions following anticipated transients. However, if the control rods and protection systems fail to function correctly, an ATWS can occur.

An ATWS event is characterized by the failure of the reactor trip portion of the protection system after an anticipated operational occurrence (AOO). This failure can occur due to malfunctions in power systems, control mechanisms, or other factors. The significance of ATWS lies in its potential to challenge established safety limits, exposing the reactor to extreme conditions of temperature and pressure. Without a prompt shutdown of the nuclear reaction, there is a risk of a rapid increase in reactor power, which could compromise safety barriers and operational safety margins.

According to Section 15.8 of the SRP Chapter 15 (NUREG-0800), an ATWS is defined as:

> ….an Anticipated Operational Occurrence (AOO) as defined in Appendix A to 10 CFR Part 50 followed by the failure of the reactor trip portion of the protection system specified in General Design Criterion (GDC) 20.

Then, the term ATWS covers a wide range of transients (Perin & Escalante, 2017). Typical AOOs that may lead to unacceptable conditions if the scram system fails include:

1) **Main Steam Isolation Valve Closure (MSIVC)**: A scenario where the isolation valve closes, potentially causing significant pressurization challenges.
2) **Turbine Trip With Bypass (TTWB)**: A sudden shutdown of the turbine while bypassing normal cooling systems.
3) **Pressure Regulator Failure – Open (PRFO)**: A failure in the pressure regulator causing it to remain open, which can disrupt system pressure control.
4) **Loss-of-Offsite Power (LOOP)**: A scenario where all external power supplies are lost, impacting core cooling and system operation.
5) **Inadvertent Opening of a Relief Valve (IORV)**: Unplanned opening of a relief valve, which can lead to pressure and coolant flow issues.

Among these scenarios, the MSIVC ATWS is particularly critical due to its identification as one of the most severe pressurization transients, with potentially catastrophic consequences if the scram system fails, given the reactor's isolation from normal cooling systems (Bolger et al., 2003).

The primary goal of this thesis is to study and document insights that can guide the development of cross-section libraries for LWR safety analyses. The focus on ATWS is driven by their complexity and the significant challenges they present to analytical tools.

3.3.2 DEC-A Transients: Anticipated Transients Without Scram (ATWS).

Anticipated Transients Without Scram (ATWS) represent a critical category of reactor events that require careful consideration within nuclear power plant operations. Understanding their historical development is essential for grasping how safety protocols and analysis techniques have evolved to address these challenges.

3.3.2.1 ATWS Historical Background.

ATWS has been a crucial focus in nuclear reactor safety research and regulation since their initial recognition in the late 1960s. The historical evolution of ATWS underscores a journey from early academic curiosity to a central element of regulatory frameworks aimed at ensuring reactor safety and reliability.

The issue of ATWS was first broached in the context of nuclear reactor licensing discussions in 1969. At this nascent stage, the concept was primarily explored from an academic perspective, lacking the urgency and practical focus that would later define its study. It was not until the 1970s and 1980s that ATWS scenarios gained prominence, driven by heightened attention to safety analyses and accident scenarios in the nuclear industry.

Early research revealed that specific transient conditions could lead to scenarios where the reactor's safety systems - particularly the reactor scram system, designed to quickly shut down the reactor - might fail. This could result in extended periods where the reactor core experienced suboptimal conditions, potentially jeopardizing safety margins and operational integrity.

The necessity for a deeper understanding of ATWS was underscored by several key events. The Browns Ferry Unit 3 fire in 1975, a significant incident in the United States, exemplified the complex challenges associated with reactor transients. Although not an ATWS event per se, it highlighted the critical need for comprehensive analysis and mitigation strategies for reactor safety. This incident, among others, prompted regulatory bodies like the U.S. Nuclear Regulatory Commission (NRC) and international counterparts to enhance their scrutiny of transient scenarios, including ATWS.

The pivotal Three Mile Island (TMI) accident in 1979 further intensified focus on reactor safety. Although TMI did not involve an ATWS event, it revealed the potential vulnerabilities in reactor systems, including the failure of automatic safety mechanisms. The incident emphasized the importance of robust safety systems and spurred a broader investigation into reactor response mechanisms during transients, contributing to a heightened regulatory emphasis on ATWS scenarios.

In response to the growing awareness of ATWS risks, regulatory frameworks began to take shape. In April 1978, the NRC published NUREG-0460, which provided preliminary results on the probability of scram failures, estimating a probability of 3×10^{-5} per demand for scram system failure (NRC, 1978). This report was instrumental in framing the regulatory approach towards ATWS.

By 1984, significant progress was made with the publication of 10 CFR 50.62, a standard that outlined requirements for reducing risk from ATWS events in Light Water Reactor Nuclear Power Plants. This regulation represented a critical milestone in formalizing the approach to ATWS risk management.

Further, the U.S. NRC issued a Regulatory Guide in 1984, which provided detailed guidance on the analysis of ATWS events. This guide established criteria for evaluating reactor safety under ATWS conditions and emphasized the necessity of comprehensive safety analysis to ensure that reactors could handle ATWS events

effectively without compromising operational safety (NRC, 1984). In December 2005, the U.S. NRC issued the Regulatory Guide RG 1.203, "Transient and Accident Analysis Methods" (US NRC, 2005), which could be used for best-estimate ATWS analysis.

3.3.2.2 Acceptance Criteria.

The acceptance criteria for ATWS events are fundamental to ensuring that nuclear reactors maintain safety and operational integrity even under conditions where automatic safety systems might fail. These criteria are designed to assess the reactor's ability to manage and mitigate the consequences of ATWS events, thereby ensuring that safety margins are preserved, and regulatory requirements are met.

The Code of Federal Regulations, 10 Part 50.62, presents the requirements for reducing risk from ATWS events for light-water-cooled nuclear power plants (Bolger et al., 2003). Moreover, the rule states that:

> …in the case of a BWR, there must be an alternate rod injection system (ARI), a stand-by liquid control system (SLC) with the capability of injecting into the reactor pressure vessel a borated water solution, and equipment to trip the reactor coolant recirculating pumps (RPT) automatically under conditions indicative of an ATWS to prevent power excursions due to void collapse during pressurization transients.

The criteria described in SRP NUREG-0800 are used to verify that acceptable limits have been met during ATWS analysis. Thus, the criteria for accepting an ATWS event should encompass a comprehensive set of inquiries such as the preservation of fuel integrity, the integrity of the containment system, the integrity of primary design features, conditions during long-term shutdown, and radiation dosage incurred during the event.

Key acceptance criteria include:

1) **Core Cooling Requirements**: This ensures that the reactor core remains within safe temperature limits, even if the reactor scram system fails. Core cooling requirements typically involve maintaining sufficient flow of coolant through the reactor core to remove heat generated by nuclear fission. The criteria specify the minimum flow rates and temperatures necessary to prevent fuel overheating and core damage during ATWS events.
2) **Reactivity Control and Shutdown**: The reactor must be capable of controlling reactivity and achieving a shutdown condition if necessary. In the event of an ATWS, the reactor's reactivity control systems should be capable of managing neutron flux levels to avoid excessive power levels. Acceptance criteria often include the evaluation of backup reactivity control mechanisms and the ability to insert control rods or use other means to stabilize the reactor core.
3) **Containment Integrity**: Acceptance criteria stipulate that the containment must remain intact to prevent the release of radioactive materials into the environment. This involves verifying the containment's design, its ability

to withstand pressure and temperature changes, and its capacity to manage potential leaks.

4) **Emergency Systems Functionality**: These systems should be capable of operating under conditions where the reactor scram system has failed, ensuring that coolant is available to the reactor core and that the containment environment is controlled.
5) **Operational Procedures and Operator Actions**: Effective operational procedures and the ability of operators to respond to ATWS events are integral to acceptance criteria. Criteria include the evaluation of operator training, emergency procedures, and decision-making processes to ensure that operators can effectively manage and mitigate ATWS scenarios. The criteria also cover the reliability and accessibility of manual override systems in case automated systems fail.

To evaluate compliance with these acceptance criteria, a combination of analytical methods, simulation tools, and physical testing is employed. Computational models and codes are used to simulate ATWS scenarios and assess the reactor's response to various conditions. Physical tests, such as full-scale or scaled-down experiments, are conducted to validate the performance of safety systems and operational procedures under simulated ATWS conditions.

Detailed descriptions of the specific thresholds delineating acceptance criteria, along with the performance measures (referred to as *Figures-of-Merit*), are expounded upon in Chapter 7.

3.3.3 State-of-the-Art of BWR ATWS Simulations.

The late 1980s and early 1990s marked a pivotal period in the evolution of simulation and modeling techniques for ATWS events. As the nuclear industry grappled with the complexities of reactor safety, researchers and engineers began developing advanced tools to simulate reactor behavior under ATWS conditions. These simulations aimed to forecast the reactor's response to various scenarios, including the failure of safety systems, and their potential impact on core cooling and overall reactor stability.

The advent of improved computational capabilities during this era catalyzed a significant enhancement in the industry's ability to model and manage ATWS scenarios. The incorporation of sophisticated models and algorithms allowed for more precise simulations of transient events, reflecting a broader understanding of the risks associated with ATWS. Modern reactors have since been equipped with advanced safety systems, control technologies, and redundant features designed to effectively handle a diverse range of transient conditions. This progress highlights the substantial advancements made since the initial recognition of ATWS risks and the commitment to improving reactor safety.

A notable advancement in the simulation of ATWS events was the development of the TRACE code by the U.S. Nuclear Regulatory Commission (NRC). Introduced in the early 1990s, TRACE represented a state-of-the-art tool for transient analysis, incorporating advanced models for thermal-hydraulic behavior.

This development allowed for a deeper understanding of how BWRs, including the BWR/6 design, respond to various ATWS scenarios (NRC, 1993). TRACE's ability to provide more accurate simulations marked a significant improvement in assessing and mitigating the risks associated with ATWS.

As the field progressed into the 2000s, further enhancements emerged with the integration of new technologies and methodologies. The shift from basic analysis to sophisticated simulations underscored a growing recognition that merely analyzing ATWS events was insufficient. Researchers and engineers began prioritizing the active mitigation of these scenarios, driven by the understanding that reactors must be equipped not only to handle anticipated transients but also to manage complex scenarios where safety systems might fail. The integration of advanced safety systems, redundant controls, and real-time monitoring technologies became crucial in modern reactor designs.

Quoting from (Yarsky, P., 2011), "... *ATWS events are analyzed to gauge consequences, quantify safety margins, and evaluate the effectiveness of mitigating actions to bring the plant to a stable, cold condition."* This statement reflects the comprehensive approach adopted in evaluating ATWS situations. Rigorous modeling, analysis, and reporting over the years have been essential in assessing the predictive capabilities of coupled thermal hydraulic/neutronics code packages for BWR ATWS events.

The ATWS analysis requirements under 10 CFR 50.62 do not necessarily mandate a full thermal-hydraulic simulation. For instance, the NuScale certification review, documented in Section 15.8 of the FSAR, notes that diverse and reliable shutdown systems reduce the frequency of ATWS events below the threshold required for detailed analysis. However, in light of safety considerations specific to MELLLA+ operation, particular scenarios of interest include ATWS events characterized by core instability or emergency depressurization.

Core instability concerns revolve around large amplitude oscillations that may arise (Baek, J. et al., 2013a), while emergency depressurization focuses on the energy transfer into containment during the mitigation period (Cheng, L. et al., 2013a).

Among various ATWS scenarios, as already stated, the MSIVC represents one of the most severe due to its high occurrence frequency and its challenge to residual heat removal systems and containment integrity. This transient has been extensively analyzed using various computer codes (Cheng, L. et al., 2016; Yarsky, P., 2013; Cheng, L. et al., 2014a; Cheng, L. et al., 2014b; Cheng, L. et al., 2015), although most previous efforts relied on point kinetics codes.

Since The MELLLA+ operational domain extends the permissible operating range of a BWR to encompass low flow rates at high power conditions, Figure 3.7, new safety concerns related to the consequences of ATWS events initiated from this state are introduced as stated in (Cheng, L. et al., 2015).

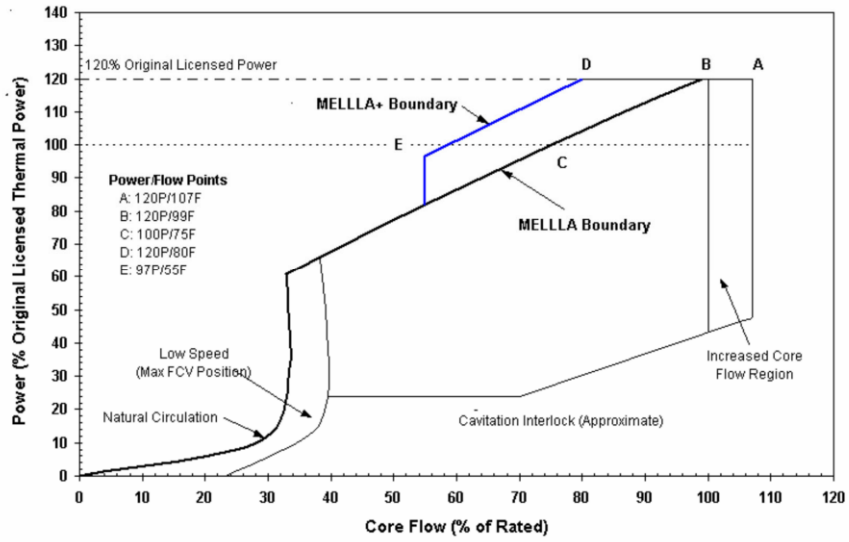

Source: NUREG-7179 (Cheng, L. et al., 2015).

Figure 3.7. Maximum Extended Load Line Limit Analysis (MELLLA +) domain.

Historically, the TRACE/PARCS code package has been utilized to explore complex transient phenomena within BWRs. Recent efforts have focused on using TRACE/PARCS to simulate hypothetical MELLLA and MELLLA+ ATWS scenarios, particularly for BWR/4 and BWR/5 designs.

Overall, reported results for ATWS simulations indicate that TRACE/PARCS effectively represent fundamental phenomena with reasonable to excellent agreement across a range of ATWS conditions, particularly at MELLLA+ operational scenarios. This endeavor aims to thoroughly investigate plant responses during transients, assess the resulting consequences, and evaluate the effectiveness of mitigation measures.

Despite the advancements, it is crucial to acknowledge that prevailing analyses often prioritize thermal hydraulic predictions, sometimes at the expense of a thorough evaluation of neutron responses and the quality of cross-section libraries. For instance, cross-section data from varying core conditions were used if deemed most accurate, but some calculations faced constraints due to limitations in cross-section data, particularly for variables like boron concentration (Cheng et al., 2010; Cheng, L. et al., 2013b). During an ATWS event, boron concentrations can reach high levels, and while power is reduced, analyzing the event sequence remains important due to potential reduced cooling in the core. Therefore, branch calculations generating cross-sections should account for the range of boron concentrations expected during ATWS events.

The focus of this thesis is to explore the pivotal role and implications of cross-section data in ATWS events. In particular, this research aims to use the TRAC-BF1/PARCS coupled code to evaluate BWR/6 performance predictions. This novel application seeks to enhance understanding of reactor responses during ATWS

scenarios, assess consequences, and improve mitigation strategies, particularly for the BWR/6 design with advanced 3D kinetics modeling. By addressing these critical aspects, the research contributes to advancing the field of reactor safety and transient analysis.

3.4 Standard Codes for Reactor Core and Transient Analyses.

To ensure comprehensive simulation coverage across various levels, from fuel pin cell to the entire nuclear power plant, an extensive selection of codes was incorporated into this thesis. This section aims to briefly introduce the various codes used, highlighting their major features and providing the essential information for understanding the main reasons for selecting them.

The section is organized sequentially, moving from lattice codes to core simulators and, finally, to plant system codes. Figure 3.8 provides a comprehensive overview of the utilized codes, offering insight into their respective functions.

Additionally, Table 3.2 lists the various versions of the codes employed for this thesis. All of the codes listed are widely used at industrial levels, ensuring a standard of quality and reliability.

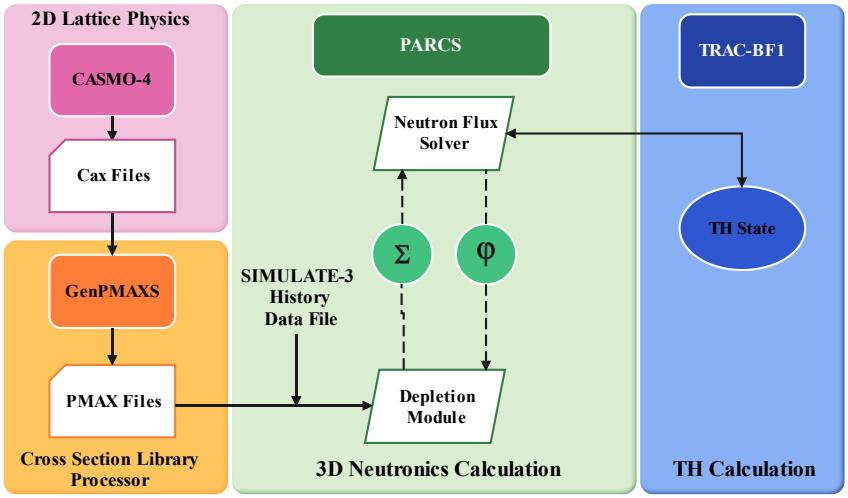

Figure 3.8. General Overview of Codes Used.

Table 3.2. Codes' Versions Used.

CASMO-4E	SIMULATE-3	GenPMAXS	PARCS	TRAC-BF1/BE
v2.05.17	v6.09.26	v6.1.3	**v3.2.mod17** v3.32	v21.01r0

While the NRC acknowledges TRACE as the leading-edge thermal-hydraulic systems code, this thesis employs TRAC-BF1 for the DEC-A transient analysis. This decision is rooted in the widespread adoption of TRAC-BF1 within the nuclear industry for BWRs, making it a pertinent choice despite TRACE's status as the state-of-the-art code endorsed by the NRC. It is important to note that everything applicable to TRACE is also applicable to TRAC-BF1 and vice versa, making either code suitable for this thesis. However, TRAC-BF1 was chosen specifically for its relevance in this context.

In the realm of neutronics, PARCS is considered the current state-of-the-art code by the NRC. For the purpose of this thesis, SIMULATE-3 will serve as the benchmark for cross-section libraries. Its selection is grounded in its extensive validation and rigorous testing across numerous cycles and core designs, cementing its credibility within the industry.

CASMO-4, SIMULATE-3, GenPMAXS, PARCS, and TRAC-BF1/BE have been selected as tools for use in this doctoral thesis due to the extensive experience gained in their management and application across various R&D and industrial projects over the past several years.

The use of all these codes has been made possible thanks to the generosity of the Nuclear Fuel Department of Iberdrola Generación Nuclear and the collaboration agreement with CAMP (The Code Application and Maintenance Program) Spain.

CAMP program is designed to ensure that the NRC's suite of analysis codes remains up-to-date, accurate, and capable of addressing the evolving needs of reactor safety assessments and regulatory requirements.

3.4.1 CASMO-4.

CASMO-4 code is a many-energy-group two-dimensional transport code developed by Studsvik, (Edenius, M. et al., 1995). It is used for burnup calculations on Boiling Water Reactor (BWR) and Pressurized Water Reactor (PWR) assemblies or pin cells. The code can deal with geometries consisting of cylindrical fuel rods of varying compositions in a square pitch accommodating rods such as those containing gadolinium, burnable absorber rods, and cluster control rods.

Some of the main features of the code are:

- The two-dimensional transport solution is based upon the Method of Characteristics (MOC) and can be carried out in several different energy group structures.

- Nuclear data for CASMO-4 are collected in a library containing microscopic cross-sections in 70 energy groups covering the range from 0 to 10MeV.
- CASMO-4 can accommodate symmetric as well as non-symmetric fuel bundles.
- Thermal expansion of dimensions and densities is performed automatically.
- Effective resonance cross-sections are calculated individually for each fuel pin.
- A fundamental mode calculation is performed to account for leakage effects.
- Gadolinium depletion and other absorber depletions are done automatically within CASMO-4 without the need for auxiliary codes.
- The microscopic depletion is calculated in each fuel pin and burnable absorber pin.

The CASMO-4 calculation process is shown in Figure 3.9. First, macroscopic cross-sections are prepared for the following micro-group calculations. Then, the macroscopic group cross-sections are calculated for the fuel assembly using the user's input data, densities, geometries, compositions, other operation parameters, and the integrated nuclear data libraries.

The effective cross-sections in the resonance energy region (4 eV to 9118 eV) for important resonance absorbers (including ^{235}U, ^{236}U, ^{238}U, ^{239}Pu, and Hf control rods) are calculated using an equivalence theorem, which relates tabulated effective resonance integrals for each resonance absorber in each resonance group to the particular heterogeneous problem under consideration. The resonance integrals calculate effective absorption and fission cross-sections for these absorbers.

The use of *Dancoff* factors accounts for the screening effect between different pins, e.g., fuel and moderator. Those factors are important parameters for cross-section self-shielding effect, (Milošević, 2001). The 1eV resonance in ^{240}Pu and 0.3 eV resonance in ^{239}Pu are adequately covered by the concentration of thermal groups around these resonances and are consequently excluded from the special resonance treatment.

The cross-sections prepared using the above process are used in a series of micro-group calculations to obtain the detailed neutron energy spectra that is used for energy condensation of the pin cells. First, a micro-group calculation is commonly performed for each pin type in the assembly.

Next, collision probabilities are determined in a simplified geometry consisting of the different material regions of the pin type. The two-dimensional macro-group calculation using an approximate and fast response matrix solution follows the micro-group calculations. It provides flux spectra for energy condensation to the group structure (from 40 to 7 energy groups), which gives the eigenvalue and the flux distribution in an assembly in a 2D transport calculation.

In single bundle calculations, a fundamental buckling mode is used for modifying the infinite lattice results obtained from the transport calculation to include leakage effects. It usually is made in diffusion theory and should be bypassed in calculations of two-by-two segments, reflectors, and fuel storage racks.

The isotopic depletion as a function of irradiation is calculated for each fuel pin and each region containing a burnable absorber. Then, the burnup calculation is carried out using a *Predictor-Corrector* approach. For each burnup step from t_{n-1} to t_n, a predictor step is first taken using the fluxes obtained from the neutron calculation at t_{n-1} to predict the number densities at t_n. As a consequence of this calculation:

- The cross-sections are then updated.
- The new spectrum calculation gives fluxes to be used in a corrector step.
- Final number densities at t_n are given by the average results from the predictor and corrector steps.

CASMO-4 also contains a module which calculates prompt and delayed gamma sources and solves the 18 group, 2D gamma transport problem such that the gamma detector response may be calculated.

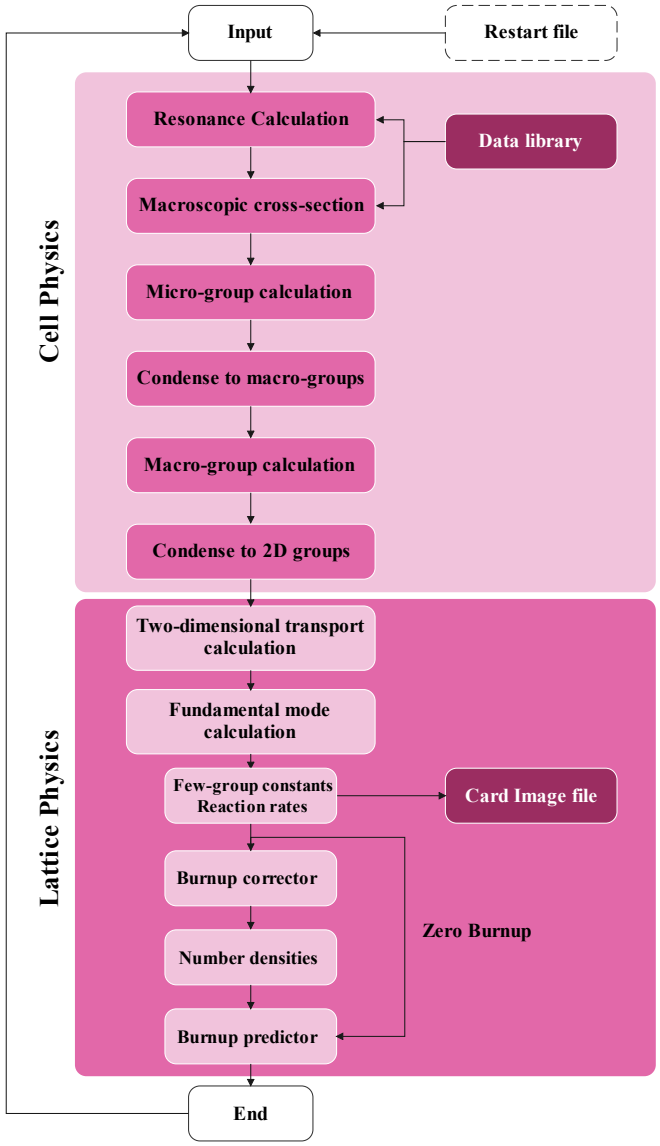

Source: Casmo-4 Manual (Edenius, M. et al., 1995).

Figure 3.9. Flow Diagram of CASMO-4.

3.4.2 SIMULATE-3.

The common practice in the industry has been to perform BWR depletion analysis with a simplified thermal-hydraulic model. One of the most popular BWR depletion codes used in the industry is SIMULATE-3. This three-dimensional, two-group, steady-state reactor core simulator performs in-core fuel management studies, core-follow, and

calculation of safety parameters. Thus, the code has been thoroughly benchmarked and validated against reactor operation (Covington, L.J. et al., 1995).

SIMULATE-3 utilizes what is known as a four-equation TH model that solves for the one-dimensional mixture mass, steam mass, mixture enthalpy, and mixture momentum equations for each axial node in each channel. Each assembly has one active channel and possibly one or more water channels. Flow rates to each channel are iteratively determined to give the same plenum-to-plenum pressure drop in each channel, and a drift flux model is used to calculate void fractions.

SIMULATE-3 employs an advanced nodal expansion method to solve the reactor core's two-group neutron diffusion theory representation without requiring normalization to fine-mesh calculations or measured data. SIMULATE-3 provides thermal-hydraulic feedback, modeling equilibrium or time-dependent Xenon and Samarium, and isotopic depletion. In addition, it allows for the generation of pin-by-pin power distributions using a pin power reconstruction technique.

The three-dimensional diffusion equation is integrated over the volume of each node to obtain the neutron balance equation. Determination of the nodal averaged scalar fluxes requires the intra-nodal flux distributions in both the fast and thermal groups derived by integrating the three-dimensional diffusion equation over two of the three directions of a node to obtain a transverse-integrated one-dimensional diffusion equation.

SIMULATE-3 explicitly models the radial and axial reflectors, and conventional albedo conditions are not required at the core periphery. The diffusion equation does, however, require a boundary condition at the outer surface of the reflector. Zero flux or zero incoming flux boundary conditions can be used. Typically, the sensitivity of the solution to the boundary condition is minimal if the reflector region is comparable in size to a fuel assembly.

The reactor power, coolant density, and fuel temperature distributions are intimately coupled in SIMULATE-3 since it performs a coupled neutronics/thermal-hydraulics iteration to find these distributions. The node-average density is calculated by evaluating the state properties of water at the average of the node inlet and outlet enthalpies.

In this thesis, the SIMULATE-3 solution serves as the benchmark code for comparing cross-section generation and modeling outcomes.

3.4.3 GenPMAXS.

GenPMAXS, which stands for Generation of the **P**urdue **Ma**croscopic **XS** set, was developed by (Downar, T. & Xu, Y., 2004) to facilitate the generation of PMAXS files from lattice physics codes such as CASMO-4, HELIOS, TRITON, and SERPENT. It serves as an interface between these detailed lattice codes and the neutronics code PARCS.

In this work, CASMO-4 has been employed as the lattice code. Consequently, GenPMAXS reads the lattice physics parameters from CASMO-4, specifically, nodal

averaged cross-sections and kinetic parameters, and converts them into a format suitable for use by PARCS, as illustrated in Figure 3.10.

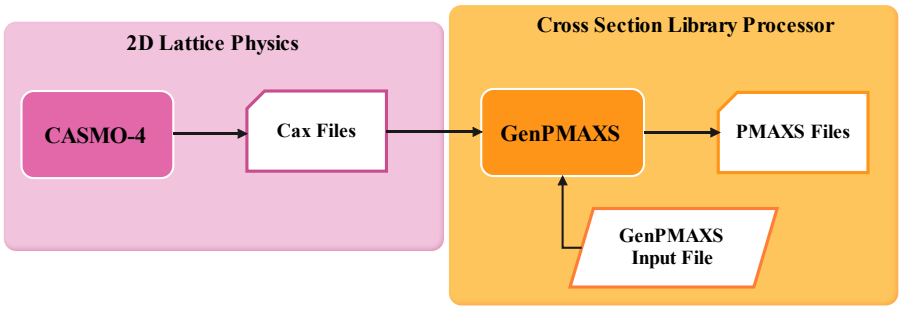

Figure 3.10. Overview of the GenPMAXS Code as the Interface between CASMO-4 and PARCS.

GenPMAXS plays an indispensable role in bridging detailed lattice physics calculations with core-level simulations in PARCS. Its ability to generate accurate, structured PMAXS files from various lattice codes underpins reliable reactor core analysis, supporting both operational efficiency and safety in nuclear reactors.

The PMAXS files generated by GenPMAXS contain all the essential data required for core simulation and depletion analysis, applicable to both steady-state and transient scenarios. These files are organized in a macroscopic cross-section format that varies according to state variables, history variables, and burnup.

Given the significant absorption cross-sections of Xenon (Xe) and Samarium (Sm), which are highly flux-dependent, their absorption cross-sections are represented using their microscopic cross-sections and number densities. This representation ensures accurate modeling of these isotopes' impact on reactor behavior.

GenPMAXS employs a structured approach to handle independent variables, classifying them into three distinct groups:

1) **Control Rod Fractions**: Reflecting the positioning and influence of control rods.
2) **Current Node Variables**: Representing the local conditions within the node.
3) **Neighbor Node Variables**: Accounting for the interactions with adjacent nodes.

Each group is treated differently, making the selection of appropriate independent variables crucial for achieving accurate simulation results that closely match reference data.

Ensuring the consistency of data during the conversion process from lattice codes to PMAXS files is paramount. GenPMAXS ensures this by verifying that the

k_{eff} values from the cross-sections align with those from the lattice results, thereby confirming the accuracy of the basic cross-sections.

3.4.4 PARCS.

PARCS, (Downar, T. et al., 2012), which stands for the Purdue Advanced Reactor Core Simulator (originally developed at Purdue University and now housed at Michigan State University), is a sophisticated three-dimensional deterministic reactor core simulator. It adeptly solves steady-state and time-dependent neutron diffusion and SP3 transport equations across both orthogonal and non-orthogonal geometries to determine the neutron flux distribution.

This code is the preferred tool for neutron diffusion calculations in thermal reactors, utilized by the U.S. NRC. Through extensive application, PARCS has demonstrated its prowess in predicting the steady-state and transient behavior of nuclear reactor cores at various burnup states specific to commercial LWRs. This has significantly bolstered its Verification & Validation (V&V) credentials and qualifications, conforming to regulatory standards (Yarsky et al., 2013; Choi et al., 2022).

As a versatile core simulator, PARCS can function independently (also known as stand-alone) or be coupled with thermal-hydraulics system codes such as TRACE5, RELAP5, and TRAC-BF1, alongside subchannel codes like COBRA-TF. These integrations, which can be executed through serial or parallel processing approaches, allow for comprehensive simulations that incorporate thermal-hydraulic feedback mechanisms.

PARCS typically employs two neutron energy groups and six neutron precursor groups; however, it can be adapted to use additional energy groups. This is particularly advantageous in fast reactor contexts, where six energy groups are often standard.

For stand-alone simulations, PARCS necessitates boundary conditions provided through 3D mappings. These mappings include data on fuel temperature, moderator temperature, boron and moderator density distributions, along with historical values. Users generally supply this information, or it is imported from external files generated by another code. In this thesis, all required data is sourced from SIMULATE-3, as detailed in Chapter 5 and Chapter 6. In terms of coupled simulations, Chapter 7 delves into predictions for thermal-hydraulic and neutronic transients using PARCS.

Key calculation features of PARCS encompass eigenvalue analyses, Xenon transient modeling, decay heat computations, pin power calculations, and adjoint calculations. Its capability to perform core eigenvalue calculations and evaluate control rod movements equips it with the necessary tools for analyzing both short-term (kinetic) and long-term (depletion) core behaviors.

Further extending its functionality, PARCS includes fuel depletion analysis. Utilizing the PMAXS format, cross-sections can integrate burnup as a fitting parameter. This dynamic adjustment of cross-sections at each time step based on burnup progression allows analysts to iteratively deplete the core, achieving a

representative equilibrium condition and deriving burnup distributions alongside their corresponding cross-sections.

Before diving deeper into the capabilities of PARCS, a more detailed discussion of the depletion model calculations is warranted. An overview of core depletion analysis is illustrated in Figure 3.11.

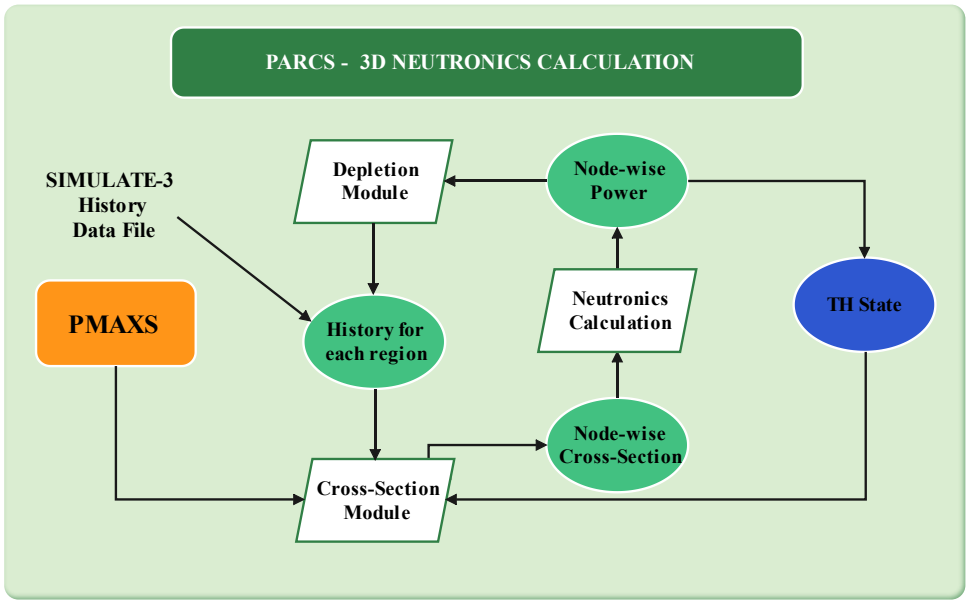

Source: GenPMAXS' Manual (Downar, T. & Xu, Y., 2004).

Figure 3.11. Overview of Core Depletion Analysis in PARCS.

The depletion module generates new burnup and historical state information that corresponds to the PARCS neutron flux solution. The cross-section module then calculates cross-sections based on this burnup and historical state information, in conjunction with the current thermal-hydraulic state. Subsequently, the PARCS neutronic module calculates the neutron flux using the cross-sections generated by the cross-section module. Finally, the node-wise power calculated by PARCS is utilized to determine the region-wise burnup increment for advancing the macroscopic cross-sections over time.

PARCS employs a macroscopic depletion method, where microscopic cross-sections and fuel number densities are not tracked individually during core depletion. Instead, the eigenvalue calculation provides the initial steady state for transient calculations. Here, the standard k_{eff} multiplier is adjusted to ensure a critical state for the transient fixed-source problem. The eigenvalue calculation in PARCS leverages the *Wielandt* eigenvalue shift method to accelerate convergence (Yee, B. C. et al., 2016).

Discretization of the balance equation in both time and space is required during the solution process. Time discretization is executed using the well-known *Theta Method*, with an exponential transformation of the group fluxes (Crank, J. & Nicolson, P., 1947). This temporal differencing yields a transient fixed-source problem at each time point, which is solved by a conditional nodal update scheme. This scheme invokes the nodal update only when there are substantial local cross-section changes and consequential local flux variations. Cross-section information is then used for neutronics calculations to obtain the power distribution across the core.

Throughout the reactor's operational lifespan, the presence of Xenon and Samarium significantly impacts reactor power. PARCS is capable of monitoring their concentrations and dynamically adjusting the absorption macroscopic cross-sections accordingly.

For relatively slow Xenon transients, PARCS employs a quasistatic calculation approach. This method bypasses the consideration of time-dependent variations in delayed neutrons, instead utilizing an eigenvalue problem solver to determine fluxes. The number densities of Xenon and Samarium are subsequently updated by solving balance equations based on the resulting fluxes. Currently, PARCS offers both equilibrium and transient options for managing the effects of Xenon and Samarium.

Multiple solution kernels are available in PARCS for spatial discretization, as illustrated in Table 3.3.

Table 3.3. PARCS Neutronics Methods: Solution Kernels.

Source: Parcs' Manual (Downar, T. et al., 2012).

Geometry Type	Kernel Name	Solution Method	Energy Treatment	Angle Treatment
Cartesian 3D	CMFD	FD	2G	Diffusion
	ANM/NEM (Hybrid)	**Nodal**	**2G**	**Diffusion**
	FMFD	FD	MG	Diffusion/SP_3
	NEMMG	Nodal	MG	Diffusion/SP_3
Hexagonal 3D	CMFD	FD	2G	Diffusion
	TPEN	Nodal	MG	Diffusion

Legend:

CMFD = Coarse Mesh Finite Difference **NEM** = Nodal Expansion Method

ANM = Advanced Nodal Method **MG** = Multigroup **FMFD** = Fine Mesh Finite Difference

PARCS incorporates a diverse array of sophisticated spatial kinetics calculation methods to deliver precise and efficient performance across various tasks. One such method is the *Coarse Mesh Finite Difference* (CMFD) formulation, which is designed

to expedite transient calculations by reducing the computational burden of resource-intensive nodal computations during periods of minimal flux spatial variation.

In PARCS, the CMFD formulation is employed to compute neutron fluxes within homogenized nodes. Specifically, a conditional update scheme is utilized to initiate higher-order nodal updates only in response to significant changes in core conditions that necessitate such adjustments. Subsequently, local two-node problems are iteratively solved during the nonlinear iteration process to correct discretization errors in the nodal interface current, which arise from the finite difference approximation in a coarse mesh structure.

In rectangular geometries, PARCS can also employ the *Advanced Nodal Diffusion Method* (ANM). This method, known for its accuracy in many applications, is typically used in calculating Light Water Reactor (LWR) simulations. However, ANM can lack robustness in near-critical two-node problems. The ANM method is quite similar to the one used in SIMULATE-3. Conversely, the *Nodal Expansion Method* (NEM) offers lower precision than ANM but provides a more robust and faster solution.

As an intermediary solution, PARCS can combine both nodal methods to simulate the reactor core. In this *Hybrid Approach*, ANM serves as the base solution, while NEM is invoked whenever the node k_{inf} approaches unity. This hybrid method has been deemed an optimal option for most cases, especially in Cartesian geometries (Downar, T. et al., 1997).

More detailed information about PARCS can be found in its user's manual (Downar, T. et al., 2012).

3.4.5 TRAC-BF1/BE.

TRAC-BF1, which stands for **T**ransient **R**eactor **A**nalysis **C**ode, was developed in the late 70's at the Idaho National Engineering Laboratory (INL) for the NRC (Borkowski, J. et al., 1992). Initially, the TRAC family of computer codes started as a tool for analyzing PWRs, known as TRAC-PF1, developed at the Los Alamos National Laboratory for the NRC. The BWR version, TRAC-BD1/MOD1, was developed jointly by the NRC and General Electric (GE) (Bolger et al., 2003).

Derived from its predecessor TRAC-PF1, TRAC-BF1 inherited foundational models but was significantly refined to address the specific challenges of simulating BWRs. TRAC-PF1 struggled to accurately capture BWR dynamics due to disparities in bundle geometries between BWRs and PWRs.

TRAC-BF1 was developed to provide robust modeling and analysis capabilities for a wide range of postulated accidents, such as large or small break LOCAs or ATWS events initiated by the closure of the Main Steam Isolation Valve (MSIVC). Consequently, TRAC-BF1 offers an unparalleled level of fidelity in representing reactor systems, encompassing both linear and non-linear phenomena across anticipated and unforeseen operational conditions.

TRAC-BF1/BE is a best-estimate thermal-hydraulic system code used for design, licensing, and operational purposes in BWRs, in both conservative and realistic

analysis modes. The code features a modular structure and detailed best-estimate models, including a three-dimensional thermal-hydraulics model.

TRAC-BF1/BE employs two-fluid, non-equilibrium, non-homogeneous two-phase flow models in both one- and three-dimensional BWR system components to solve the six-equation finite difference scheme of field equations. These equations describe the thermal-hydraulic behavior of the coolant, the energy flow in the fuel and structural components, and the generation of nuclear power in the reactor core.

The code uses a staggered-mesh scheme where velocities (V) are defined at the mesh-cell surfaces, while volume properties such as pressure (p), gas volume fraction (α), temperature (T), internal energy (e), and density (ρ) are defined at the mesh cell center. This results in scalar field equations (mass and energy) applying to a given mesh cell, while momentum equations apply at the interfaces between mesh cells in the three component directions.

Additionally, unique features of the code include:

- Non-homogeneous critical flow model.
- Boron transport model, enhanced with a second-order modified Godunov scheme (Barrachina, T. et al., 2013; Barrachina, T. et al., 2015).
- Two-phase level tracking model.
- Reactivity feedback model, including the effect of soluble boron.
- Balance of plant component models, such as turbines, feedwater heaters, and steam condensers.
- Mechanistic separator-dryer model.
- A comprehensive control system model.
- Restart capability.

The default kinetic model in TRAC-BF1/BE is the constant power or point-kinetics model. However, the code has undergone iterative enhancements, culminating in its current capability to conduct both 1D and 3D kinetics calculations when coupled with PARCS.

The Universitat Politècnica de València spearheaded the development, implementation, and validation of the 1D kinetics functionality within TRAC-BF1/BE. Additionally, the coupling of TRAC-BF1/BE and PARCS for parallel processing to enable transient simulations incorporating 3D power dynamics was a collaborative effort between the Universitat Politècnica de València and Iberdrola Generación Nuclear (Jambrina et al., 2012; Jambrina, A. et al., 2013).

TRAC-BF1/BE is applicable to operating BWR/2, BWR/3, BWR/4, BWR/5, and BWR/6 designs. More information can be found in its user manual.

3.5 Summary.

Chapter 3 delves into the advanced methodologies and tools pivotal to nuclear data processing, emphasizing their critical role in modern reactor analysis. The chapter begins by establishing the foundational importance of cutting-edge nuclear data processing technologies, setting the stage for a comprehensive exploration of their impact on reactor safety and performance.

The section on reactor core analysis underscores the integration of thermal-hydraulic and neutronics coupled calculations. This analysis is essential for understanding the core behavior across a spectrum of operational scenarios. By merging advanced thermal-hydraulic and neutronic models, engineers achieve a holistic view of reactor core dynamics. The continual evolution of computational tools and coupled simulation techniques enhances the precision and reliability of these analyses, thereby ensuring the safe and efficient operation of nuclear reactors.

Transient analysis forms a cornerstone of nuclear reactor design and operation. It ensures that reactors can effectively manage a wide range of scenarios, from anticipated operational occurrences to beyond design basis accidents. This analysis is crucial for the ongoing refinement of reactor design, operational procedures, and regulatory standards. By advancing transient analysis techniques and incorporating innovative safety features, the nuclear industry strives to uphold the highest standards of safety and reliability, thereby maintaining the secure operation of reactors.

The decision to focus on ATWS scenarios in this thesis underscores its significance in challenging existing safety standards and fostering advancements in technology and operational protocols. This proactive approach is essential for mitigating serious incidents and safeguarding nuclear facilities worldwide.

Extensive research and documentation in the literature reveal various strategies for managing ATWS scenarios. These include enhancements to reactor control systems and emergency cooling systems. Advanced thermal-hydraulic and neutronic simulation models have been developed to predict reactor behavior during an ATWS and evaluate the effectiveness of mitigation measures.

The chapter concludes with a detailed examination of the most-common codes used for reactor core analysis. It provides an in-depth look at CASMO-4, SIMULATE-3, GenPMAXS, PARCS, and TRAC-BF1, highlighting their unique features and applications in reactor core analysis. This final section demonstrates how these codes contribute to a more precise and reliable understanding of reactor core behavior, further advancing the field of nuclear reactor safety.

Chapter 4
Cross-Section Generation & Modeling for BWRs

4.1 Introduction.

BWR fuel assemblies present significant complexities due to several factors, including substantial enrichment splitting, the presence of large water rods, gaps between fuel assemblies, the channel box, and control rod insertion. These complexities pose challenges in accurately predicting fuel behavior during reactor operation.

Fuel depletion analysis focuses on predicting long-term changes in reactor fuel composition caused by fuel burnup. These changes impact the reactor's operational lifespan, stability, and control.

Accurate predictions of reactor behavior under both steady-state and transient conditions are, therefore, crucial for safety analysis. Such predictions also aid in optimizing the fuel cycle and enhancing the overall performance of the reactor. Consequently, due to the considerable variation in core parameters over a reactor cycle, a suitable set of cross-sections is necessary to accurately predict reactor behavior under all conditions.

4.2 Cross-section Modeling.

Figure 4.1 contains a schematic view of the various dynamic interactions usually incorporated in a time-dependent consideration of the reactor state.

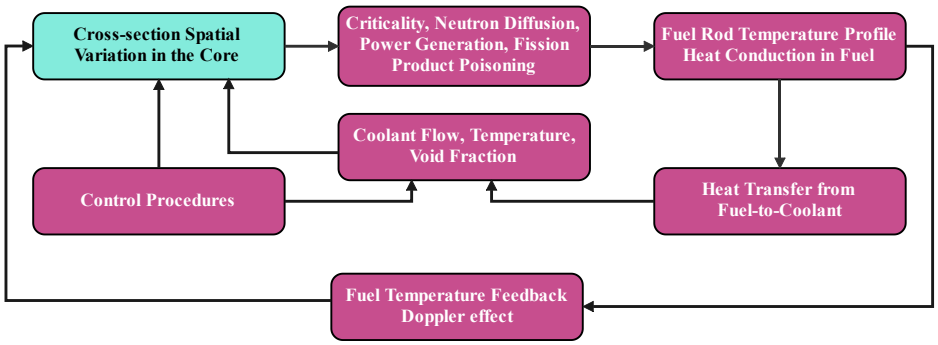

Source: (Silvennoinen, P., 1976).

Figure 4.1. Flow Chart Reactor Core Dynamics.

As seen in Figure 4.1, many of the reactivity feedback mechanisms directly affect the neutron flux and power distributions and, therefore, may cause variations of the cross-sections. These variations, as described in (Fujita et al., 2014), can be assorted in two different phenomena or effects:

- I**nstantaneous effect**: appears when the core state variables undergo instantaneous changes while maintaining invariant the fuel composition. It is captured by branch calculations in the lattice code.
- **History effect**: comes into the game as the burnup progresses and the fuel composition changes due to variations of exposure-averaged core state variables. It is captured by history depletion calculations in the lattice code.

All macroscopic cross-section data are generated from lattice physics assembly calculations as functions of node-wise exposure, instantaneous variables, and related history parameters as

$$\Sigma = \Sigma(EXP, VOI, TFU, TMO, CR, HVOI, HTFU, HTMO, HCR) \qquad \textbf{Equation 4.1}$$

Where Σ represents the macroscopic cross-section, EXP the exposure, VOI the void fraction, TFU the fuel temperature, TMO the moderator temperature, CR the control rod insertion, $HVOI$ the void history, $HTFU$ the fuel temperature history, $HTMO$ the moderator temperature history, and HCR the control rod history.

Looking closer to Equation 4.1, one can start imagining that the core state variables will change accordingly with the burnup, and hence, variations of the cross-sections as the cycle advances are expected due to their heavy dependence on core conditions.

For example, the instantaneous void content, VOI, is the amount of void currently in the moderator whereas, the historical void content in the moderator, $HVOI$, represents the void level at which the fuel has been depleted. In BWR core calculations, it is imperative to accurately capture the history effect since a sizeable variation of the control rod insertion and the void fraction is expected.

The specific inclusion of the instantaneous and history effects in Equation 4.1 yields into

$$\begin{aligned}\boldsymbol{\Sigma}(\boldsymbol{EXP},\boldsymbol{VOI},\boldsymbol{TFU},\boldsymbol{TMO},\boldsymbol{CR},\boldsymbol{HVOI},\boldsymbol{HTFU},\boldsymbol{HTMO},\boldsymbol{HCR}) \\ \approx \boldsymbol{\Sigma}_{\boldsymbol{base}}(\boldsymbol{EXP},\boldsymbol{VOI}_{\boldsymbol{base}},\boldsymbol{TFU}_{\boldsymbol{base}},\boldsymbol{TMO}_{\boldsymbol{base}},\boldsymbol{CR}_{\boldsymbol{base}}) \\ + \Delta\boldsymbol{\Sigma}_{\boldsymbol{inst}}(\boldsymbol{EXP},\boldsymbol{VOI},\boldsymbol{TFU},\boldsymbol{TMO},\boldsymbol{CR}) \\ + \Delta\boldsymbol{\Sigma}_{\boldsymbol{hist}}(\boldsymbol{EXP},\boldsymbol{HVOI},\boldsymbol{HTFU},\boldsymbol{HTMO},\boldsymbol{HCR})\end{aligned} \qquad \textbf{Equation 4.2}$$

Where the subscripts $base$, $inst$, and $hist$ represent the base condition, the instantaneous, and the history effects, respectively.

In view of Equation 4.2, it is easily deduced that the macroscopic cross-sections can be pieced together as the sum of a base cross-section and a collection of partial cross-sections which would require calculating all the possible combinations among the burnup, state variables, and depletion history variables.

Although *"the more, the merrier"* is very desirable, calculating every variety of core state and depletion parameters could become unmanageable and be impractical for assembly-average core calculations as also stated by (Fujita, T., 2015). Besides, it is also having to be known a priori which is not always possible.

As a compromised solution, a limited number of combination sets is selected and calculated by the lattice code. Then, during the core calculation, each node will be identified by a specific combination of state values and depletion variables, determining the selection and reconstruction of the macroscopic cross-sections from a particular set.

In addition, the cross-terms among both effects must also be considered. Once the feedback parameters are chosen, there are still two more things to consider: the definition of the feedback parameter domain range and the number of mesh points inside the selected domain. Defining the mesh points properly is crucial for lattice code calculations because, once the feedback variables have been chosen, the interpolation errors strictly depend on the selected range, as pointed out by (Sánchez-Cervera, et al., 2014b). This issue will be widely covered in the forthcoming Chapter 5.

4.2.1 Instantaneous Effect.

Cross-section modeling for coupled 3D simulations is based on the generated in the so-called base branch and depletion calculations from the lattice physics code and assembled into the cross-section library.

In each step the lattice physics code uses constant fuel composition. The branch calculations capture the instantaneous effect that is caused by the immediate and local changes in the significant core parameters; therefore, lattice branches have no dependence on the exposure.

The instantaneous effect is estimated by the branch calculations from several depletion points of the depletion calculation on the *Nominal (Base)* condition.

Usually, the standard calculation of the change of the fuel composition on a given cycle is performed employing the following base conditions:

1) nominal power,
2) core-averaged values of thermal-hydraulic parameters as the moderator density, or the fuel temperature, and
3) withdrawn control rods since the majority of control rods are in that position during full power operation.

The concept of the base condition scheme is shown in Figure 4.2. Regarding the selection of the number of depletion steps, usually, the burnup points should be closer to each other the faster the isotope composition of the fuel is changing.

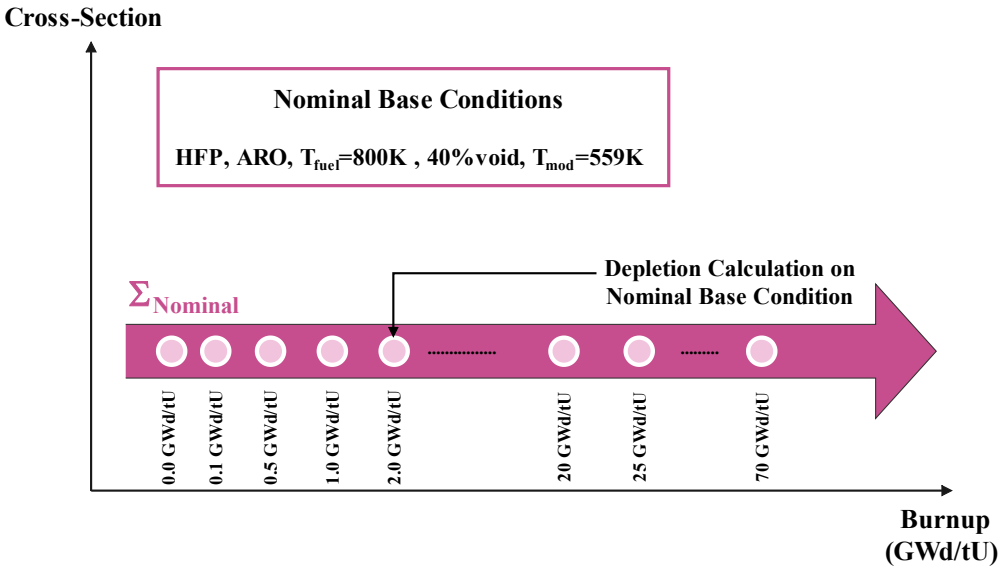

Figure 4.2. Example of Nominal Base Calculation.

During the lattice code branch calculations, the state variables ought to be changed one-by-one to cover as many different core conditions as possible. This concept is shown in Figure 4.3. In practice, however, a few state variables are modified at the same time.

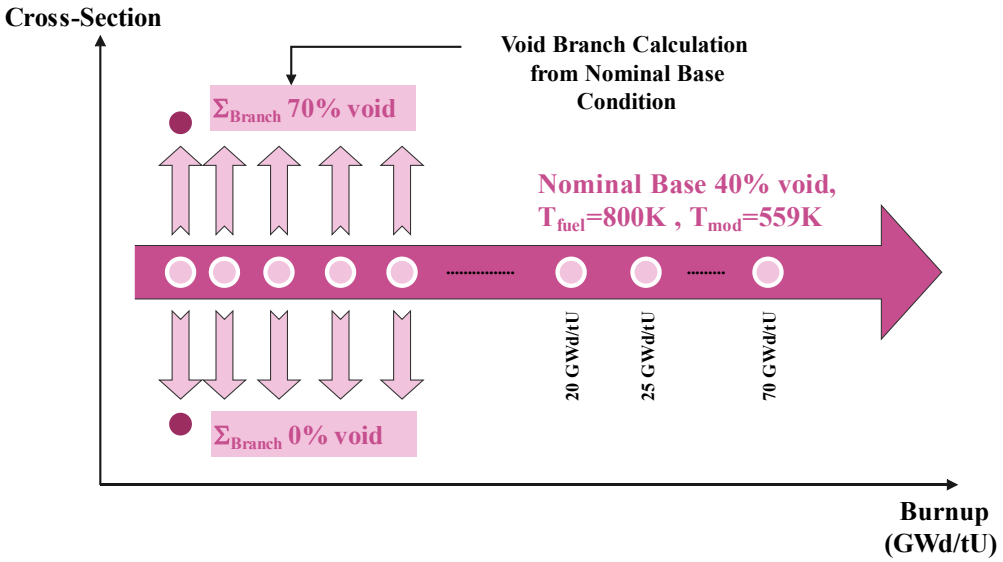

Figure 4.3. Example of Branch Calculation from Nominal Base Condition.

In view of the Figure 4.3, the branch calculations (voids at 0% and 70%) are performed from several depletion points of the depletion calculation on the nominal condition at 40% void. Therefore, the macroscopic cross-sections will vary accordingly as stated by (Fujita et al., 2014) as follows:

$$\Delta\boldsymbol{\Sigma}_{inst}(\boldsymbol{EXP}, \boldsymbol{X}_{base} \rightarrow \boldsymbol{X}') = \boldsymbol{\Sigma}_{branch}(\boldsymbol{EXP}, \boldsymbol{X}') - \boldsymbol{\Sigma}_{base}(\boldsymbol{EXP}, \boldsymbol{X}_{base}) \qquad \textbf{Equation 4.3}$$

where X is one of the core state variables. Note that the left-hand side represents the variation due to the instantaneous change of the core state variable X from the base condition X_{base} for a given burnup to the perturbed condition X'. This concept is shown in Figure 4.4.

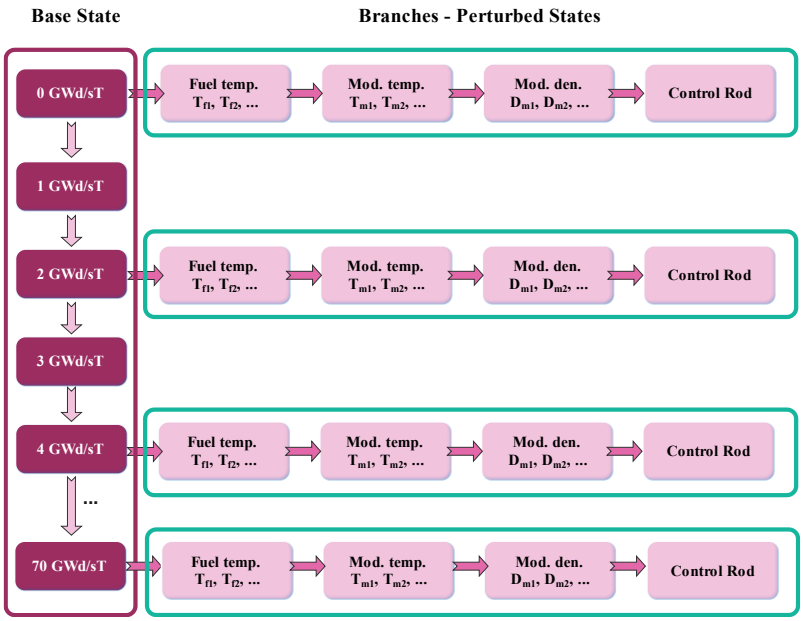

Figure 4.4. Example of Base State and Branch Calculations.

4.2.2 History Effect.

History effect arises from the variation of fuel composition caused by changes in core state variables during the depletion process. As the fuel burns, the behavior of cross-sections is expected to change because the future properties of the fuel are influenced by its current properties during depletion.

To capture the impact of previous changes in the reactor on the current reactor state, history parameters are introduced as a function of time. In the particular case of BWRs, the cross-section burnup dependence is a three-dimensional vector encompassing exposure, spectral history, and control rod history.

The main spectral history effect on fission and absorption cross-sections, as mentioned by (Iwamoto, T. & Yamamoto, M., 1999), is attributed to the historical moderator density, which determines the isotopic depletion of the fuel and the distribution of spectrum flux. Thus, the most significant history effects in a BWR stem from void fraction and control rod histories.

Depending on the thermal-hydraulic conditions and the control rod movement for a given cycle N, the fuel will deplete differently in both space and time; thus, resulting in changes to the radial power distribution at each depletion step. This effect persists in cycle $N + 1$ and onwards until the fuel is discharged from the core.

As an illustrative example, consider two nodes with the same void fraction (e.g., 45%) and exposure (e.g., 35 GWd/tU), but the first node has been depleted at 50% void

fraction while the second node has been depleted at 60% void fraction. Despite their current void fractions being equal, their reactivities differ because the depletion neutron spectrum is harder (higher energies) at 60% void fraction compared to 50%. Thus, the operating histories impact the depleted isotope.

Furthermore, the cross-term effect for history effects needs to be taken into account. The dependencies of macroscopic cross-sections on history variables are determined by conducting separate lattice physics assembly depletion calculations, referred to as *Off-nominal Calculations*. These calculations involve modifying the state variables from the nominal core-averaged depletion calculation to off-rated values for each history effect.

It is important to note that the lattice physics code does not need to precisely replicate the operating history of a node in order to provide cross-sections to the core simulator code. Instead, a series of history depletion calculations are performed, wherein specific state variables are periodically changed from the base calculation case to different instantaneous parameters (branch calculations). This approach ensures that sufficient cross-section information is generated for the core simulator code, as depicted in Figure 4.5.

The justification for off-nominal calculations on assembly depletion is straightforward. Suppose a calculation is solely performed at averaged-core conditions. In that case, the neutron behavior will be modeled inaccurately because the cross-sections at the bottom of the core will be generated based on over-moderated conditions and under-moderated conditions at the top of the core, as outlined in (Watson & Ivanov, 2002). Hence, correctly modeling off-nominal values is essential for highly accurate cross-section sets.

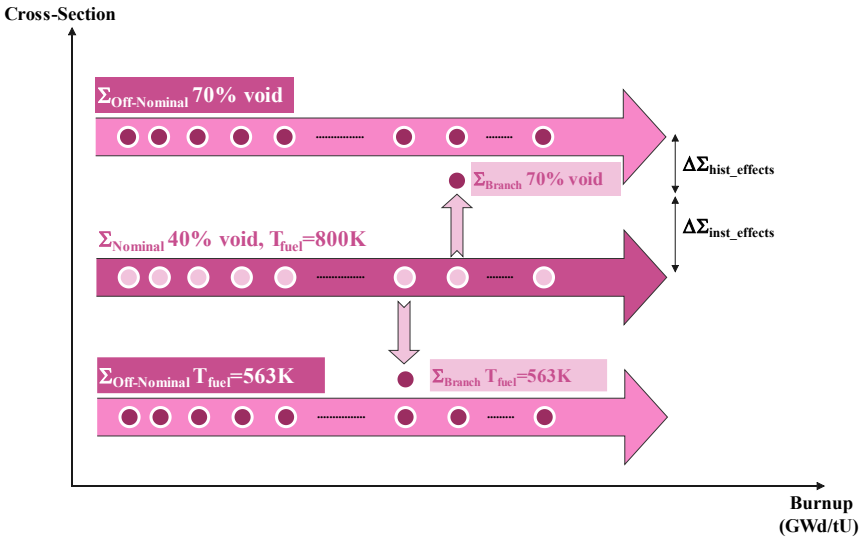

Figure 4.5. Example of Off-Nominal Calculation Scheme from Nominal Base Condition.

4.2.3 Control Rod Effect.

With power reactors operating as they do at high power densities and high temperatures, it is important to maintain a power distribution as flat as possible and as constant as possible, reference (Cochran, R. G. & Tsoulfanidis, N., 1999).

The power control during regular operation can be performed adjusting reactivity using either:

1) Control rod reactivity.
2) Recirculation flow reactivity.

Putting aside the latter and focusing on the former, the control rods are composed of a strong neutron absorber and perform an important function utilized in two ways:

1) to change the degree of reactor criticality for the purpose of raising or lowering the power level, and
2) to keep a reactor critical by compensating the fuel depletion either being inserted to compensate positive depletion reactivity effects (e.g., depletion of solid burnable poisons like Gadolinium), or withdrawn to balance the negative depletion reactivity effects (e.g., depletion of the ^{235}U in the fuel).

Because the moderator at the bottom part of the core is in liquid state while at the upper part is mostly steam, without any control rods, the power at the bottom part would be much higher than that at the upper half of the core. By inserting the control rods from the bottom in BWRs, the flux and the power are suppressed at the bottom half and the overall axial power distribution becomes more uniform as intended by the core designers.

Control Rods (CRs) are blades that can be alternate space inserted in between four fuel assemblies from the bottom. The blades are combined together in a cruciform-design control rod, see Figure 4.6.

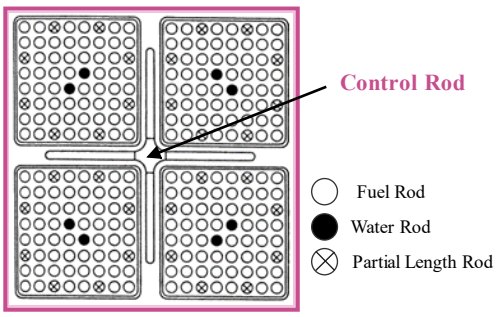

Source: (Cochran, R. G. & Tsoulfanidis, N., 1999).

Figure 4.6. Example of a Cruciform Control Rod for a BWR Fuel.

Control rods can be classified depending on their *"main mission within the core"*. In that sense, there are mainly two types of CRs:

1) Reactivity-binding: denominated as deeply inserted control rods (typically positioned between 6% and 18% withdrawal).
2) Power-shaping: denominated as shallow control rods (positioned between 50% and 85% withdrawal).

The presence of deep rods primarily impacts core reactivity while having minimal impact on the axial power distribution. As the cycle progresses and there is a requirement to increase reactivity to sustain power levels, these control rods are gradually withdrawn from the core.

Shallow rods, on the other hand, offer the ability to shape axial power and control thermal quantities like Linear Heat Generation Rate (LHGR). These CRs also have a significant influence on core stability. The withdrawal and insertion sequences of these rods are pre-programmed by core designers before each operating cycle.

Control rods are generally categorized as *Black or Gray*. Black control rods act as solid neutron absorbers, while gray control rods serve as milder neutron absorbers, allowing some neutrons to escape. The trend in reactor design favors the use of gray control rods due to their lesser impact on neutron flux and power distribution distortions.

The gray factor is associated with the total absorption cross-section of the control rod, which depends on the absorbing material and its density. A control rod may have several axial compositions with different gray factors, which have to be considered during lattice calculations.

There are nodal codes that assume that the associated gray factor of a control rod is 100% for a given axial composition. In other words, the nodal code assumes that the corresponding axial node of the control rod has a 100% absorption capacity, resembling a black control rod. Consequently, if the actual control rod used deviates from this assumption, significant local errors may arise when performing core follow, depletion, or rod sequence exchange simulations. Nevertheless, other codes do not incorporate the gray factor separately, as it has already been accounted for during the prior determination of cross-sections by the lattice code.

To accurately predict long-term depletion effects, it is necessary to track the reactivity changes of control rods. Over time, the burnup of absorber material in the control rod will affect its reactivity worth. The strong radial power tilt in a fuel bundle when a control rod is present leads to a corresponding radially tilted burnup, with the corner near the control rod experiencing less burnup and the opposite corner experiencing more. This results in a harder neutron spectrum and Plutonium build-up in the fuel pin rows adjacent to the control rod.

Failure to account for these effects in core simulation calculations can lead to underestimated power levels and erroneous internal power distributions in bundles located near control rods for extended periods.

The *Control Rod History Effect* refers to the lasting impact of a control rod on power and burnup distributions of fuel bundles in the core from which the control rod has been removed. Therefore, it is crucial to track the history of control rod behavior over time for each node and incorporate differential cross-section data for this effect into the cross-section library file.

4.3 Reflector Modeling.

All LWRs utilize reflectors in the form of the coolant surrounding the core. The large local power changes near the core-reflector interface require accurate reflector cross-sections to preserve the reaction rates of the reflector and the leakages at the interface as described by (Lee, C. H. et al., 2006).

In early nodal methods, the modeling of reflector regions surrounding the core employed albedo-type boundary conditions (Bahadir, T., 2015). These conditions were applied either at the core periphery or the baffle-reflector interface. Albedo coefficients, determined through separate transport calculations, were used. However, power distribution errors in these approaches could reach magnitudes as high as 10-15%. When modern nodal methods were developed, and more significant accuracy was obtained, the use of albedo boundary conditions became undesirable.

Modern methods employ explicit modeling of reflector regions in nodal reactor calculations. Typically, reflector and baffle calculations are performed in a 1D slab geometry known as *Spectral Geometry*. These calculations must be conducted separately from the fuel segment calculations (Shim et al., 2016). These models assume that a single set of discontinuity factors and homogenized cross-sections can be applied to all reflector nodes (Ragusa et al., 2005). The concept of discontinuity factors has been previously discussed in Chapter 3.

While discontinuity factors show weak dependence on position, cross-sections can significantly differ between inner and outer corner reflector nodes as will be explored in Chapter 5. It is worth noting that the accuracy of the reflector model is a result of the calculation of discontinuity factors for the reflector.

GenPMAXS, an example of modern methods code, is utilized to generate nodal cross-sections based on the results of a lattice code calculation. In the case of side reflectors, the 1D reflector model depicted in Figure 4.7 is typically employed for cross-section generation.

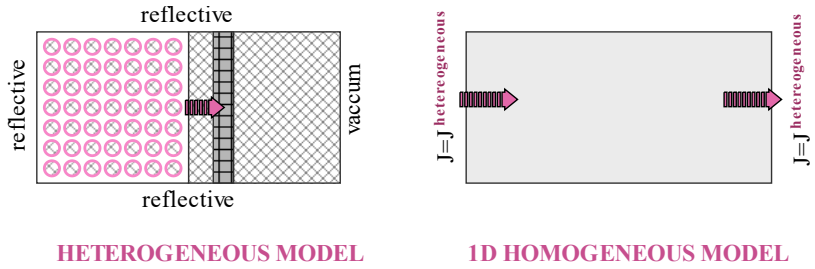

Source: GenPMAXS Manual (Downar, T. & Xu, Y., 2004).

Figure 4.7. Example of Reflector Model for Cross-Section Generation.

This approach involves solving 1D diffusion equations within the homogeneous reflector region to determine the surface-averaged fluxes of the reflector. The calculation ensures that the average flux and currents on surfaces are preserved, using information derived from lattice calculations, as stated in the GenPMAXS manual (Downar, T. & Xu, Y., 2004).

For the corner reflector region cross-section, solving the 2D homogeneous diffusion equation presents serious difficulties. An approximation can be represented by correcting the scattering cross-section as follows:

$$r_{2D} = \frac{P_{FA} - d}{P_{FA}} \qquad \textbf{Equation 4.4}$$

where P_{FA} and d denote the fuel assembly pitch and shroud thickness, respectively.

Typically, three types of reflector cross-sections are required for three-dimensional core calculations: top, bottom, and radial reflector, (Downar, T. & Xu, Y., 2004).

The top and bottom reflectors can have distinct structures, which may require different cross-sections. The determination of cross-sections is primarily dependent on the composition, i.e., steel and water mixture.

Nevertheless, radial reflector modeling is an entirely different story. There are three kinds of locations of radial reflector in term of how many faces are connected to fuel assemblies:

1) the side reflector which has one face connected to fuel assembly,
2) the corner reflector which has two faces connected to fuel assemblies, and
3) the outer reflector which is not connected to fuel assemblies.

In the context of this dissertation, CASMO-4 has been employed as lattice code employed. Reflector calculations in CASMO-4 are exclusively conducted at zero exposure, utilizing 25 energy groups (Edenius, M. et al., 1995). This approach is justified as the reflector primarily consists of water and does not undergo significant depletion.

However, it is important to recognize that the thermal-hydraulic conditions of the reflector impact the historical effects on adjacent fuel elements. As a result, in the specific case of a modeling a BWR, consideration of the moderator temperature dependency, encompassing both instantaneous and historical effects, must be considered for the bottom and radial reflectors while consideration of the void fraction dependency, encompassing both instantaneous and historical effects, for the top reflector.

4.4 Overview of PARCS Cross-section Model.

According to (Odar, F. et al., 2003), in the earlier versions of PARCS dating back to the late 1990s, cross-section functionalization relied on the *Partial Derivatives Model*, depicted as follows:

$$
\begin{aligned}
&P(C_b, T_f, T_m, D_m, \alpha, \alpha_{CR},) \\
&\quad = P(C_{b,0}, T_{f,0}, T_{m,0}, D_{m,0}, \alpha_0\ \alpha_{CR,0}) \\
&\quad + \frac{\partial P}{\partial C_b}\Big|_{C_{b,0}} (C_b - C_{b,0}) + \frac{\partial P}{\partial \sqrt{T_f}}\Big|_{T_{f,0}} \left(\sqrt{T_f} - \sqrt{T_{f,0}}\right) \\
&\quad + \frac{\partial P}{\partial T_m}\Big|_{T_{m,0}} (T_m - T_{m,0}) + \frac{\partial P}{\partial D_m}\Big|_{D_{m,0}} (D_m - D_{m,0}) \\
&\quad + \frac{1}{2}\frac{\partial^2 P}{\partial D_m^2}\Big|_{D_{m,0}} (D_m - D_{m,0})^2 + \frac{\partial P}{\partial \alpha}\Big|_{\alpha_0} (\alpha - \alpha_0) \\
&\quad + \frac{1}{2}\frac{\partial^2 P}{\partial \alpha^2}\Big|_{\alpha_0} (\alpha - \alpha_0)^2 + \frac{\partial P}{\partial \alpha_{CR}}\Big|_{\alpha_{CR,0}} (\alpha_{CR} - \alpha_{CR,0})
\end{aligned}
$$

Equation 4.5

In this context, the subscript 0 indicates the base case. The variable P is quite versatile, encompassing parameters such as microscopic and macroscopic cross-sections, assembly discontinuity factors, or kinetic parameters.

Initially, the model exhibited high efficiency but lacked the desired level of accuracy. This was primarily due to an assumption that the partial derivatives with respect to one variable were independent of variations in other variables, resulting in only first-order accuracy. Additionally, it overlooked cross-term effects between variables, further limiting accuracy. This limitation was highlighted in (Stålek & Demazière, 2008). Furthermore, the model did not incorporate burnup or history variables, as it was not designed for depletion calculations. Consequently, enhancements were necessary to broaden the scope and improve features of the code.

After years of code development, benchmarking efforts, and continuous enhancements, the cross-section functionalization in PARCS, which is currently considered adequate for LWRs, is expressed as shown in Equation 4.6.

$$
\begin{aligned}
&P(b, H, \alpha_{CR}, D_m, C_b, T_f, T_m) \\
&\quad = P(b, H, \alpha_{CR,0}, D_{m,0}, C_{b,0}, T_{f,0}, T_{m,0}) \\
&\quad + \left.\frac{\partial \Sigma}{\partial \alpha_{CR}}\right|_{(b,H,\alpha_{CR,ref})} (\alpha_{CR} - \alpha_{CR,0}) \\
&\quad + \left.\frac{\partial \Sigma}{\partial D_m}\right|_{(b,H,\alpha_{CR},D_{m,ref})} (D_m - D_{m,0}) \\
&\quad + \left.\frac{\partial \Sigma}{\partial C_b}\right|_{(b,H,\alpha_{CR},D_m,C_{b,ref})} (C_b - C_{b,0}) \\
&\quad + \left.\frac{\partial \Sigma}{\partial \sqrt{T_f}}\right|_{(b,H,\alpha_{CR},D_m,C_b,T_{f,ref})} \left(\sqrt{T_f} - \sqrt{T_{f,0}}\right) \\
&\quad + \left.\frac{\partial \Sigma}{\partial T_m}\right|_{(b,H,\alpha_{CR},D_m,C_b,T_f,T_{m,ref})} (T_m - T_{m,0})
\end{aligned}
\qquad \textbf{Equation 4.6}
$$

Where H represents history variables, b is the burnup, and again P encompasses the same parameters as Equation 4.5.

Sensitivity studies have shown that the sequence of independent variables in Equation 4.6 significantly impacts the accuracy of the cross-section model, as outlined in the GenPMAXS manual, reference (Downar, T. & Xu, Y., 2004). Therefore, the sequence adopted in Equation 4.6 for the dependency of each partial derivative is the recommended one, where the independent variables are arranged in decreasing order of influence on the partial derivatives.

A key difference from Equation 4.5 is that the partial derivatives with respect to a given variable now consider variations in some of the other variables. Because the partial derivatives are influenced by the reactor's actual operating conditions, there is no longer a need for quadratic dependency on moderator density/void fraction, (Stålek & Demazière, 2008).

Consequently, PARCS cross-sections are now calculated based on four instantaneous state variables:

1) Control rod insertion (i.e., effective rodded fractions),
2) Moderator density/void fraction,
3) Soluble poison concentration, and
4) Fuel temperature.

Note that there is no explicit dependency on the moderator temperature. This is because, in cases involving LWRs, the dependency on moderator density already encompasses the effects of moderator temperature.

Additionally, five history variables (H), are incorporated:

1) Control rod history,
2) Coolant density history,
3) Coolant soluble poison history,
4) Fuel temperature history, and
5) Coolant temperature history.

Returning to Equation 4.6, the subscript 0 denotes the base case, while the subscript ref represents the reference point. This reference point is defined as the midpoint between the instantaneous value and the base value. In a generic form, this relationship can be expressed as in Equation 4.7:

$$v_{ref} = \frac{v + v_0}{2} \qquad \textbf{Equation 4.7}$$

where v is the instantaneous value. Thus, the reference point itself depends on the instantaneous value. This method provides a second-order accuracy in estimating the cross-sections, as outlined in the GenPMAXS manual.

During core calculations performed by PARCS, the required cross-section parameters for specific reactor operating conditions are obtained through multi-dimensional linear interpolations with respect to the history variables, burnup, and instantaneous variables. Hence, PARCS reads the branch/history information and constructs the so-called *Tree-leave Structure*, illustrated in Figure 4.8, which serves as a specific three-level storage arrangement, as referenced in (Downar, T. & Xu, Y., 2004).

At the highest level, the structure represents the history cases, while the second level represents the instantaneous state with two possible values, i.e., 0 for the base value and 1 for the perturbed one. Finally, fuel burnup is the last variable in the tree structure. In view of Figure 4.8, the dark pink bolded tree structure represents the base case within the set of history variables, as detailed in (Stålek & Demazière, 2008).

Using a tree-leave structure instead of a table allows for non-uniform spacing between branches/histories and non-equidistant points in each linear interpolation. However, there is a trade-off between memory requirements and computational speed.

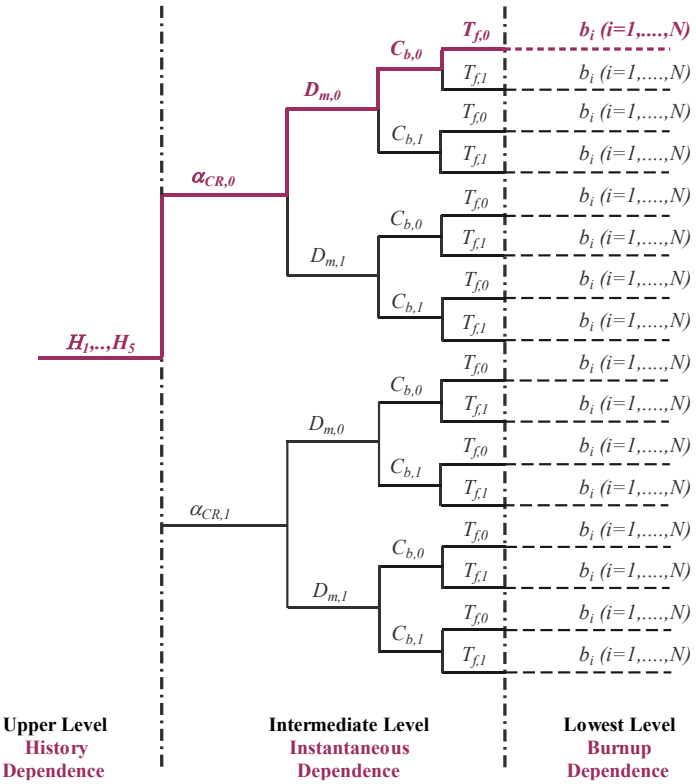

Source: (Stålek & Demazière, 2008).

Figure 4.8. PARCS Cross-Section Tree-Leave Structure.

However, it is important to highlight that the hierarchical structure employed for branch and history calculations does not align with the functionalization of data in CASMO-4/SIMULATE-3. As discussed in (Demazière, C. et al., 2012), the data in CASMO-4/SIMULATE-3 results from the summation of base values and partials. Each component is a function of up to three variables, particularly in the context of LWRs applications, as referenced in (Ver Planck, D.M. et al., 1995).

A concise overview of the cross-section model in CASMO-4/SIMULATE-3 will be presented in Subsection 4.6.

4.5 PMAX: Cross-section Files for PARCS.

This section provides a high-level summary of the PMAXS file structure. The given information is mostly extracted from the GenPMAXS Manual (Downar, T. & Xu, Y., 2004).

Recalling from Chapter 3, the most common cross-section files used by PARCS for core simulation and depletion analysis purposes are the PMAXS files. PMAXS files

provide the principal macroscopic cross-sections, the microscopic cross-sections of Xenon/Samarium, the group-wise form functions with several different branch states for the appropriate fuel burnup states, and all of the correct kinetics data.

Because the macroscopic cross-sections in PARCS are constructed with the assumption of a linear superposition of the partial cross-sections on a base reference state, PMAXS has to support all required information for representing the macroscopic cross-sections as:

$$\Sigma(Cr,S,N,H) = C_{01}\Sigma\left(\frac{C_1}{C_{01}},S,N,H\right) + \sum_{i=2}^{N_c} C_i\Sigma(C_i,S,N,H) \qquad \textbf{Equation 4.8}$$

Where C_{01} is the sum of the unrodded fraction and the first composition fraction in the current node

$$C_{01} = 1 - \sum_{i=2}^{Nc} C_i$$

And $\Sigma(Cr,S,N,H)$ is determined by Equation 4.9 as

$$\Sigma(Cr,S,N,H) = \Sigma^r(H) + Cr\left.\frac{\partial\Sigma}{\partial Cr}\right|_{(Cr/2,H)} + \sum_{j=2}^{Ns}\Delta S_j\left.\frac{\partial\Sigma}{\partial S_j}\right|_{(Cr,S_j^m,N^r,H)} + \sum_{j=1}^{4}\left(\sum_{k=1}^{Nn} n_{j,k}\left.\frac{\partial\Sigma}{\partial n_k}\right|_{(Cr,S,N_{j,k}^m,H)}\right) \qquad \textbf{Equation 4.9}$$

Where C represents the fractions for each type of control rod, S represents the state variables of the current node, N represents state variables of the neighbor node, and H represents the history variables with the burnup.

As gathered from Equation 4.9, a reference cross-section is modified with contributions from the control rod insertion and from the other independent variables which are determined by using the product of a partial cross-section, $\partial\Sigma/\partial x$, and the amount of the perturbation for each independent variable.

The partial derivatives of cross-sections are taken at the mid-point between the reference state and the current node state. These partials are obtained by piece-wise interpolating the pre-tabulated data and providing a second-order accurate cross-section's estimate.

At this point, it is worth mentioning that the sequence of independent variables in Equation 4.8 and Equation 4.9 is far from being random. Actually, it is fixed and essential for organizing the data in the PMAXS file.

The 12 independent instantaneous variables (listed below in the specific order that should be provided) that PMAXS and PARCS currently accept are:

1) CR control rod fraction (required).
2) DC density of coolant.
3) PC soluble poison concentration in coolant.
4) TF temperature of fuel.
5) TC temperature of coolant.
6) IC impurity of coolant.
7) DM density of moderator.
8) PM soluble poison concentration in moderator.
9) TM temperature of moderator.
10) IM impurity of moderator.
11) DN density difference between neighbor and current assembly.
12) BN burnup difference between neighbor and current assembly.

This sequence was established based on the magnitude of the dependencies of the neutronic properties with respect to these variables as summarized in Table 4.1.

Table 4.1. Dependencies of k_{inf} Partial Derivatives to Each Variable.

Source: GenPMAXS Manual (Downar, T. & Xu, Y., 2004).

	k_{inf}	$\partial k_{inf}/\partial D_c$	$\partial k_{inf}/\partial P_c$	$\partial k_{inf}/\partial \sqrt{T_f}$	$\partial k_{inf}/\partial T_c$
D_c	Very strong	Very strong	Very strong	Strong	Very strong
P_c	Strong	Very strong	Mild	Mild	Very strong
$\sqrt{T_f}$	Mild	Strong	Weak	Weak	Strong
T_c	Weak	Weak	Almost none	Almost none	Very strong

Since the data is structured in a macroscopic cross-section format as a function of the state variables, the history variables, and the burnup, several PMAXS requirements must be fulfilled such as:

1) Every branch, except the reference branch, should have a base branch. The base branch has reference values for the variables of the current branch and the same state values as the current branch for all other state variables. This requires all branches must be derived from the reference branch by changing one state variable for each branch from its base branch.
2) All histories have the same branches which include the number of branches and the state value of each branch.

3) The same branch in different histories should have the same burnup points.

4.5.1 Generating Branches.

Since the process of generating branches can be easily misunderstood, it could be handy to employ an example while going through the explanation.

Let us imagine that there are six states at which cross-sections are provided from the lattice code. The starting point is to select the reference state, labeled as Ref. The states with reference parameters but with control rods inserted are called control rod branches and labeled as CR.

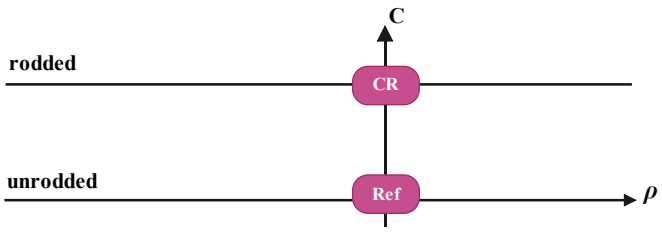

The values of the independent variables at this state are assigned as reference values and directly stored in the reference branch as raw cross-section data. The difference of the cross-sections between the CR state and the Ref state are stored in the control rod (rodded) branch and the partial derivatives of cross-section differences with respect to the rod fraction are computed and stored.

Next, a brand-new branch state needs to be created by changing the value of one independent variable from the reference state or from any branch state already generated by this process. This branch will be named after the variable that has been changed for generating this branch state (Control Rod (CR) branch, Density Coolant (DC) branch, Fuel Temperature (TF) branch, and so on and so forth).

On the other hand, the changed variable is referred to as a branch variable for this type of branch. The branch states in each type of branch have reference values for all independent variables after the branch variable and, a value different from the reference value is used for the branch variable.

Continuing with our example, as shown below, the moderator/coolant density has been selected as the variable to be modified generating four additional conditions labeled as DC_1, DC_2, DC_3, DC_4.

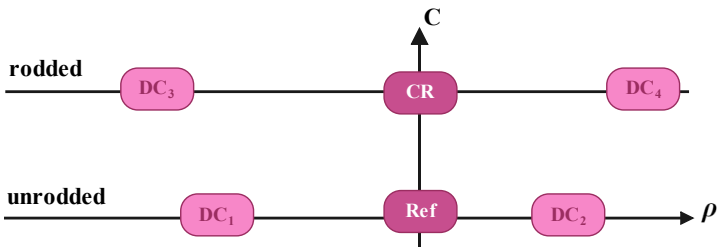

These four brand-new branches are called the density branches of the moderator density branch state, and the moderator density is the branch variable of the moderator density branch. The partial derivatives for the mid-point between a branch state and its base state are stored in the branch. These partial derivatives are computed by second order central differencing as

$$\left.\frac{\partial \Sigma}{\partial x_k}\right|_{X^m} = \frac{\Sigma\left(X^i\right) - \Sigma\left(X^{B(i)}\right)}{x_k^i - x_k^r} \qquad \textbf{Equation 4.10}$$

Where $X^i = \left(X_1^i, X_2^i, \ldots, X_n^i\right)$ is the vector for the variables of state i, $X^{B(i)}$ is the vector for the variables of the base state of state i, X^m is the vector for the mid-point between state i and its base state r, and x_k is the branch variable of state i.

Therefore, the partial derivatives with respect to the moderator density are computed with data from the six states and stored as four branch cases as DC_{1m}, DC_{2m}, DC_{3m}, and DC_{4m}. At this point, all branches have already been created and it would be possible to calculate the cross-sections at any given point.

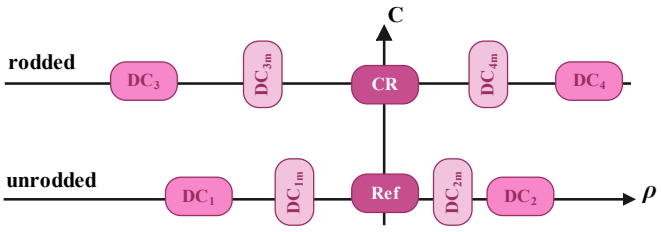

Going back to our example, let us compute the **cross-section for Point 1** at given conditions (c, DC),

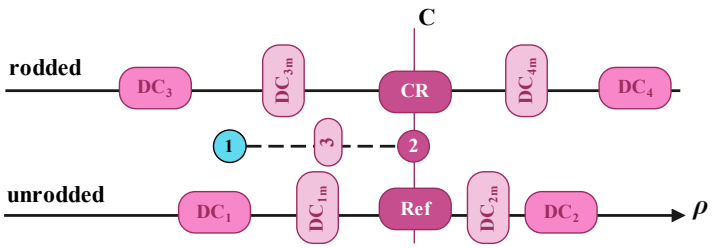

Source: GenPMAXS Manual (Downar, T. & Xu, Y., 2004).

Figure 4.9. Example of Computing Cross-Sections at the Desired Point 1.

Yet, the feedback formulation can be simplified as

$$\Sigma(c, DC) = \Sigma^{ref} + c\frac{\partial\Sigma}{\partial Cr}\Big|_{(Cr/2)} + (DC - DC^r)\frac{\partial\Sigma}{\partial DC}\Big|_{(c,DC_m)} \qquad \textbf{Equation 4.11}$$

The first term on the right-hand side of the equation, Σ^{ref}, is the cross-section at the reference state. The second term is the contribution from insertion of the control rod (depicted as Point 2 in Figure 4.9). The third term is the density of coolant term and is computed as the difference between Point 1 and Point 2.

The partial derivative with respect to density of coolant at Point 3 is obtained by linear interpolation between the partial derivatives with respect to moderator density at DC_{1m}, DC_{2m}, DC_{3m}, and DC_{4m}.

An important observation needs to be addressed before going further on the explanation. Even though the derivatives are defined at the mid-point, the state variable values for the midway-point are not used in the interpolation. Only the values of the original states are used, and therefore only the values of the original states are stored as branch information in PMAXS.

Thus, the formula for computing the partial derivative is given by:

$$\frac{\partial\Sigma}{\partial DC}\Big|_{(c,DC_m)} = w_1\frac{\partial\Sigma}{\partial DC}\Big|_{(0,DC_{1m})} + w_2\frac{\partial\Sigma}{\partial DC}\Big|_{(0,DC_{2m})} + w_3\frac{\partial\Sigma}{\partial DC}\Big|_{(1,DC_{3m})} + w_4\frac{\partial\Sigma}{\partial DC}\Big|_{(1,DC_{4m})} \qquad \textbf{Equation 4.12}$$

Where the weights for the four points are determined by linear interpolation as

$$w_1 = (1-c)\frac{DC - DC_2}{DC_1 - DC_2} \qquad w_2 = (1-c)\left(1 - \frac{DC - DC_2}{DC_1 - DC_2}\right)$$
$$w_3 = c\frac{DC - DC_4}{DC_3 - DC_4} \qquad w_4 = c\left(1 - \frac{DC - DC_4}{DC_3 - DC_4}\right)$$

Although the branch cases have a multi-dimensional structure, they are listed sequentially as one-dimensional cases in PMAXS with the branch information given at the beginning of each file.

4.5.2 Generating Histories.

The dependencies of the cross-section data to the history variables (except burnup) are treated with partial derivatives with respect to these history variables as follows:

$$\Sigma(\bar{H},B) = \Sigma(\bar{H}^r,B) + \sum_{j=2}^{nh} \Delta h_j \left.\frac{\partial \Sigma}{\partial h_j}\right|_{(\bar{H}_j^m,B)} \qquad \textbf{Equation 4.13}$$

Where Σ represents the cross-sections at reference state and all partial derivations with respect to all instantaneous variables which are needed in Equation 4.8, $\bar{H}^r = (h_1^r, \dots, h_{nh}^r)$ is the reference history state, $\bar{H} = (h_1, \dots, h_{nh})$ is the combination of all history variables except burnup, which represents the history state of interest, and $\bar{H}_j^m = (h_1, \dots, h_{j-1,}(h_j + h_j^r)/2, +h_{j+1}^r, \dots, h_{nh}^r)$ accounts for the middle point between $\bar{H}$ and $\bar{H}^r$ with respect to the j^{th} history value $\Delta h_j = h_j + h_j^r$.

History dependences and the burnup dependence of the cross-section data are treated by piece-wise linear interpolation. Thus, the cross-section data at burnup b is computed as:

$$\Sigma^i(\bar{H}^j, b) = \frac{b_k^{i,j} - b}{b_k^{i,j} - b_{k-1}^{i,j}} \Sigma^i(\bar{H}^j, b_{k-1}^{i,j}) + \frac{b - b_k^{i,j}}{b_k^{i,j} - b_{k-1}^{i,j}} \Sigma^i(\bar{H}^j, b_k^{i,j}) \qquad \textbf{Equation 4.14}$$

Where Σ^i represents the cross-section data in i^{th} branch, $\bar{H}^j$ history case of j^{th}history case, $b_k^{i,j}$ is first burnup point in i^{th} branch of j^{th} history case which be greater than b.

Employing a procedure analogous to that used for generating branches, let us imagine that the **cross-section at Point 13**, depicted in Figure 4.10, needs to be addressed. In order to accurately determine the cross-section at Point 13, it is needed to identify both historical and instantaneous conditions that will impact the calculation for this specific point.

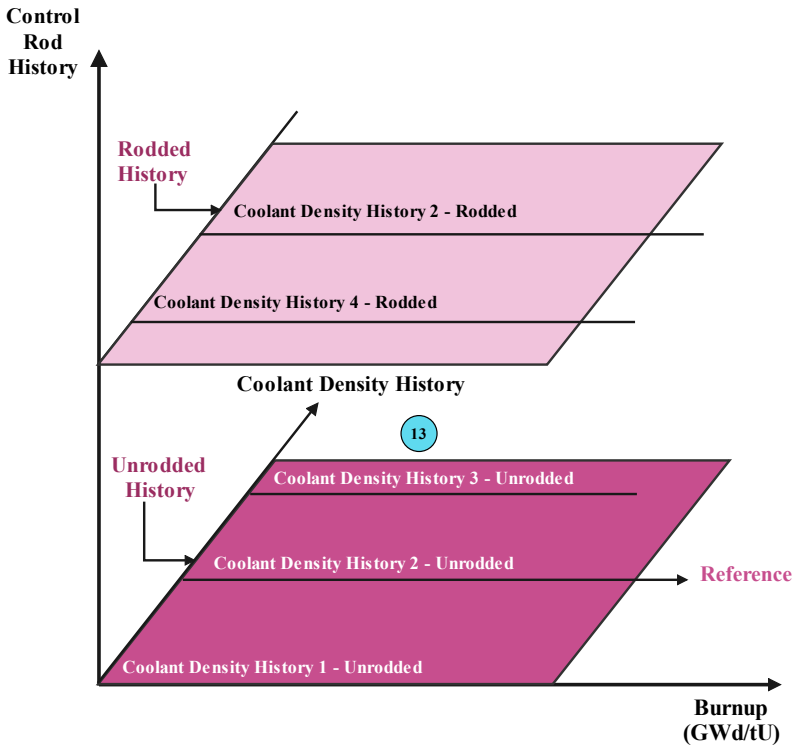

Figure 4.10. Example of Computing History Dependence for Point 13.

In the example shown in Figure 4.10, control rod history and coolant density history are taken as the first and second history variables, respectively. The fuel burnup will always be the last history variable in the tree-structure of PMAXS as was already illustrated in Figure 4.8.

The calculation begins by identifying the points associated with the reference history case, corresponding to the *Unrodded Coolant Density History 2* marked in Figure 4.10.

These identified points, denoted as Points 3, 4, and 5 (highlighted in dark blue) in Figure 4.11, serve as the reference for the analysis. By establishing this framework, a comprehensive understanding of the factors influencing the cross-section at Point 13 is ensured.

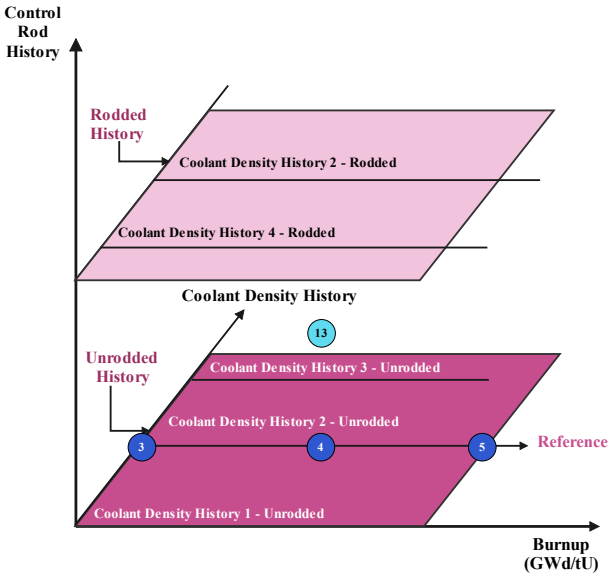

Figure 4.11. Example of Computing History Dependence for Point 13. Step #1.

Subsequently, the points associated with the *Rodded Coolant Density History 2* are identified. These points are marked in yellow and designated as Points 10, 11, and 12, respectively, in Figure 4.12.

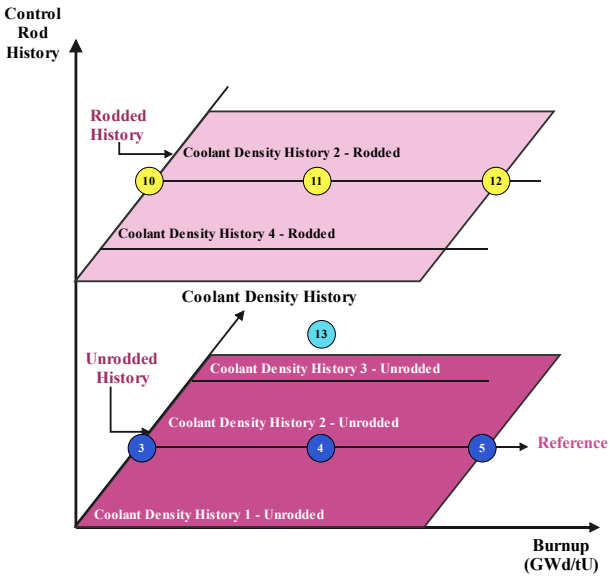

Figure 4.12. Example of Computing History Dependence for Point 13. Step #2.

After acquiring the pertinent points for the rodded/unrodded reference histories, the next step involves identifying additional points associated with the remaining *Coolant Density History Cases* 1, 3, and 4.

These points, marked in green, are illustrated in Figure 4.13.

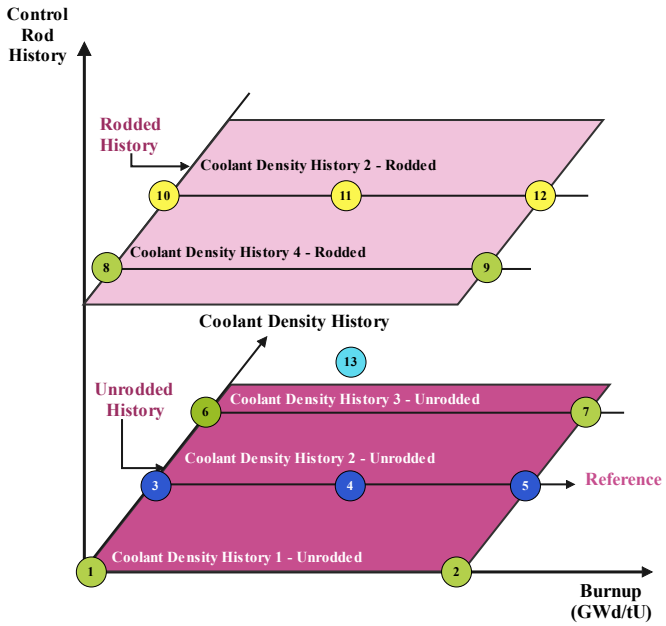

Figure 4.13. Example of Computing History Dependence for Point 13. Step #3.

Note that the locations of the history state points in PMAXS can be irregular as described in the GenPMAXS Manual (Downar, T. & Xu, Y., 2004).

Hence, to fully characterize the cross-sections at Point 13 with respect to the historical variables, a total of 12 burnup points categorized into 5 history cases are used.

Once these historical parameters are identified, the instantaneous variables, their linear interpolations, and the corresponding partial derivatives must be addressed.

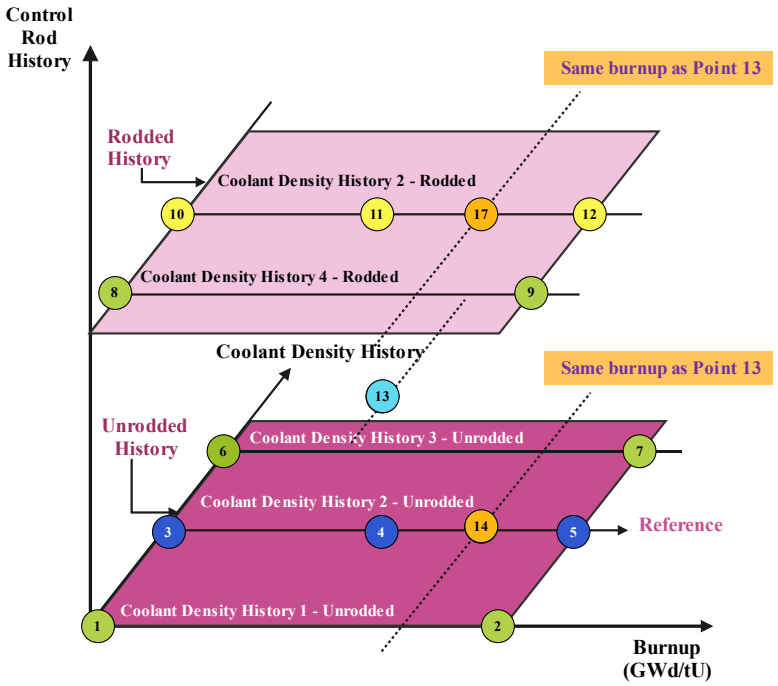

Figure 4.14. Example of Computing History Dependence for Point 13. Step #4.

This procedure commences with the calculation of Points 14 and 17, situated in the reference history case and the rodded reference history plane, respectively, as depicted in Figure 4.14. These points are selected due to their matching burnup with Point 13.

Point 14 is determined through linear interpolation between Points 4 and 5, while Point 17 is computed via linear interpolation between Points 11 and 12.

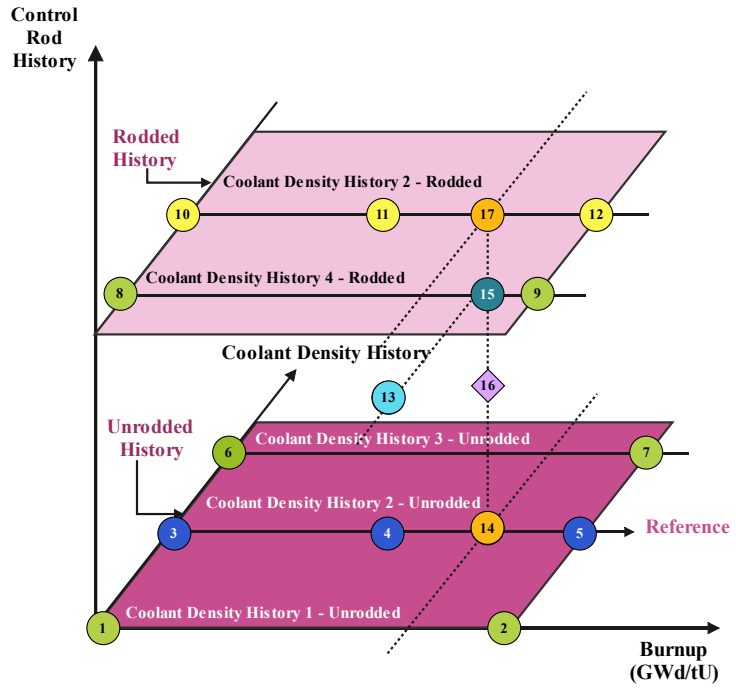

Figure 4.15. Example of Computing History Dependence for Point 13. Step #5.

Drawing from the branch generation section, it becomes evident that Point 15 is essential for obtaining the cross-section for Point 13 given their shared control rod history as seen in Figure 4.15.

Point 15, situated at the same coolant density history as Point 14, is computed using Point 16, which in turn is determined by Points 14 and 17. This step-by-step process ensures the accurate determination of cross-sections for Point 13.

Last step involves calculating all necessary linear interpolations, indicated by orange circles, and partial differences, denoted by violet rhombuses, as depicted in Figure 4.16.

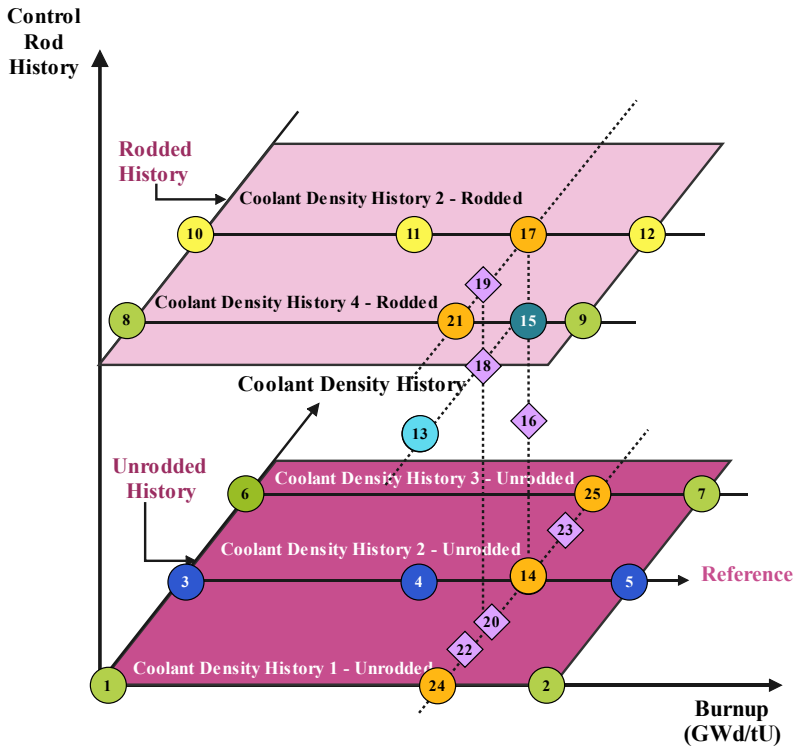

Source: GenPMAXS Manual (Downar, T. & Xu, Y., 2004).

Figure 4.16. Summary of Computing History Dependence for Point 13.

The cross-section data at Points 1, 2 and 6, 7 serve as the basis for calculating the cross-sections at Points 24 and 25 through linear interpolation.

Cross-section data at Point 21 is determined via linear interpolation between Points 8 and 9.

Partials at Point 19 are obtained by finite differencing between Points 14 and 21.

The partials at Point 20 are computed by linear interpolation between the partials at Points 22 and 23 which require cross-sections at Points 14, 24 and 25.

Point 18 is obtained by linear interpolation between Points 19 and 20.

Finally, Point 13 is determined by summing the products of the difference in coolant density history between Points 13 and 15 and the partial derivatives concerning moderator density history at Point 18.

In summary, to characterize the cross-sections at Point 13, a total of 24 points categorized into history cases, instantaneous branches, linear interpolation and partial derivates are utilized.

4.5.3 PMAX Data Structure.

After scanning the history and branch information from the lattice code file, GenPMAXS builds the PMAXS branch structure, maps the input branches to the PMAXS branches, reads cross-section data of the input branches from the lattice file, and generates cross-sections for reference branches of all histories and partial derivatives for all other branches of PMAXS.

This is performed by following this sequence:

1) A branch is selected as the reference branch from all branches in all histories which is closest to the desired reference state. The reference state is specified in the input file by the user.
2) Select a history from all histories which has state values closest to the reference state as the reference history.
3) Construct a PMAXS branch structure with the information from the branches in the reference history.
4) Map input branches in the non-reference history to PMAXS branches.
5) Generate cross-section partials for all non-reference branches in the reference history moving backwards from the last type of the branch to the first type.
6) Generate cross-section partials for all non-reference branches in the non-reference history and if necessary, create or correct cross-section data for the reference branch in non-reference histories. As in the previous steps, the branches are processed backwards, from the last type to the first.

Using this process, all input branches of the reference history are mapped to PMAXS branches and expected to be reproduced when needed by PARCS. All the information contained in the PMAXS file is structured in a hierarchical system as illustrated in Figure 4.17. Kinetic parameters are treated as history- and burnup-dependent only parameters.

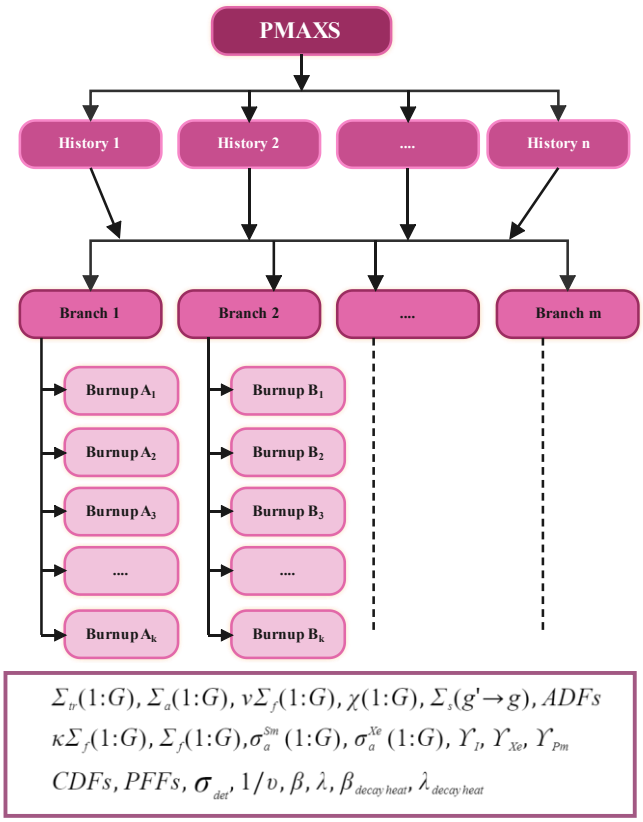

Figure 4.17. PMAXS' Data Structure.

4.6 Generating PMAXS files from CASMO-4.

In the standard industrial approach, the generation of PMAXS cross-section files from CASMO-4 results typically involves using the S3C option, as documented in the available literature (Hursin et al., 2017).

This option automatically establishes a hierarchical structure for branch and history calculations, covering the various reactor states encountered during steady-state and transient analyses. This structure is utilized to construct the library, incorporating both micro and macroscopic cross-sections derived from CASMO-4 calculations. Further information on the S3C history/branch structure can be found in CASMO-4 manual (Rhodes, J. & Edenius, M., 2004).

During CASMO-4 calculations, the output data, known as CAX files, are organized into blocks containing cross-section data and state values for history and branch cases. The thermal-hydraulic model of SIMULATE-3 provides the

thermal-hydraulic conditions for each node within the reactor, which are subsequently used to obtain nodal cross-section values.

The conversion of data from the CASMO-4/SIMULATE-3 framework to the PARCS framework is a non-trivial task due to differences in data representation (Stålek & Demazière, 2008). According to (Ver Planck, D.M. et al., 1995), each material constant P (namely macro and micro cross-section, discontinuity factor, and fission products and detector data) can be expressed as:

$$P(A,B,C) = P(A_0,B_0,C_0) + \Delta P_A(A) + \Delta P_B(A,B) + \Delta P_C(A,B,C) \qquad \textbf{Equation 4.15}$$

Where $P(A_0,B_0,C_0)$ is the base value and

$$\Delta P_A(A) = \int_{A_0}^{A} \frac{\partial}{\partial A'} P(A',B_0,C_0)dA' \qquad \textbf{Equation 4.16}$$

A' being the primary variable,

$$\Delta P_B(B) = \int_{B_0}^{B} \frac{\partial}{\partial B'} P(A,B',C_0)dB' \qquad \textbf{Equation 4.17}$$

B' being the primary variable and A the secondary variable, and

$$\Delta P_C(C) = \int_{C_0}^{C} \frac{\partial}{\partial C'} P(A,B,C')dC' \qquad \textbf{Equation 4.18}$$

C' being the primary variable, B the secondary variable, and A the tertiary variable.

Thus, given the last four equations, it could be expected that the CASMO-4 raw multi-dimensional data are obtained by adding a series of tables with partial functions. Whether data from the CASMO-4 lattice calculations are not available for constructing the tables, second-order Lagrangian interpolation is used to generate the missing values. The data construction can be graphically represented as

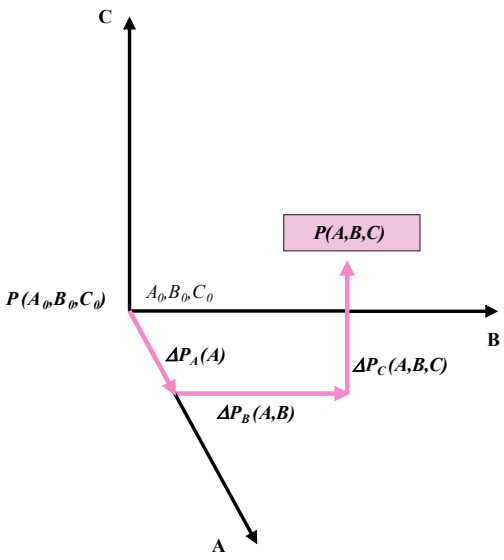

Source: (Demazière, C. et al., 2012).

Figure 4.18. Construction of the Two-group Cross-sections in CASMO-4/SIMULATE-3.

Then, the additional dependencies of the data are modeled by 1D tables of the derivatives of the data as a function of burnup, b, and can be expressed in a generic form as

$$P(b, B, C, \ldots\ldots, Z) = P(b, B_0, C_0, \ldots\ldots, Z_0) + \Delta P_B(b) + \Delta P_C(b) + \cdots + \Delta P_Z(b) \qquad \textbf{Equation 4.19}$$

where

$$\Delta P_B(b) = \int_{B_0}^{B} \frac{\partial}{\partial B'} P(b, B', C_0, \ldots\ldots, Z_0) dB'$$

$$\Delta P_C(b) = \int_{C_0}^{C} \frac{\partial}{\partial C'} P(b, B_0, C', \ldots\ldots, Z_0) dC' \qquad \textbf{Equation 4.20}$$

$$\Delta P_Z(b) = \int_{Z_0}^{Z} \frac{\partial}{\partial Z'} P(b, B_0, C_0, \ldots\ldots, Z') dZ'$$

Table 4.2 contains an example of the histories and branches for a typical BWR fuel assembly from the CASMO-4 S3C automatic history/branch matrix card. In this example, the moderator temperature is never intended to change by itself and changes together with the moderator density and the fuel temperature.

Table 4.2. Example of Histories and Branches for BWR Fuel Assembly with S3C Card.

Source: GenPMAXS Manual (Downar, T. & Xu, Y., 2004).

Index	Descriptions	CR	DC	PC	TF	TC
1	H1	0	0.738	0	813	560
2	DC	0	0.458	0	813	560
3	DC	0	0.177	0	813	560
4	CR	1	0.738	0	813	560
5	TF	0	0.738	0	560	560
6	DC/TF/TC	0	0.998	0	293	293
7	CR/DC/TF	1	0.998	0	293	293
1	H2	0	0.458	0	813	560
2	DC	0	0.738	0	813	560
3	DC	0	0.177	0	813	560
4	CR	1	0.458	0	813	560
5	TF	0	0.458	0	560	560
6	DC/TF/TC	0	0.998	0	293	293
7	CR/DC/TF/TC	1	0.972	0	353	353
1	H3	0	0.177	0	813	560
2	DC	0	0.738	0	813	560
3	DC	0	0.458	0	813	560
4	CR	1	0.177	0	813	560
5	TF	0	0.177	0	560	560
6	DC/TF/TC	0	0.998	0	293	293
7	CR/DC/TF	1	0.998	0	293	293
8	DC/TF/TC	0	0.972	0	353	353
9	DC/TF/TC	0	0.862	0	475	475
10	CR/DC/TF/TC	1	0.972	0	353	353
11	CR/DC/TF/TC	1	0.862	0	475	475
12	DC/PC/TF/TC	0	0.998	0.1	293	293
13	DC/PC/TF/TC	0	0.998	660	293	293
1	H4	1	0.458	0	560	560
1	H5	1	0.458	0	813	560
2	CR	0	0.458	0	813	560

As seen, there are still two or three variables changed in the same branch so the branch structure can be different from the input branch structure in PMAXS which

strongly encourages one change at a time. The mapping of input branches to PMAXS branches for all histories is given in Table 4.3.

Table 4.3. Branch Mapping for all Histories of BWR Fuel Assembly.

Source: GenPMAXS Manual (Downar, T. & Xu, Y., 2004).

PMAXS Index	CAX Index	Type	CR	DC	PC	TF
Reference History						
1	1	RE	0	0.458	0	813
2	4	CR	1	0.458	0	813
3	2	DC	0	0.738	0	813
4	3	DC	0	0.177	0	813
5	6	DC	0	0.998	0	293/813
6	7	DC	1	0.998	0	293/813
7	5	TF	0	0.458	0	560
CR History						
1	2	RE5	0	0.458	0	813
2	1	CR	1	0.458	0	813
Lower DC History						
1	3	RE3	0	0.458	0	813
2	4	CR	1	0.177/0.458	0	813
3	2	DC	0	0.738	0	813
4	1	DC	0	0.177	0	813
5	6	DC	0	0.998	0	293/813
6	7	DC	1	0.998	0	293/813
7	5	TF	0	0.177/0.458	0	560
Higher DC History						
1	2	RE1	0	0.458	0	813
2	4	CR	1	0.738/0.458	0	813
3	1	DC	0	0.738	0	813
4	3	DC	0	0.177	0	813
5	6	DC	0	0.998	0	293/813
6	7	DC	1	0.998	0	293/813
7	5	TF	0	0.738/0.458	0	560
TF History						
1	1	TF4	0	0.458	0	560

As noted, not all input branches in non-reference histories are mapped in PMAXS, or even some PMAXS branches may lack corresponding input branches due to potential differences in the number of branches. Specifically, CR and TF histories have fewer branches than the reference history, and there are multiple input branches in the lower density history that are not mapped to PMAXS branches.

This situation results in CAX files generated by the S3C expansion approach potentially containing histories and branches that do not meet PMAXS requirements and thus cannot be directly converted to PMAXS. Indeed, several PARCS calculations using S3C PMAXS files have been reported as failing to converge, highlighting that the S3C branch/history sets may not be suitable for PARCS models, as discussed in (Hursin et al., 2017).

These identified issues served as the catalyst for the in-depth examination of cross-section modeling for BWRs presented in this dissertation.

4.6.1 Verification and Validation Procedure of the PMAXS Files.

The lack of compatibility between the data formats of the PMAXS files and SIMULATE-3 library files presents a significant challenge in converting between the two formats. While not a critical issue, it necessitates a meticulous process to ensure accurate reconstruction of data from CASMO-4 in order to utilize the cross-section sets for practical applications in PARCS. Consequently, each cross-section set must undergo thorough verification and validation.

The verification procedure involves retrieving data from the SIMULATE-3 library file, encompassing all feasible combinations of instantaneous variables, history variables, and burnup values. Subsequently, PARCS input files are constructed for each variable set.

Considering the extensive number of combinations due to dependencies on history and instantaneous variables, manual execution of this process is impractical and laborious. Therefore, to ensure pragmatic and efficient operations, a Python program was developed for automated validation of the cross-sections.

The program reads the content of the PMAXS files and extracts information pertaining to history conditions and instantaneous variables. It subsequently generates PARCS input files, assuming a single segment in the core at a time and neglecting reactor leakages. This validation process employs an infinite homogeneous reactor, with the infinite multiplication factor, k_∞, serving as the performance indicator. Once the input is prepared, PARCS is executed.

The k_∞ value calculated by PARCS must precisely match the one computed by CASMO-4 under identical conditions and burnup. If this requirement is met, the cross-sections are deemed valid. Conversely, if the k_∞ values differ, the cross-sections are considered invalid, necessitating the calculation of new sets before performing whole core calculations.

This verification and validation procedure for cross-section sets has been previously employed and documented in other studies (Demazière, C. et al., 2012).

4.7 Cross-section Generation Guidelines for BWRs.

The intricate interplay between neutrons, fuel, and coolant within a nuclear reactor core forms the cornerstone of nuclear power generation. Fission events, primarily initiated by thermal neutrons, are heavily influenced by the temperature of the fuel. Accurate calculations of cross-sections, fundamental to understanding neutron interactions, necessitate precise knowledge of fuel temperature. Concurrently, the coolant within the reactor core serves a pivotal role as a neutron moderator, contributing significantly to the overall feedback mechanism.

Notably, changes in coolant density or control rod positions not only impact burnup but also induce shifts in the neutron spectrum, thereby affecting the distribution of plutonium and fission product inventories. These phenomena have been extensively discussed in literature, reference (Silvennoinen, P., 1976).

In a typical BWR core under normal operating conditions, the moderator/coolant transitions from a liquid state in the lower regions to a steam phase in the upper areas. This transition leads to a substantial change in moderator density from the inlet to the outlet core fuel assembly. To accurately capture the behavior of the fuel throughout its operational lifespan, cross-section sets must encompass a comprehensive range of core conditions such as:

- different instantaneous and history void fractions to simulate the spatial variation of the moderator density,
- different moderator and fuel temperatures due to double effect: to simulate different condition, configuration, and operation points of the reactor and to account for phenomena such as the Doppler effects,
- the presence of control rods, and
- burnup/depletion.

As the water flows through the core and the boiling occurs, its subcooled conditions at the inlet, with a corresponding density of about 0.76 g/cm^3, will be varied all the way up to the outlet, with a related density of about 0.2 g/cm^3, with an average density that is typically around 0.43 g/cm^3.

Therefore, a wide range of moderator density distribution must be considered for the instantaneous and the history effects while generating cross-sections because, as already stated during the whole chapter, the void fraction is the major contributor of the feedback effect on the axial power distribution in a BWR. Also, the impact of control rod history needs to be handled, as pointed out while discussing the history effects in Subsection 4.2.2.

For industrial applications, the standard approach taken for a coupled fuel/fluid/neutronics analysis is to calculate the fuel temperature, moderator density, and soluble boron concentration (if applicable) by the thermal-hydraulic code. The control fraction is provided, via input, to the neutronics code. All those parameters need to be considered to estimate the instantaneous cross-sections.

The historic control rod and moderator density values are provided by a steady-state core-follow simulator, which has followed the core operation since the initial loading up to the time of the transient to be calculated.

Therefore, it seems reasonable that, to perform a specific calculation, one would choose the cross-section set that applies best to the problem. In this way, the US Nuclear Regulatory Commission (NRC) released in 2012 a cross-section generation guidance report (NUREG/CR-7164 (Wang, D. et al., 2013)) whose main objective was to answer the question of *"how many histories and branches were sufficient to have converged results applicable for BWR analysis"*. The given guidelines came as a result of a comparison of several cross-sections sets calculated using different methodologies and codes and were intended to be applicable to all BWR designs.

In order to furnish some quantitative insight into the BWR cross-section modeling, the NUREG/CR-7164 generated three cross-section sets with CASMO-4, HELIOS, and TRITON, and converted them to PMAXS format files to perform TRACE/PARCS calculations using three different BWRs models, which were:

1) Single-CHAN model,
2) Oskarshamn plant model, and
3) Ringhals plant model.

Cross-section-wise, a Peach Bottom fuel type with the 7×7 lattice was chosen for this study due to the availability of the data. All the fuel specifications regarding the performed cross-section sensitivity analysis, as well as the three BWR model detailed descriptions, are available at the reference (Wang, D. et al., 2013).

To conduct the study, it was found appropriate to cover the moderator density ranges from 0.03591 g/cm^3 (100% void) up to 0.73808 g/cm^3 (0% void) in 10% void spacing. Besides, there was one additional density at 1.0 g/cm^3 for representing cold depressurized conditions.

Thus, the cross-section set consisted of 12 uncontrolled history coolant densities (HDCs, Cr = 0) and 12 controlled (HDCs, Cr = 1), each history having 12 coolant densities (DC) branches, see Figure 4.19. This cross-section set was used as the reference PMAXS file.

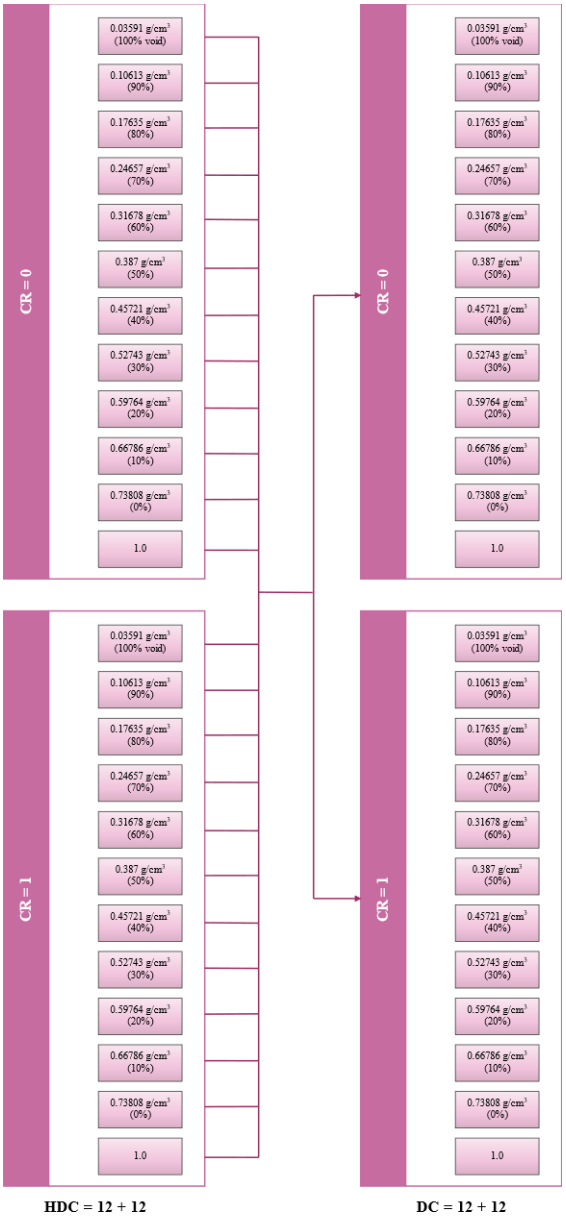

Source: NUREG-CR7164 (Wang, D. et al., 2013).

Figure 4.19. PMAXS Histories (HDC) and Instantaneous Moderator Density Branches (DC). NUREG-CR7164 Reference Case.

For the sensitivity analysis of instantaneous and history effects, the PMAXS reference file was broken down into small PMAXS files to estimate how many

branches and histories were providing similar results to the reference one. All the subdivided PMAXS files are described in (Wang, D. et al., 2013).

The results for the steady-state and transient calculations were compared for each history, including HDC and HCR, and each branch by means of the core eigenvalue (k_{eff}), the 3D power peaking factor (P_{xyz}), the core radial assembly power peaking factor (P_{xy}), and the core axial power peaking factor (P_z).

The radial peaking factor is defined as the power in hot channel divided by the power in average channel. The axial peaking factor is defined as the ratio of the maximum heat power to the average heat flux. Both are helpful indicators of the state of the core and, therefore, were selected to compare the different cross-section sets and to draw conclusions from the obtained results.

However, little regard was devoted to the axial and radial power profiles while performing the study. As it will be seen further in the next chapter, both power profiles will be differential elements when modeling cross-sections.

Going back to the modeling guidelines, the main conclusion extracted from the history analysis was that neither steady-states nor transients were susceptible to the DC and CR histories. On the other hand, the branch effect analysis showed that, even though steady-states might not be highly sensitive to the DC branches, the transients show sensitivity, particularly in the core upper region, if the void fraction is above the range of the DC branches.

Based on the above-mentioned results, the NUREG/CR-7164 recommendations were as follows, see Figure 4.20.

1) For the **history** effect, three moderator density values at **0**, **40**, and **70%** at a single **950 K** fuel temperature.
2) Four **instantaneous** moderator density values at **0**,**40**, **70,** and **90%** void fraction.
3) Three **instantaneous** fuel temperatures of **500**, **950**, and **1500 K**.
4) For **all cases**, branches for **controlled** and **uncontrolled** bundles are needed.

In addition:

1) A coolant density branch for accurately modelling **cold depressurized** conditions.
2) If **boron** injection is needed, boron branches should be included.

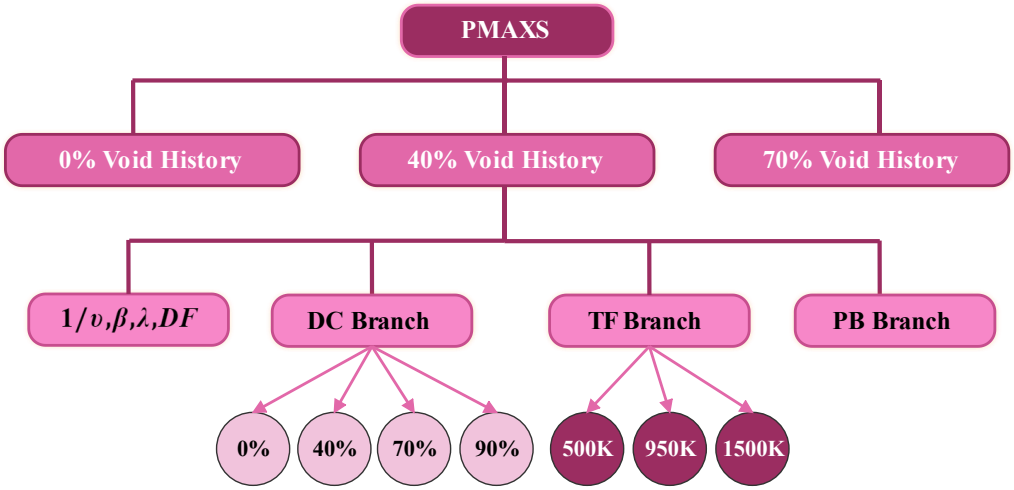

Source: NUREG-CR7164 (Wang, D. et al., 2013).

Figure 4.20. Example of PMAXS Structure following the NUREG/CR-7164 Guidelines.

Furthermore, general assumptions for the moderator density, the moderator temperature, and the cross-term effect treatments have to be considered while modeling cross-sections for BWRs.

Those assumptions, which are not explicitly provided by the NUREG/CR-7164 but have been reported in different cross-section's modeling previous works, reference (Fujita et al., 2014; Cacuci, D. G. (Ed.)., 2010), are as follows:

1) The selected saturation temperature at the reactor pressure normal operation conditions (about 70 MPa) corresponds to 561.4 K.
2) The moderator temperature will remain constant at 561.4 K for void fractions higher than 0%.
3) The void fraction will remain constant at 0% for moderator temperatures lower than the saturation temperature.

These assumptions are supported by the fact that in BWRs, at hot operating conditions, the coolant enters the reactor at a slightly subcooled temperature but reaches saturation conditions within the first three nodes of the bottom of the core. Once the temperature reaches saturation conditions, it does not change and all heat from the fuel goes into boiling the water.

Therefore, there is no cross-section dependence on moderator temperature at operating conditions and the moderator temperature dependence comes into play mostly at coast-down or shutdown conditions.

On the other hand, unlike PWRs, BWRs can go critical at any zero-power temperature. Thus, the lattice code will have to generate enough cross-section data for

accurately modeling criticality conditions beyond normal conditions, i.e., Hot Zero Power (HZP) conditions. This is usually doable by selecting temperatures between cold conditions (293 K) and HZP conditions (561.4 K).

Overall, for most BWR applications, the PMAXS structure shown in Table 4.4 and Table 4.5 would provide sufficiently accurate results. Nonetheless, it must be highlighted that specific studies may require a different structure as a designer's task to ensure the applicability of the cross-section set to the particular application.

Table 4.4. Recommended History Branches.

Source: NUREG-CR7164 (Wang, D. et al., 2013).

Moderator Density (kg/cm^3)	Void (%) at 70 MPa	Control Rod (0 out/1 in)	Fuel Temperature (K)
738	0	0	950
457	40		
247	70		
738	0	1	
457	40		
247	70		

Table 4.5. Recommended Instantaneous Branches.

Source: NUREG-CR7164 (Wang, D. et al., 2013).

Moderator Density (kg/cm^3)	Void (%) at 70 MPa	Control Rod (out/in)	Fuel Temperature (K)
738	0	0	500 950 1500
457	40		
247	70		
106	90		
738	0	1	500 950 1500
457	40		
247	70		
106	90		
1000	0	0	293 500 950
		1	293 500 950

4.8 Summary.

The chapter discussion delves into the intricacies of neutronics modeling, which involves representing a physical reactor system using approximate numerical models. These models must accurately capture the reactor's behavior across a range of conditions, including steady-state and transient scenarios.

A critical component of neutronics modeling is the precise representation of cross-sections, which dictate the interactions of neutrons with the diverse materials within the reactor. This aspect is particularly crucial for BWR fuel assemblies due to their complexity arising from factors such as enrichment splitting and control rod insertion. Therefore, the careful selection and definition of cross-section sets are essential to ensure accurate core calculations.

Fuel depletion analysis plays a pivotal role in forecasting the long-term changes in reactor fuel composition resulting from burnup during operational phases and how these changes are compensated. Such predictions significantly influence the reactor's operational lifespan, stability, and control. Accurately capturing these changes requires

sophisticated models that account for local effects and historical data, ensuring that the predictions align closely with actual reactor behavior.

Moreover, the ability to confidently anticipate BWR core behavior - including eigenvalue, reactivity, and thermal limits - is of paramount importance in demanding operating domains such as Extended Power Uprate (EPU) and Maximum Extended Load Line Limit Analysis Plus (MELLLA+). The severe economic implications concerning cycle energy production and fuel costs for the operating fleet further underscore the necessity for accurate foresight.

To ensure precise calculations during transient scenarios, it is imperative to have a well-defined set of cross-sections capable of accurately representing the reactor's behavior under various conditions. The absence of an appropriate cross-section set may necessitate reliance on extrapolation or assumptions, potentially leading to non-physical, unrealistic, or inaccurate outcomes. Accurate cross-section data ensures reliable predictions and robust safety analyses, which are crucial for maintaining the integrity and efficiency of nuclear power plants.

The significance of properly capturing both local and historical effects cannot be overstated. Local effects pertain to the specific conditions within different parts of the reactor core, while historical effects involve the cumulative impact of past operational events and changes in fuel composition. Integrating these effects into neutronics models enhances the fidelity of simulations, leading to better predictions of reactor behavior.

NUREG-CR7164 serves as a pivotal guideline in this context, providing comprehensive methodologies and best practices for nuclear data processing and modeling. It emphasizes the importance of high-fidelity simulations and the use of advanced computational tools to improve the accuracy of reactor analyses. The insights from NUREG-CR7164 form the starting point of our studies, guiding the development of robust cross-section libraries and enhancing our understanding of reactor dynamics.

Chapter 5
Cross-section Modeling: Code-to-Code Results

5.1 Introduction.

The operation of BWRs has grown significantly more complex due to factors such as higher flow rates, increased power levels, advanced fuel designs, and intricate control blade manipulation. Concurrently, extending fuel cycles has narrowed the operational margins of these reactors. This convergence of factors underscores the heightened complexity and challenges inherent in analyzing BWRs.

Accurate prediction of reactor behavior under steady-state and transient conditions necessitates actual reactor data to assess simulation software performance, crucial for adhering to modern software quality standards.

Hence, this chapter seeks to evaluate the precision of the CASMO-4/GenPMAXS/PARCS computational sequence when analyzing modern BWR operation using currently available BWR fuels.

The sequence CASMO-4/GenPMAXS/PARCS has already been assessed for several types of reactors. Various reports and publications have been generated for PWRs and older BWRs regarding transient tests and depletion analysis for Peach

Bottom Unit 2 Cycles 1-3 (Choi et al., 2022), and Edwin Hatch Unit 1 Cycles 1-3 (Yarsky et al., 2013).

However, although these assessments are high quality, the operational approach to BWRs has changed dramatically since the 1980s when these reactors began operation.

Therefore, core-follows of two cycles of a BWR/6 reactor, designated as Cycle A and B, are modeled in PARCS and used to calculate core-follow eigenvalues alongside radial and axial assembly power distributions. Predictions by PARCS will be compared against the plant core-follow computer SIMULATE-3, serving as the reference for each simulated case.

Code-to-code benchmarks serve as an excellent verification tool. Given the extensive validation basis of the CASMO-4/SIMULATE-3 package, along with its widespread industrial applications, results are highly reliable, making code-to-code comparison a comprehensive analysis tool.

This code-to-code comparison is intended for steady-state performance parameters and two-group nuclear cross-sections for BWR fuel lattices and cores.

5.2 Study Cases: Cycles A & B.

Cycle A corresponds to a cycle running on a 12-month schedule with only two different mechanical fuel types at the core (named Types 1 & 2), corresponding to 9 unique segments of 2D fuel lattice neutronics configurations.

On the other hand, Cycle B is a 24-month length cycle with four different mechanical fuel types (Types 3 to 6). In this case, 70 CASMO-4 lattices altogether were calculated to produce the nuclear data library needed for Cycle B analysis.

The corresponding fuel bundle core loading pattern for both cycles is shown in Figure 5.1.

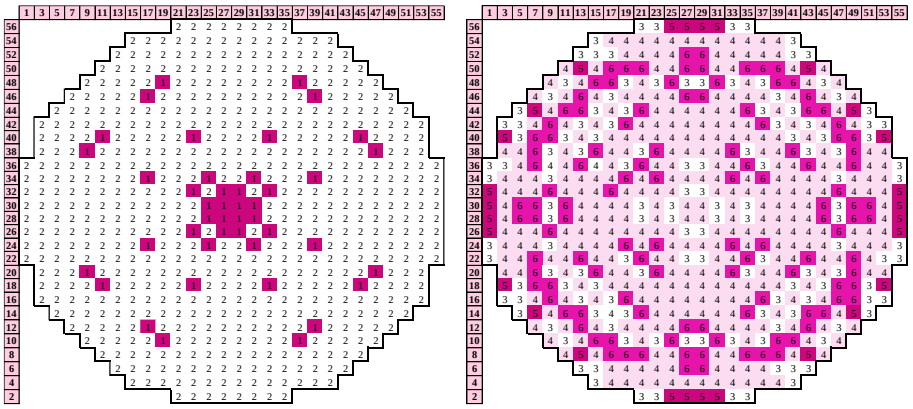

Figure 5.1. Core Fuel Loading Pattern for Cycles A (left) and B (right).

Although the core is intended to be loaded so that the power profile across the core is as flat as possible, individual assemblies do not all produce the same power. Instead, each assembly has a specific thermal power, depending on its fuel enrichment, poison content, and core location.

In practice, the online computer at the power plant records the fractions of average power produced by each assembly. These fractions are determined from signals proportional to the assembly power obtained by detectors periodically inserted in certain assemblies. In BWRs, these detectors are called Traversing In-core Probes (TIPs). The comparison between the measured and calculated data will be discussed in more detail in Chapter 6.

Bundle designs for a 12- or 24-month cycle length are quite different mainly because of the energy demand requirements. As expected, of the six mechanical fuel types, Types 1 and 2 correspond to the earliest fuel designs, 8x8 pin array types, with the lowest ^{235}U enrichment content and fewer gadolinia-rods.

Assembly 3 to 6 are a 10x10 pins per bundle configuration designs with internal water rods. The most important reason for increasing the number of pins in an assembly is to get a larger heat transfer area and, thereby, lower fuel temperature for a given power. Conversely, higher power in the assemblies can allow the reactor to run with a more optimized core design. The neutron leakage can be decreased by low-leakage loading, and the build-up of Pu can be increased by spectral shift operation.

Types 3 to 6 represent modern BWR fuel designs whose common feature is the use of multiple kinds of part-length fuel rods to get more moderator-to-uranium ratio in the upper part of the fuel and, thus, to increase the coolant flow in the upper regions of the flow channel.

Other features of modern fuel designs are complex water rod geometries within the bundles to get a smooth power distribution in the assembly and a significant loading of gadolinia-rods.

All six types have a heated length of 381 cm with axially varying average bundle enrichment and blankets of natural uranium at the top and bottom of the assembly to keep the neutron leakage down. Spacer grids have also been considered in the modeling and analysis.

The available data for Cycles A & B include two core-follow plant computer decks for near full power conditions, which provided all the thermal-hydraulic parameters of the plant with the operating conditions, i.e., power, flow rate, inlet temperature, and subcooling inlet enthalpy.

The main difficulty for Cycle A was the lack of complete operating data. The analysis will only consider the first half of the cycle just right before a shutdown condition due to a SCRAM event, which happened at around half of the scheduled cycle. The rest of the data for this cycle was unavailable and, thus, will be omitted.

While Cycle A only covers Beginning-Of-Cycle (BOC) up to Middle-Of-Cycle (MOC) conditions, Cycle B assesses a complete core-follow simulation, i.e., depletion

characteristics from the BOC through the End-Of-Cycle (EOC), including Coast-down conditions. For this cycle, the complexity of the core is mainly due to the high number of different fuel assembly types loaded from different vendors.

All histories, as well as the control rod pattern, are provided at each depletion step. This measured information is used to develop a PARCS model for both cycles.

Even though all the available depletion steps are modeled and compared against data, only a selected number of steps for both cycles will be shown and discussed herein. These steps have been chosen to cover as many characteristic and interesting cycle points as possible. The operating conditions of the selected steps are shown in Table 5.1.

Table 5.1. Selected Operating Condition Points.

Fuel Cycle	Core-Averaged Cycle Exposure (GWd/st)	Relative Power (%)	Relative Flow (%)
A	0.695 (5% Cycle Exposure)	101.9	81.0
A	2.536 (25%)	102.0	80.8
A	4.478 (50%)	101.9	82.5
B	0.891 (5% Cycle Exposure)	111.7	92.0
B	4.515 (25%)	111.9	90.1
B	9.100 (50%)	111.7	91.6
B	13.502 (75%)	111.3	95.2
B	15.908 (90%. Coast-Down Starts)	108.8	99.8
B	17.110 (95%)	104.4	99.5

The axial Relative Power Fraction (RPF) predicted by SIMULATE-3 at the analyzed cycle exposure conditions for both cycles is shown in Figure 5.2.

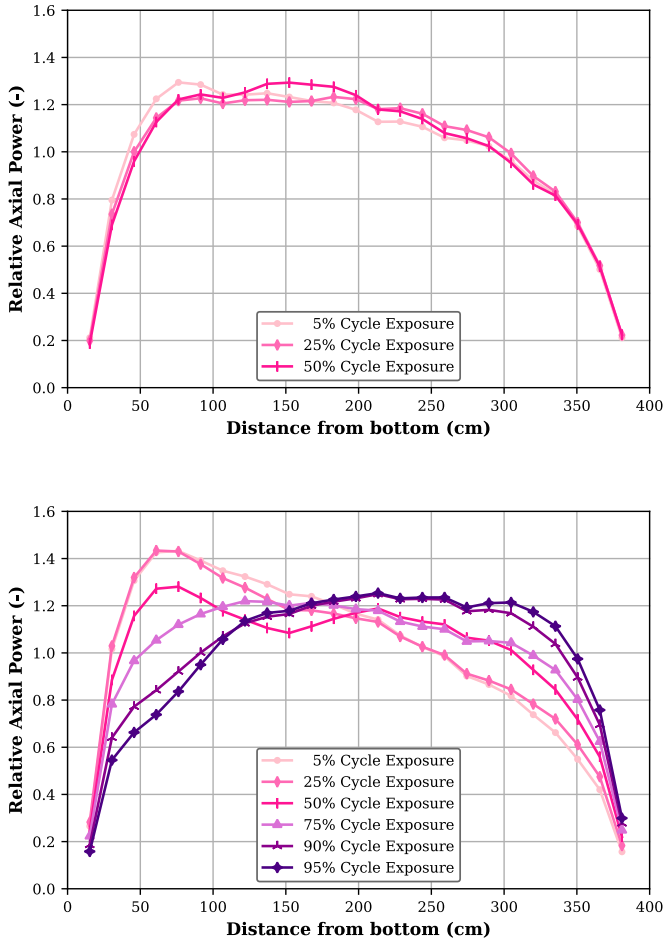

Figure 5.2. Axial Power Profile predicted by SIMULATE-3. Cycle A (top) and Cycle B (bottom).

As the cycle progresses, the axial power shifts to the top of the bundle. Further, the spectrum shift effects, in combination with high recirculation flow at the end of the cycle (stretch-out and coast-down), give a transition from bottom-peaked to top-peaked power.

Power and void distributions in the core follow each other as *Siamese Twins*; where there is a high power, there is always a high void, and vice versa. Therefore, a quality calculation of the void distribution is necessary to obtain an accurate power distribution.

According to (Stacey, W. M., 2018), fuel depletion and compensating control actions affect the reactor power distribution over the lifetime of the fuel in the core.

Depletion of the fuel will be the greatest where the power is the greatest. The initial positive reactivity effect of depletion will then enhance the power peaking. At later times, the negative reactivity effects will cause the power to shift away to regions with higher k_{eff}. Therefore, at the end-of-cycle, the radial power distribution is relatively more concentrated in the center of the core.

The radial RPFs predicted by SIMULATE-3 for Cycles A and B are illustrated in Figure 5.3 and Figure 5.4, respectively.

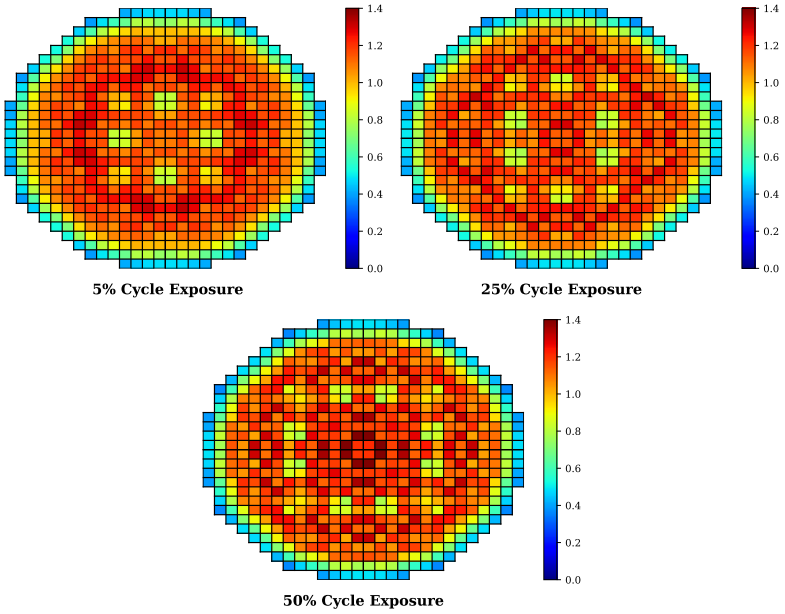

Figure 5.3. Radial Power Profile predicted by SIMULATE-3. Cycle A.

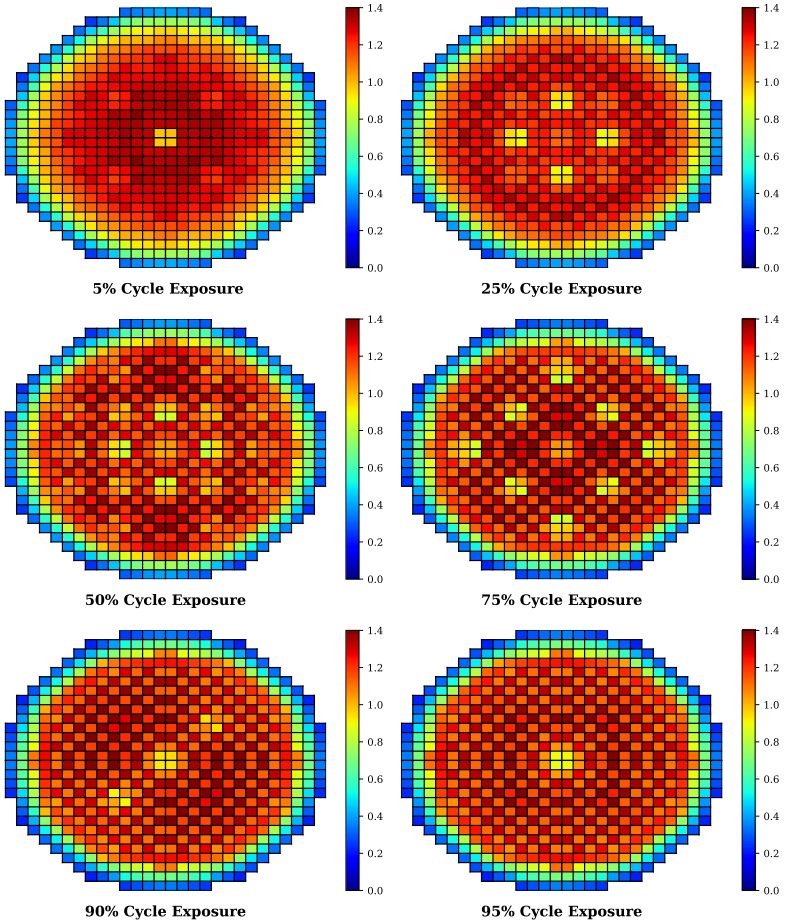

Figure 5.4. Radial Power Profile predicted by SIMULATE-3. Cycle B.

As discussed in Chapter 4, the control rod history effect has to be accounted for. To reduce and compensate for this effect, the core is operated by alternating between control blades that are inserted to control reactivity, meet thermal limits, and ensure the power is evenly distributed to prevent the shadowing of the fuel.

The radial control density also follows the radial power distribution, meaning there will be a concentration of control rods in the central part of the core. In conventional BWR operations, four basic control rod patterns, designated as A1, A2, B1, and B2 patterns as described in reference (General Electric Company, 2001), are used to develop operating control rod pattern sequences throughout each cycle.

A typical sequence interval can last from 8 weeks to 16 weeks. The sequences are arranged such that the rods within the sequence are evenly distributed throughout the core. For any given period of operation, only rods in a single sequence will be inserted into the core, while all rods in the other three sequences will be entirely withdrawn. In

BWRs the objective of power flattening is observed in the programming of control rod insertion and withdrawal sequences together with the coolant flow control alternative.

Control rod pattern sequences can be appreciated at a glance in the radial power distributions as the cycle progresses for Cycles A and B.

The power distribution is directly dependent on the exposure history or distribution through the reactivity feedback associated with fuel burnup alongside fission product and poison productions. Usually, the highest burnt fuel is placed in peripheral positions in the core because it gives a low neutron leakage out of the core and high power in the center.

Axial exposure distribution for both cycles at the selected operating condition points is plotted in Figure 5.5. From this, it can be seen that even if the core has had a void distribution that forces the power to be bottom-peaked during most of the cycle, at EOC, generally, the exposure shape of an assembly is somewhat less regular axially. The reason why the exposure is so smooth at the end can be accounted for by the spectrum shift operation and the build-up of Pu at the top of the fuel.

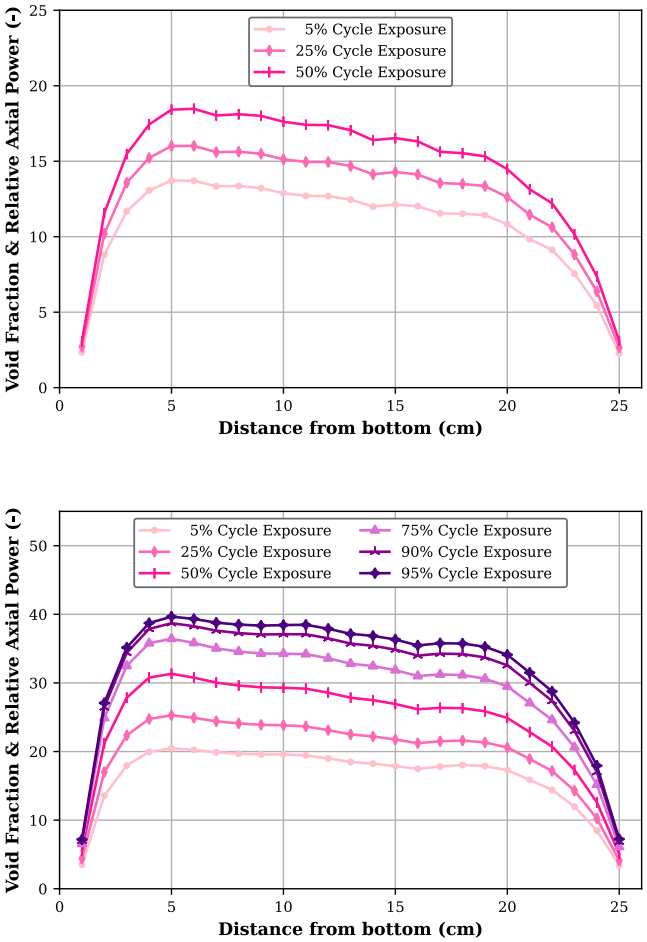

Figure 5.5. Core Average Exposure Profiles. Cycle A (top) and Cycle B (bottom).

It is important to highlight that between Cycles A & B, over ten cycles have been depleted, and operational changes have occurred, such as power uprate (with the corresponding increase of the planted rated power output), cycle-time schedule extension (from a 12-month cycle to a 24-month cycle), higher fuel enrichment, higher core voiding conditions, and the use of fuels with more modern designs and more pins in a mixed core with different vendors.

These differences in core design and operation might show in the results of the core-follow for each of the cycles, especially at those points with control rod exchange sequences or another significative event.

5.3 PARCS Model.

The set-up full-core PARCS model for both cycles presents the following features:

1) PARCS models 740 assemblies: 624 fuel assemblies and 116 reflector assemblies around the periphery of the core.
2) Axially, the active core is divided into 25 nodes that are 15.24 cm (6") tall. The total active core length is 381 cm. Two additional axial nodes account for the top and bottom reflectors, totaling 27 axial layers. The axial reflectors are set to twice the height of an active node (30.48 cm or 12").
3) The axial nodalization accounts for material changes in fuel design, exposure, and history variations.
4) Radially, the core is divided into 30 nodes 15.24 cm (6") wide, each corresponding to one fuel assembly, plus a radial reflector of also 15.24 cm. This radial fuel spacing (pitch) is standard for BWR.
5) 145 control rods provide reactivity control. The control rods are defined to have 48 axial positions (aka notches) spaced 7.62 cm (3"). The fully inserted condition (ARI – all rods in) is set at 0 notches; the fully withdrawn (ARO – all rods out) state is set at 48.
6) Equilibrium Xenon/Samarium is considered for all calculated depletion steps.
7) The neutronic mesh is defined to coincide with the thermal-hydraulic mesh.
8) The boundary conditions are set for zero flux at all four boundaries (North, East, South, West).
9) Appropriate rotated discontinuity factors are used. Note that there is an offset of 90-degrees anti-clockwise between the convention in SIMULATE-3 and PARCS.
10) The complete reactor histories up to Cycle A and B were simulated and recovered to account for the historical effects, e.g., primarily void and control histories, and to accurately evaluate the core condition at the start of both cycles.
11) All history variables for each fuel segment corresponding to either Cycle A or B are extracted from the SIMULATE-3 depletion files.

Additionally, for Cycle A:

1) The core loading is as follows: there are 44 fuel assemblies of Type 1, and the remaining 580 are Type 2 fuel assemblies. All assemblies are BWR old fuel designs with 8x8 pin arrangement with a pin enrichment range between 2.0 and 4.0 wt.% ^{235}U.
2) 21 plant data provided steps from BOC through MOC conditions.
3) Accumulated average core exposure of 4.478 GWd/st.

And, for Cycle B:

1) The core loading is as follows: there are 136 fuel assemblies of Type 3, 343 fuel assemblies of Type 4, 28 fuel assemblies of Type 5, and the remaining 117 are Type 6.

2) All assemblies are BWR modern fuel designs with 10x10 pins per bundle designs with a pin enrichment range between 2.0 and 4.95 wt.% ^{235}U.
3) 243 provided plant data steps ranging from BOC to EOC conditions.
4) Accumulated average core exposure of 18.006 GWd/st.

5.4 Cross-Section Reference Library Set – Set 1.

All fuel and reflector specifications for each fuel lattice segment in Cycles A and B were provided as CASMO-4 inputs.

Initially, these CASMO-4 models were used with SIMULATE-3, employing the S3C default input option for the history/branch matrix. This preliminary approach aimed solely at understanding cross-section generation and modeling. However, the typical S3C case matrix output from CASMO-4 does not fully align with the inherent requirements of GenPMAXS for generating cross-section interpolation data. The simulation results using the S3C library are not included here, as they fall outside the scope of this dissertation.

To ensure that the CASMO-4 outputs were correctly converted to the PMAXS format for subsequent use in PARCS, a different history/branch matrix needed to be defined and implemented in the CASMO-4 inputs.

This new library, referred to as ***Set 1***, was established based on the guidance provided in NUREG/CR-7164 for BWR lattice modeling, as discussed in Chapter 4. Set 1 will serve as the reference library for the cross-section generation analysis performed in this thesis.

Axially, top and bottom reflectors were included and set to 30.48 cm tall. Radially, reflector cross-sections were modeled in detail with eight orientations as North (N), East (E), West (W), South (S), Northeast (NE), Northwest (NW), Southwest (SW), and Southeast (SE). This differentiation accounts for the radial core location, determining whether they adjoin one edge of the assembly, and considers the varying amounts of stainless-steel baffle, which influence the spectrum (Bahadir, T., 2015).

Once the reflector cross-sections are adequately modeled and validated, and assuming the reactor geometry remains unchanged, there is no need to recalculate them for different cycle simulations. Therefore, the same reflector cross-sections will be used for both Cycle A and Cycle B.

The initial history-branch matrix structure details for Set 1 library are given in Table 5.2 and Table 5.3, where CR, VOI, TFU, and TMO correspond to control rod, void fraction, fuel temperature, and moderator temperature, respectively.

Table 5.2. Branches Used in Reference Set Library – Set 1.

Number	Type	CR	VOI (%)	TFU (K)	TMO (K)	Depletion/Branch
Base Case (BC)	BASE	Out	40	792.4	561.4	Nominal Depletion
1	VOI	Out	0	792.4	561.4	Branch from BC
2	VOI	Out	70	792.4	561.4	Branch from BC
3	VOI	Out	90	792.4	561.4	Branch from BC
4	VOI/TFU	Out	0	562.0	561.4	Branch from BC
5	VOI/TFU	Out	0	1500.0	561.4	Branch from BC
6	VOI/TFU	Out	40	562.0	561.4	Branch from BC
7	VOI/TFU	Out	40	1500.0	561.4	Branch from BC
8	VOI/TFU	Out	70	562.0	561.4	Branch from BC
9	VOI/TFU	Out	70	1500.0	561.4	Branch from BC
10	VOI/TFU	Out	90	562.0	561.4	Branch from BC
11	VOI/TFU	Out	90	1500.0	561.4	Branch from BC
12	CR/VOI	In	0	792.4	561.4	Branch from BC
13	CR/VOI	In	40	792.4	561.4	Branch from BC
14	CR/VOI	In	70	792.4	561.4	Branch from BC
15	CR/VOI	In	90	792.4	561.4	Branch from BC
16	CR/VOI/TFU	In	0	562.0	561.4	Branch from BC
17	CR/VOI/TFU	In	0	1500.0	561.4	Branch from BC
18	CR/VOI/TFU	In	40	562.0	561.4	Branch from BC
19	CR/VOI/TFU	In	40	1500.0	561.4	Branch from BC
20	CR/VOI/TFU	In	70	562.0	561.4	Branch from BC
21	CR/VOI/TFU	In	70	1500.0	561.4	Branch from BC
22	CR/VOI/TFU	In	90	562.0	561.4	Branch from BC
23	CR/VOI/TFU	In	90	1500.0	561.4	Branch from BC
24	VOI/TMO	Out	0	792.4	545.0	Branch from BC
25	VOI/TFU/TMO	Out	0	293.0	293.0	Branch from BC
26	VOI/TFU/TMO	Out	0	562.0	293.0	Branch from BC
27	VOI/TFU/TMO	Out	0	792.4	293.0	Branch from BC
28	CR/VOI/TMO	In	0	792.4	545.0	Branch from BC
29	CR/VOI/TFU/TMO	In	0	293.0	293.0	Branch from BC
30	CR/VOI/TFU/TMO	In	0	562.0	293.0	Branch from BC
31	CR/VOI/TFU/TMO	In	0	792.4	293.0	Branch from BC

Table 5.3. Histories Used in Reference Set Library – Set 1.

Number	Type	CR	VOI (%)	TFU (K)	TMO (K)	Depletion/Branch
Base Case (BC)	BASE	Out	40	792.4	561.4	Nominal Depletion
1	HVOI	Out	0	792.4	561.4	Depletion from BC
2	HVOI	Out	70	792.4	561.4	Depletion from BC
3	HCR/HVOI	In	0	792.4	561.4	Depletion from BC
4	HCR/HVOI	In	40	792.4	561.4	Depletion from BC
5	HCR/HVOI	In	70	792.4	561.4	Depletion from BC
6	HVOI/HTFU	Out	40	562.0	561.4	Depletion from BC
7	HVOI/HTFU	Out	40	1500.0	561.4	Depletion from BC
8	HCR/HVOI/HTFU	In	40	562.0	561.4	Depletion from BC
9	HCR/HVOI/HTFU	In	40	1500.0	561.4	Depletion from BC

Typically, for LWRs, the total fuel burnup is around 30 to 55 GWd/st, on average, depending on the different lengths of time within the core. Thus, it is essential to perform lattice depletions to a final exposure that is guaranteed to encompass the entire operating lifetime of the bundle, e.g., up to 70 GWd/st. The burnup points used by CASMO-4 in the depletion calculations for obtaining the reference library Set 1 are outlined in Table 5.4.

Table 5.4. Selected Burnup Points Used in Reference Set Library – Set 1.

Burnup Points (GWd/st)									
0.0	0.5	1.0	2.0	4.0	6.0	8.0	10.0	15.0	20.0
25.0	30.0	35.0	40.0	45.0	50.0	55.0	60.0	65.0	70.0
							Total	**Points**	**20**

All lattice calculations have been performed using CASMO-4 with a standard library based on data from ENDF/B-IV. The cross-sections are tabulated in coupled 70/18 neutron and gamma energy group structures. Finally, CASMO-4 output files, CAX files, were converted into PMAXS files using the code GenPMAXS version 6.1.3.

5.5 Core-Follow Analysis.

The parameters of interest when comparing PARCS and SIMULATE-3 are the core criticality, k_{eff} , alongside the relative power fractions, *RPF*.

The relative difference between the calculated eigenvalue and the reference is expressed in pcm and obtained according to the expression:

$$\frac{\Delta k_{eff}}{k_{eff}} = \left(\frac{k_{eff}^{calculated\,(PARCS)}}{k_{eff}^{reference(SIMULATE)}} - 1 \right) \times 10^5 \qquad \textbf{Equation 5.1}$$

The relative difference in terms of power distributions is expressed in % and obtained as follows:

$$\frac{\Delta RPF}{RPF} = \left(\frac{RPF^{calculated\,(PARCS)}}{RPF^{reference\,(SIMULATE)}} - 1 \right) \times 100 \qquad \textbf{Equation 5.2}$$

Equation 5.3 will be used for both axial and radial relative power differences. Finally, the Root Mean Square (RMS) errors will be formulated as follows:

$$RMS_{RPF} = \sqrt{\frac{\sum \left(\frac{RPF^{calculated\,(PARCS)}}{RPF^{reference\,(SIMULATE)}} - 1 \right)^2}{N}} \times 100 \qquad \textbf{Equation 5.3}$$

Where N is the number of fuel assemblies in the core.

In conventional BWR core analysis, with the prediction exactness for licensing and operational margins in mind, there is no regulatory requirement to obtain a predetermined level of accuracy on power distribution calculations.

Uncertainty is typically included in the calculation of Specified Acceptable Fuel Design Limits (SAFDL - requirement specified in GDC 10, 10CFR50 Appendix A). If a licensee uses an inaccurate method, they have to apply additional conservative margins to their calculations.

Although other sources of inaccuracy (e.g., thermal-hydraulic conditions and correlations) tend to dominate these conservative margins, conventionally, neutronic calculations have a goal to maintain errors lower than **5% on the axial power and 2% on the radial or bundle power**. These power distribution inaccuracies are confirmed periodically during the cycle using the detectors, e.g., TIP measurements, as will be discussed in Chapter 6.

Similarly, with respect to inaccuracies in the calculation of k_{eff}, there are no regulatory requirements. The only impact to reactor operation is the potential of miscalculating the point of criticality as control rods are withdrawn during cycle startup. The safety impact is minimal because the approach to criticality is monitored with the source-level neutron detectors.

Nevertheless, licensees conventionally impose a **500 pcm** limit on the allowed dk/k inaccuracy to ensure the fidelity of these calculations and allow for accurate calculations of power distributions.

5.5.1 Cross-section Reference Library Set 1 Results.

Effects related to the designed cross-section reference library are assessed first. Comparisons of SIMULATE-3 and PARCS calculations for the eigenvalue and the core-average axial and radial power distributions for all selected points using the cross-section library Set 1 are shown in Table 5.5. Such results will be considered as a starting point for reconsidering the branch/history structure matrix of the cross-section library if needed.

Table 5.5. PARCS vs. SIMULATE-3 Results. Cross-section (XS) Set 1.

Fuel Cycle	Core Average Cycle (GWd/st)	PARCS k_{eff}	$\Delta k_{eff}/k_{eff}$ (pcm)	Axial RPF RMS (%)	Radial RPF RMS (%)	Maximum Radial Peak (%)
A	0.695	0.99971	67	10.57	1.48	4.42
A	2.536	0.99842	48	10.49	1.46	5.20
A	4.478	0.99931	51	9.78	2.13	6.39
B	0.891	1.00364	6	5.16	0.68	2.57
B	4.515	1.00130	10	5.62	1.02	2.25
B	9.100	1.00065	-15	6.98	1.61	3.30
B	13.502	1.00069	-46	8.66	2.15	4.09
B	15.951	1.00030	-108	11.97	2.15	5.52
B	17.110	0.99837	-101	12.87	1.60	4.65

Discrepancies between SIMULATE-3 and PARCS are less than 110 pcm in terms of k_{eff} and within 2.2% in terms of radial RMS for all analyzed points. There is a slight overprediction of k_{eff} for Cycle A, while it turns into a slight underprediction for Cycle B as the cycle progresses. As stated in (Sánchez-Cervera, et al., 2014b), the total error in k_{eff} is due to error contributions from all cross-sections at once.

Axial power results show a lack of agreement between both codes, becoming more noticeable as the cycle progresses. The error increase with burnup might be an indication that the history variables are not properly modeled; thus, a large number of cross-section extrapolations are needed, which might be causing such poor axial power predictions.

Relative radial power difference, core-average axial power shape, and the relative axial difference between the two calculations are shown in Figure 5.6 for Cycle A and Figure 5.7- Figure 5.8 for Cycle B.

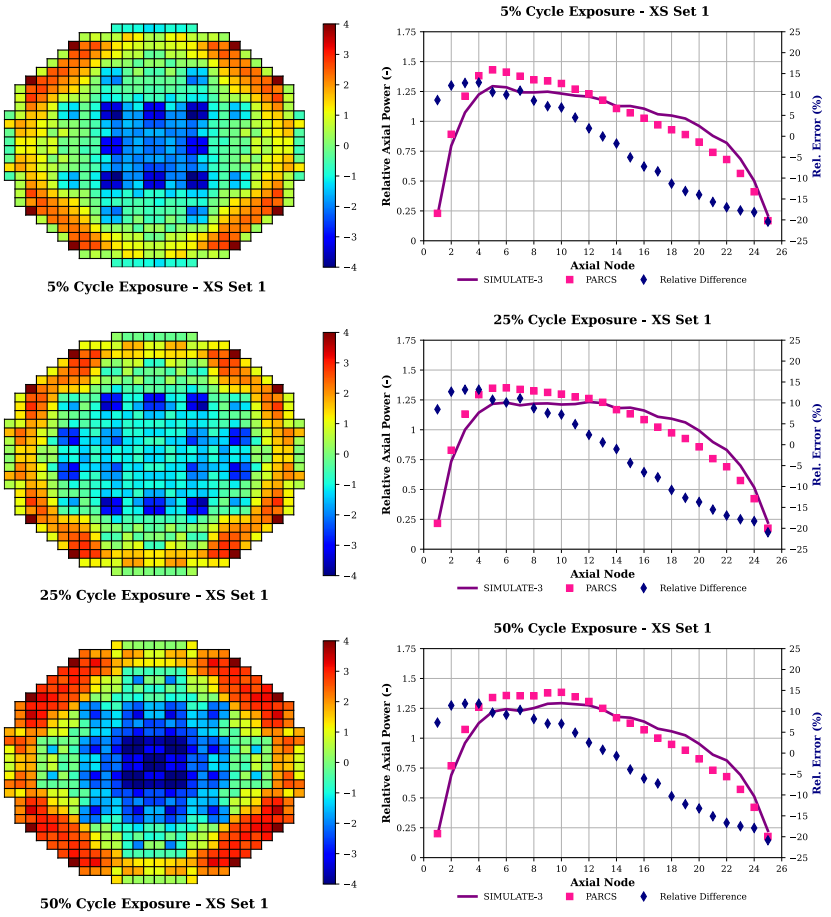

Figure 5.6. Relative Radial and Axial Power Errors (%). XS Set 1. Cycle A.

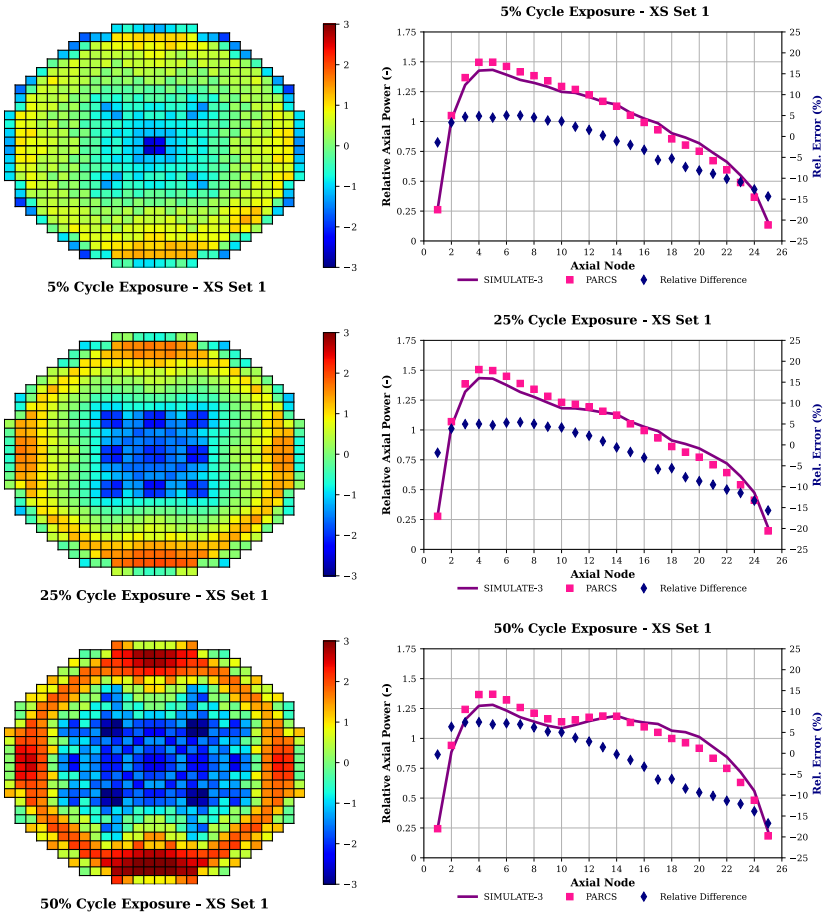

Figure 5.7. Relative Radial and Axial Power Errors (%). XS Set 1. First Half of Cycle B.

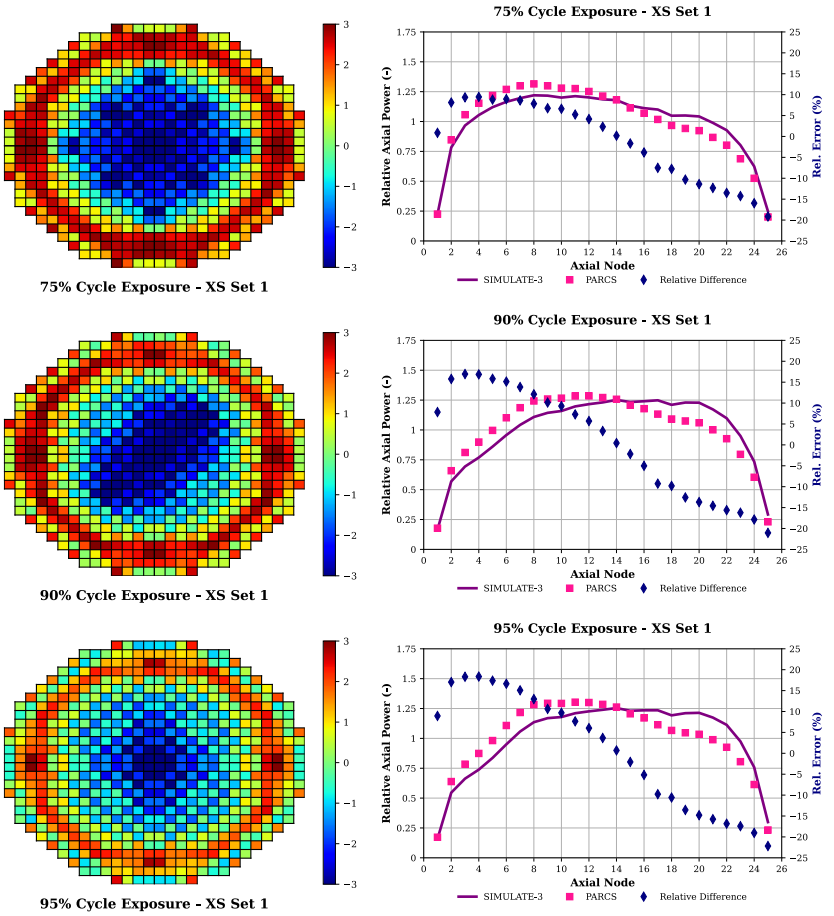

Figure 5.8. Relative Radial and Axial Power Errors (%). XS Set 1. Second Half of Cycle B.

For the radial power distribution, there is a clear tendency to underestimate the power in those fuel elements with control rods, as well as an overestimation of the power in some peripheral channels. This trend can be seen in both cycles for most of the analyzed points.

The higher differences are concentrated in the assemblies near the radial reflectors, where PARCS overpredicts the power by up to 6.5% compared to SIMULATE-3. This might suggest an underestimation of radial neutron leakage by PARCS, especially noticeable in the second part of the cycle and in some reflectors adjacent to fuel assemblies.

Axially, a constant deviation of the PARCS results from the reference data can be noticed, i.e., the axial power shape is more peaked at the bottom core for all analyzed cases independently of core exposure. Thus, it seems that PARCS tends to calculate higher void fractions in the subcooled region at the inlet of the core. Also, the axial

leakage of neutrons through the top and bottom reflectors might be erroneously estimated.

The significant errors in estimating the power distributions along all the analyzed points indicate that the cross-section reference library designed following the NUREG/CR-7164 (Wang, D. et al., 2013), indications is not adequately characterizing the reactor conditions for either of the simulated cores. Thus, it would be necessary to reconsider the history/branch matrix structure to find proper cross-section sets that best suit our purposes.

As aforementioned, the prediction of nodal power, and hence, the reactor power, is characterized by both instantaneous and historical variables. Therefore, the cross-section library domain range should include as many state and history variable conditions as possible to reduce cross-section extrapolations. Proper identification of density ranges, i.e., of void fraction ranges, is essential during the cross-section modeling process since, as seen in Chapter 4, the void fraction is one of the key parameters for BWRs simulations both for state and historical variables.

With this in mind, Figure 5.9 illustrates the distributions of history nodal moderator densities and fuel temperatures for cycles A and B. The solid blue line represents the respective lower and upper history boundaries of the cross-section library Set 1, i.e., 0% void (corresponding to a density of 0.73511 kg/cm^3) and 550 K fuel temperature for the lower boundaries whereas 70% void (corresponding to a density of 0.24723 kg/cm^3) and 1500 K for the upper boundaries.

It is interesting to compare the moderator density vs. fuel temperature node conditions for Cycle A and B. As seen, Cycle B, with more modern fuel elements and working under extended power uprate conditions, presents lower and flatter fuel temperature distribution and higher void fractions than Cycle A.

Looking at Figure 5.9, it can be gathered that the selected 70% void fraction, which has traditionally been considered as moderation conditions at the top of the BWR fuel assembly during regular operation, is not enough to cover the core domain.

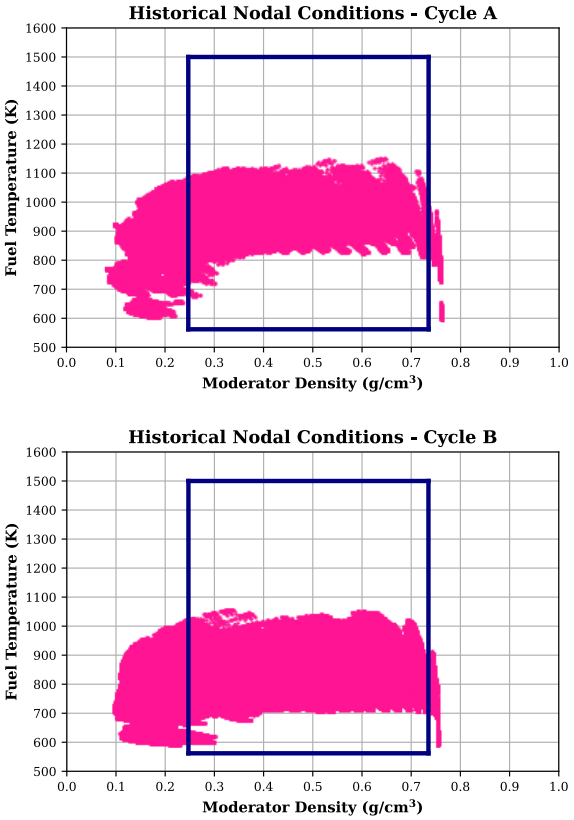

Figure 5.9. Set 1. History Matrix Structure Boundaries. Cycle A (top) and Cycle B (bottom).

Actually, as shown in Figure 5.10, about 50% of the moderator density points are out of the history domain (i.e., greater than 70%) for each cycle and, hence, calculated through cross-section extrapolations.

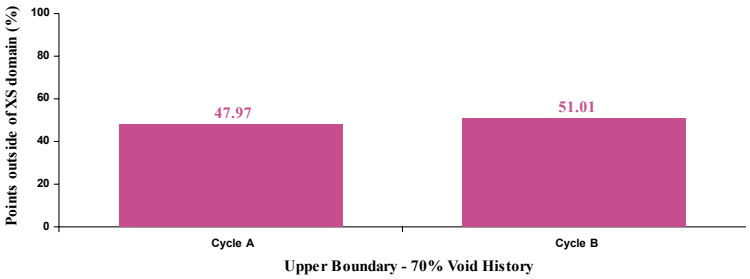

Figure 5.10. Set 1. Points Outside of Void History Upper Boundary.

The study carried out in the NUREG/CR-7164, presented that both absorption and fission cross-section curves showed more non-linearity at high void fractions than at low void fractions. Then, the extrapolation of the cross-sections from the 70% void might overestimate the cross-sections at high void faction and could explain the poor agreement power-wise between SIMULATE-3 and PARCS using the Set 1 library because macroscopic cross-sections have a strong dependence on the history effects of moderator density and control rod position.

Following the same approach for the state variables, Figure 5.11 illustrates both nodal moderator density and fuel temperature instantaneous distributions for Cycles A and B.

The solid blue line delineates the lower and upper instantaneous boundaries of Set 1. Specifically, these boundaries are defined as 0% void at moderator temperatures of 293 K and a fuel temperature of 550 K for the lower limit, and 90% void with a fuel temperature of 1500 K for the upper limit.

An intermediate boundary is also indicated at 0% void and a fuel temperature of 792 K, applicable when moderator densities fall below the saturation temperature under nominal operating conditions. The dashed blue lines represent intermediate void fraction branches at 0% (with a moderator temperature of 562 K), 40%, and 70%, respectively.

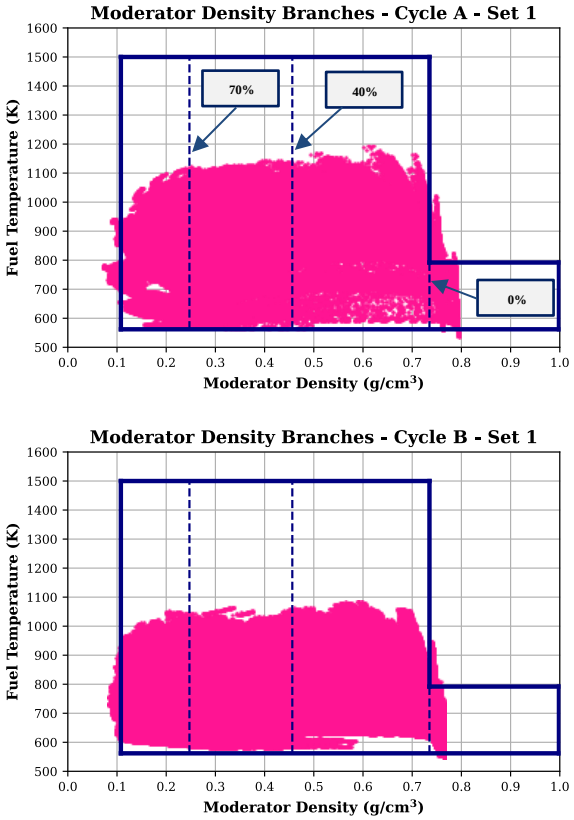

Figure 5.11. Set 1. Moderator Density Branch Matrix Structure Boundaries. Cycle A (top) and Cycle B (bottom).

As illustrated in Figure 5.11, it can be considered that the selected void fraction branches, i.e., 0%, 40%, 70%, and 90%, should provide sufficient accuracy for BWR transient analysis as was already concluded at the NUREG/CR-7164 guidelines (Wang, D. et al., 2013).

However, because the set of branch cases may not form a regular mesh, it is interesting to know beforehand the distribution of the instantaneous nodal density within the reactor to optimize the meshing points in areas with a more extensive distribution or more significant variability.

This way, it is also intended to try to avoid interpolations as much as possible since it is known that k_{eff} error due to the cross-section interpolation error generally increases with burnup. For controlled moderator density branches, it is suggested that the same density branch structure be used.

Figure 5.12 illustrates the moderator density histogram for both cycles, while Table 5.6 presents the percentage distribution of the nodes within the considered void fraction ranges of the employed branches.

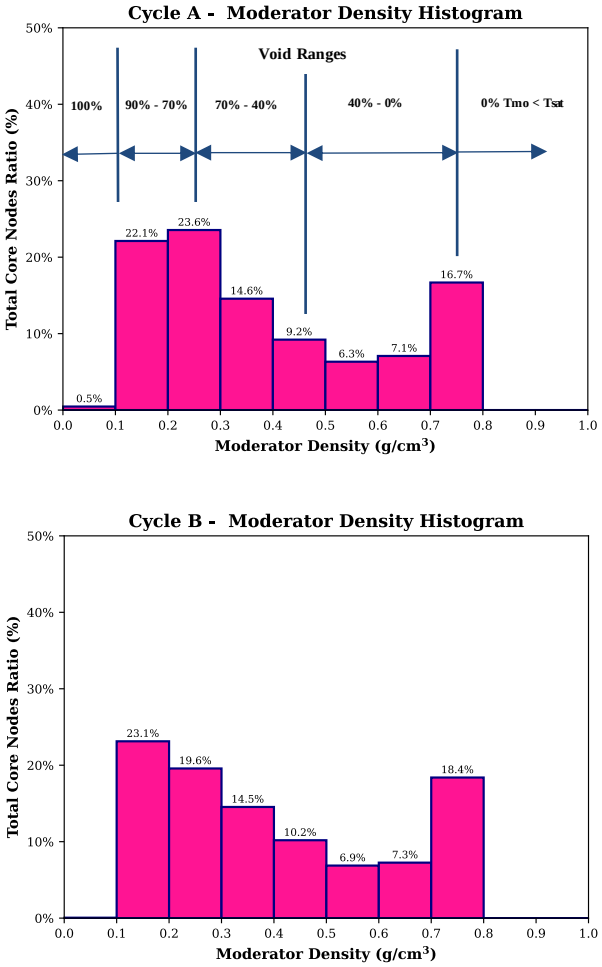

Figure 5.12. Instantaneous Moderator Density Distributions. Cycle A (top) and Cycle B (bottom).

Table 5.6. Nodal Moderator Density Distributions by Branch.

	Void Range (0%)	Void Range (0% - 40%)	Void Range (40% - 70%)	Void Range (70% - 90%)	Void Range (90% - 100%)
Cycle A	8.4%	26.4%	31.0%	33.9%	0.5%
Cycle B	9.2%	28.5%	29.4%	32.9%	0.0%

As seen in Table 5.6, approximately 30% of the nodes are within each void fraction range of interest, meaning that a refinement of the branches could be interesting to study the impact of the mesh points, i.e., the interpolations in the power predictions. Thus, the objective is to define a proper domain range where all state values and history parameters could adequately characterize the core reactor under steady-state or transient conditions independently of the simulated cycle or the fuel designs.

Since the number of different fuel lattice segments composing the core of Cycle A is considerably smaller than the number of core segments constituting Cycle B (9-to-70), only Cycle A cases are hereafter considered and used to perform the cross-section analysis of different modeled libraries.

Then, the withdrawn conclusions from Cycle A analysis will be used on Cycle B to obtain reasonable general model guidelines which are intended to cover different fuel designs, cycles, and operational and accidental transient conditions. The results corresponding to Cycle B will be shown in Section 5.6.

5.5.2 Analysis of the Influence of the Instantaneous/History Effect.

In order to cover a whole given operating range, different sets of operating conditions and branch cases are customarily modeled. The expected range has to be enfolded by selecting an adequate range for the independent variables based on the type of plant and event to be modeled, see Table 5.7.

Table 5.7. Typical Calculation Types Performed by Lattice Codes.

Source: (Stålek & Demazière, 2008).

REACTOR TYPE	TYPES OF CALCULATIONS PERFORMED FOR THE FUEL
BWR	• Void histories depletion • Branch cases from void histories depletion for different values of α, α_{CR}, T_f • Cold branches and cold rodded branches from void histories depletion • Void history depletion with a control rod and control rod branch

Each point (T_f, T_m, P_m, α) represents one possible core state during the transient. Yet, the level of required mesh refinement, i.e., the number of branches, is not the same for all state variables and, therefore, cannot be equally distributed along the variable domain ranges. In addition, not all cross-sections are equally affected by changes in the state variables and, thereby, not all parameters of interest, such as k_{eff}, are influenced in the same way. Consequently, the mesh should be refined considering the physical behavior and the expected associated phenomena (Sánchez-Cervera et al., 2014a).

BWRs have a strong axial variation in moderator density requiring a branch structure that captures the non-linear impact of density on the cross-sections (Downar, T. et al., 2012). Depending on the height in the core, the water will have a varying void content, i.e., a varying fraction of steam volume in the water. The void ranges from 0% at the bottom of the core to about 90% at the top.

In the available literature, it is usually recommended to account for a moderator density finer mesh as density decreases. For this reason, more definition was added to the high void distributions to the Set 1 library and another extra branch at 20% void fraction for accounting for the non-linearity in the interpolations from 0% to 40% void range. This new-brand library was labeled as ***Set 2a***.

A comparison of Set 1 and Set 2a libraries moderator density branch structures is shown graphically in Figure 5.13.

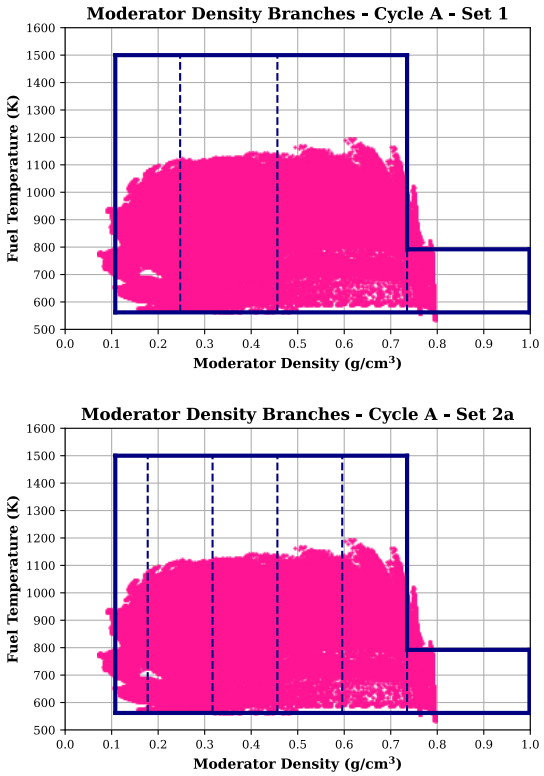

Figure 5.13. Instantaneous Moderator Density Branch Structure for Set 1 (top) and Set 2a (bottom).

For a more comprehensive differentiation, the branches added from one library to another are highlighted in Table 5.8.

Table 5.8. Void History/Branch Matrix Structure Conditions for Set 1 and Set 2a.

XS Set Library	History Parameter	Off-Nominal Lower Boundary	Nominal History	Off-Nominal Upper Boundary	Branch Parameter	Selected Branches (%)
Set 1	HVOI	0%	40%	70%	VOI	0/40/70/90
Set 2a	HVOI	0%	40%	70%	VOI	0/20/40/60/80/90

Comparisons of the axial and radial power predictions between Set 1 and Set 2a libraries are presented in Figure 5.14 and Figure 5.15, respectively.

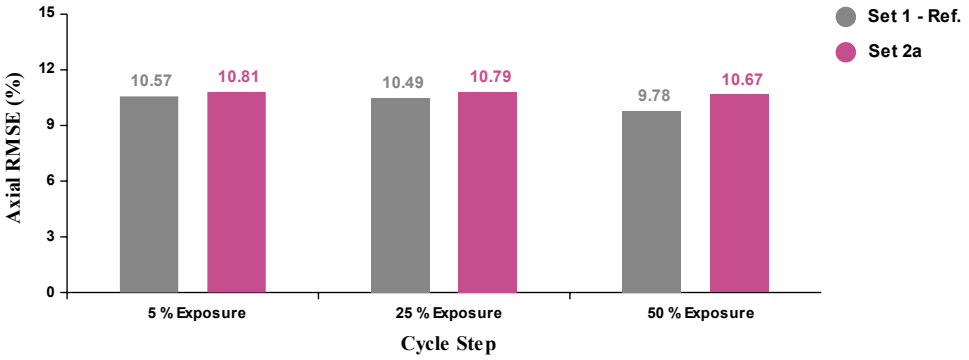

Figure 5.14. Axial RMSEs (%). Set 1 vs. Set 2a.

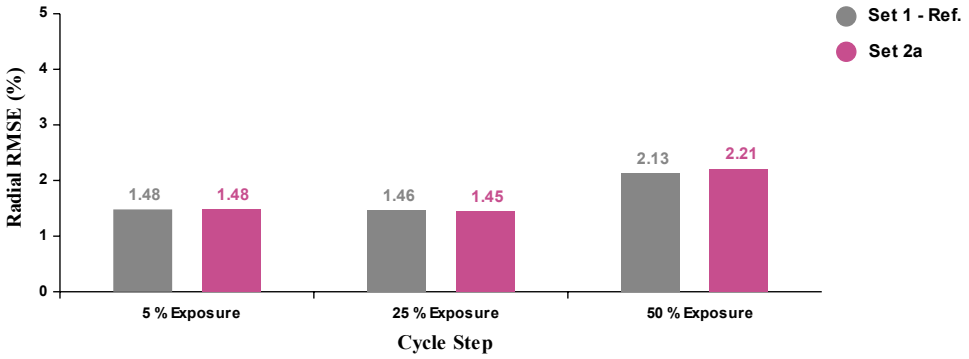

Figure 5.15. Radial RMSEs (%). Set 1 vs. Set 2a.

As can be seen, adding more branches causes only marginal differences in the power predictions and indicates that BWR steady-state results are not highly sensitive to moderator density instantaneous branch effects, at least while the operating conditions of the reactor remain invariant. Even so, off-nominal reactor conditions and

transients may be sensitive to the structure of moderator density branches as will be discussed later in this chapter.

Given the obtained results, especially the high errors in the prediction of the axial power distribution, it may seem that the poor agreement between PARCS and SIMULATE-3 is not a consequence of the branch structure but is more likely to come from the history matrix structure.

As already discussed, history variables are defined as burnup-weighted values of the instantaneous state parameters. Thus, history effects should be included in cross-sections to account for the hardening of the neutron spectrum throughout a cycle.

For BWRs, the history effect of moderator density on the neutron spectrum is much greater than that of other state parameters and is therefore strongly recommended to be included in the cross-section generation. Moderator density histories that are upper than 80% void fraction, i.e., 90%, are recommended for high power density reactors to improve cross-section evaluation in the upper core region.

For this reason, the redefinition of the moderator density histories is addressed next, maintaining the same branches modeled as in library Set 2a.

Table 5.9 contains the void history matrix structure conditions for the libraries designated as ***Set 2b***, ***Set 2c***, and ***Set 2d*** where the off-nominal void upper boundary has been gradually extended for the different cross-section set libraries from 70% to 95%.

Table 5.9. Void History/Branch Matrix Structure Conditions for Set 2a to Set 2d.

XS Set Library	History Parameter	Off-Nominal Lower Boundary	Nominal History	Off-Nominal Upper Boundary	Branch Parameter	Selected Branches (%)
Set 2a	HVOI	0%	40%	70%	VOI	0/20/40/60/80/90
Set 2b	HVOI	0%	40%	**80%**	VOI	0/20/40/60/80/90
Set 2c	HVOI	0%	40%	**90%**	VOI	0/20/40/60/80/90
Set 2d	HVOI	0%	40%	**95%**	VOI	0/20/40/60/80/90

The extension of the off-nominal upper boundaries is shown graphically in the following figures.

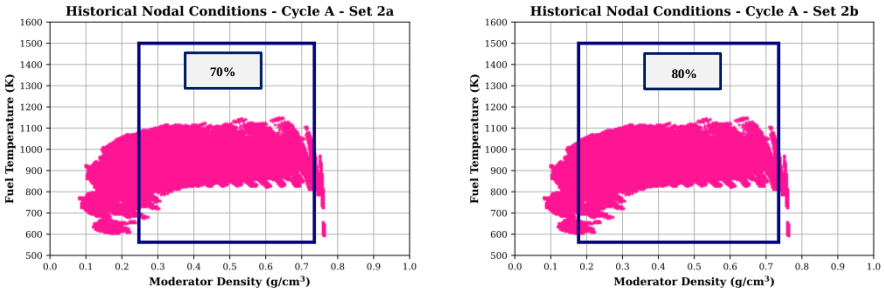

Figure 5.16. History Matrix Structure Boundaries. Set 2a (left) and Set 2b (right).

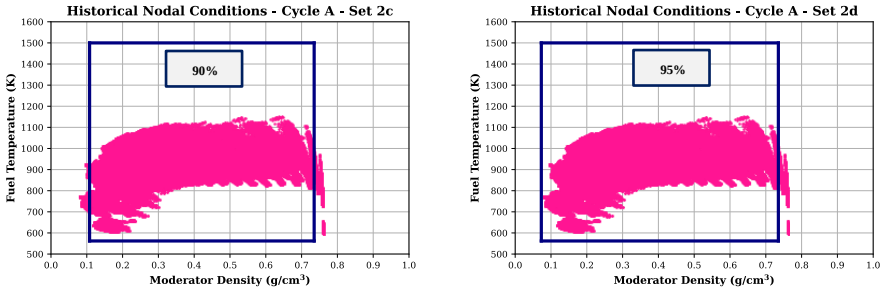

Figure 5.17. History Matrix Structure Boundaries. Set 2c (left) and Set 2d (right).

Expanding the upper bound of void history results in fewer nodes falling outside the domain range, as illustrated in Figure 5.18. Consequently, this reduction in nodes outside the range diminishes the necessity for extrapolations to determine the cross-section of a specific node. As a result, a more accurate prediction of nodal power is expected.

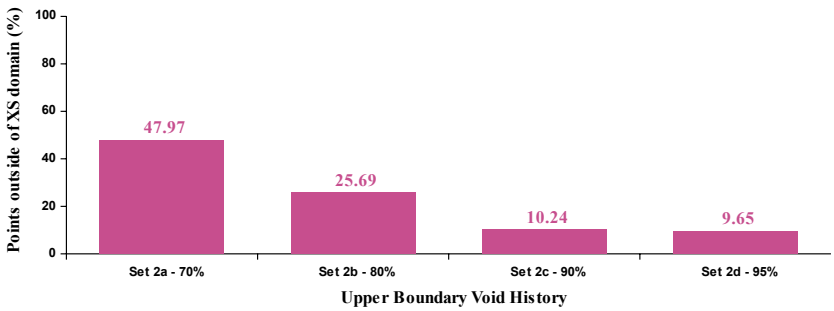

Figure 5.18. Points Outside of Cross-Section History Domains.

It is notable that the percentage of nodes outside the Set 2d (95% void) domain mesh is not solely due to the high void fraction, but also from liquid state points at moderator temperatures lower than those corresponding to the saturation pressure as seen in Figure 5.19.

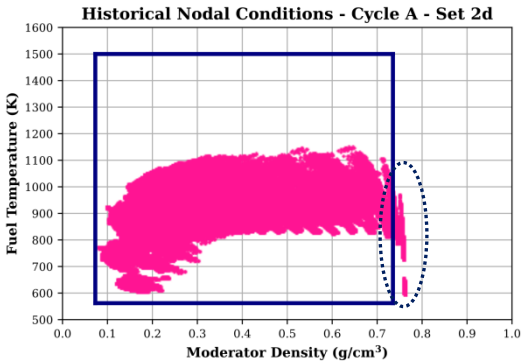

Figure 5.19. History Matrix Structure Boundaries Set 2d (95% upper void).

Consequently, these lower moderator temperatures introduce a bias in the calculations for points outside the domain of interest. By using this bias as a reference and subtracting it from the total points outside the domain across all cases, the number of points outside the history domain for each cross-section set library is recalculated, as depicted in Figure 5.20.

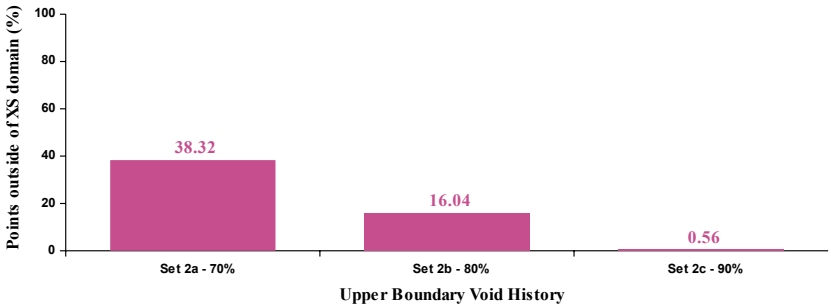

Figure 5.20. Points Outside of Cross-Section History Domains without Set 2d's Bias.

The comparison of k_{eff} and power distributions between PARCS and SIMULATE-3, utilizing libraries Set 2a to Set 2d, is summarized in Table 5.10 to Table 5.12.

Table 5.10. History Impact. XS Sets Results for 5% Exposure Cycle.

XS Set Library	PARCS k_{eff}	$\Delta k_{eff}/k_{eff}$ (pcm)	Axial RPF RMS (%)	Radial RPF RMS (%)	Maximum Radial Peak (%)
Set 1	0.99971	67	10.57	1.48	4.42
Set 2a	0.99970	66	10.81	1.48	4.38
Set 2b	1.00019	115	5.22	1.03	4.66
Set 2c	1.00033	129	3.74	0.92	4.74
Set 2d	1.00038	134	3.28	0.90	4.79

Table 5.11. History Impact. XS Sets Results for 25% Exposure Cycle.

XS Set Library	PARCS k_{eff}	$\Delta k_{eff}/k_{eff}$ (pcm)	Axial RPF RMS (%)	Radial RPF RMS (%)	Maximum Radial Peak (%)
Set 1	0.99842	48	10.49	1.46	5.20
Set 2a	0.99841	47	10.79	1.45	5.09
Set 2b	0.99903	109	4.10	1.12	5.48
Set 2c	0.99920	126	2.50	1.07	5.61
Set 2d	0.99927	133	2.06	1.07	5.68

Table 5.12. History Impact. XS Sets Results for 50% Exposure Cycle.

XS Set Library	PARCS k_{eff}	$\Delta k_{eff}/k_{eff}$ (pcm)	Axial RPF RMS (%)	Radial RPF RMS (%)	Maximum Radial Peak (%)
Set 1	0.99931	51	9.78	2.13	6.39
Set 2a	0.99900	20	10.67	2.21	6.43
Set 2b	0.99986	106	3.16	1.47	6.62
Set 2c	1.00001	121	1.95	1.34	6.69
Set 2d	1.00012	132	1.49	1.29	6.74

Discrepancies between SIMULATE-3 and PARCS are consistently less than 135 pcm in terms of k_{eff} and within 1.5% in terms of radial RMS. Across all cross-section libraries, there is a slight tendency for k_{eff} to be overpredicted, with this trend becoming slightly more pronounced as the history domain expands. However, these discrepancies remain constant across all points analyzed within the same library.

With the expanded history matrix, the power distributions show an outstanding improvement, with better results gradually obtained as the history domain broadens; as illustrated in Figure 5.21 and Figure 5.22.

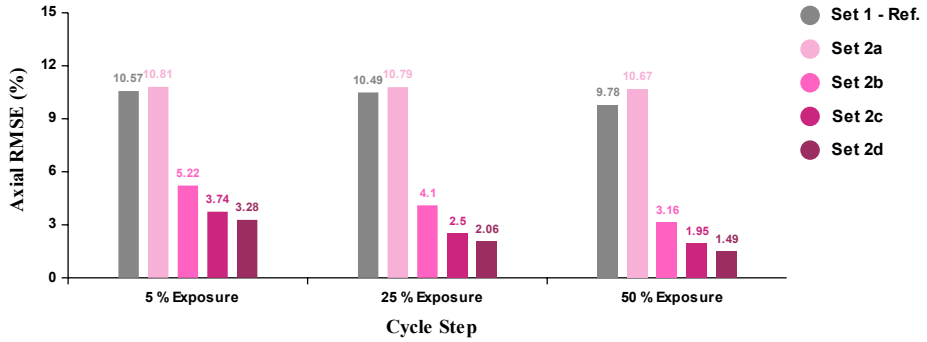

Figure 5.21. Axial RMSEs (%). Set1 vs. Set 2a-2d.

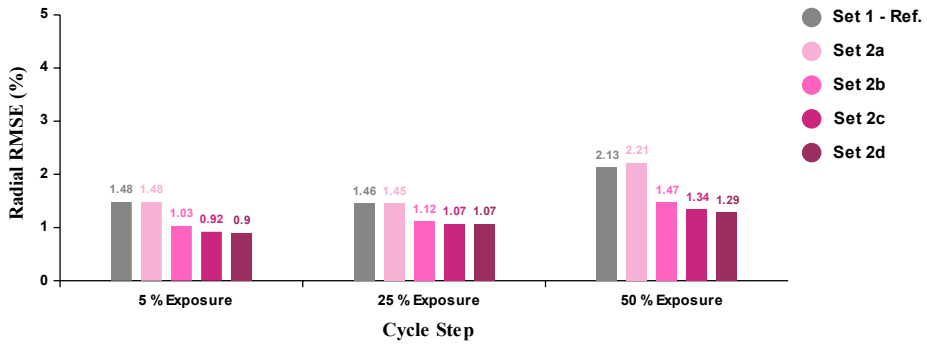

Figure 5.22. Radial RMSEs (%). Set1 vs. Set 2a-2d.

The reduction in errors observed as burnup increases suggests that historical effects are accurately accounted for, resulting in fewer cross-section extrapolations required for estimating nodal power distribution.

Although the 95% history shows the best accuracy compared to the reference, Set 2c library corresponding to 90% void history will be selected instead because some studies have found convergence difficulties for high void fractions (Wang, D. et al., 2013), because as the void fraction increases, the neutron spectrum becomes harder which raises concern about the predictability of lattice codes for fuel regions with very high void.

The 95% void branch might be used to replace the 90% branch if cross-sections at 95% void could be calculated accurately with a Monte Carlo calculation to confirm the

accuracy of the lattice code. Nonetheless, this validation is beyond the scope of this thesis.

Moreover, it is worth noting that error reductions between Set 2c (90% void) and Set 2d (95% void) are less pronounced. This observation could be attributed to the minimal difference in water density between 90% and 95% void fractions, or even between 95% and 100% void fractions. Consequently, the lattice code perceives only a marginal change in water densities within these specific ranges, potentially resulting in very similar cross-sections.

Thus, selecting Set 2c library, the RMS difference at BOC has been reduced axially from 10.52% to 3.74% (a reduction of approximately 64%) and radially from 1.48 to 0.92% (a reduction of about 37%). Moreover, at MOC conditions, the axial improvement is even more remarkable, with the RMS difference reduced from 9.78% to 1.95% (corresponding to an error reduction of around 80%).

For libraries Set 2a and Set 2c, relative radial and axial power differences at all analyzed points between SIMULATE-3 and PARCS are shown in Figure 5.23 and Figure 5.24, respectively.

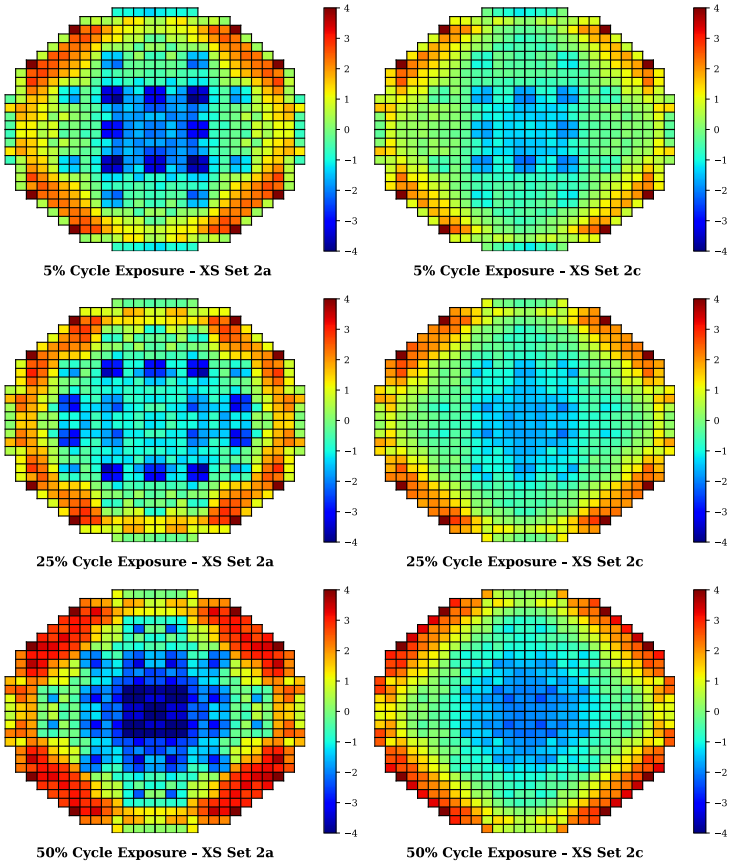

Figure 5.23. Relative Radial Power Errors (%). Set 2a vs. Set 2c.

For the radial power distribution, the tendency to underestimate the power in those fuels with control rods, as well as an overestimation of the power in some peripheral channels is still present. However, as can be seen, the underprediction of the power in the center of the core or near to control rods is less pronounced because the control blade and spectral history effects might be better captured with 90% off-nominal void fraction boundary conditions.

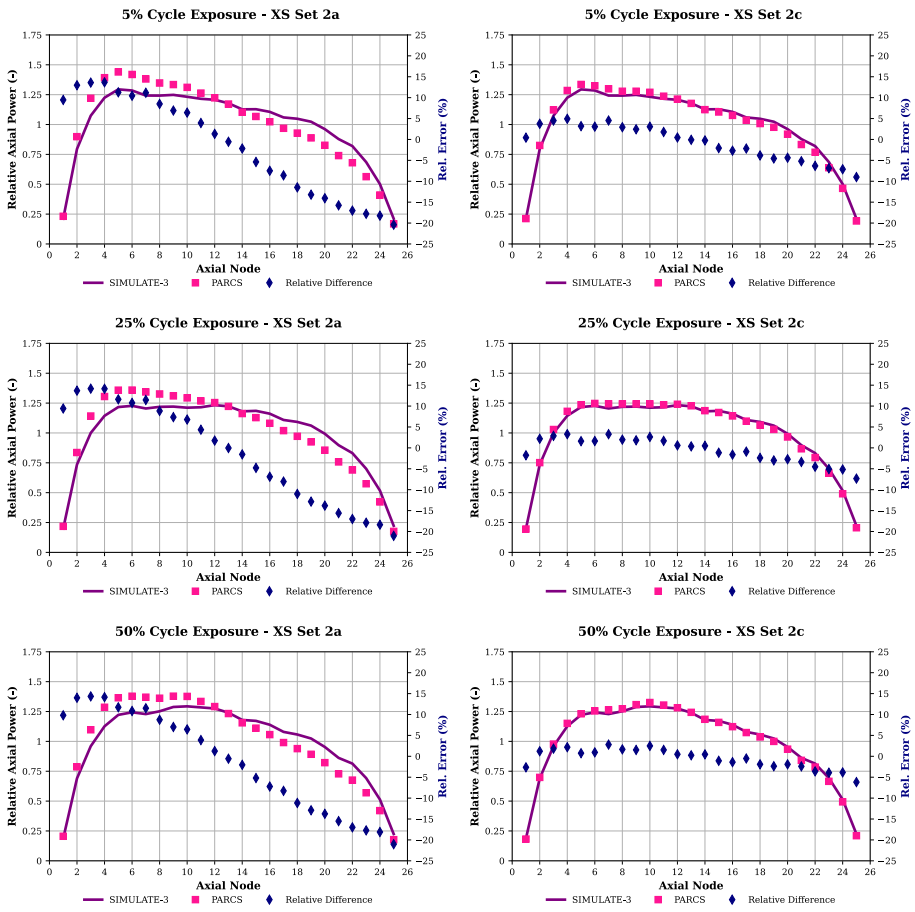

Figure 5.24. Relative Axial Power Errors (%). Set 2a vs. Set 2c.

For the axial power distribution, the significant discrepancies between SIMULATE-3 and PARCS due to its tendency to estimate a more peaked power at the bottom core that was seen with 70% void as an off-nominal upper boundary are no longer present when using 90% void as upper boundary history.

The overall obtained results do not correspond to the conclusions reported in the NUREG-CR7164 guidelines regarding the sensitivity analysis performed on moderator density history effects where (1) it was said that neither BWR steady-state nor transient analysis was highly sensitive to moderator density history effects (nor control rod history effects), and (2) it was found that three moderator density histories at 0%, 40%, and 70% (or 80%) voids were good enough for most BWR applications.

Therefore, based on the analysis conducted, the NUREG-CR7164 guidelines should be reevaluated to account for modern fuel bundles, high exposure levels, and power uprates.

On the other hand, when considering the history/branch matrix structure, the user should ensure that the range of anticipated application for the history/state parameters has been sufficiently covered in order to avoid the need for excessive cross-section table extrapolation. Yet, if there is no other choice, PARCS allows cross-section extrapolations for both instantaneous and history variables in the neutronic calculations when characterizing the reactor.

In PARCS, the parameter used to set the cross-section extrapolation range for instantaneous variables only applies to the branch type variable for each type of branch, whereas the parameter used to set the cross-section extrapolation range for history variables only applies to history variables.

The user gives the cross-section extrapolation ranges through the input deck. However, using too large of an extrapolation range can lead to unphysical cross-sections, which might result in a code failure. Therefore, the extrapolation option should be used with caution.

Comparisons of the power predictions using Set 2a (70% void off-nominal boundary) and Set 2b (80% void off-nominal boundary) libraries allowing cross-section extrapolations, up to 25% and 15% respectively, are presented in Figure 5.25 and Figure 5.26.

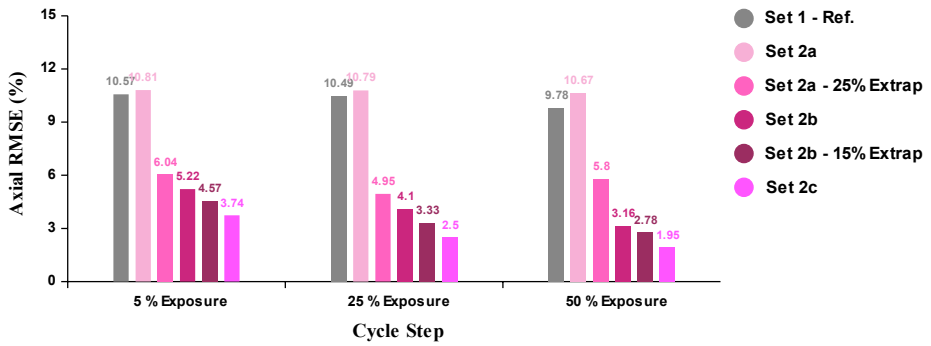

Figure 5.25. Axial RMSEs (%). Cross-Section Extrapolations.

Axially, there is a straightforward improvement in the estimation of the power distribution if, for the same library, the option to use cross-section extrapolations is selected. This leads to a reduction of around 50% in the axial RMS, as seen for Set 2a library results. The error reduction is less apparent for Set 2b library but still present in all analyzed points. Radially, the results align with those observed axially.

Nevertheless, the obtained results for both axial and radial RMSEs indicate that the best option for modeling BWR cross-sections is to use a library which sufficiently covers the range of applications for the history/state parameters without the need for cross-section extrapolations.

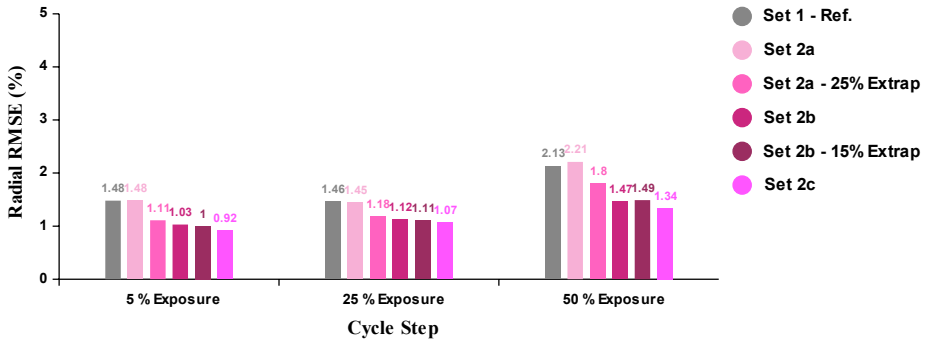

Figure 5.26. Radial RMSEs (%). Cross-Section Extrapolations.

Therefore, it seems more appropriate to select Set 2c library with an off-nominal upper boundary of 90% void instead of 70% or 80% voids even with the use of cross-section extrapolations.

Once the upper limit of the cross-section off-nominal calculations has been set, it seems convenient to re-study the effect of the branch refinement to determine whether the branches have an impact on the power distributions once the histories are suitably covered.

Alongside the moderator density branch mesh redefinition, the value of the nominal calculation will be modified from 40 to 45%. As seen in Figure 5.27 and Figure 5.28, a nominal value of 45% is more appropriate because it is closer to the average void core operation value at BOC conditions for both Cycles A and B during almost the whole cycles and it also corresponds to the mid value between the off-nominal limits of 0 and 90%, which might be more suitable for linear interpolations and the node characterization.

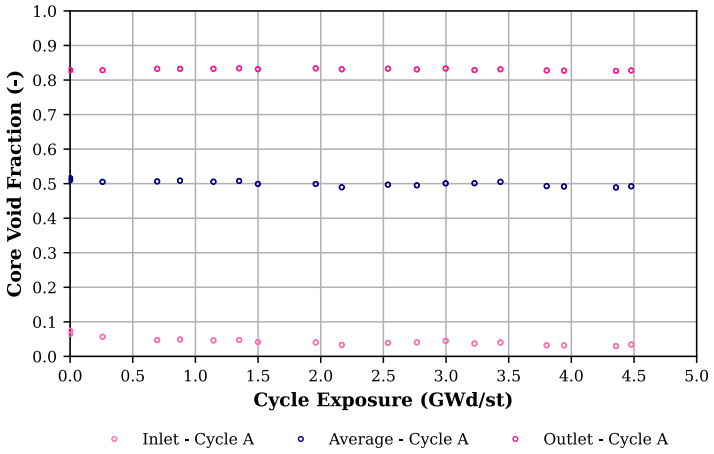

Figure 5.27. Instantaneous Void Fraction vs. Exposure. Cycle A.

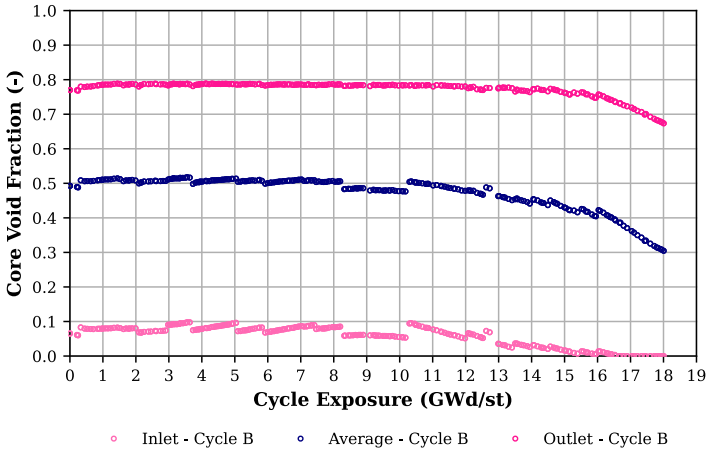

Figure 5.28. Instantaneous Void Fraction vs. Exposure. Cycle B.

Since BWR assemblies are very heterogeneous and the two-phase flow occurs in the reactor core during the operation, it is considered convenient to vary the entire 0-100% void fraction range by void fraction increases in approximately 10% steps.

This library is labeled as ***Set 3a*** and will be used as a reference library. Library Set 3a has been broken down into two libraries with less branches to study the branch mesh impact. Figure 5.29 contains the instantaneous void matrix structure conditions for the libraries designated as ***Set 3a***, ***Set 3b***, and ***Set 3c***.

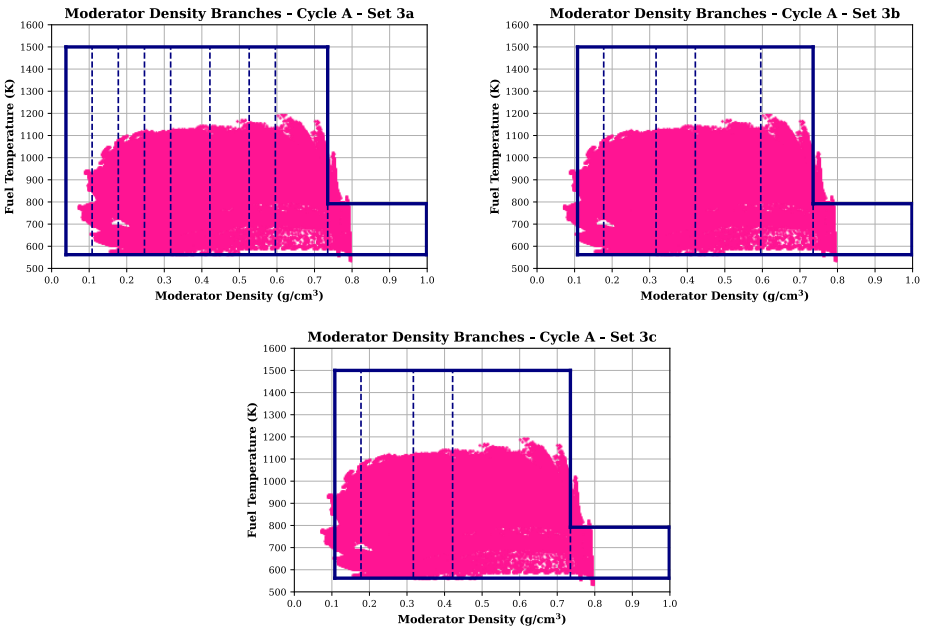

Figure 5.29. Instantaneous Void Branch Structure. Set 3a - Set 3b - Set 3c.

For a more comprehensive differentiation, once again, the changes from one library to another are highlighted in Table 5.13.

Table 5.13. Void History/Branch Matrix Structure Conditions for Set 2c, Set 3a, 3b, and 3c.

XS Set Library	History Parameter	Off-Nominal Lower Boundary	Nominal History	Off-Nominal Upper Boundary	Branch Parameter	Selected Branches (%)
Set 2c	HVOI	0%	40%	90%	VOI	0/20/40/60/80/90
Set 3a	HVOI	0%	45%	90%	VOI	0/20/30/45/60/70/80/90/100
Set 3b	HVOI	0%	45%	90%	VOI	0/20/45/60/80/90
Set 3c	HVOI	0%	45%	90%	VOI	0/45/60/80/90

Comparisons of the power predictions among Set 2c and Set 3a, 3b, and 3c libraries are presented in Figure 5.30 and Figure 5.31.

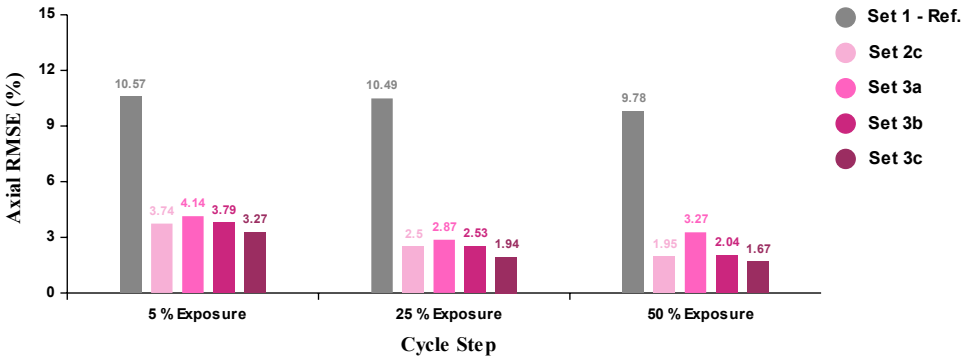

Figure 5.30. Axial RMSEs (%). Set 2c vs. Set 3a, 3b, and 3c.

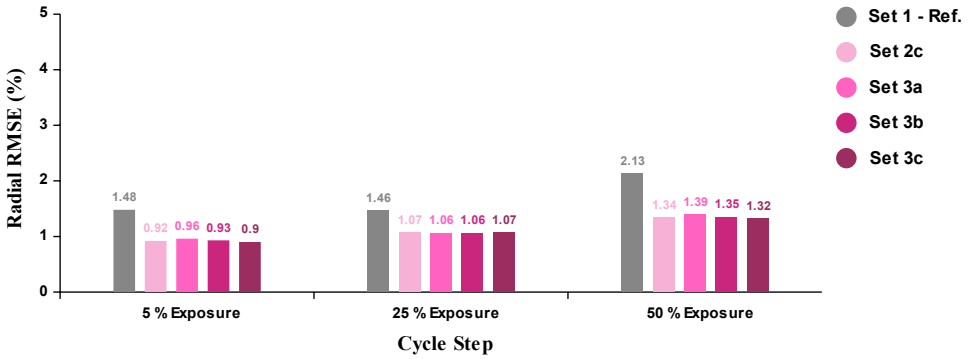

Figure 5.31. Radial RMSEs (%). Set 2c vs. Set 3a, 3b, and 3c.

As shown in Figure 5.30 and Figure 5.31, sensitivity analysis of moderator density instantaneous branch effects causes only marginal differences in the power predictions, especially for the radial power estimation, and indicates that BWR steady-state results are not highly sensitive to moderator density branch effects at least while the operating conditions of the reactor remain invariant.

Interestingly, the library with a finer density mesh exhibits poorer agreement with the reference assembly-wise axial predictions, a result that may initially seem paradoxical but aligns with the findings illustrated in Figure 5.14 concerning the fines branch matrix prior to expanding the history upper boundaries.

These comparisons, however, are intrinsic to a code-to-code analysis, and thus, the relative errors are significantly influenced by the reference code and its library. Consequently, one possible reason behind the higher errors could be the absence of the same branches in the reference library. Nonetheless, these results suggest that only a few branches may be sufficient, rather than an excessively fine definition of them.

The comparison of k_{eff} and power distributions between PARCS and SIMULATE-3, utilizing libraries Set 1, Set 2a, and Set 3a to Set 3c, is summarized in Table 5.14 to Table 5.16.

Table 5.14. Branches Impact. XS Sets Results for 5% Exposure Cycle.

XS Set Library	PARCS k_{eff}	$\Delta k_{eff}/k_{eff}$ (pcm)	Axial RPF RMS (%)	Radial RPF RMS (%)	Maximum Radial Peak (%)
Set 1	0.99971	67	10.57	1.48	4.42
Set 2c	1.00033	129	3.74	0.92	4.74
Set 3a	1.00027	123	4.14	0.96	4.74
Set 3b	1.00031	127	3.79	0.93	4.76
Set 3c	1.00026	122	3.27	0.90	4.76

Table 5.15. Branches Impact. XS Sets Results for 25% Exposure Cycle.

XS Set Library	PARCS k_{eff}	$\Delta k_{eff}/k_{eff}$ (pcm)	Axial RPF RMS (%)	Radial RPF RMS (%)	Maximum Radial Peak (%)
Set 1	0.99842	48	10.49	1.46	5.20
Set 2c	0.99920	126	2.50	1.07	5.61
Set 3a	0.99913	119	2.87	1.06	5.55
Set 3b	0.99918	124	2.53	1.06	5.60
Set 3c	0.99913	119	2.04	1.07	5.60

Table 5.16. Branches Impact. XS Sets Results for 50% Exposure Cycle.

XS Set Library	PARCS k_{eff}	$\Delta k_{eff}/k_{eff}$ (pcm)	Axial RPF RMS (%)	Radial RPF RMS (%)	Maximum Radial Peak (%)
Set 1	0.99931	51	9.78	2.13	6.39
Set 2c	1.00001	121	1.95	1.34	6.69
Set 3a	0.99988	108	2.27	1.39	6.69
Set 3b	0.99996	116	1.94	1.35	6.67
Set 3c	0.99993	113	1.67	1.32	6.64

Results of simulations using the Set 3c library, 45% void as nominal conditions, have better agreement with the SIMULATE-3 reference case than those from the Set 2c library with 40% void as nominal depletion conditions.

Discrepancies between SIMULATE-3 and PARCS are consistently less than 130 pcm in terms of k_{eff} and within 1.4% in terms of radial RMS. These results support the change to use 45% void as nominal depletion conditions because it is closer to the average void fraction at which the reactor operates under normal conditions, as illustrated in Figure 5.32 and Figure 5.33.

Thus, it might be concluded, from the performed analysis, that five moderator density branches at 0%, 45%, 60%, 80%, and 90% voids provide sufficient accuracy for most BWR applications.

However, transients may be sensitive to the structure of moderator density branches, especially when the core upper region has void fractions that are outside the range of moderator density branches.

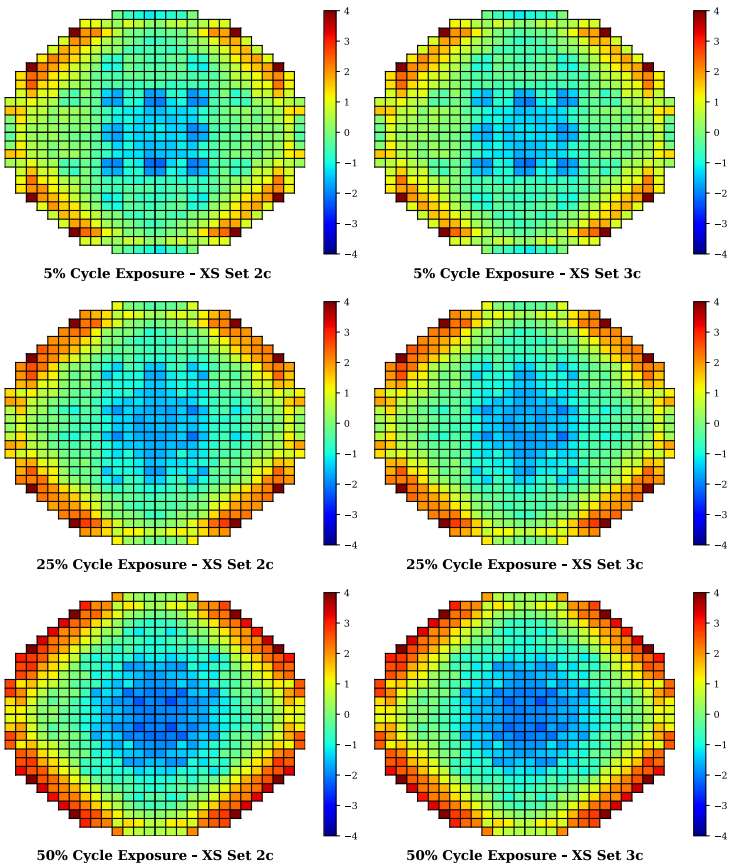

Figure 5.32. Relative Radial Power Errors (%). Set 2c vs. Set 3c.

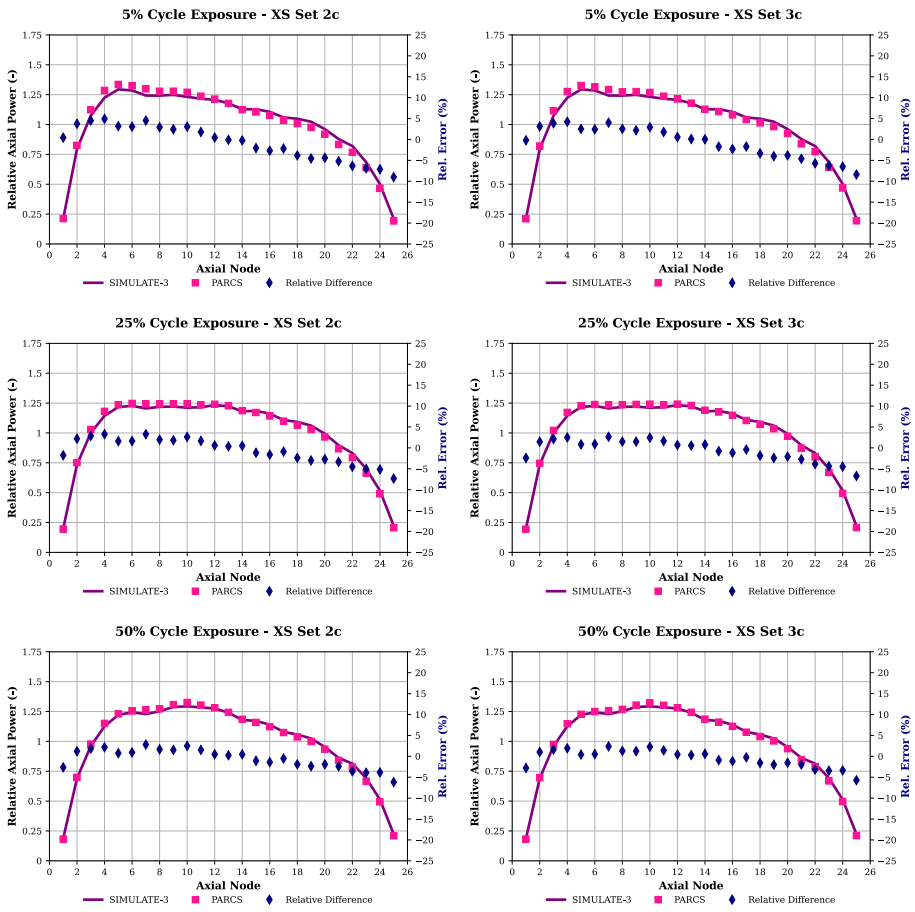

Figure 5.33. Relative Axial Power Errors (%). Set 2c vs. Set 3c.

In conclusion, the recommended history-branch matrix structure details of the Set 3c library are given in Table 5.17 and Table 5.18. Next, the analysis of the impact of the burnup points for both history and instantaneous variables will be undertaken.

Table 5.17. Branches Used in the Selected Cross-Section Library – Set 3c.

Number	Type	CR	VOI (%)	TFU (K)	TMO (K)	Depletion/Branch
Base Case (BC)	BASE	Out	45	792.4	561.4	Nominal Depletion
1	VOI	Out	0	792.4	561.4	Branch from BC
2	VOI	Out	60	792.4	561.4	Branch from BC
3	VOI	Out	80	792.4	561.4	Branch from BC
4	VOI	Out	90	792.4	561.4	Branch from BC
5	VOI/TFU	Out	0	562.0	561.4	Branch from BC
6	VOI/TFU	Out	0	1500.0	561.4	Branch from BC
7	VOI/TFU	Out	45	562.0	561.4	Branch from BC
8	VOI/TFU	Out	45	1500.0	561.4	Branch from BC
9	VOI/TFU	Out	60	562.0	561.4	Branch from BC
10	VOI/TFU	Out	60	1500.0	561.4	Branch from BC
11	VOI/TFU	Out	80	562.0	561.4	Branch from BC
12	VOI/TFU	Out	80	1500.0	561.4	Branch from BC
13	VOI/TFU	Out	90	562.0	561.4	Branch from BC
14	VOI/TFU	Out	90	1500.0	561.4	Branch from BC
15	CR/VOI	In	0	792.4	561.4	Branch from BC
16	CR/VOI	In	45	792.4	561.4	Branch from BC
17	CR/VOI	In	60	792.4	561.4	Branch from BC
18	CR/VOI	In	80	792.4	561.4	Branch from BC
19	CR/VOI	In	90	792.4	561.4	Branch from BC
20	CR/VOI/TFU	In	0	562.0	561.4	Branch from BC
21	CR/VOI/TFU	In	0	1500.0	561.4	Branch from BC
22	CR/VOI/TFU	In	45	562.0	561.4	Branch from BC
23	CR/VOI/TFU	In	45	1500.0	561.4	Branch from BC
24	CR/VOI/TFU	In	60	562.0	561.4	Branch from BC
25	CR/VOI/TFU	In	60	1500.0	561.4	Branch from BC
26	CR/VOI/TFU	In	80	562.0	561.4	Branch from BC
27	CR/VOI/TFU	In	80	1500.0	561.4	Branch from BC
28	CR/VOI/TFU	In	90	562.0	561.4	Branch from BC
29	CR/VOI/TFU	In	90	1500.0	561.4	Branch from BC
30	VOI/TMO	Out	0	792.4	545.0	Branch from BC
31	VOI/TFU/TMO	Out	0	293.0	293.0	Branch from BC
32	VOI/TFU/TMO	Out	0	562.0	293.0	Branch from BC
33	VOI/TFU/TMO	Out	0	792.4	293.0	Branch from BC
34	CR/VOI/TMO	In	0	792.4	545.0	Branch from BC
35	CR/VOI/TFU/TMO	In	0	293.0	293.0	Branch from BC
36	CR/VOI/TFU/TMO	In	0	562.0	293.0	Branch from BC
37	CR/VOI/TFU/TMO	In	0	792.4	293.0	Branch from BC

Table 5.18. Histories Used in the Selected Cross-Section Library – Set 3c.

Number	Type	CR	VOI (%)	TFU (K)	TMO (K)	Depletion/Branch
Base Case (BC)	BASE	Out	45	792.4	561.4	Nominal Depletion
1	HVOI	Out	0	792.4	561.4	Depletion from BC
2	HVOI	Out	90	792.4	561.4	Depletion from BC
3	HCR/HVOI	In	0	792.4	561.4	Depletion from BC
4	HCR/HVOI	In	45	792.4	561.4	Depletion from BC
5	HCR/HVOI	In	90	792.4	561.4	Depletion from BC
6	HVOI/HTFU	Out	45	562.0	561.4	Depletion from BC
7	HVOI/HTFU	Out	45	1500.0	561.4	Depletion from BC
8	HCR/HVOI/HTFU	In	45	562.0	561.4	Depletion from BC
9	HCR/HVOI/HTFU	In	45	1500.0	561.4	Depletion from BC

5.5.3 Analysis of the Influence of the Burnup Mesh Points.

During operation of a reactor its material compositions change because of exposure to the neutron flux and because of radioactive decay. These changes affect important quantities like multiplication factor and power distribution, reference (Studsvik Scandpower, 2008). This topic was already described in Chapter 3 when the Bateman equation was discussed.

Since the cell composition changes with burnup as well as the conditions in the moderator and the fuel, the neutron spectrum also changes. Change in the neutron spectrum in turn means that the average microscopic cross-sections may have to be recalculated in every step.

The macroscopic cross-sections are certainly calculated for every step and for every region of the core. Lattice physics codes like CASMO-4 take these changes into account.

As stated in (Ott, K. O. & Neuhold, R. J., 1985), time-dependent phenomena in nuclear reactors may be subdivided into three distinctively different classes:

1) *Short-time phenomena*, which typically occur in time intervals of milliseconds to seconds; in special cases, the time intervals may extend to many minutes.
2) *Medium-time phenomena*, which occur over hours or days corresponding to the mean buildup and decay times of certain fission products that strongly affect the reactivity.
3) *Long-time phenomena*, with variations developing over several months or years.

These time-dependent phenomena basically include changes in the neutron flux as well as causally related changes in the reactor system, i.e., composition or temperature.

Medium- and long-time phenomena are of interest for the sake of the influence of the burnup mesh points in cross-section libraries.

Medium-time phenomena are generally associated with the buildup burnup and beta decay of ^{135}Xe and ^{149}Sm. ^{135}Xe is formed as the result of the decay of ^{135}I and is also produced directly in fission. ^{149}Sm is not formed directly in fission but appears as the result of the decay of ^{149}Nd which decays from ^{149}Pm which may be assumed to be produced directly in fission.

These two fission products are strong neutron absorbers because of their very high thermal neutron capture cross-sections and, particularly for ^{135}Xe, its relatively large fission yield. Thus, to capture the Xe/Sm effects is fundamental for building adequate cross-section libraries.

Long-time phenomena include particularly the burnup and buildup of fissionable isotopes, as well as the buildup, beta decay, and burnup of most of the fission products.

The reactivity effects of fuel depletion must be compensated to maintain criticality over the fuel burnup cycle. The major compensating elements are the control rods, although Burnable Poisons (BP) at selected locations in the core can also be used to compensate the negative reactivity effects of fuel depletion.

BPs are nuclides that have a large absorption cross-section which is converted into a nuclide with a low absorption cross-section as the result of neutron absorption. Experience has shown that the use of burnable poisons offers advantages for better fuel utilization over use of control rods alone (Cochran, R. G. & Tsoulfanidis, N., 1999).

Gadolinium (Gd) is commonly used in BWR as a burnable poison to reduce the reactivity of fresh bundles and to shape the power distributions during core depletion.

The axial Gd designs can be made in many different ways. The most common way is to have more Gd in the lower sections and less in the upper parts. However, fuel pins containing Gd deplete in a complicated manner and, usually, many radial rings need to be modeled to accurately follow Gd depletion and the fission distribution profile within the pellet, (Smith, K. & Forget, B., 2013).

When the Gd content has been burnt, the maximum reactivity in the fresh fuel happens. Then, to determine the right depletion steps for Gd is essential for building good cross-section libraries.

For fuel mixtures that contain gadolinium, a time step size of around 2 GWd/st can introduce significant errors into the results from the lattice physics code. This sensitivity is caused by the large spatial self-shielding of the ^{155}Gd and ^{157}Gd isotopes that create rapid changes in the thermal flux distribution across the fuel pellet as the gadolinium depletes. To accurately capture the depletion rate of the gadolinium, time step sizes on the order of 0.2-0.5 GWd/st are typically required at the lattice level.

For the specific case of CASMO-4, there are two possible depletion cases for BWRs:

1) Depletion steps without Gd. Use of the following steps: 0.1, 0.5, 1.5, 2.5, 5, 7.5, 10, and every 2.5 MWd/st up to 100 MWd/st.

2) Depletion steps with Gd. After initial steps of 0.1 and 0.5 MWd/st, steps of 0.5 MWd/st are used until the ^{155}Gd is depleted. Thereafter, the same depletion steps are used as for a bundle without Gd.

Anyhow, the depletion steps for Gd depletion are hardwired if the code detects that the input contains Gd. The user can request additional steps but not eliminate the default steps. This restriction is to preserve the fidelity of the depletion calculation, reference (Knott et al., 1995).

In CASMO-4, a *Predictor-Corrector* approach is used for the burnup calculation which permits the use of relatively large burnup intervals, while maintaining the accuracy of the results. For each burnup step, the depletion is calculated twice; first using the spectra at the start of the step and then, after a new spectrum calculation, using the spectra at the end of the step.

Thus, in going from the time t_{n-1} to t_n, a *Predictor* step is first taken using the fluxes obtained from the neutron calculation at t_{n-1}. The predictor step provides predicted number densities at t_n. The cross-sections are then updated, and the new spectrum calculation gives fluxes to be used in a *Corrector* step after which final number densities at t_n are given by the average value of the results from the predictor and corrector steps.

Average number densities from these two calculations are used as start values for the next burnup steps. All the calculations assumed that the conditions changed at the end of each depletion step and stayed constant throughout the step.

Table 5.19 summarizes the burnup points' recommendations for the lattice code calculation if one wants to catch up properly with the associated depletion phenomena. The step length may be given in time units or terms of burnup. Obviously, the latter is more meaningful since the burnup causes changes in the fuel.

Table 5.19. Summary of Typical Burnup Step Lengths.

Burnup Lengths	Reason
From 0 to 0.5 GWd/st: points at 0, 0.1, and 0.5	Fission Products. Mainly Xe/Sm
From 1 to 10 GWd/st: steps of 0.5 GWd/st	Burnable Absorbers. Mainly Gd
Up to 70 GWd/st: steps of 2.5 or 5 GWd/st	Fuel Depletion. Actinide Production

Following these recommendations, two more libraries have been modeled in addition to the selected library Set 3c. Before going further with the description of the libraries and their employed burnup points, it is worth noting that there is a distinction in CASMO-4 between burnup points for the depletion and the branches.

Users can select the number of burnup points for depletion and branches, although the default option for depletion can also be chosen. In that sense, because, as

aforementioned, the Gd depletion burnup points are hardwired in CASMO-4, the fission products, and burnable absorbers effects will typically be captured and considered in the built library. Thus, the discrepancies seen in using different numbers of burnup points will be more likely related to the branches.

The range of burnup exposure included in the lattice physics calculation should be sufficient to cover the maximum anticipated exposure for all fuel assemblies in the core. This is needed to avoid over-extrapolation of cross-sections at high burnups. Thus, the three analyzed libraries are designed to cover a burnup up to 70 GWd/st.

Table 5.20, Table 5.21, and Table 5.22 contain the selected burnup points for each of the three libraries composed to analyze the impact of the burnup points on the predictions of the 3D power distribution for Cycle A. The burnup points added from one library to another are highlighted.

Table 5.20. Burnup Points for CASMO-4. Set 3c-b20 library.

Burnup Points (GWd/st)									
0.0	0.5	1.0	2.0	4.0	6.0	8.0	10.0	15.0	20.0
25.0	30.0	35.0	40.0	45.0	50.0	55.0	60.0	65.0	70.0
							Total	**Points**	**20**

Table 5.21. Burnup Points for CASMO-4. Set 3c-b46 library.

Burnup Points (GWd/st)									
0.0	**0.1**	0.5	**1.0**	**1.5**	2.0	**2.5**	**3.0**	**3.5**	4.0
4.5	**5.0**	**5.5**	6.0	**6.5**	**7.0**	**7.5**	8.0	**8.5**	**9.0**
9.5	10.0	**12.5**	15.0	**17.5**	20.0	**22.5**	25.0	**27.5**	30.0
32.5	35.0	**37.5**	40.0	**42.5**	45.0	**47.5**	50.0	**52.5**	55.0
57.5	60.0	**62.5**	65.0	**67.5**	70.0				
							Total	**Points**	**46**

Table 5.22. Burnup Points for CASMO-4. Set 3c-b78 library.

Burnup Points (GWd/st)									
0.0	0.1	0.5	1.0	1.5	2.0	2.5	3.0	3.5	4.0
4.5	5.0	5.5	6.0	6.5	7.0	7.5	8.0	8.5	9.0
9.5	10.0	10.5	11.0	11.5	12.0	12.5	13.0	13.5	14.0
14.5	15.0	15.5	16.0	16.5	17.0	17.5	18.0	18.5	19.0
19.5	20.0	20.5	21.0	21.5	22.0	22.5	23.0	23.5	24.0
24.5	25.0	25.5	26.0	26.5	27.0	27.5	28.0	28.5	29.0
29.5	30.0	32.5	35.0	37.5	40.0	42.5	45.0	47.5	50.0
52.5	55.5	57.5	60.0	62.5	65.0	67.5	70.0		
							Total	**Points**	**78**

Set 3c-b20, ***Set 3c-b46***, and ***Set 3c-b78*** represent 20, 46, and 78 burnup points, respectively. Set 3c-b46 models a refined mesh up to 10 GWd/st whereas Set 3c-b78 represents a finer mesh up to 30 GWd/st.

Graphical representations of axial and radial RMSEs for the analyzed points are presented in Figure 5.34. Overall, there exists excellent concordance between the axial and radial power distributions computed by PARCS and those by SIMULATE-3 under identical conditions. This alignment is particularly noteworthy during BOC conditions, where the 46-burnup points library accurately predicts the power distribution with exceptional precision.

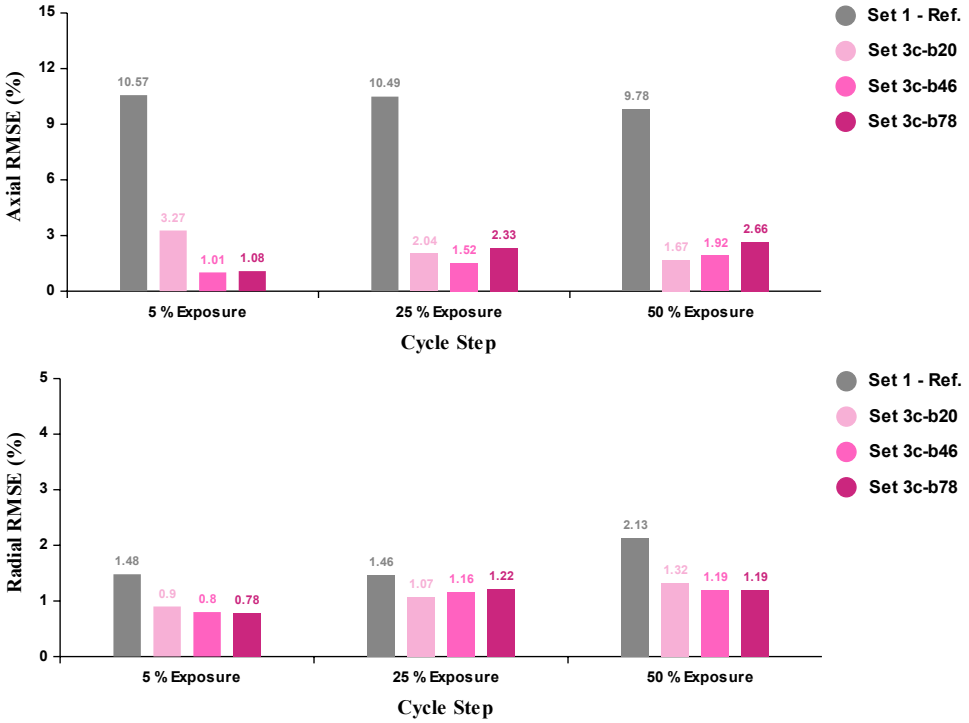

Figure 5.34. Axial and Radial RMSEs (%). Burnup Points Impact.

The impact of varying burnup points in cross-section modeling is shown in Table 5.23 to Table 5.25. These tables provide a comparative analysis of SIMULATE-3 and PARCS calculations for eigenvalue and core average axial and radial power distributions across three different libraries.

Discrepancies between SIMULATE-3 and PARCS remain consistently below 125 pcm in terms of k_{eff} and within 1.32% in terms of radial RMS. Notably, a systematic overprediction of k_{eff} by approximately 120 pcm is observed for the 20-burnup library, while a slight underprediction, escalating as the cycle progresses, is evident for the 78-burnup library. Nevertheless, these estimations of k_{eff} and radial RMS errors align closely with those previously observed for the branch impact analysis.

Table 5.23. Burnup Points Impact. 5% Exposure Cycle Results.

XS Set Library	PARCS k_{eff}	$\Delta k_{eff}/k_{eff}$ (pcm)	Axial RPF RMS (%)	Radial RPF RMS (%)	Maximum Radial Peak (%)
Set 3c-b20	1.00026	122	3.27	0.90	4.74
Set 3c-b46	0.99933	29	1.01	0.80	4.48
Set 3c-b78	0.99890	-14	1.08	0.78	4.38

Table 5.24. Burnup Points Impact. 25% Exposure Cycle Results.

XS Set Library	PARCS k_{eff}	$\Delta k_{eff}/k_{eff}$ (pcm)	Axial RPF RMS (%)	Radial RPF RMS (%)	Maximum Radial Peak (%)
Set 3c-b20	0.99913	119	2.04	1.07	5.63
Set 3c-b46	0.99809	15	1.52	1.16	5.56
Set 3c-b78	0.99761	-33	2.33	1.22	5.54

Table 5.25. Burnup Points Impact. 50% Exposure Cycle Results.

XS Set Library	PARCS k_{eff}	$\Delta k_{eff}/k_{eff}$ (pcm)	Axial RPF RMS (%)	Radial RPF RMS (%)	Maximum Radial Peak (%)
Set 3c-b20	0.99993	113	1.67	1.32	6.64
Set 3c-b46	0.99872	-8	1.92	1.19	6.41
Set 3c-b78	0.99822	-58	2.66	1.19	6.34

Relative radial power differences, core-average axial power shape, and relative axial differences related to the impact of different burnup points libraries are shown in Figure 5.35 through Figure 5.38.

A priori, the most accurate results were expected from the 78-burnup points library. However, it is found that there is no evident improvement in power distribution estimations when using this library in comparison to the 46-burnup points, as the power errors seem to bounce around without a clear trend toward an improvement in the results with a finer burnup mesh, but a significant difference in computational time for the lattice code calculations for 46- or 78-burnup points.

The error bouncing trends can be recalled when looking at the relative errors between the Set3c-b46 and Set3-b78 libraries. Thus, it seems plausible there might be a

limit to enhancements on the cross-section libraries burnup-points wise. However, further work will be required to demonstrate this conclusively.

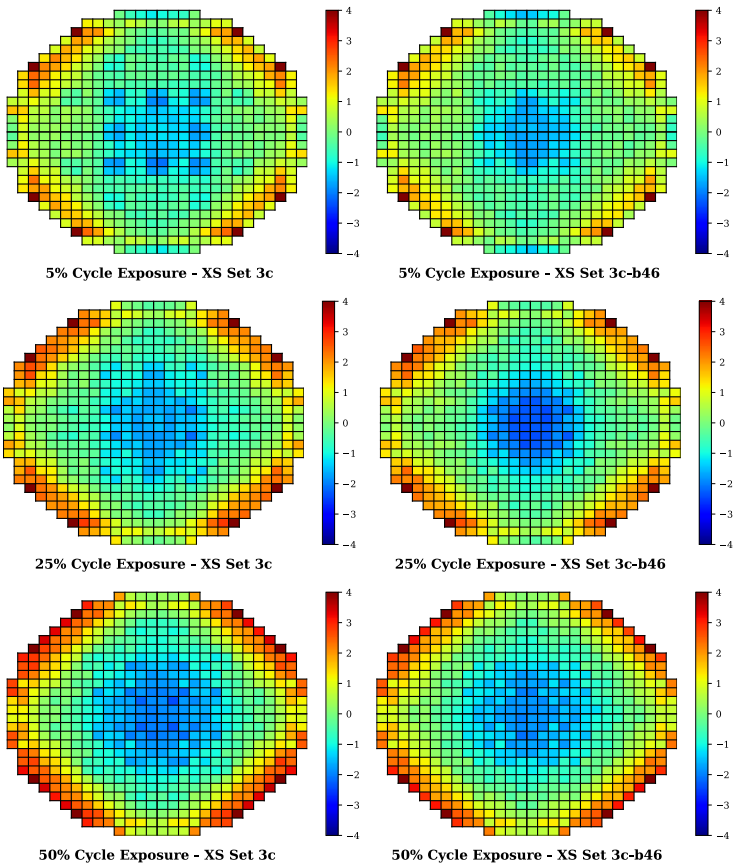

Figure 5.35. Relative Radial Power Errors (%). Set 3c vs. Set 3c-b46.

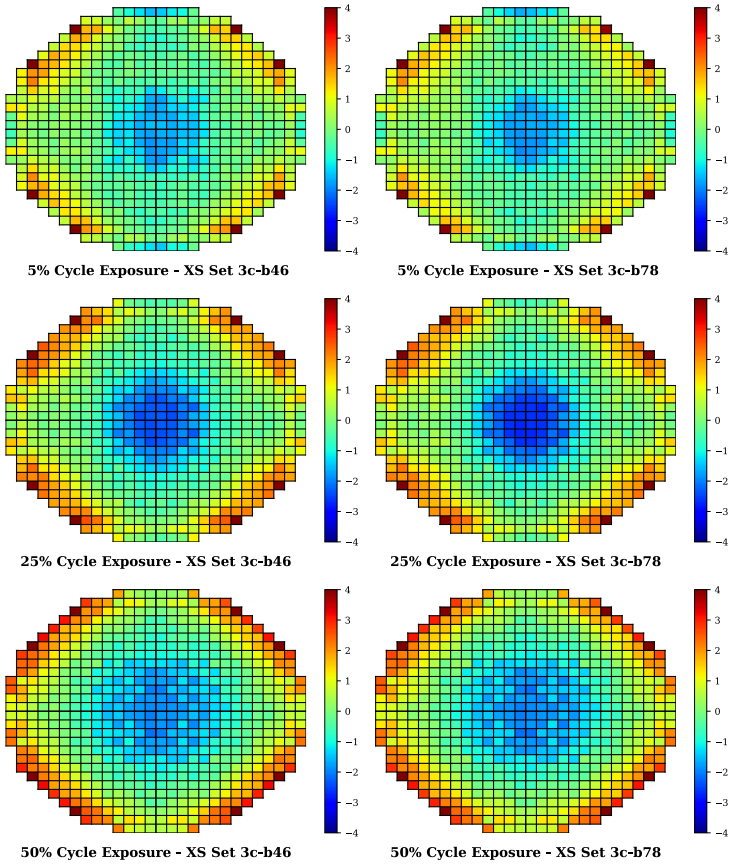

Figure 5.36. Relative Radial Power Errors (%). Set 3c-b46 vs. Set 3c-b78.

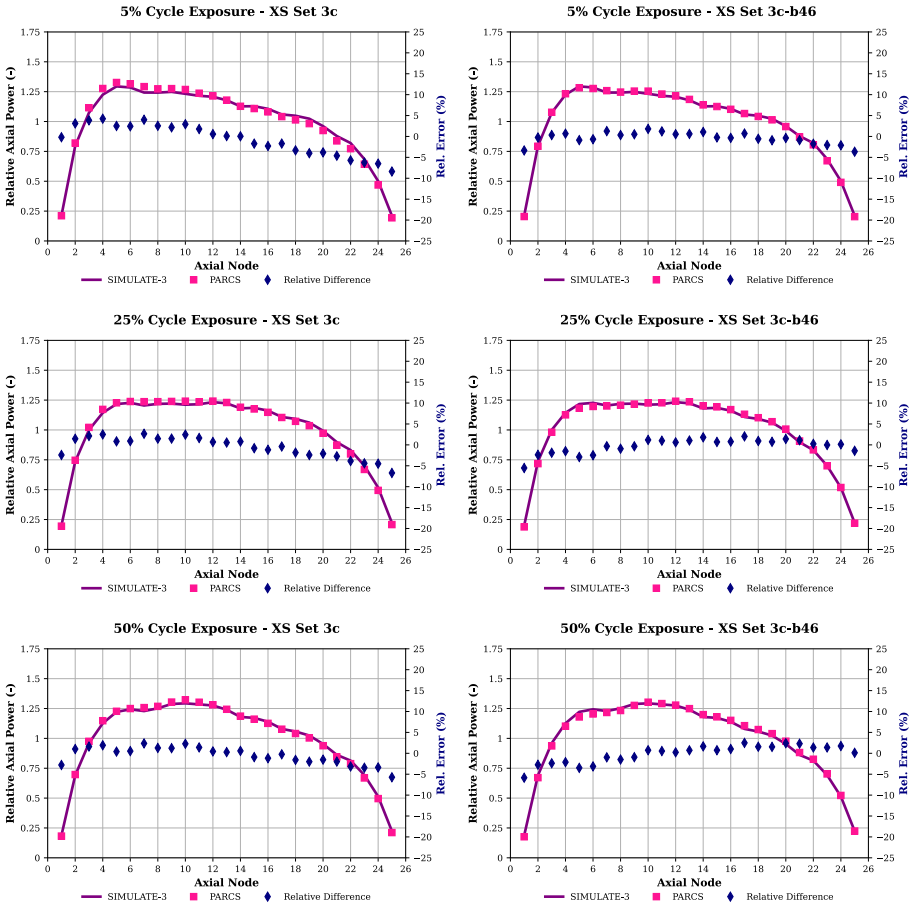

Figure 5.37. Relative Axial Power Errors (%). Set 3c vs. Set 3c-b46.

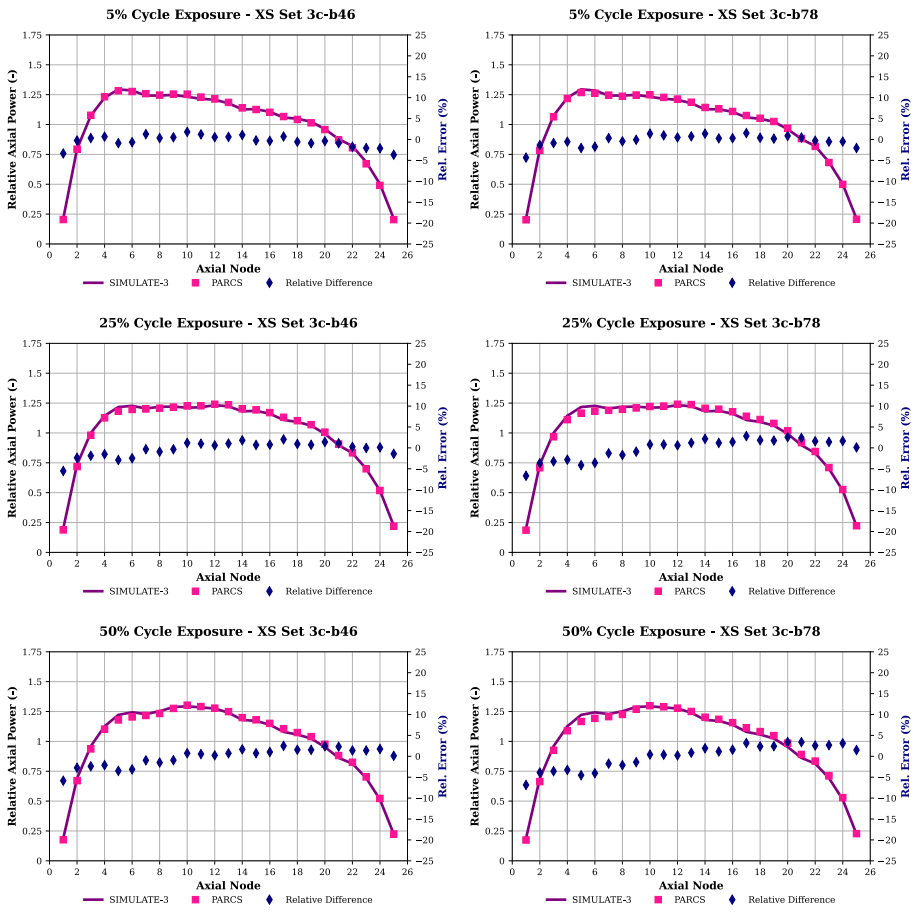

Figure 5.38. Relative Axial Power Errors (%). Set 3c-b46 vs. Set 3c-b78.

To conclude the study of the cross-section modeling for BWRs, the next comparison shows the axial power profiles predicted by SIMULATE-3 and PARCS using the initial library, ***Set 1***, and the two libraries selected in the analysis of the history/branch matrix and the impact of the burnup points, i.e., ***Set 3c*** and ***Set 3c-b46***, respectively.

The improvement in power prediction is outstanding due to the comprehensive coverage of the reactor's expected operating conditions by the modeled history/branch matrix, the chosen mesh variables, and the selected burnup points. This extensive coverage minimizes the need for cross-section extrapolations, which are the primary sources of errors, resulting in an excellent estimation of power distribution.

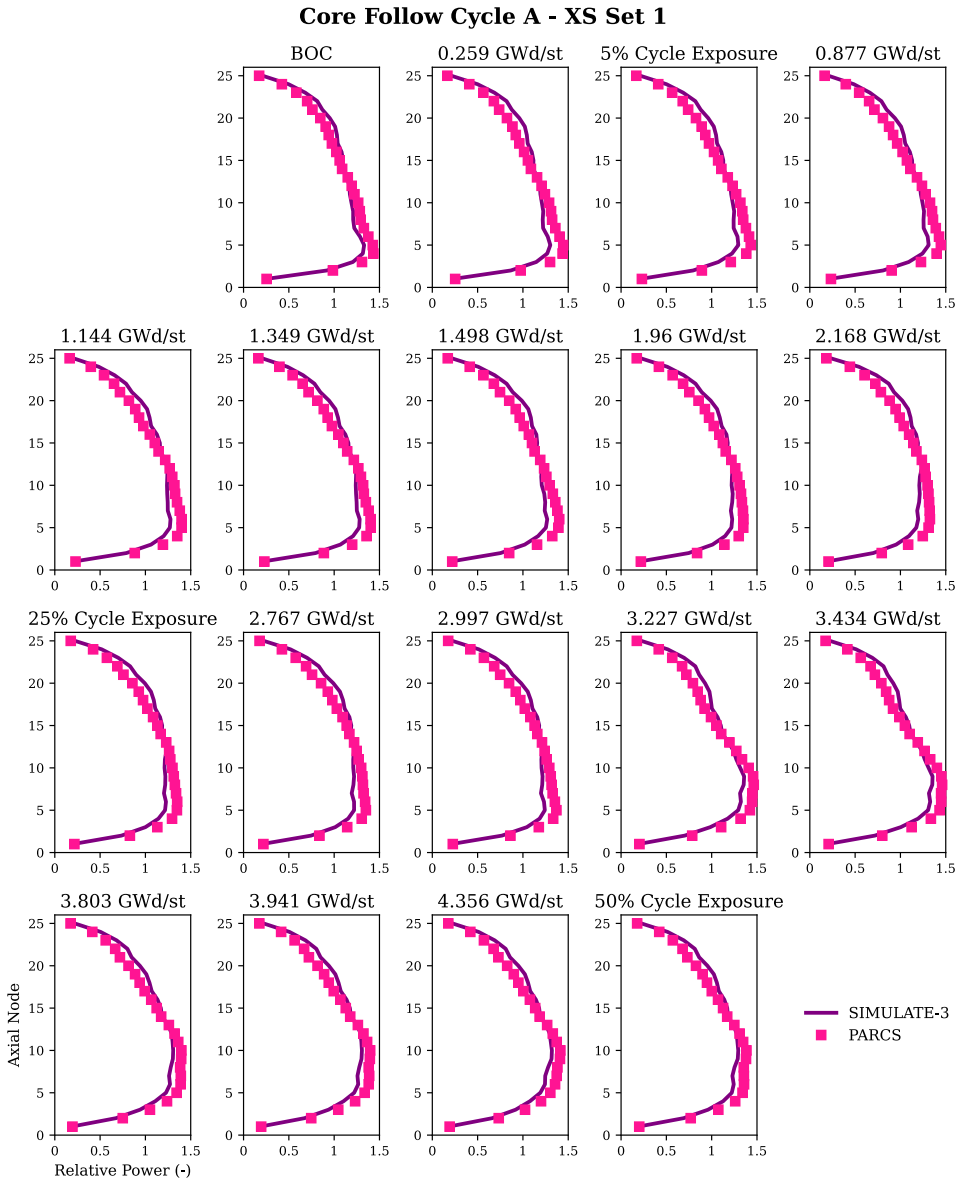

Figure 5.39. PARCS Axial Power Distributions. Cycle A Core Follow. XS Set 1.

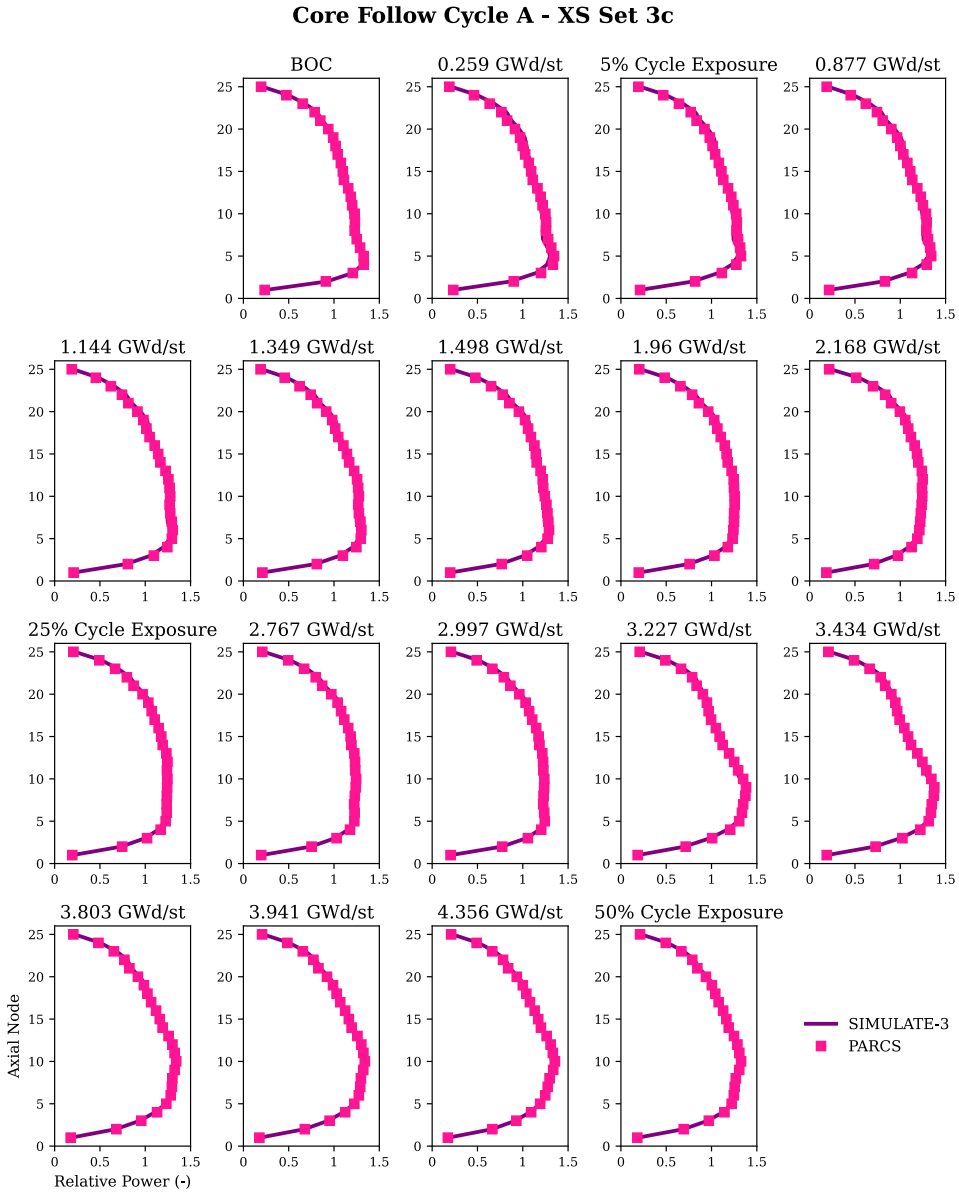

Figure 5.40. PARCS Axial Power Distributions. Cycle A Core Follow. XS Set 3c.

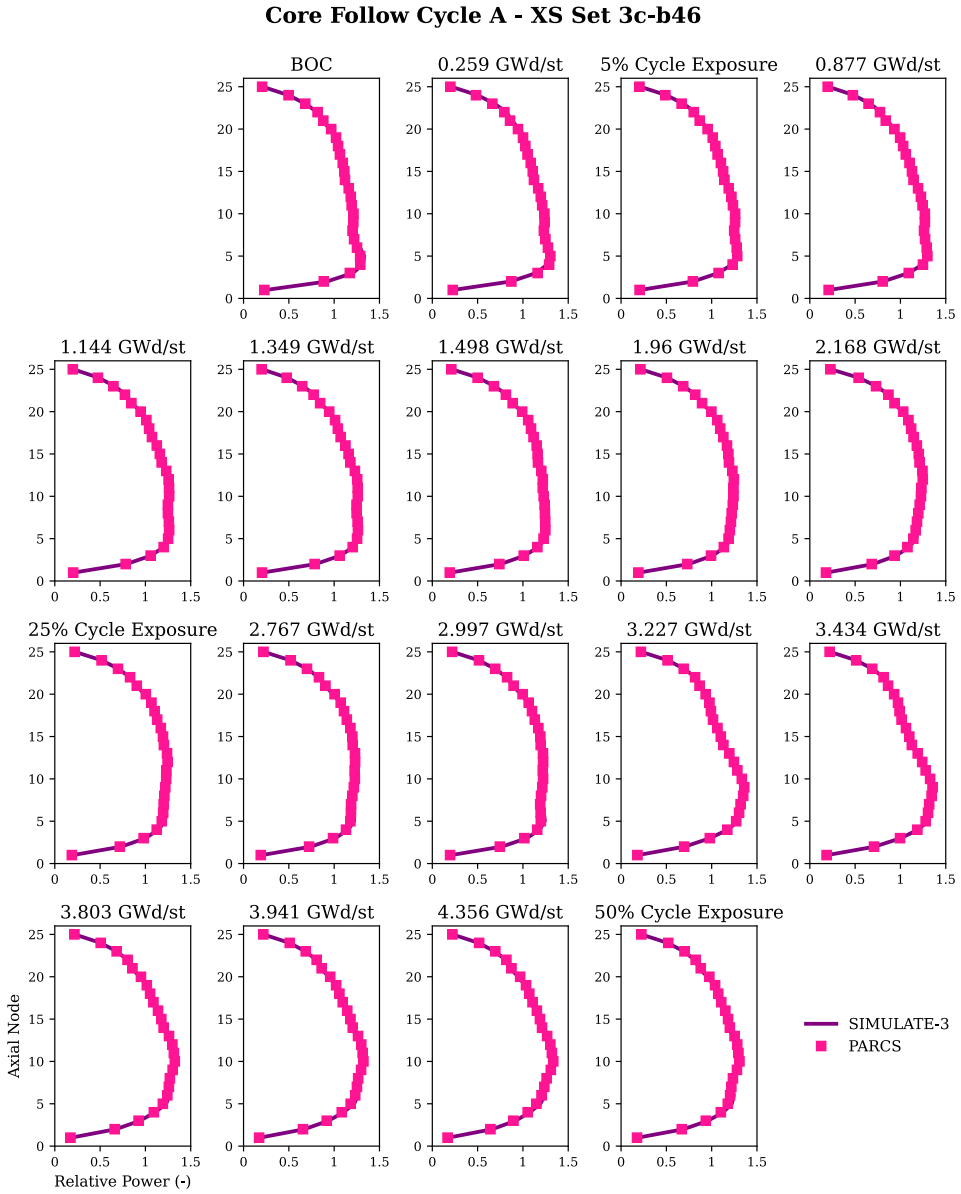

Figure 5.41. PARCS Axial Power Distributions. Cycle A Core Follow. XS Set 3c-b46.

In conclusion, it appears that the best-suited cross-section library for our modeling purposes is the ***Set 3c-b46 library***. This library mesh will also be used to model the library required to simulate Cycle B core follow, as outlined at the beginning of this chapter.

5.6 Core Follow Cycle B Results.

Once the Set 3c-b46 library has been selected, the 70 unique fuel segments corresponding to Cycle B have to be modeled and run with CASMO-4 to produce the nuclear data library needed for Cycle B analysis. Recalling from Section 5.2, Cycle B assesses a complete core-follow simulation, i.e., depletion characteristics from the BOC through the EOC, including coast-down conditions. Moreover, all histories and the control rod patterns are available at each depletion step.

Figure 5.42 illustrates the distributions of history and instantaneous nodal moderator densities and fuel temperatures for Cycle B. The solid blue line represents the boundaries of the Set 3c-b46 library while the dotted blue lines represent the void branching. As seen, almost all nodes in Cycle B are covered by the Set 3c-b46 library, so a very accurate power prediction is expected using this library.

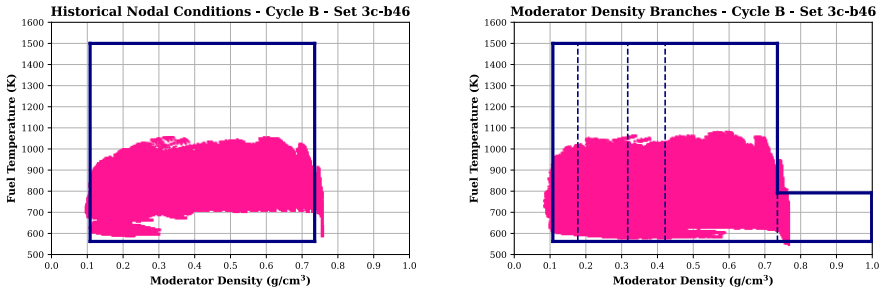

Figure 5.42. History (left) and Instantaneous (right) Moderator Density Boundaries. Set 3c-b46.

Utilizing the Set 3c-b46 library, significant enhancements are observed in the accuracy of predictions, see Figure 5.43 and Figure 5.44.

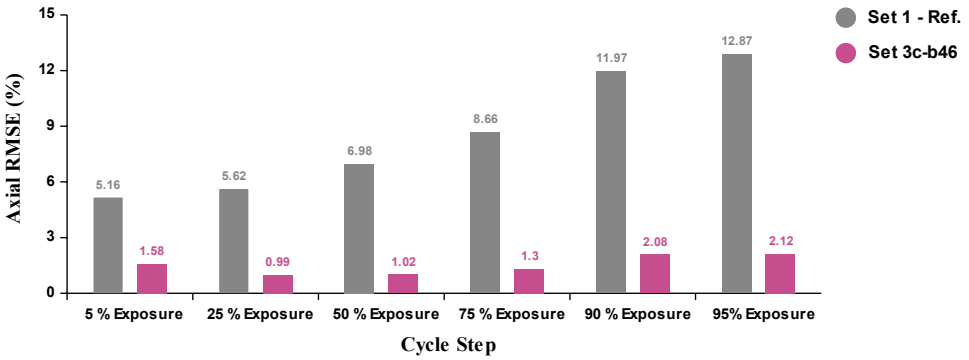

Figure 5.43. Axial RMSEs (%). Set 1 vs. Set 3c-b46. Cycle B.

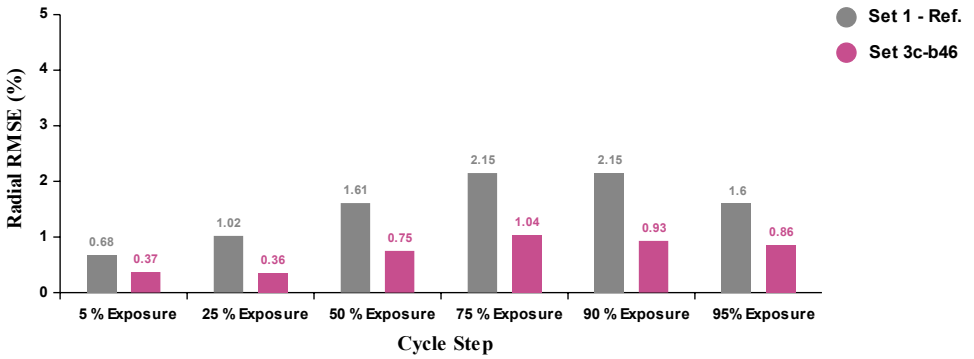

Figure 5.44. Radial RMSEs (%). Set 1 vs. Set 3c-b46. Cycle B.

At BOC conditions, the RMEs difference is notably reduced both axially, from 5.16% to 1.58% (representing an error reduction of approximately 69%), and radially, from 0.68% to 0.37% (reflecting a reduction of about 45%).

Remarkably, the axial improvement is even more pronounced at MOC conditions, with an error reduction of around 85% (from 6.98% to 1.02%), and at EOC conditions, with an error reduction of about 83% (from 12.87% to 2.12%).

This reduction in errors with increasing burnup indicates the accurate capture of historical effects, resulting in fewer cross-section extrapolations required for estimating nodal power distribution.

Overall, outstanding improvements are observed when employing the Set 3c-b46 library in comparison to Set 1 across all selected points of Cycle B.

The comparison of k_{eff} and power distributions between PARCS and SIMULATE-3 utilizing both Set 1 and Set3c-b46 libraries is detailed in Table 5.26 and Table 5.27.

Discrepancies between SIMULATE-3 and PARCS are consistently below 60 pcm for k_{eff} when employing the Set 3c-b46 library, and within 1.1% in terms of radial RMS. It is noteworthy that both libraries, Set 1 and Set 3c-b46, exhibit a similar trend, initially showing a slight overprediction of k_{eff} at BOC, which transitions to a slight underprediction as the cycle progresses.

Table 5.26. PARCS vs. SIMULATE-3 Results. Cycle B. XS Set 1.

Fuel Cycle	Core Average Cycle (GWd/st)	PARCS k_{eff}	$\Delta k_{eff}/k_{eff}$ (pcm)	Axial RPF RMS (%)	Radial RPF RMS (%)	Maximum Radial Peak (%)
B	0.891	1.00364	6	5.16	0.68	2.57
B	4.515	1.00130	10	5.62	1.02	2.25
B	9.100	1.00065	-15	6.98	1.61	3.30
B	13.502	1.00069	-46	8.66	2.15	4.09
B	15.951	1.00028	-108	11.97	2.15	5.52
B	17.110	0.99837	-101	12.87	1.60	4.65

Table 5.27. PARCS vs. SIMULATE-3 Results. Cycle B. XS Set 3c-b46.

Fuel Cycle	Core Average Cycle (GWd/st)	PARCS k_{eff}	$\Delta k_{eff}/k_{eff}$ (pcm)	Axial RPF RMS (%)	Radial RPF RMS (%)	Maximum Radial Peak (%)
B	0.891	1.00373	15	1.58	0.37	2.44
B	4.515	1.00141	21	0.99	0.36	1.53
B	9.100	1.00060	-20	1.02	0.75	2.11
B	13.502	1.00068	-47	1.30	1.04	2.83
B	15.951	1.00081	-55	2.08	0.93	2.75
B	17.110	0.99883	-55	2.12	0.86	3.06

The improvement in power prediction for the radial power distribution is notably significant, as illustrated in Figure 5.45 and Figure 5.46. Notably, the tendency to underestimate power in fuels with control rods, as well as the overestimation of power in some peripheral channels, which were prominently observed with the Set 1 library, is less pronounced when employing the Set 3c-b46 library. This improvement is attributed to the significantly more accurate radial power estimation, resulting in overall lower errors.

The largest differences are observed in assemblies adjacent to the radial reflectors, where PARCS overpredicts power by up to a 2.5% difference compared to SIMULATE-3. This observation corroborates the previous finding of PARCS underestimating radial neutron leakage, as observed in the study of Cycle A.

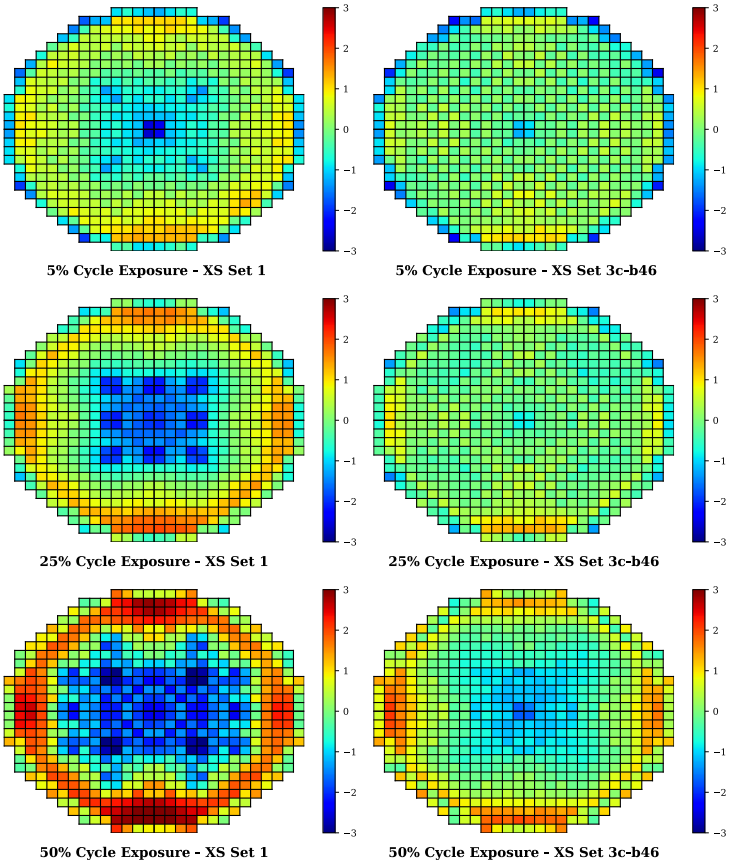

Figure 5.45. Relative Radial Power Errors (%). XS Set 1 vs. Set 3c-b46. First Half of Cycle B.

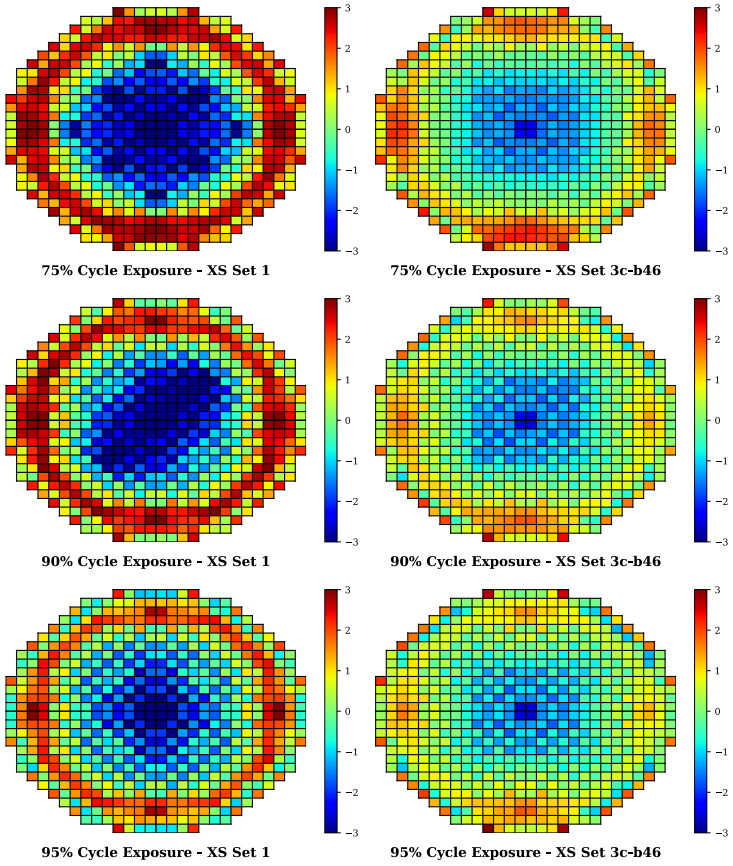

Figure 5.46. Relative Radial Power Errors (%). XS Set 1 vs. Set 3c-b46. Second Half of Cycle B.

Axially, as depicted in Figure 5.47 and Figure 5.48, the PARCS assembly-wise power prediction with Set 3c-b46 shows excellent agreement with the reference SIMULATE-3, making the enhanced cross-section library design very perceptible and remarkable.

One of the key conclusions from this study is the identification of significant errors when utilizing the Set 1 library across all analyzed points. This finding underscores the inadequacy of the current NUREG-CR714 recommendations for modeling BWR cross-section libraries, particularly in the context of modern fuel assemblies and the more demanding reactor operating conditions.

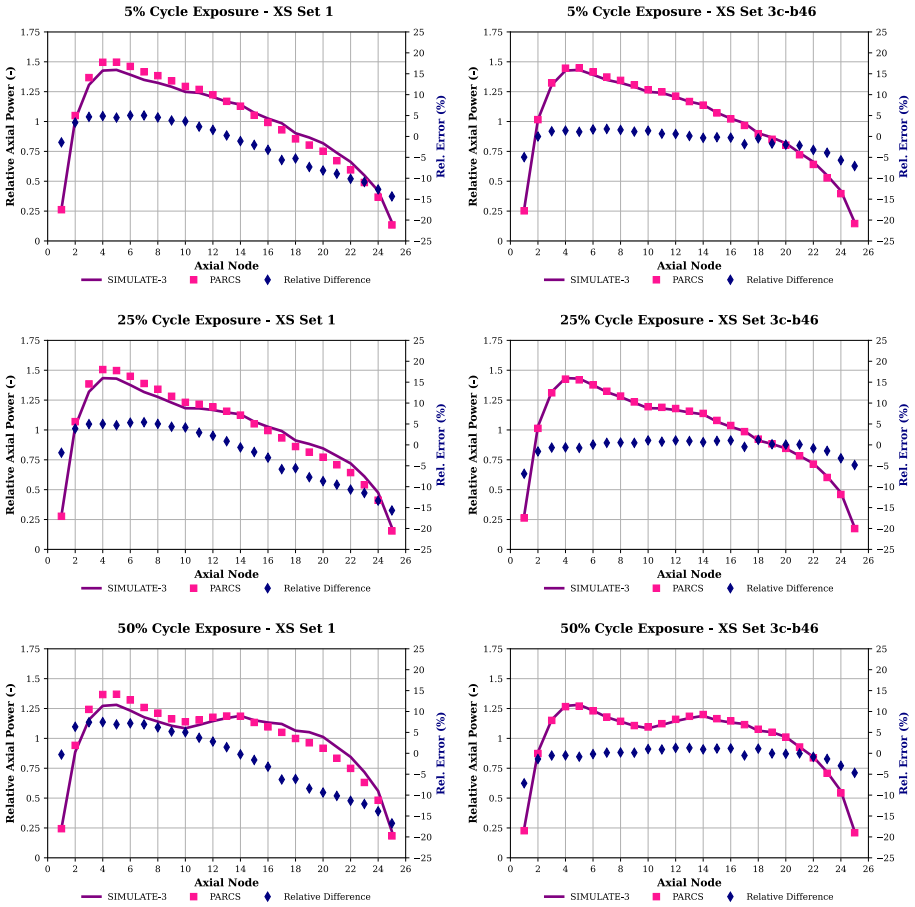

Figure 5.47. Relative Axial Power Errors (%). XS Set 1 vs. Set 3c-b46. First Half of Cycle B.

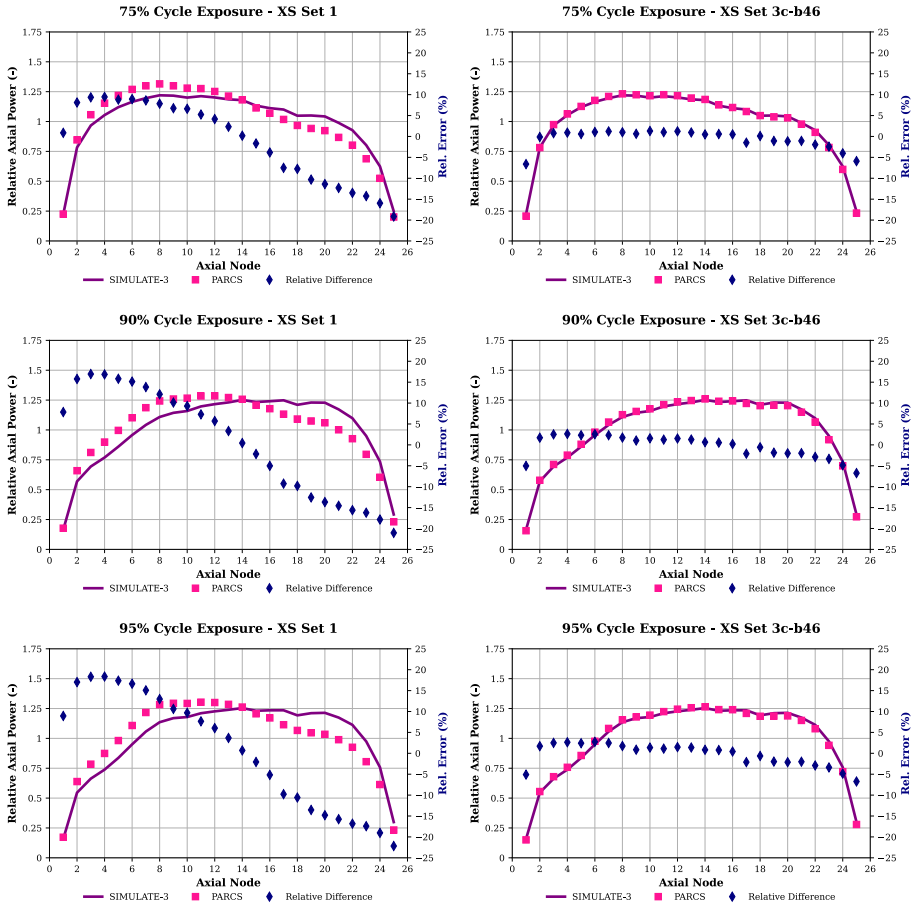

Figure 5.48. Relative Axial Power Errors (%). XS Set 1 vs. Set 3c-b46. Second Half of Cycle B.

To provide a comprehensive analysis, the entire Cycle B operational conditions were modeled using PARCS. Comparisons with SIMULATE-3 covered core k_{eff}, axial power shape RMS, and radial power shape RMS.

As shown in Figure 5.49, the core k_{eff} values from both SIMULATE-3 reference results and PARCS are closely aligned at the start of the cycle. However, discrepancies gradually increase to approximately 80 pcm as the cycle progresses, as illustrated in Figure 5.50. Importantly, PARCS exhibits excellent accuracy in predicting the expected $k_{eff} = 1$ eigenvalue.

Figure 5.51 highlights the differences between SIMULATE-3 and PARCS for the axial RMS across both Set 1 and Set 3c-b46 libraries. Notably, the agreement remains within 2% for most of the cycle with the Set 3c-b46 library. However, towards the end of the cycle, both libraries show an increase in axial RMS, with the Set 1 library

reaching errors up to 14%. A detailed discussion on the discrepancies in power predictions at the end of the cycle will be provided in Section 5.6.1.

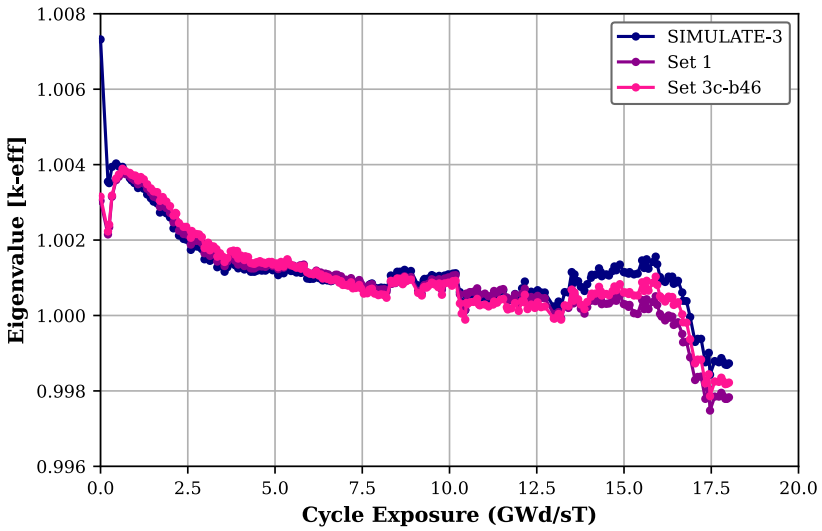

Figure 5.49. Core k_{eff}. Cycle B Core Follow. Set 1 vs. Set 3c-b46.

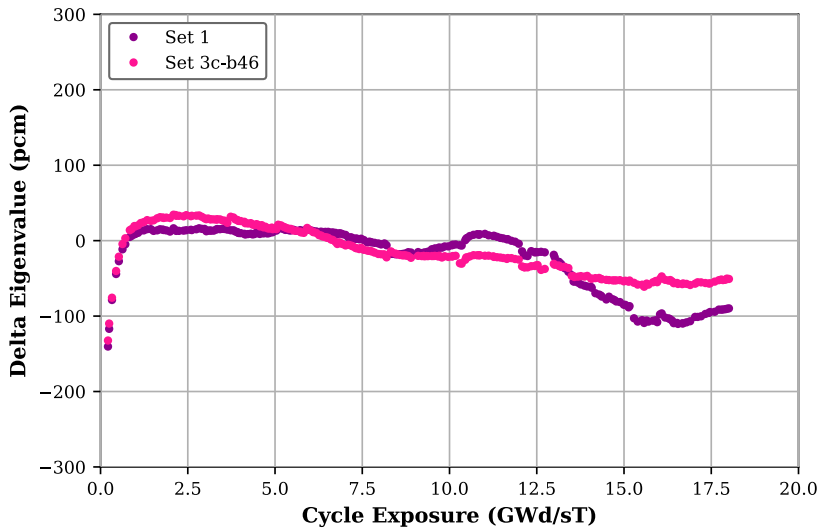

Figure 5.50. Delta k_{eff} (pcm). Cycle B Core Follow. Set 1 vs. Set 3c-b46.

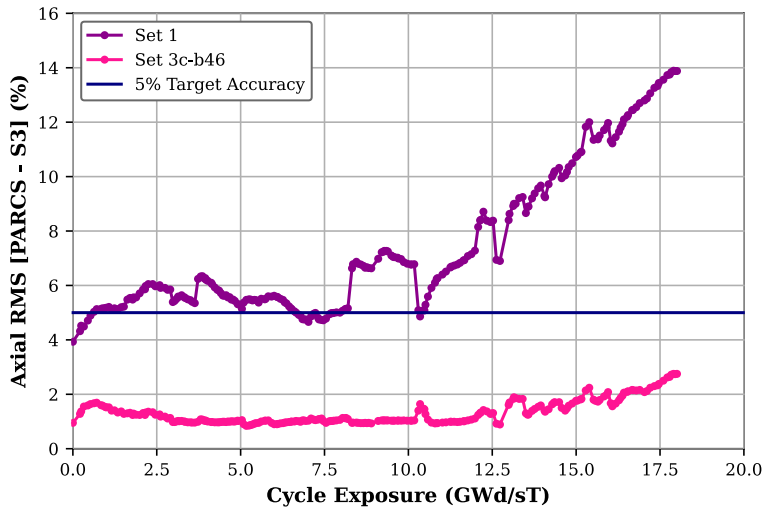

Figure 5.51. PARCS Axial RMS Difference from SIMULATE-3 (%). Cycle B Core Follow. Set 1 vs. Set 3c-b46.

Furthermore, the radial power shape differences, as shown in Figure 5.52, remain within 1.5% throughout the entire cycle. Radial errors tend to increase as the cycle progresses.

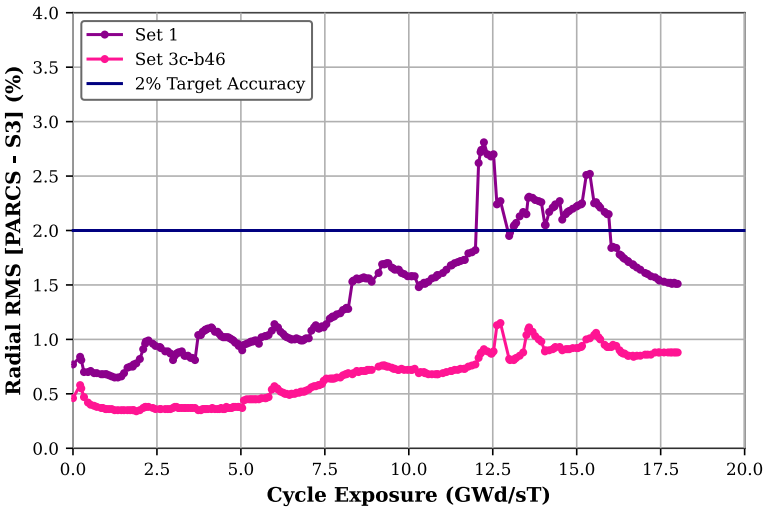

Figure 5.52. PARCS Radial RMS Difference from SIMULATE-3 (%). Cycle B Core Follow. Set 1 vs. Set 3c-b46.

It is worth noting that the weighting options for history parameters can be linear or non-linear. Non-linear weighting assigns greater importance to recent time-instantaneous state parameters compared to older time history values. Given the results, it is possible that SIMULATE-3 and PARCS employ different history weighting approaches. SIMULATE-3 may use non-linear weighting while PARCS utilizes linear weighting, a factor that warrants detailed analysis in future research.

In conclusion, the power distributions calculated by PARCS show excellent agreement with those by SIMULATE-3 under identical conditions, particularly when using the **Set 3c-b46 library**. This highlights the effectiveness of the enhanced cross-section library design in accurately modeling modern fuel assemblies and reactor operating conditions.

5.6.1 Coast-down Conditions Modeling.

After the full power end-of-cycle has been reached, the reactor can be either shut down for refueling or still made critical at lower thermal output through core *Stretch-out* or *Coast-down*.

According to the NRC library (*US-NRC Library - Glosary*, 2021), coast-down is *"an action that permits the reactor power level to decrease gradually as the fuel in the core is depleted"*. In other words, the Coast-down stage is when the reactor continues operating at less than full power at a normal EOC in order to maintain criticality by reducing the core-average voids and fuel temperature, thus increasing reactivity and cycle length, see Figure 5.53.

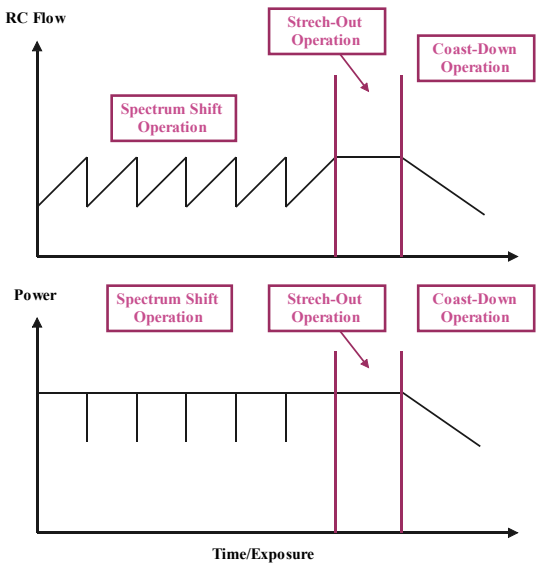

Figure 5.53. Typical General Electric (GE) BWR Operation Phases.

During the spectrum shift operation, where the core is operated at maximum power and minimum flow, a high production of ^{239}Pu due to the resonance capture of neutrons in ^{238}U occurs. This production, in combination with increasing the recirculation flow, allows a significant extension of the full power period afterwards.

At the end-of-cycle, the excess reactivity of the core is essentially zero. As a result of the lower temperature due to the negative temperature/power coefficient, three effects tend to increase the reactivity of the core as described in (Cochran, R. G. & Tsoulfanidis, N., 1999):

1) If the moderator temperature decreases, the density increases which is equivalent to adding more moderator in the core and increasing the positive core reactivity.
2) If the temperature is reduced, the Doppler effect is also reduced. Such a reduction amounts to the addition of positive reactivity in the core.
3) If the power is reduced, the negative reactivity contribution due to fission products is also reduced.

In the early 80s, a great deal of interest was intended on evaluating Coast-down as a means to improve uranium utilization in LWRs and, thus, focused on modeling coast-down as a fuel management strategy. Many studies were conducted, proving that coast-down does not severely compromise any neutronic or thermal-hydraulic constraints (Lobo, 1980).

Leaving aside the fuel management strategy and focusing on the adequate characterization of the coast-down conditions, during the coast-down phase, the reactor and steam supply system parameters are changed from their typical operating values, as illustrated next. The onset of the coast-down phase is denoted by a dark pink marker in the following graphs, see Figure 5.54, indicating a shift in the operating conditions maintained up to that point in the cycle. Similarly, a zone of interest at the cycle's end is highlighted (pale pink) in the total core flow plot. This zone demonstrates a continuous rise in the Recirculation Flow (RC) towards maximum flow during the final third of reactor operation, aimed at counterbalancing reactivity.

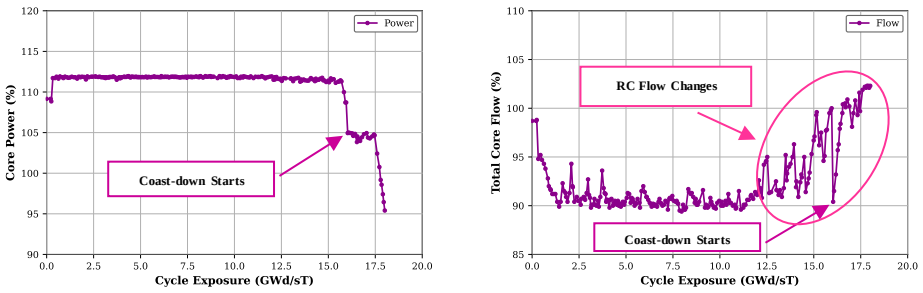

Figure 5.54. Total Power and Core Flow Conditions during Cycle B.

The fluctuations in flow rates during the final third of the cycle manifest in the axial and radial power distribution predictions generated by PARCS. This impact is particularly pronounced in the axial RMEs errors compared to those estimated by SIMULATE-3, as illustrated in Figure 5.55.

Axial power predictions show substantial deviations from SIMULATE-3 at EOC, especially during the stretch-out and coast-down stages when using the Set 1 library. Although the upward trend in axial errors continues with the Set 3c-b46 library, the deviations are less pronounced and remain within acceptable accuracy limits.

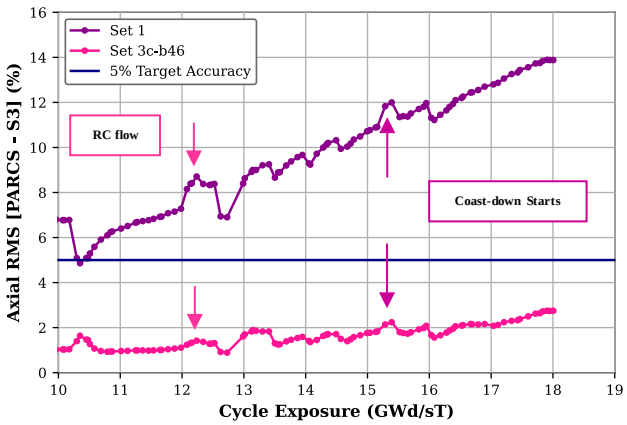

Figure 5.55. Axial Power RMSEs (%). Set 1 and Set 3c-b46. Coast-down Phase.

On the other hand, radial power predictions display different behavior during these phases. Figure 5.56 demonstrates that as the coast-down phase commences, radial power errors decrease following an initial overshoot of the accuracy target during the phase of increasing the recirculation flow. Moreover, the discrepancies observed when using the Set 3c-b46 library are less evident due to consistently low errors throughout the entire core-follow simulation period.

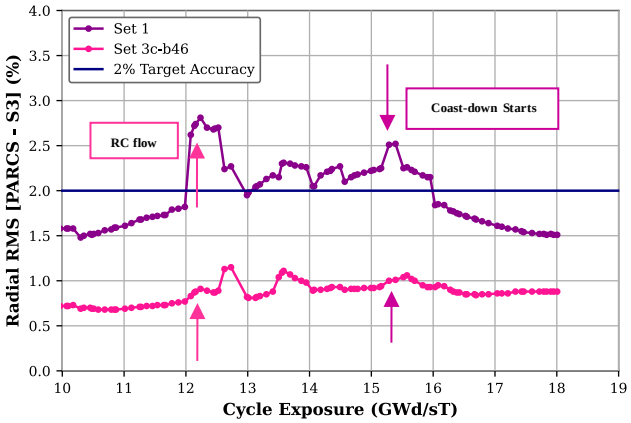

Figure 5.56. Radial Power RMSEs (%). Set 1 and Set 3c-b46. Coast-down Phase.

Traditionally, deficiencies in nodal analysis methods are often attributed to inaccuracies stemming from BWR history effects, as well as the prediction of moderator densities and fuel temperature. Considering the observed discrepancies in power distribution predictions by PARCS, it seems convenient to examine the evolution of the nodal distribution of the moderator density throughout the cycle.

At EOC conditions, the rise in subcooled flow, coupled with the decline in reactor saturation pressure, see Figure 5.57, may lead to a shift in the nodal distribution of void fraction towards lower void branches.

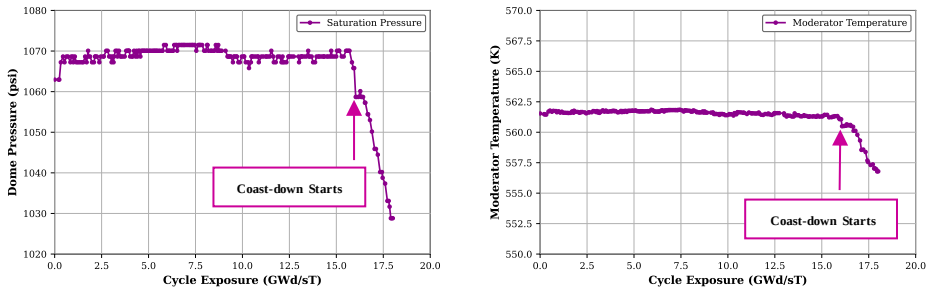

Figure 5.57. Dome Pressure and Moderator Temperature Conditions during Cycle B.

The progression of the nodal moderator density distribution throughout the cycle is illustrated in Figure 5.58.

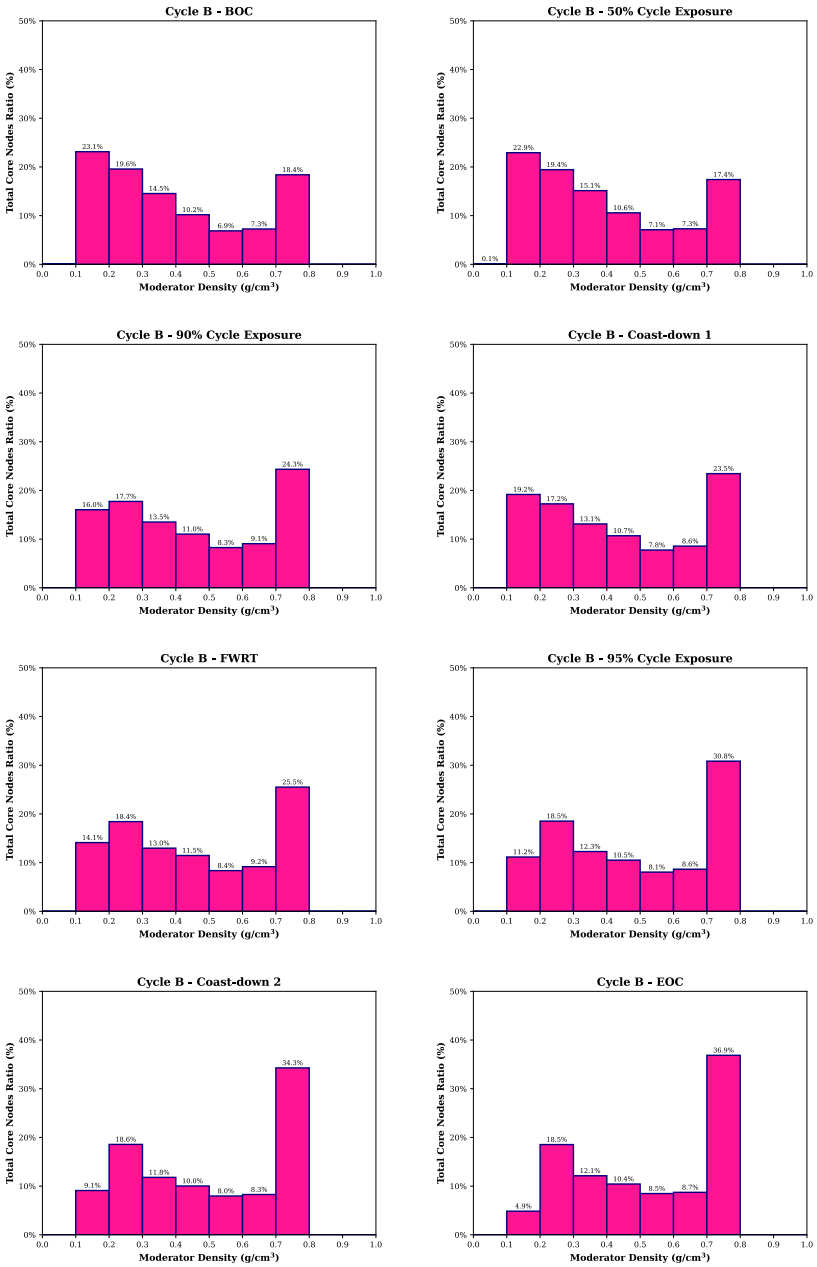

Figure 5.58. Evolution of the Nodal Moderator Density Distributions along Cycle B.

As depicted in Figure 5.58, the Coast-down phase comprises three distinct stages labeled as (1) Coast-down #1, (2) FWRT (Feedwater Reduced Temperature), and (3) Coast-down #2.

During Coast-down #1, there is a gradual reduction in power to 105% of the Original License Thermal Power (OLTP), accompanied by a gradual increase in core flow. This phase transitions into the FWRT stage, characterized by a decrease in feedwater temperature. The concurrent increase in core flow and decrease in temperature aim to introduce positive reactivity into the core to maintain power levels. Finally, Coast-down #2 begins as power continues to decrease until shutdown, while the core flow remains relatively constant.

The increase in moderator density observed in the nodal distribution towards the end of the cycle is closely linked to these three phases, as well as the decrease in reactor saturation pressure, which contributes to the shift in nodal voids. Consequently, as moderator density increases, the density mesh for liquid states must be accurately determined to capture associated phenomena during Coast-down and EOC conditions, given the changing nodal moderator density distribution throughout the cycle.

Indeed, Figure 5.58 illustrates a clear movement of nodal distribution from high voids towards low voids at the EOC. Notably, 90% void fraction nodes represent 23% of the core at BOC, but only 4.5% at EOC. Conversely, 0% void fraction nodes represent less than 20% of the core at BOC, but around 40% at EOC conditions.

The errors observed in Figure 5.55 indicate the potential need for a finer mesh in the lower void branches of the branch structure. This refinement would enhance the accuracy in capturing the decrease in average void fraction at EOC, i.e., from 50% to 30%, as shown in Figure 5.59.

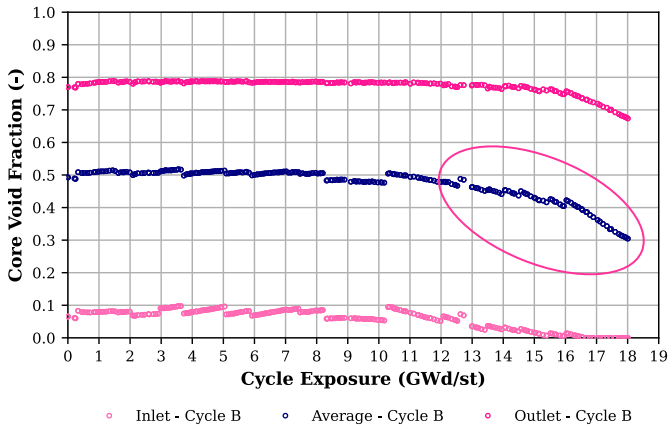

Figure 5.59. Core Void Fraction vs. Exposure. Cycle B.

To account for the concurrent increase in moderator density and decrease in saturation pressure, void branching in the moderator temperature branches must be appropriately modeled.

Accordingly, three distinct void moderator temperature matrix structures have been modeled and tested to ascertain the optimal approach for accurately predicting power/void distribution within the reactor during the coast-down phase. The changes from Set 3c-b46 library to the new libraries modeled are highlighted.

Table 5.28. Void-Moderator Temperature History/Branch Matrix Structure Conditions. Designed Coast-down Sets.

XS Set Library	Branch Parameter	Value	Nominal History	Branch Parameter	Selected Branches (%)
Set 3c-b46	TMO	561.4	45%	VOI	0/45/60/80/90
Set 3c-b46	TMO	545	N/A	VOI	0
Set Coast-down #1	TMO	561.4	45%	VOI	0/**20**/45/60/80/90
Set Coast-down #1	TMO	545	N/A	VOI	0
Set Coast-down #2	TMO	561.4	45%	VOI	0/**20**/45/60/80/90
Set Coast-down #2	TMO	545	N/A	VOI	0/**20**
Set Coast-down #3	TMO	561.4	45%	VOI	0/**20**/45/60/80/90
Set Coast-down #3	TMO	**500**	N/A	VOI	0/**20/45/60/80/90**

As outlined in Table 5.28, Set Coast-down #1 library introduces an intermediate branch at 20% void fraction and the moderator temperature corresponding to normal operation saturation pressure. This addition aims to reduce the need for linear interpolations between 0% and 40% void branches, which becomes necessary due to the increased number of nodes in the lower void fraction range.

In contrast, the Set Coast-down #2 library includes an additional branch for lower void fractions at lower moderator temperatures, aiming to capture void migration during the latter part of the cycle, attributed to decreasing pressure and moderator temperature.

Conversely, the Set Coast-down #3 library is designed to cover the entire moderator density range at lower moderator temperatures. Notably, the moderator temperature is set to 500 K, instead of 545 K, to encompass a wider range of pressures, with a focus on scenarios involving transients such as Anticipated Transient Without Scram (ATWS) with Automatic Depressurization System (ADS) activation.

Axial and radial power predictions for Cycle B core follow are depicted in Figure 5.60 and Figure 5.61, respectively. Despite the theoretical expectation that cross-sections should be parameterized over the reactor operating space, encompassing factors such as fuel temperature, control rod presence, moderator density, and

temperature, Figure 5.60 and Figure 5.61 reveal poor agreement between PARCS and SIMULATE-3 when employing the Coast-down #2 and #3 libraries.

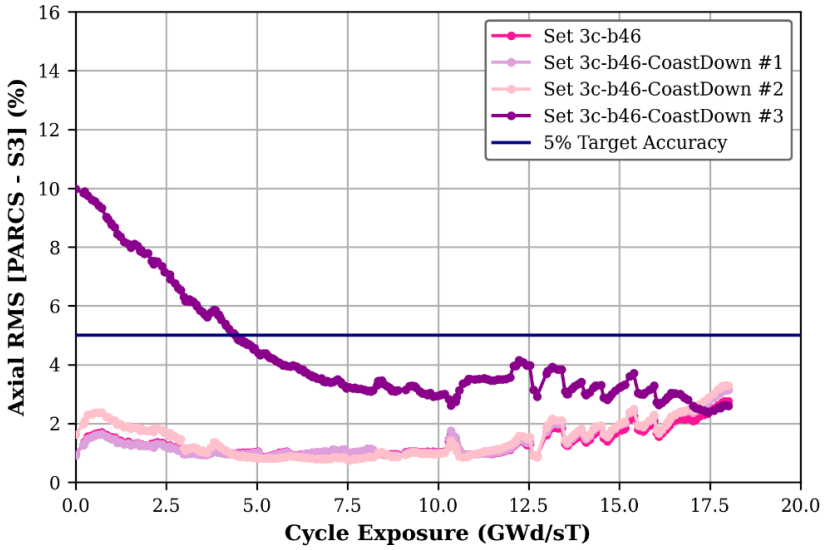

Figure 5.60. Axial RMSEs (%). Cycle B Core-Follow.

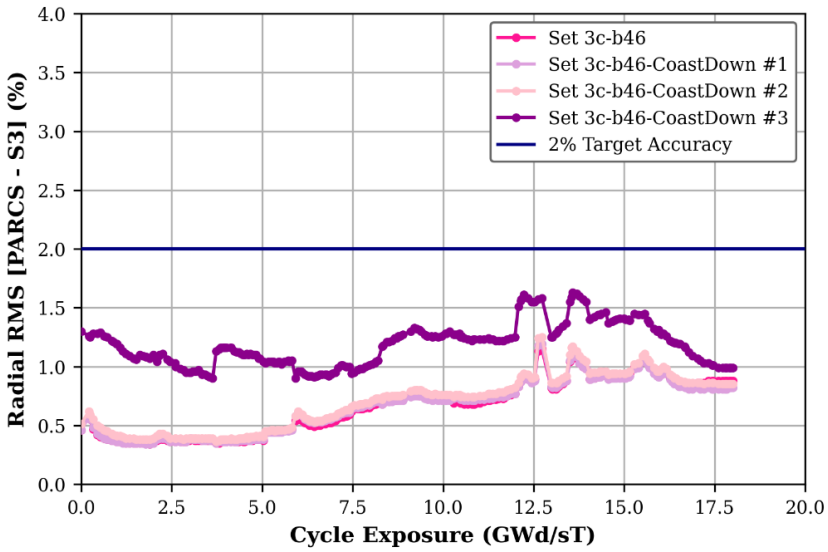

Figure 5.61. Radial RMSEs (%). Cycle B Core-Follow.

As outlined in the PARCS Manual (Downar, T. et al., 2012), BWRs exhibit significant axial variation in moderator density, necessitating a branch structure that captures the non-linear impact of density on cross-sections. While it is suggested that moderator temperature is largely a second- or third-order effect that can be disregarded in the branch structure of BWR cross-sections, the results obtained using Set Coast-down #2 and #3 libraries suggest otherwise regarding moderator temperature.

The discrepancies arise from GenPMAXS's limitation in parameterizing cross-sections based on multiple moderator temperatures, particularly when the temperature branches include void fraction branches greater than 0%. While this issue is only mildly evident with the Set Coast-Down #2 library at BOC conditions, it becomes significantly more pronounced with the Set Coast-Down #3 library throughout the entire cycle.

The code appears to establish reference nominal values and cross-section derivatives based on a moderator temperature of 500 K, rather than aligning with the nominal moderator temperature of 561.4 K, which corresponds to the reactor's nominal saturation pressure for most of the operational cycle. As a result, the accuracy of nodal-wise power predictions, especially in the axial direction, is compromised under normal operating conditions for the majority of the cycle.

However, as the moderator temperature and saturation pressure decrease, the RMSEs also reduce because the GenPMAXS parameters gradually converge towards the reactor's actual operating conditions. This alignment mitigates some of the inaccuracies in the power predictions.

Based on the obtained results, it becomes evident that if there is a necessity to model evolving core conditions throughout a cycle, particularly concerning pressure saturation and, consequently, moderator temperatures, PARCS may not accurately predict the 3D power distributions. This limitation arises from GenPMAXS's inability to effectively handle the parameterization of moderator temperature alongside moderator density and fuel temperature.

Therefore, there is a compelling need to enhance the capabilities of GenPMAXS in this aspect and it is strongly recommended to address this limitation to ensure more precise and comprehensive modeling of BWR core behavior under varying operational conditions.

5.7 Summary & Conclusions.

Accurately predicting reactor behavior under both steady-state and transient conditions necessitates using actual reactor data to rigorously assess the performance of simulation software; thus, ensuring compliance with contemporary software quality standards. In this context, this chapter has undertaken a critical evaluation of the CASMO-4/GenPMAXS/PARCS computational sequence in analyzing modern BWR operations with currently available BWR fuels.

The evaluation focused on comparing predictions from PARCS against the plant core-follow computer SIMULATE-3, including eigenvalue calculations and radial and axial assembly power distributions. This comparison has served as the benchmark for validating PARCS's predictions. The core-to-core comparison concentrated on steady-state performance parameters and two-group nuclear cross-sections for BWR fuel lattices and cores.

Benchmarking involved the depletion of two distinct cycles: Cycle B, which utilized modern fuel designs, and Cycle A, which featured earlier fuel versions. This broad scope of testing aimed to cover a comprehensive range of BWR fuel burnup scenarios, from BOC through the burnup level associated with peak reactivity that nears the point of gadolinium depletion for Cycle A, and from BOC to coast-down conditions for Cycle B.

It is noteworthy that between Cycles A and B, over ten additional cycles have been depleted, reflecting substantial operational changes. These changes included power uprates, extending the cycle duration from 12 to 24 months, increasing fuel enrichment, encountering more severe core voiding conditions, and integrating modern fuel designs with higher pin counts from various vendors.

The data available for Cycles A and B encompassed two core-follow plant computer decks under near full power conditions, providing comprehensive thermal-hydraulic parameters of the plant, such as power, flow rate, inlet temperature, and subcooling inlet enthalpy. Detailed histories and control rod patterns were provided at each depletion step to develop a robust PARCS model for both cycles.

To analyze the impact of different cross-section libraries, three distinct calculations were performed focusing on histories, branches, and burnup points. These analyses aimed to enhance technical modeling for BWR cross-section libraries, particularly for safety analyses involving burnup credit.

The initial analysis utilized the Set 1 library, established based on the guidance provided in NUREG/CR-7164 for BWR lattice modeling, as discussed in Chapter 4. Although Set 1 served as the reference library, significant errors were observed across all analyzed points, indicating that current NUREG/CR-7164 recommendations are insufficient for characterizing modern fuel assemblies and more demanding reactor operating conditions.

The high errors, particularly in predicting axial power distributions, suggested that the discrepancies between PARCS and SIMULATE-3 were likely due to the history matrix structure rather than the branch structure. The results highlighted that

eigenvalue predictions and power distribution calculations were highly sensitive to the cross-section library modeling methodology, with history effects having the most substantial impact due to their strong dependence on moderator density and control rod position.

The findings suggest a need to reconsider NUREG/CR-7164 guidelines for history modeling, especially with modern fuel bundles, high exposure, and power uprates. For instance, the study indicated that a 90% void fraction, as opposed to the current 70% boundary condition, is more suitable for accurately reflecting reactor conditions.

The sensitivity analysis revealed that BWR steady-state results are generally not highly sensitive to moderator density branch effects, although this might not apply to all transients. Users are advised to ensure that computed cross-section branches and histories are relevant to specific analyses. From the history and local values sensitivity analysis, **Set 3c** was identified as the cross-section set closest to the SIMULATE-3 reference.

In the burnup point analysis, three distinct cross-section libraries were derived from Set 3c: Set 3c-b20, Set 3c-b46, and Set 3c-b78, corresponding to 20, 46, and 78 burnup points, respectively. Set 3c-b46 features a refined mesh up to 10 GWd/st, while Set 3c-b78 employs a more granular mesh extending to 30 GWd/st. These libraries were meticulously designed to capture the nuances of depletion phenomena accurately.

The analysis revealed that employing a large time step size, approximately 2 GWd/st, can lead to substantial errors, particularly when dealing with gadolinium-containing fuels. To address this issue, smaller time step sizes - around 0.5 GWd/st - were found to be more suitable for precise gadolinium depletion modeling.

Furthermore, introducing a finer depletion step between 0 and 0.5 GWd/st, specifically at 0.1 GWd/st, significantly enhanced power predictions at BOC, primarily by mitigating the effects of Xenon.

Contrary to initial expectations, no significant improvement in power distribution estimations was observed when using the 78-burnup points library compared to the 46-burnup points library. The power errors exhibited fluctuation without a clear trend, and the computational time for lattice code calculations was notably longer for the 78-burnup points library. The observed error trends suggest a possible limit to the benefits of increasing burnup points in cross-section libraries. Further investigation is needed to confirm this conclusively.

Regarding coast-down modeling, traditional deficiencies in nodal analysis methods have often been attributed to inaccuracies related to BWR history effects and predictions of moderator densities and fuel temperatures. Considering the discrepancies in power distribution predictions by PARCS, examining the evolution of nodal distribution of moderator density throughout the cycle becomes crucial.

At EOC conditions, increased subcooled flow and decreased reactor saturation pressure may shift the nodal distribution of void fraction towards lower void branches. Specifically, nodes with a 90% void fraction, which represented 23% of the core at

BOC, decreased to only 4.5% at EOC. Conversely, 0% void fraction nodes increased from less than 20% at BOC to around 40% at EOC.

To accommodate the concurrent increase in moderator density and decrease in saturation pressure, void branching in moderator temperature branches must be appropriately modeled. Results have shown that PARCS may not accurately predict 3D power distributions due to GenPMAXS's limitations in parameterizing moderator temperature alongside moderator density and fuel temperature. This limitation underscores the urgent need to enhance GenPMAXS's capabilities for more precise modeling of BWR core behavior under varying operational conditions.

In conclusion, the use of the **Set 3c-b46** library has demonstrated outstanding improvements in comparison to Set 1 across all selected points of Cycle B. This improvement is attributed to the library's comprehensive coverage of the reactor's expected operating conditions, minimizing the need for cross-section extrapolations and resulting in an excellent estimation of power distribution.

The successful demonstration of PARCS's capability to model modern fuels with large water rods, part-length rods, and significant gadolinium loading highlights its effectiveness. However, the analysis also revealed additional factors requiring attention, such as the impact of a high number of burnup points and the weighting of linear/non-linear state variables/histories, which necessitate further scrutiny in future research endeavors.

Chapter 6
Cross-section Modeling: Code-to-TIPs Results

6.1 Introduction.

In commercial LWRs, the power distribution in the core is affected by several operational parameters, making it challenging to assume a constant power distribution. Core power distribution information is required to satisfy a number of fundamental reactor safety and operational requirements. Therefore, local power production within the core is routinely monitored to assure the integrity of the fuel cladding, to plan for and perform reactor control maneuvers in the near term, and to evaluate the performance of the reactor core with the exposure as stated in (Fisher, 1977).

To obtain accurate in-core power distribution measurements, LWR vendors provide additional instrumentation for supervision, such as *Traversing In-core Probes* (TIPs), which play a crucial role in the core operational strategy's decision-making process and are essential for ensuring safety, control, and performance evaluation. Given the increasing complexity and size of nuclear plants, the significance of these functions has increased significantly.

Direct measurement of in-core power distributions and related quantities is impractical in practice. Therefore, indirect methods are employed, using computer

codes to predict detailed core performance while measured power distributions are used to confirm and validate these predictions. Simulating the TIP response is a key element for core simulators, enabling the reliable use of TIP measurements to validate predictions and assess the accuracy of calculated radial and axial power distributions by comparing them with measured in-core instrument reaction rates. Consequently, validation against TIPs at various burnup steps of Cycle B is also performed in this thesis.

TIPs measurements are used herein to validate the capability of PARCS to model advanced BWR fuel designs and to calculate 3D power distributions for actual reactor operating conditions. This analysis encompasses the evaluation of different cross-section sets employed in previous code-to-code comparisons. Consequently, the validation of the selected cross-section libraries, as modeled in Chapter 5, is achieved through comparisons against TIP measurements.

6.2 Traversing In-Core Probe (TIP) Description.

Continuous monitoring of the three-dimensional power profile within a reactor core becomes imperative for the operation of BWRs due to the influence of two-phase coolant flow and power peaking on Critical Power Ratio (CPR), as outlined in (Harfst, W., 1985). Such monitoring not only enhances operational efficiency but also contributes significantly to safety performance (Fridström, R., 2010).

In BWRs, the measurement of neutron flux density is carried out at specific locations using in-core detectors positioned within tubes located in the narrow water gaps between four fuel assemblies, as illustrated in Figure 6.1.

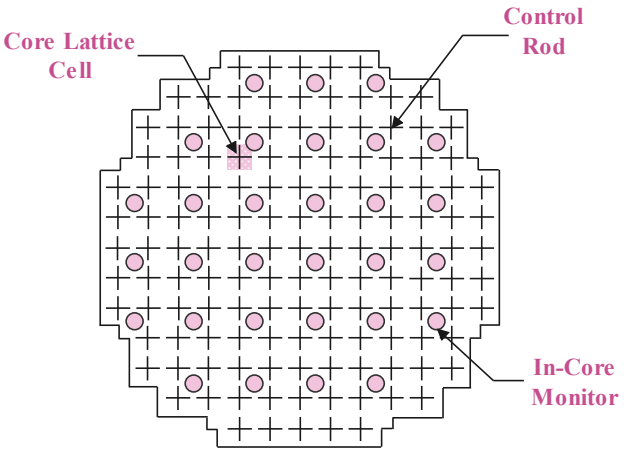

Source: (Kok, K. D. (Ed.)., 2016).

Figure 6.1. Typical BWR Core Arrangement.

In BWRs, core supervision systems have always been based on a combination of calculated and measured power data. Consequently, all modern supervision systems are based on a core simulator (3D nodal code) running online with data collection from the process (i.e., heat balance calculated power, recirculation flow, control rod pattern, and core inlet temperature) that are adaptively adjusted to match Local Power Range Monitor (LPRM) measured data.

The online computer at the power plant measures and records the power fraction for all assemblies determined from signals proportional to the assembly power obtained by detectors periodically inserted in specific assemblies.

As stated in (Harfst, W., 1985), the main functions of the neutron monitoring system are:

- monitoring the neutron flux density at all reactor's operating conditions,
- determining the total power generated by fission, and
- monitoring the spatial power density distribution in the reactor core.

In a BWR, there are three in-core neutron/gamma detector systems covering different power/flux regions in the reactor operation, namely:

1) SRM (Source Range Monitor),
2) IRM (Intermediate-Range Monitor), and
3) LPRM (Local Power Range Monitor).

The need for a different monitoring system occurs because neutron flux density varies over approximately 11 decades between shut-down and full power; thus, this range cannot be covered by just a single monitoring system. A typical radial layout of the detectors in the core is shown in Figure 6.2.

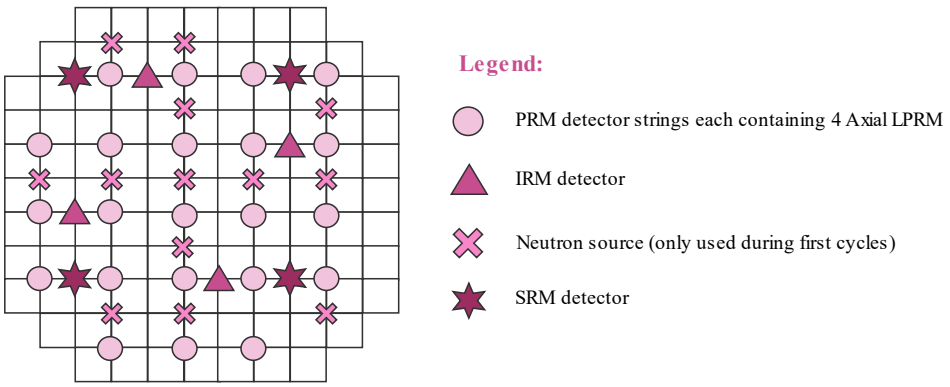

Figure 6.2. In-Core Detectors Radial Layout Example.

As described in (Bozzola, S., 1982), the SRM monitors the core nuclear performance during the initial nuclear start-up phase. In contrast, the core monitoring is performed through the IRMs at low power levels, view Figure 6.3.

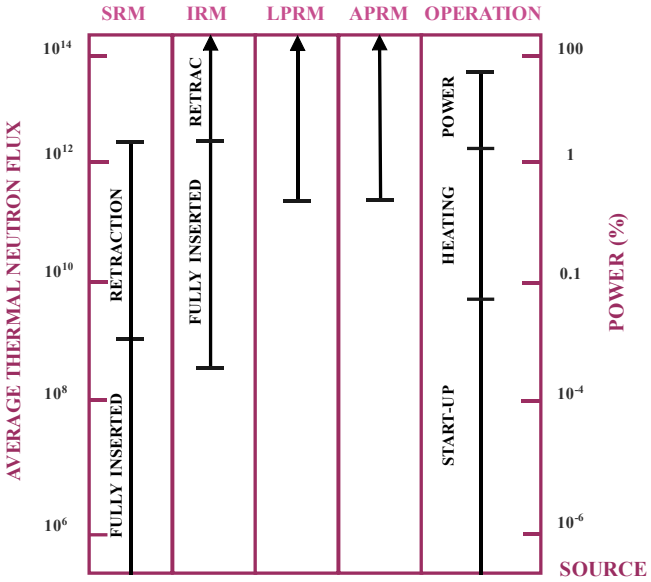

Source: (Bozzola, S., 1982).

Figure 6.3. Indicative Ranges of the Neutron Monitoring System.

LPRM detectors are combined to give the so-called APRM (Average Power Range Monitor), which measures the average value for the core. LPRMs are typically grouped into four APRM systems so that each APRM system covers determined axial levels of the core.

Due to the harsh conditions with high radiation during core operation, all the detectors must often go through a calibration process (Bozzola, S., 1982). Thereby, to be able to calibrate the Power Range Monitor (PRM) system (LPRM and APRM) during power operation, there is a TIP system installed.

The TIP detector can be positioned to measure all the LPRM radial positions, which are fission detectors fixed in the reactor core, whereas the TIP is typically a gamma detector but, in some cases, is a neutron detector. All the LPRMs are connected to a switch below the reactor vessel, and inside each LPRM detector string there is a tube for the TIP detector.

Running TIP detectors through all LPRM string locations gathers axial power shape information with a high axial definition for each inch of active core height in all radial positions. Gamma rays measured by the TIP estimate neutron flux because the thermal neutron flux can be directly linked to the power because fission predominantly occurs due to thermal neutrons. Gamma rays in the core are directly related to fission.

When control rods are moved, they can cause changes in the axial power distribution within the reactor core. These changes can be significant enough to require

control rod pattern adjustments. Adjusting the control rod pattern can affect the axial power shape more significantly than changes made by adjusting the recirculation flow rate.

Regular monitoring of the axial power distribution is necessary to ensure that the reactor core remains within safe limits. This is where the TIP system comes into play. The TIP system measures the neutron flux at different axial locations within the reactor core (US NRC, 2011).

The TIP detectors are placed within the reactor core and are used to collect data on the neutron flux at different axial locations. This data is collected monthly and used by the plant process computer to estimate the power distribution within the reactor core and to check conformance with thermal limits.

The process computer also uses the TIP data to determine adjustments needed to LPRM calibrations to compensate for uranium depletion, neutron spectrum changes, and detector sensitivity changes. This ensures that the power distribution within the reactor core remains within safe limits and that the reactor operates safely and efficiently.

After the data collection, the TIP detectors are returned to storage locations in the reactor building.

In summary, TIP measurement has these three primary purposes:

1) to calibrate the LPRM detectors,
2) to provide data for the online core supervision system, and
3) to verify the power distribution calculated by the core simulator.

6.3 TIPs Plant Measurements.

As stated in (Giust et al., 2004), TIP data can be considered our best reference measurement *"…safely consider that the TIP values are the closest thing to the truth of what is going on inside the core."*

Accordingly, modeling the TIP response is a critical component of core simulators so that TIP measurements can be used to validate their predictions, and their results can be used to predict the power in the core reliably. Comparisons between measured and calculated in-core instrument reaction rates are used to infer the accuracy of the estimated radial and axial power distributions.

Thus, TIPs measurements are used herein with a dual purpose: (1) to validate the capability of PARCS to model advanced BWR fuel designs and (2) to calculate 3D power distributions for actual reactor operating conditions using the different cross-section sets modeled in Chapter 5 to validate their suitability in core power estimations.

To verify and validate the TIP response calculated by PARCS, a subset of steps from Cycle B has been simulated using PARCS and compared against measured 3D power distributions derived from periodic TIP measurements conducted at the plant.

The selected steps encompass the complete depletion of Cycle B, including the beginning-of-cycle (BOC), four intermediate points (MOC), and the end-of-cycle (EOC), all under full power conditions. Each step varies in terms of coolant flow, control rod patterns, and inlet subcooling. These steps aligned with the available TIP measurements obtained during the given cycle.

Cycle B, spanning 24 months, typically entails approximately 24 TIP measurements, as these measurements are usually performed monthly. However, due to detector failures, four consecutive measurements were disregarded towards the end of the cycle. Consequently, the selected EOC state, corresponding to an approximate burnup of 16 GWd/st, does not precisely coincide with the actual end-of-full power operation but rather represents a measurement taken just before the coast-down phase.

Regarding the BOC conditions, a specific point near the initiation of the cycle, approximately at a burnup of 0.25 GWd/st, was chosen because gamma TIP measurements were available for this particular point.

Table 6.1 overviews the selected points, presenting their corresponding core average burnup, rated thermal power, and total core flows.

Table 6.1. Selected TIP Measurements from Cycle B.

TIP Measurement	Cycle Step	Exposure (GWd/st)	Power (%)	Total Flow (%)
TIP_M#1 - BOC	Paso 02	0.247	108	98
TIP_M#5 - MOC 1	Paso 25	2.150	111	92
TIP_M#9 - MOC 2	Paso 76	5.412	111	90
TIP_M#13 - MOC 3	Paso 121	8.349	111	91
TIP_M#17 - MOC 4	Paso 161	11.364	111	90
TIP_M#20 - EOC	Paso 193	14.054	111	91

The control rod positions associated with each selected point are displayed in Figure 6.4. Control rod patterns will be changed along the cycle to maintain the radial power distribution as flat as possible while compensating for the loss of reactivity due to the fuel burnup.

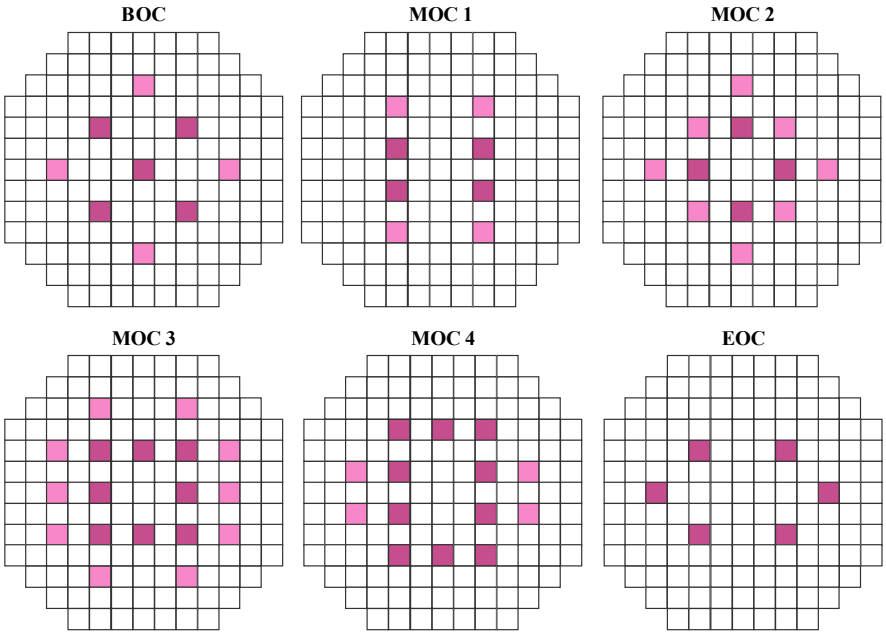

Figure 6.4. Control Rod Patterns at Selected TIP Measurement Points.

The figure's legend provides the following color-coding scheme: white color represents fully withdrawn control rods, pale pink indicates control rods in shallow positions (referred to as power shaping control rods), and dark pink means control rods in deep positions (known as reactivity binding control rods) as described in Chapter 5.

Given that inserted control rods significantly impact the core by causing localized distortions in the neutron flux, more significant discrepancies between measured and calculated data are expected to be observed in detectors located near inserted control rods. This effect can be attributed to the control blade history effect, as mentioned in (Bozzola, S., 1982).

The available dataset comprises TIP strings situated at 33 distinct radial locations, each with 24 axial measurement locations. The specific locations where TIP measurements were conducted are specified in Figure 6.5.

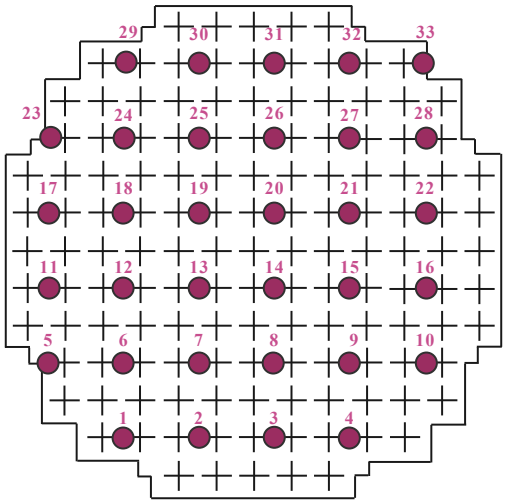

Figure 6.5. Location of the 33 TIP Detectors.

According to the CASMO-4 (Rhodes, J. & Edenius, M., 2004) and SIMULATE-3 Manuals (Covington, L.J. et al., 1995), a detector response calculation is performed at each CASMO-4 base/branch step with two-group reaction rate cross-sections and stored as part of the nuclear data library.

In the SIMULATE-3 reaction rate calculation, nodal properties are used to evaluate the microscopic cross-sections and instrument form-functions at the local conditions in order to predict the most accurate values of the reaction rates. Then, the reaction rates in the detectors are reconstructed using the intranodal fluxes evaluated at the detector locations, the CASMO-4 detector form-functions, and the microscopic cross-section for the detector.

Finally, the TIP response is averaged for the four assemblies surrounding the detector. The instrument form-functions and microscopic cross-sections are functionalized versus all the available depletion and state point variables. This is important because the detector's microscopic cross-section depends on the fuel assembly's exposure and moderator densities.

Note that the plant TIPs are gamma detectors, which do not necessarily represent the bundle power, but that of the few closest pins. These differences in modeling the detectors may lead to inaccuracies, especially around areas with singularities such as part length rods, rods with Gadolinium, or the tip of inserted control rods.

On the other hand, the detector response calculation in PARCS is based on an approximate response calculation approach. The TIP detectors are modeled using the built-in detector feature of PARCS, which means that a simple option to average the power of the four adjacent bundles was used for these detectors, and data was generated at 25 axial locations for comparison with plant measurements.

Then, the calculated response approach taken in PARCS involves the following steps:

1) Normalize all measured 33 x 24 TIP signals (33 strings, 24 axial locations) to 1.0.
2) Obtain the 3D nodal power from the two core simulators, PARCS and SIMULATE-3, and calculate at each of the 33 x 24 TIP measurement locations the average nodal value of the four assemblies neighboring each TIP measurement to approximate the flux levels at the physical location of the TIP measurement, and then renormalize to 1.0 according to SIMULATE-3. SIMULATE-3 and PARCS TIP responses data are generated at 25 axial locations for comparison with plant measurements that provide 24 axial locations; thus, a SIMULATE-3-to-TIP and PARCS-to-TIP axial locations correspondence needs to be considered.
3) Estimate the difference between Step 2 and Step 1 at each of the 33 radial locations and calculate the Root Mean Square Errors (RMEs) of nodal-, axially-, and radially-averaged differences.

A key concern is that TIP measurements are difficult from the experimental point of view. The detector position must be adjusted remotely without reliable confirmation of its position. In addition, it is a time-consuming operation, and licensees tend to move fast over the data collection steps.

Confirmation of the measurements is performed at a later time; thus, measurement errors are likely and occur frequently. During data analysis, it is customary to remove data points that deviate *"too much"* from the calculated points. For example, if all the measurements on an axial string agree well with calculated values but one of the elevations has a large error, it is customarily assumed that it was due to a measurement error (e.g., because of incorrect positioning of the TIP detector).

As analysis hypothesis, any single TIP comparison that deviates more than 10% from the measured data, and there is no sample of similar divergence in the rest of the positions, will be discarded and eliminated from the statistics based on the assumption that the measurement was incorrect due to unforeseen errors (e.g., inaccurate axial positioning, external noise, etc.).

This hypothesis is necessary since all the positions' quality is crucial. A significant error in one position (likely due to an experimental measurement error and unrelated to the calculation) may lead to a power shift in other parts due to power normalization. The 10% criterion is based on experience with the performance of many simulation codes.

Moreover, to make a meaningful comparison between the core plant simulator and PARCS, the same number of points at exact locations will be removed from SIMULATE-3 and PARCS TIP response calculations.

So, the average error is evaluated as the standard deviation of the difference between the measured TIP and the calculated TIP response by either SIMULATE-3 or PARCS as:

$$X_d^n = (TIP_{calculated} - TIP_{measured})_d^n \qquad \textbf{Equation 6.1}$$

Where n is the number of axial nodes, which is equal to 24 in total, and d represents the number of detectors equals to 33 in total.

Thus, the nodal and axial root mean squares will be defined as follows:

Nodal Deviation:

$$RMS_{nodal} = \sqrt{\frac{\sum_1^N (X_d^n)^2}{N}} \times 100 \qquad \textbf{Equation 6.2}$$

Where N is the total number of nodes, i.e., 24 x 33. The total nodal deviation is often referred to as *Nodal Precision*.

The comparison between calculated and measured reaction rates is conducted on a node-to-node basis, encompassing the entire set of measured nodes. This set is determined by multiplying the number of detector positions by the number of nodes. This parameter indicates the code's capability to accurately compute the average nodal distribution compared to the measured distribution.

Axial Deviation:

$$RMS_{axial} = \sqrt{\frac{\sum_{d=1}^{33} (X_d^n)^2}{33}} \times 100 \qquad \textbf{Equation 6.3}$$

Where $n = 1 \ldots 24$, i.e., the number of axial nodes. The axial deviation refers to the disparity observed between the calculated and measured axially-averaged reaction rates. It quantifies the extent to which the computed values deviate from the measured values along the axial direction.

Since the impact of using different cross-section sets on the radial level is practically negligible as explained in Chapter 5, the radial RMS errors will not be included herein.

All simulations were conducted using **PARCS version 3.32**. The simulations assumed equilibrium Xenon/Samarium conditions for all selected measurements and utilized the history files provided by SIMULATE-3, along with the operational conditions of the plant.

6.4 PARCS TIP Response Calculations.

The nodal RMS errors for local power level across all 792 points (obtained by multiplying the 24 axial points by 33 TIP locations) are presented for three different conditions: BOC, several MOC points, and EOC. Additionally, the axial RMS power differences (%) between the TIP measurements and the TIP responses calculated by SIMULATE-3 and PARCS core simulators are included.

Figure 6.6 to Figure 6.29 provide a detailed comparison of the average axial power distribution within the core, as obtained from authentic TIP measurements, with the corresponding calculations performed by the core simulators SIMULATE-3 and PARCS.

In these comparisons, the PARCS nodal power levels were averaged radially across the four assemblies surrounding each TIP measurement location, approximating the flux levels at the physical position of the TIP measurement.

The solid line represents the power measured by the TIP detectors, while the triangular dots and circles represent the power calculated by SIMULATE-3 and PARCS, respectively.

The vertical axis represents the total axial height of the detector (365.76 cm) divided into 24 nodes, each with a height of 15.24 cm. The horizontal axis displays the relative axial power normalized to a core average of 100%.

All PARCS calculations will be presented for each simulated condition, considering each cross-section library employed (Set 1, Set 3c, Set 3c-b46, and Set 3c-b78).

The results will be further discussed in their respective subsections, providing a more comprehensive analysis and interpretation.

6.4.1 BOC Condition Results.

A summary of the relative differences between calculations and measurements for the several cases analyzed is reported in Table 6.2. It can be seen that SIMULATE-3 exhibits the closest agreement with the TIP measurements for both nodal and axial power estimations, aligning with the expected outcome.

Table 6.2. Comparison of Nodal and Axial RMSEs (%). BOC Condition. All XS Libraries

RMSE (%)	SIMULATE-3	Set 1	Set 3c	Set 3c-b46	Set 3c-b78
Nodal	4.831	7.946	5.114	5.580	5.517
Axial	3.265	4.098	3.714	4.269	4.187

In terms of the PARCS-calculated TIP responses, the results indicate that all nuclear data libraries adequately handle the instantaneous variables. The agreement among the PMAXS cross-section libraries remains consistent, with nodal RMS discrepancies ranging between 5% and 6%, and axial disparities between 3.7% and 4.3%.

Regarding the rejected points due to a power deviation exceeding 10%, 184 out of 792 (accounting for 23.2% of the total) have been excluded from the statistics during BOC conditions for both SIMULATE-3 and PARCS.

Notably, library Set 1 displays the largest discrepancies in nodal-wise predictions. The impact of cross-section extrapolation becomes apparent from 70% void upwards. These findings confirm the previously highlighted issues concerning this specific nuclear data library, as discussed in Chapter 5.

When comparing Set 1 and Set 3c libraries, the discrepancies between PARCS and the TIP data show a reduction from 8% to 5.1% in terms of nodal RMS (a decrease of approximately 36%) and from 4.1% to 3.7% in terms of axial RMS (a reduction of around 10%). This improvement in power distribution predictions by PARCS is observed as the history range is broadened from 70% to 90%, even though the state variables play the most relevant role in BOC conditions.

However, when using libraries with higher burnup points (libraries b46 and b78), no improvement is observed in power distribution estimations. While qualitatively, these libraries behave as expected, the unexpected and counterintuitive outcome in terms of RMSEs suggests there might be a limit to enhancements depending on the specific characteristics of the analyzed case. Further investigations will be necessary to provide conclusive evidence in this regard.

The axial power comparison depicted in Figure 6.6 to Figure 6.9 showcases the overall accuracy of PARCS in predicting axial power shapes for most detectors.

Although PARCS lacks a proper gamma field model to simulate gamma TIP measurements, overall, a very good agreement is achieved between PARCS and the

measured TIPs at BOC. Additionally, a good correlation is observed between PARCS and SIMULATE-3 regarding power distributions across the core, with errors of a similar order of magnitude.

However, it is worth noting that significant differences emerge near the locations of inserted control rods, particularly at detectors number 7, 8, 9, 13, 14, 15, 19, 20, and 21, regardless of the cross-section libraries utilized in the study.

A more detailed analysis reveals that these discrepancies predominantly manifest in the lower axial half of the core, which is consistent with the operational characteristics of BWRs, where control rods are inserted from the bottom of the core. Consequently, this suggests that the model employed by PARCS to represent the behavior of control rods might be subject to inaccuracies, mainly when multiple control rod definitions are utilized, as it is the case in Cycle B.

Moreover, the effect of not considering the variation of the cross-sections and neutron kinetic parameters in the reflector region due to the instantaneous moderator density is apparent in the larger discrepancy observed close to the top and the bottom of the active core. These two issues have been previously observed in Forsmark calculations, as reported in (Demazière, C. et al., 2012).

Finally, slight deviations are observed in the peripheral detectors, where PARCS generally yields higher overall channel power levels compared to the TIP data. In these instances, PARCS tends to overestimate the power peaking in the axial direction, implying lower void fractions in the subcooled region at the core inlet.

Despite this discrepancy, PARCS succeeds in accurately reproducing the overall axial power profile in its simulations.

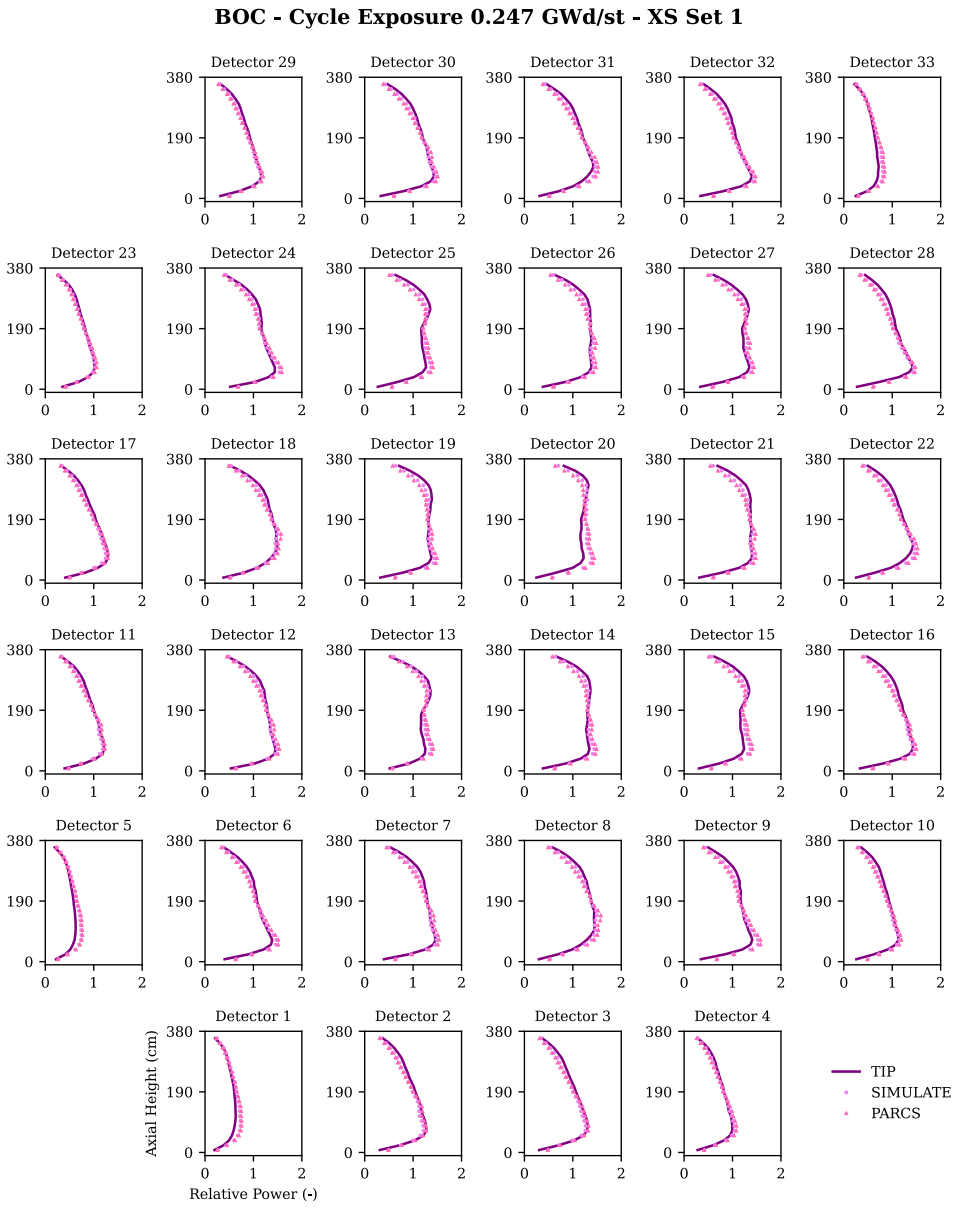

Figure 6.6. BOC - TIPs Data. Measured vs. Calculated. XS Set 1.

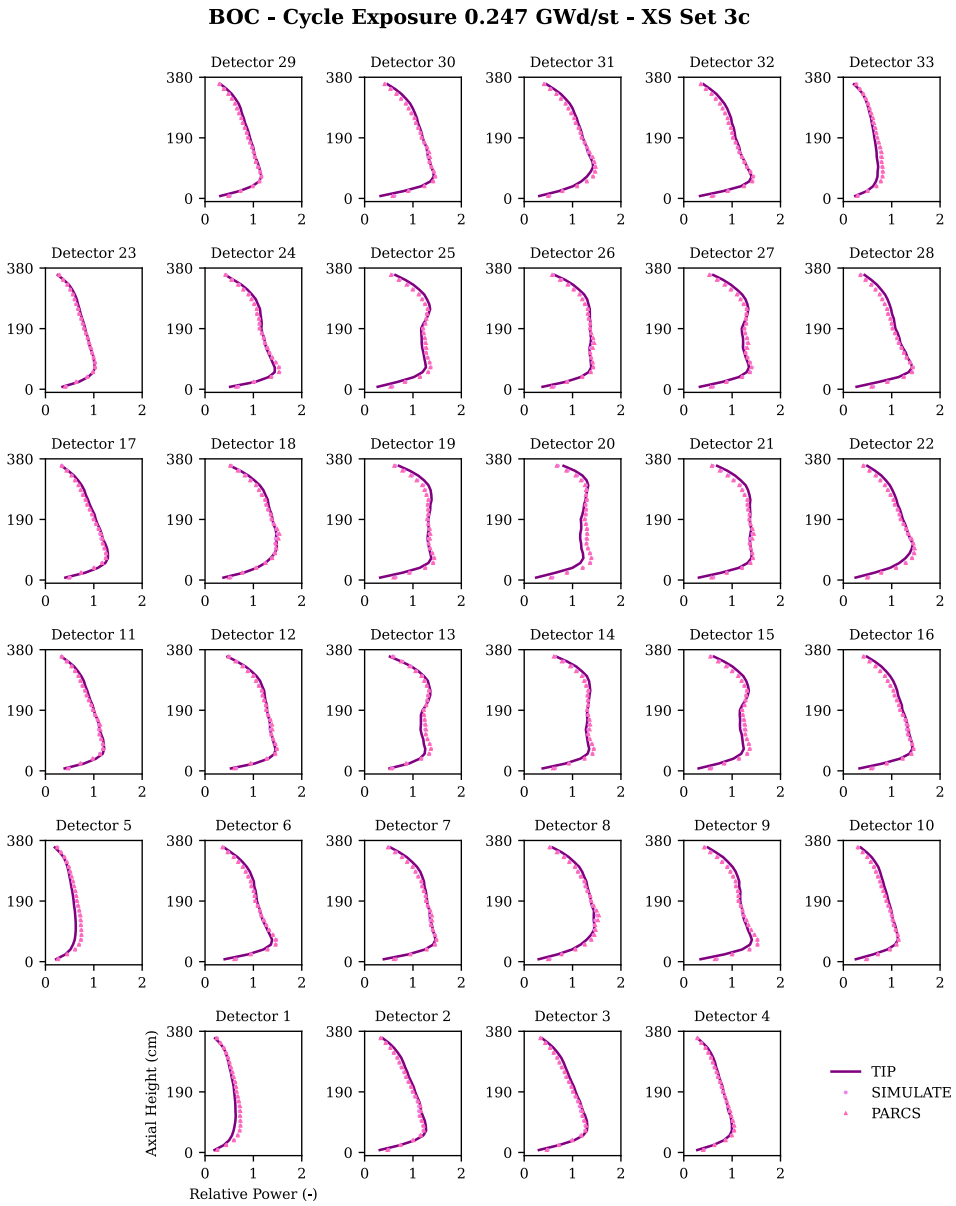

Figure 6.7. BOC - TIPs Data. Measured vs. Calculated. XS Set 3c.

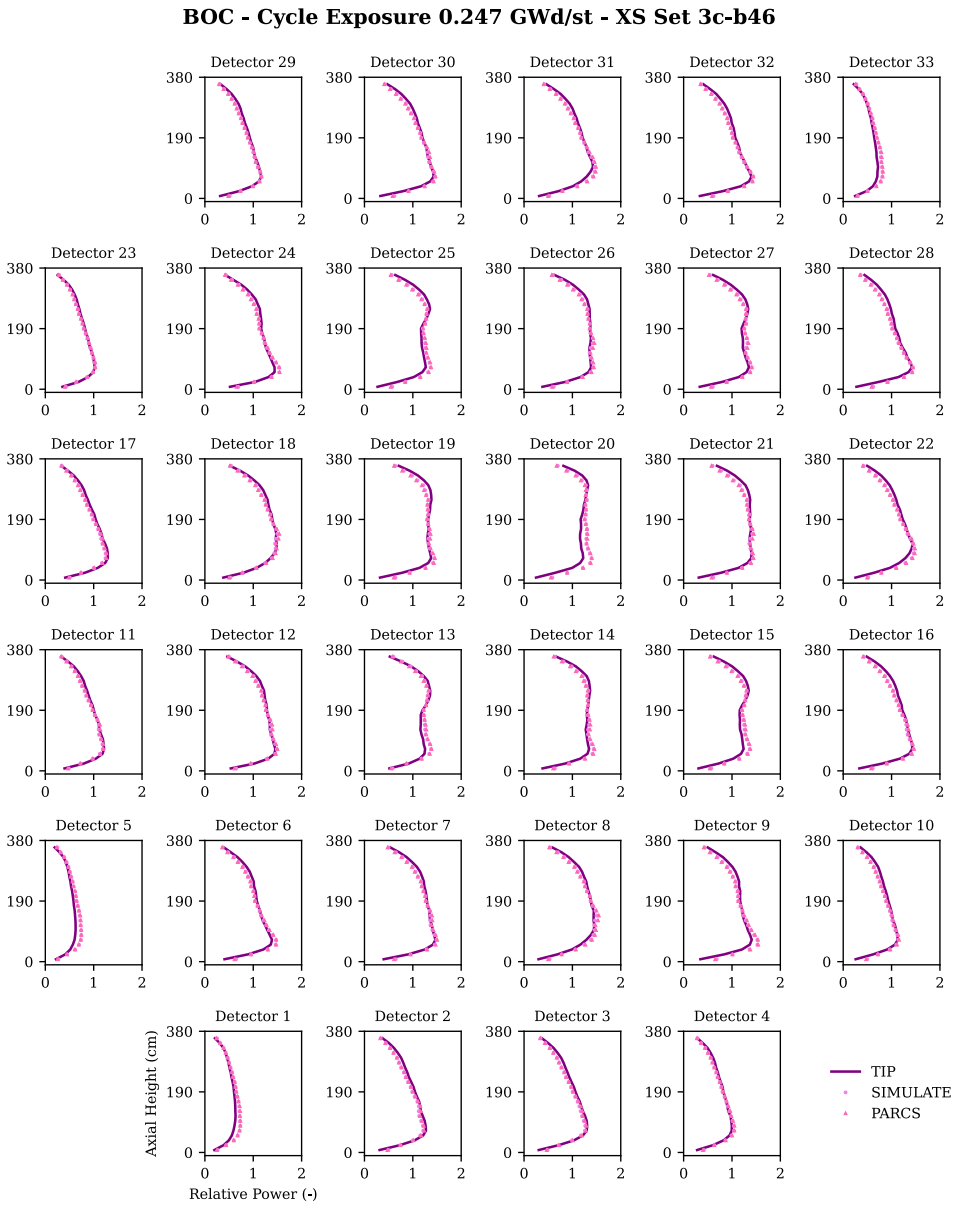

Figure 6.8. BOC - TIPs Data. Measured vs. Calculated. XS Set 3c-b46.

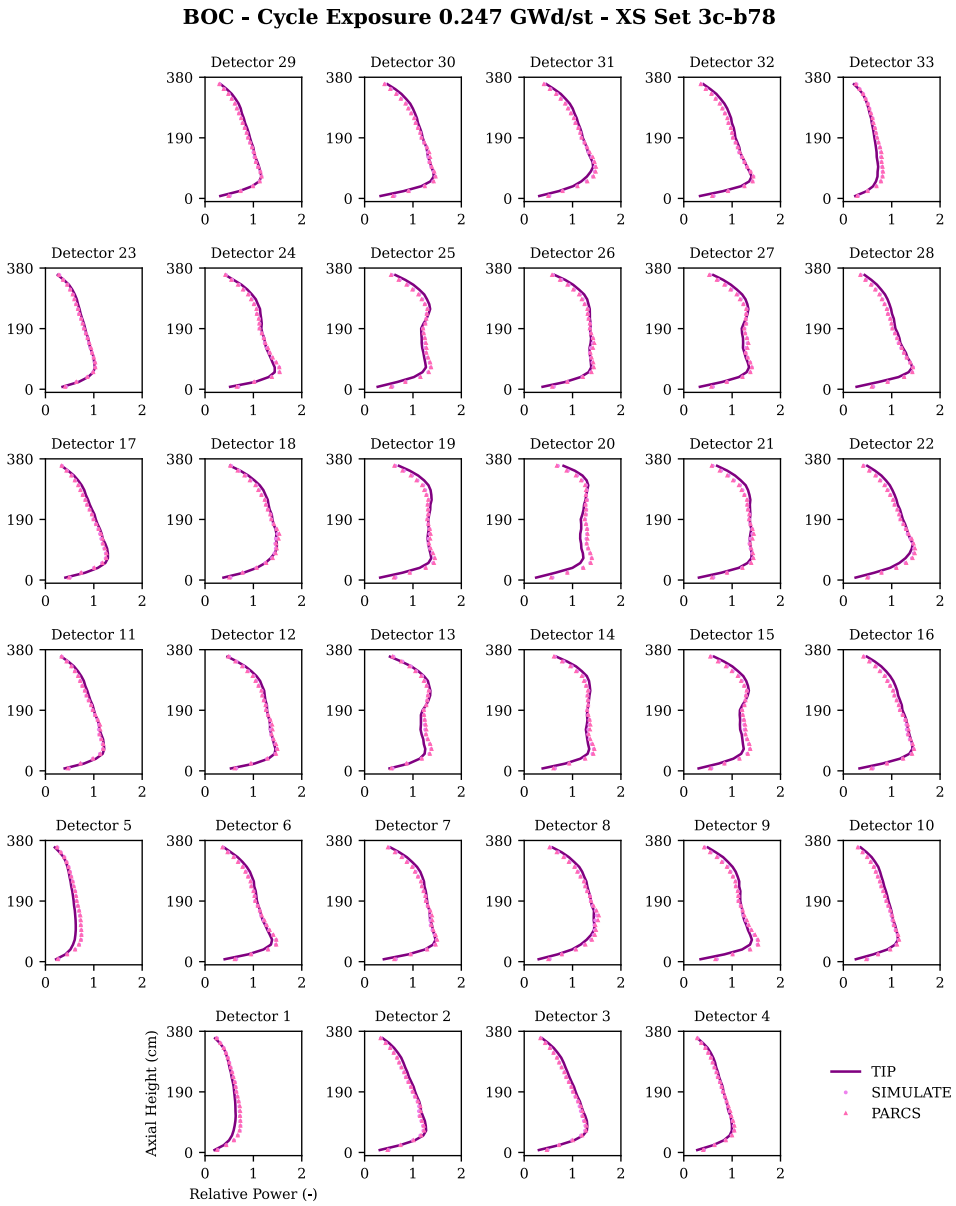

Figure 6.9. BOC - TIPs Data. Measured vs. Calculated. XS Set 3c-b78.

6.4.2 MOC Condition Results.

As seen in Table 6.3, the comparison among Set 3c, b46, and b78 libraries reveals no significant differences, as all three libraries yield nearly identical results for power distributions. However, it is worth noting that library b46 exhibits a slightly better agreement with TIPs on average for the four MOC condition points. Set 1 significantly deviates from the plant data and lacks coverage for the entire range of reactor operations.

Once and again, the best agreement between the experimental data and the core simulator is between TIP and SIMULATE-3.

Table 6.3. Comparison of Nodal and Axial RMSEs (%). MOC Conditions. All XS Libraries.

RMSE (%)	SIMULATE-3	Set 1	Set 3c	Set 3c-b46	Set 3c-b78
Nodal 1	3.969	7.196	4.290	4.461	4.455
Nodal 2	4.541	7.047	4.527	4.465	4.455
Nodal 3	4.132	7.196	4.469	3.947	3.947
Nodal 4	4.845	8.699	4.102	4.519	4.547
Axial 1	1.98	3.825	2.611	2.746	2.746
Axial 2	1.761	2.899	2.202	2.059	2.044
Axial 3	1.121	3.829	2.778	1.803	1.791
Axial 4	3.264	4.615	2.631	3.255	3.297

Overall, the PARCS TIP responses demonstrate that all nuclear data libraries accurately handle instantaneous and historical variables. The agreement between TIPs and all PMAXS cross-section libraries is excellent, with nodal RPF RMS below 5% and axial RPF RMS below 3.3%.

Regarding the points rejected due to power deviation exceeding 10%, the following points have been excluded from the statistics for each MOC case: 110 points for MOC #1, 112 points for MOC #2, 120 points for MOC #3, and 151 points for MOC 4. Consequently, the rejected points account for 13.9%, 14.1%, 15.2%, and 19.1% of the total for MOC #1, MOC #2, MOC #3, and MOC #4, respectively. These values represent the lowest number of rejected points observed thus far, and although they increase with exposure, they remain below 20% of the total.

In general, PARCS values demonstrate excellent agreement with TIPs for all the analyzed MOC measurements when predicting axial power shapes, as observed in Figure 6.10 to Figure 6.25. These results suggest that all libraries adequately capture the Gd effect.

The errors near the locations of inserted control rods have decreased in comparison to the BOC results, particularly when the control rods move to implement the

pre-programmed exchange sequences during regular cycle operation, as was already depicted in Figure 6.4. This finding confirms that the control rod history, which seems to be fairly accounted by PARCS, significantly influences the axial power distribution.

As previously discussed, there continues to be a slight axial deviation in the peripheral detectors, consistent with the observations made during the analysis of the results at BOC, as well as a similar trend of discrepancies persists in the power estimations at the bottom and top reflectors by PARCS when compared to the TIPs.

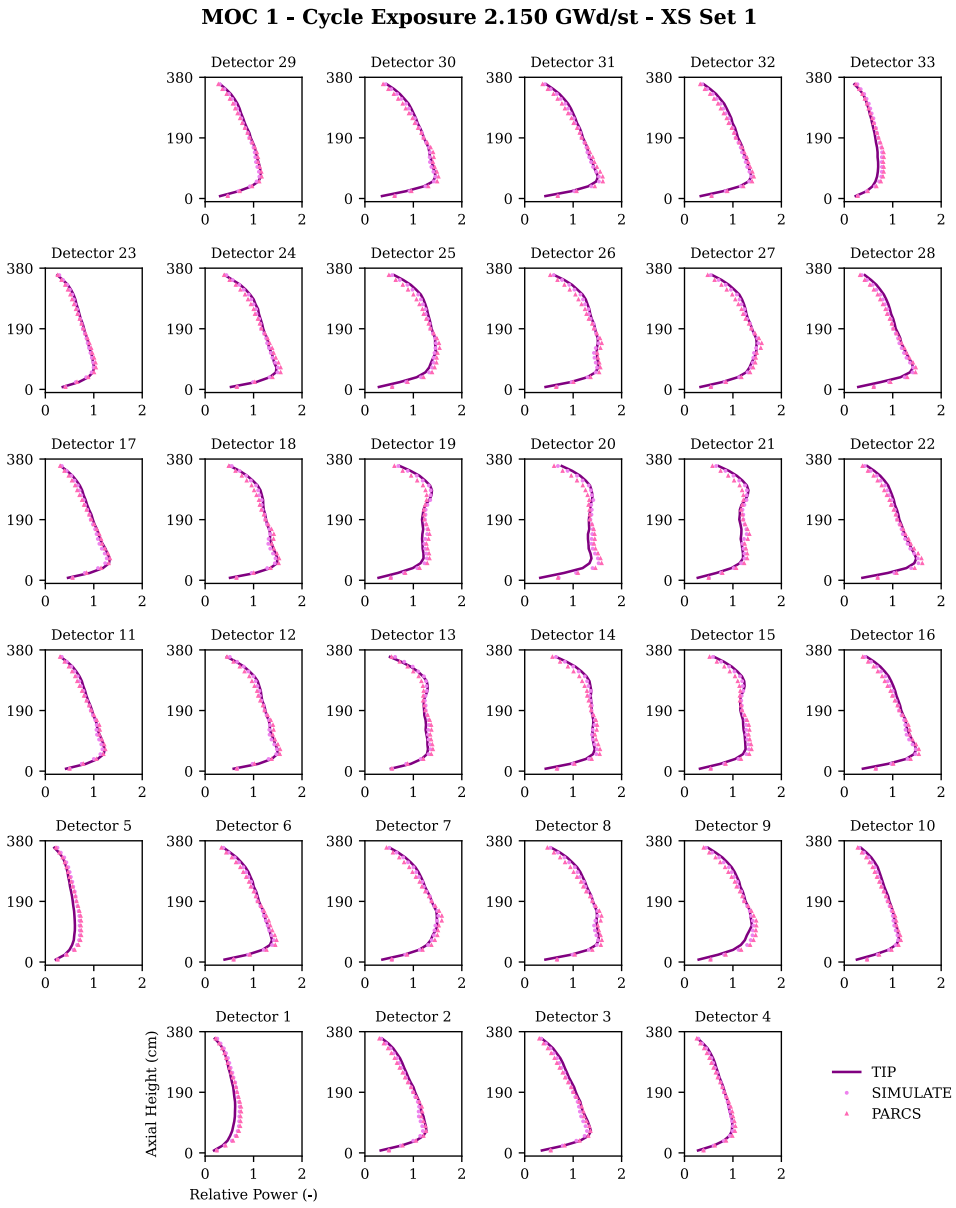

Figure 6.10. MOC #1 - TIPs Data. Measured vs. Calculated. XS Set 1.

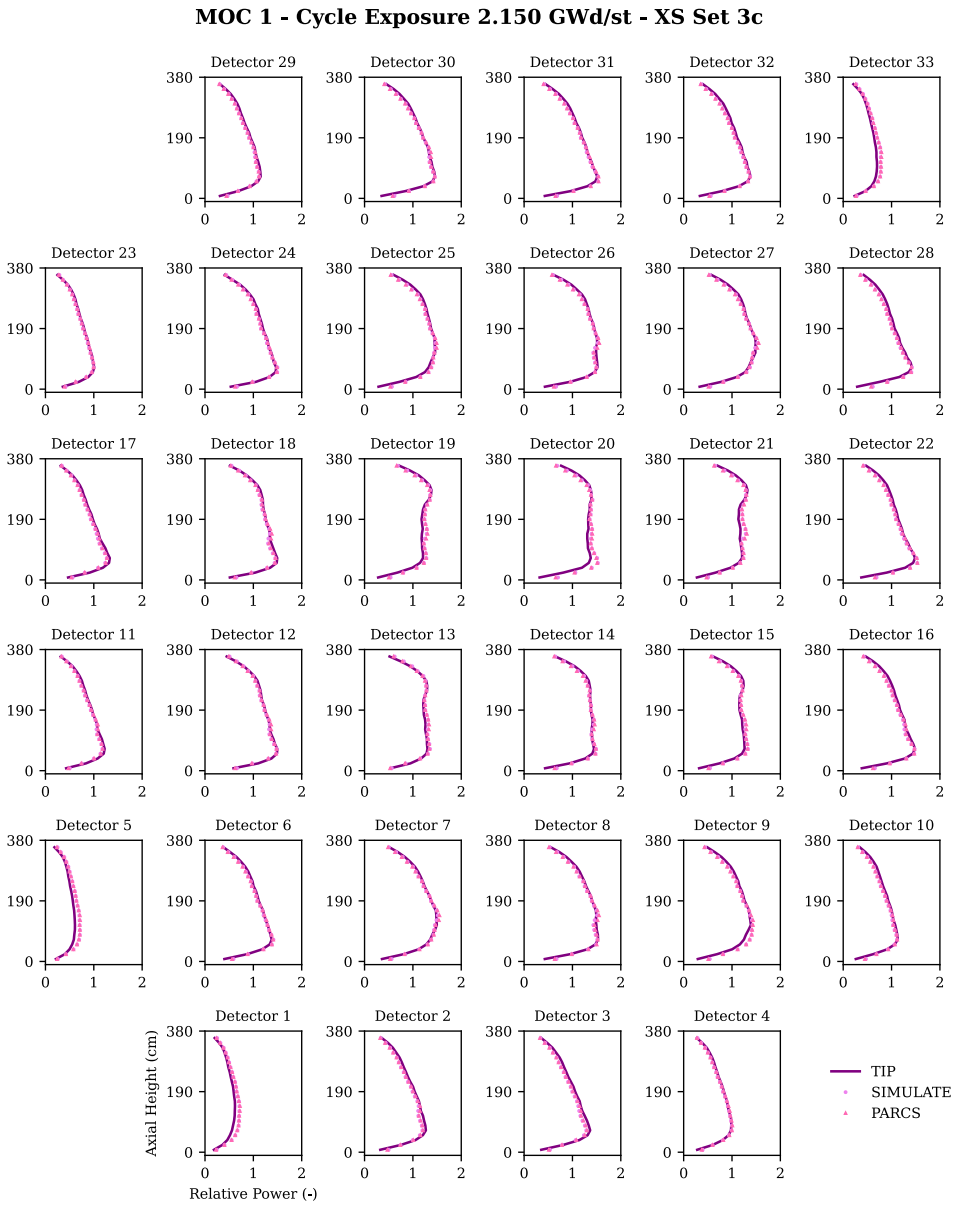

Figure 6.11. MOC #1 - TIPs Data. Measured vs. Calculated. XS Set 3c.

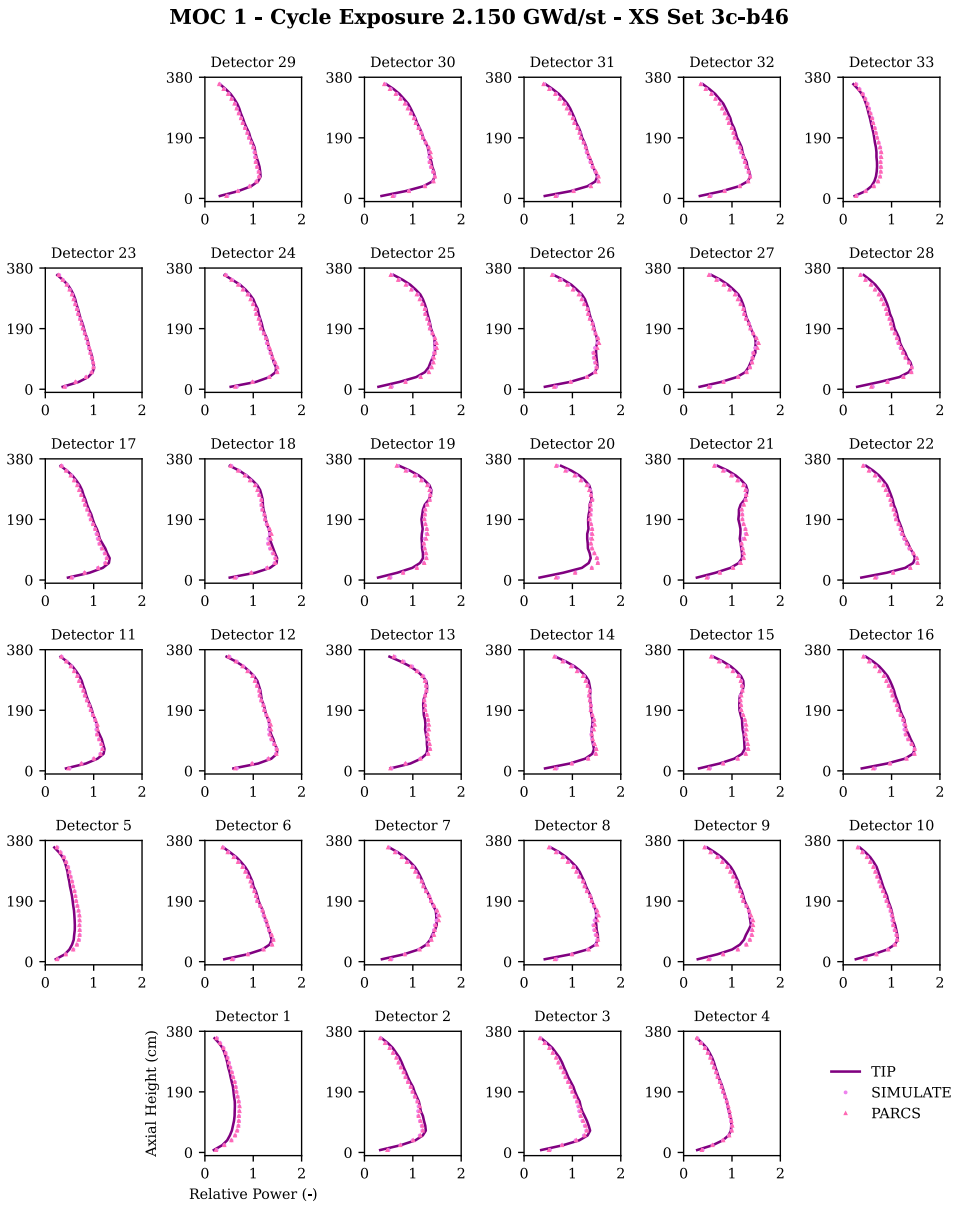

Figure 6.12. MOC #1 - TIPs Data. Measured vs. Calculated. XS Set 3c-b46.

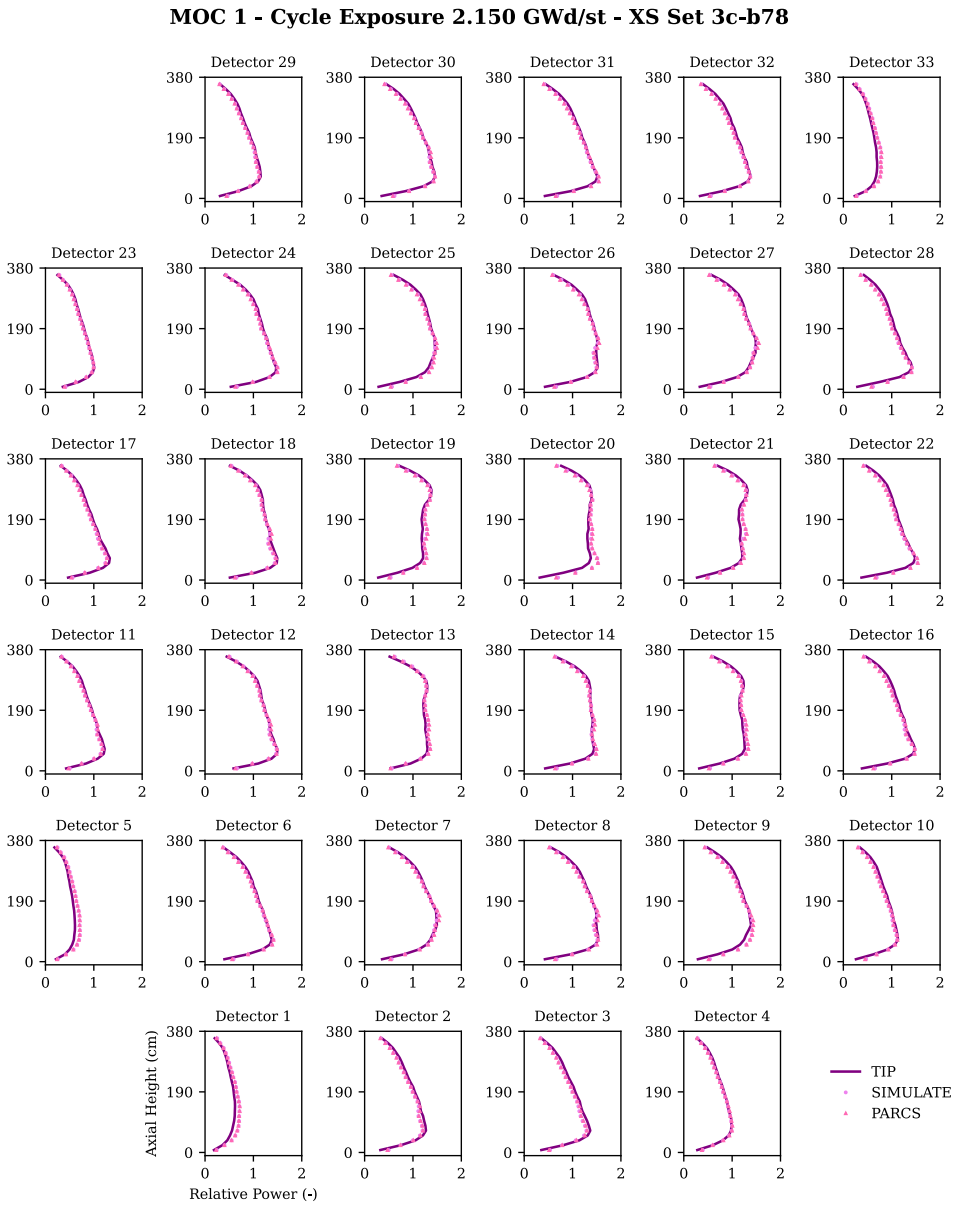

Figure 6.13. MOC #1 - TIPs Data. Measured vs. Calculated. XS Set 3c-b78.

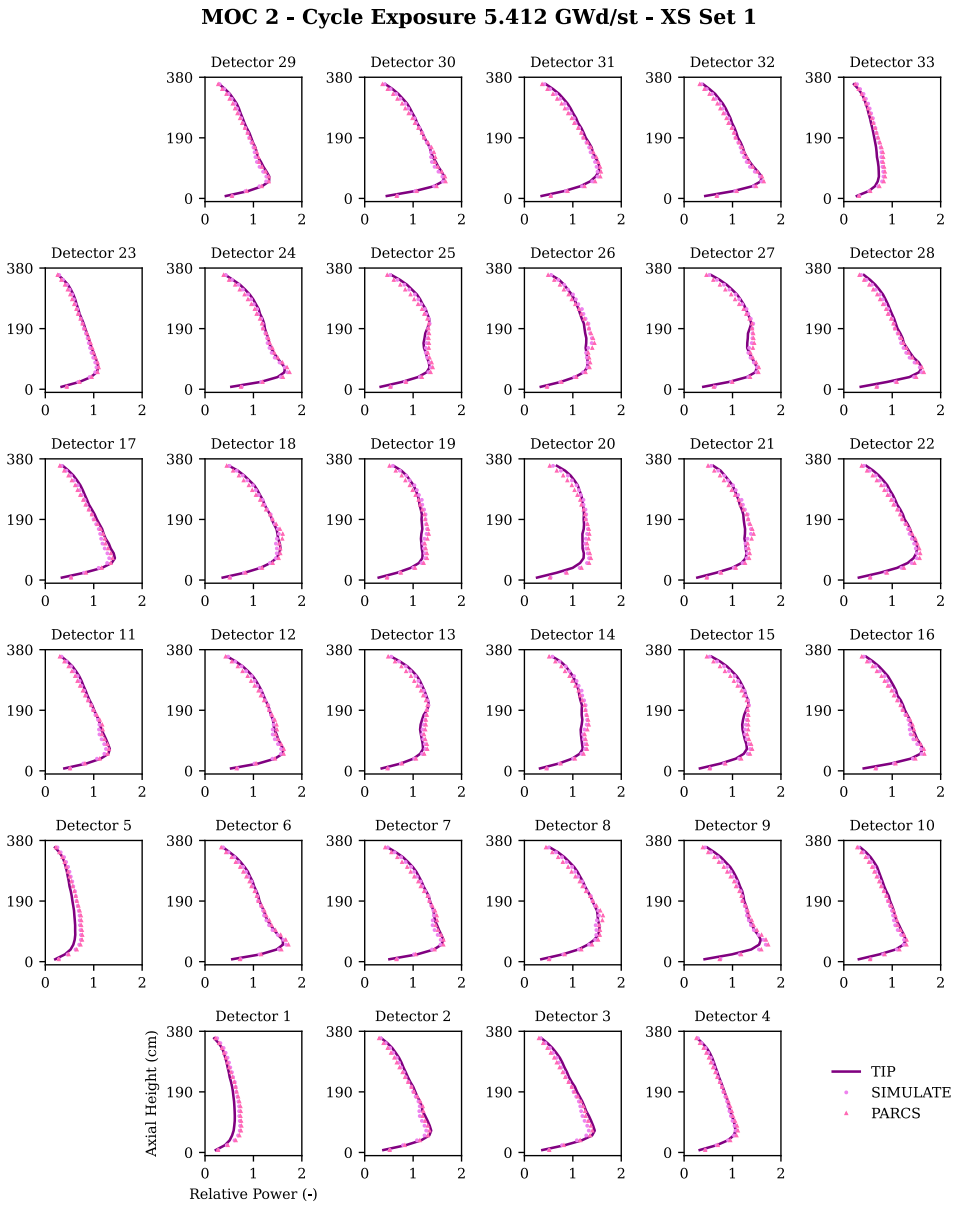

Figure 6.14. MOC #2 - TIPs Data. Measured vs. Calculated. XS Set 1.

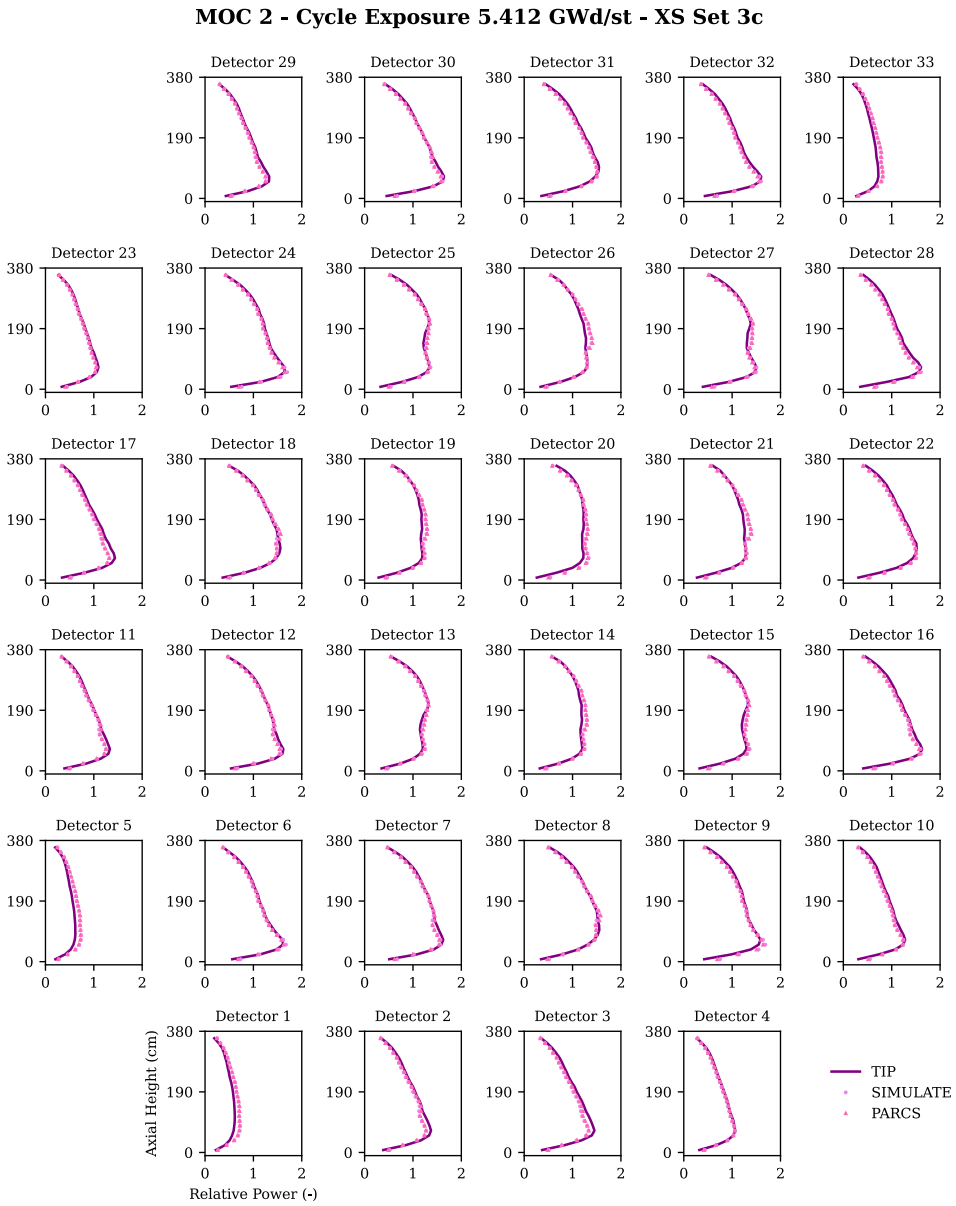

Figure 6.15. MOC #2 - TIPs Data. Measured vs. Calculated. XS Set 3c.

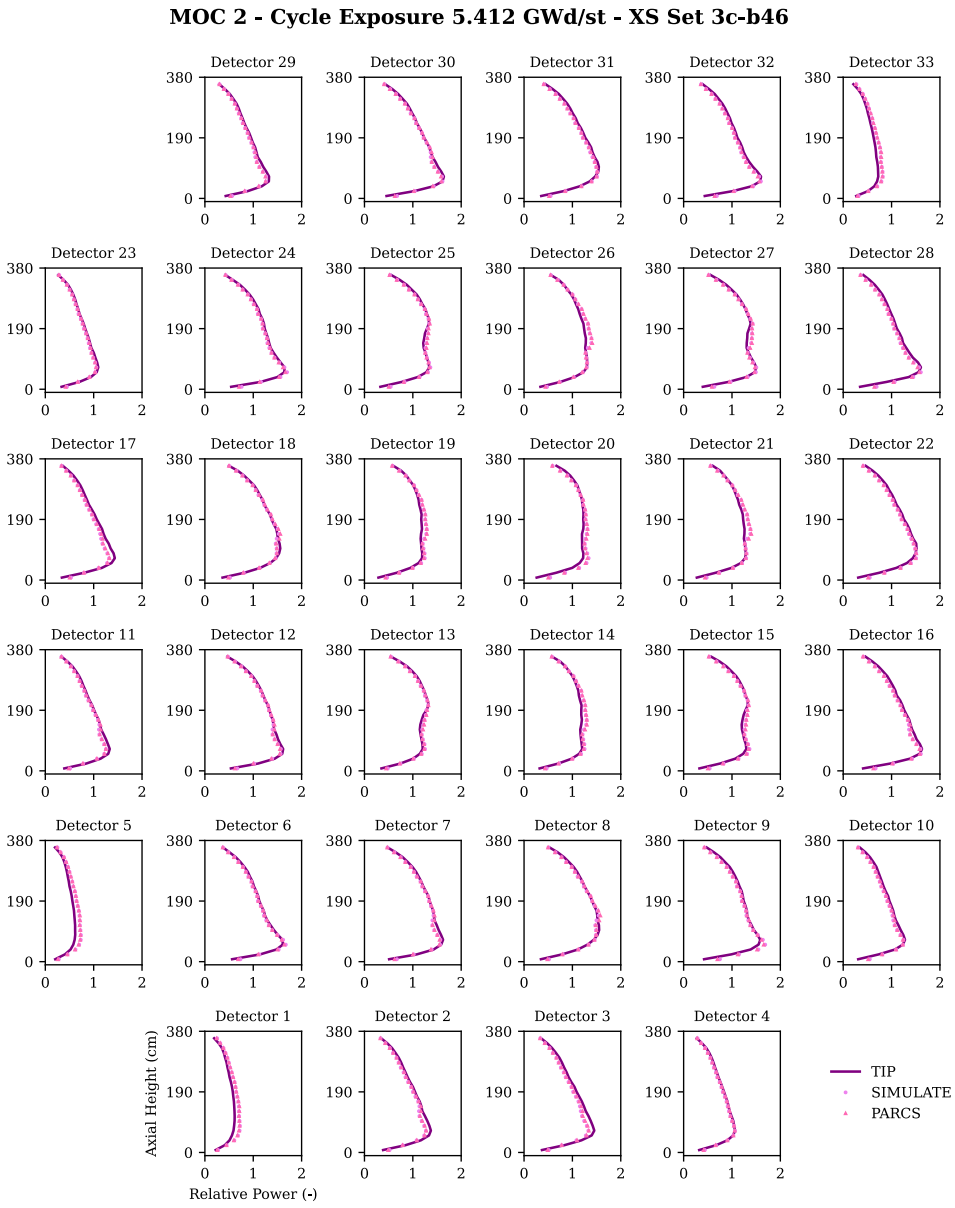

Figure 6.16. MOC #2 - TIPs Data. Measured vs. Calculated. XS Set 3c-b46.

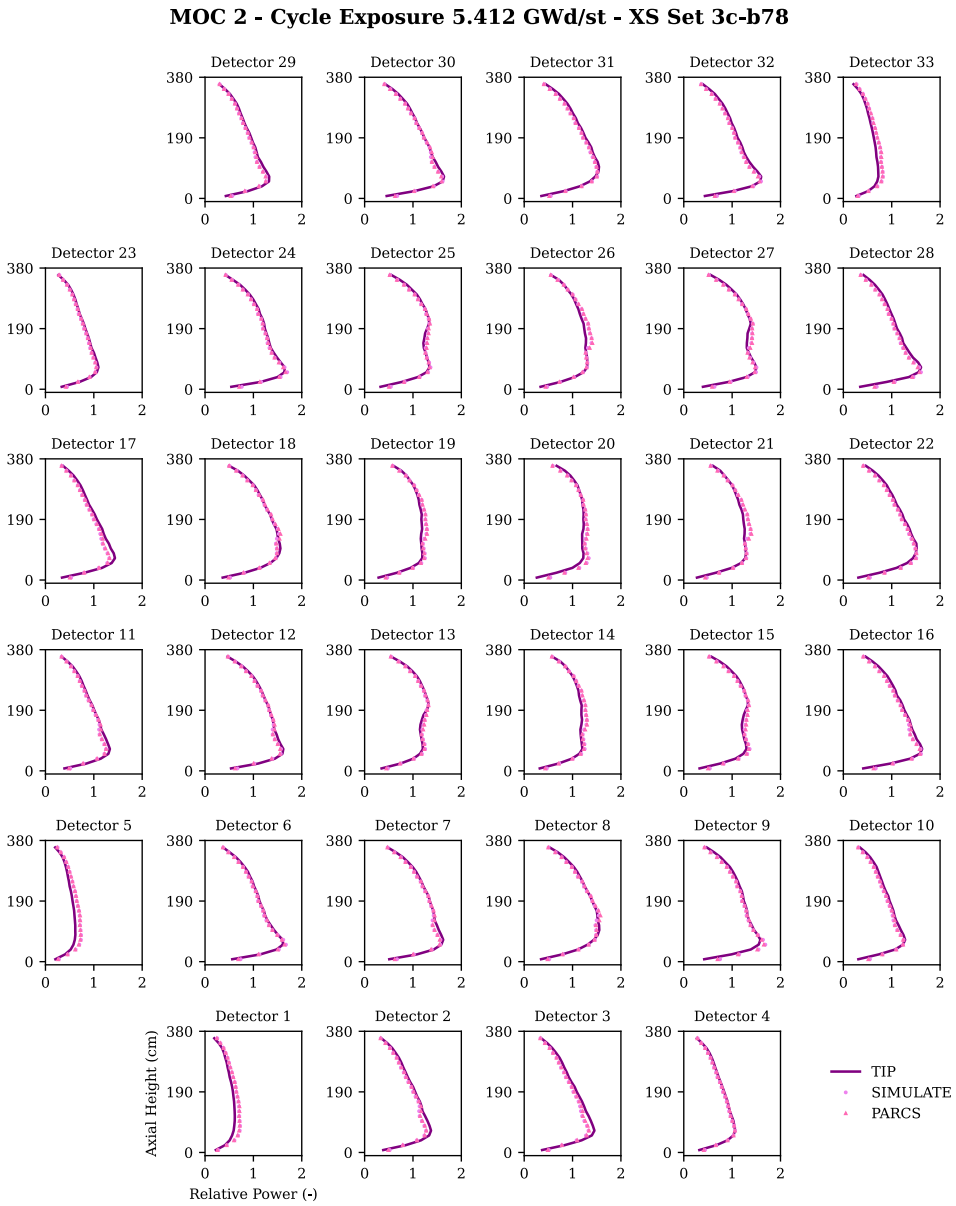

Figure 6.17. MOC #2 - TIPs Data. Measured vs. Calculated. XS Set 3c-b78.

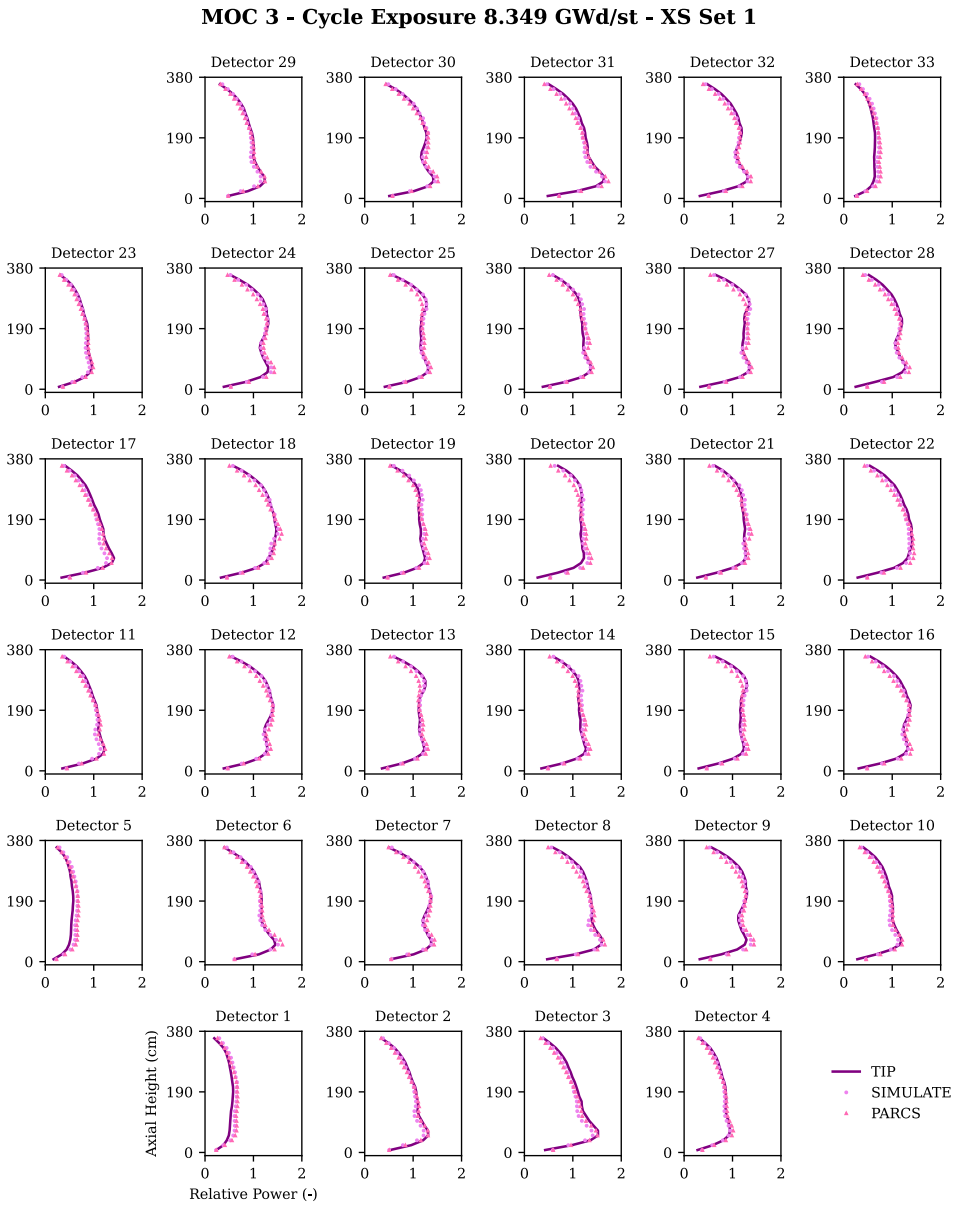

Figure 6.18. MOC #3 - TIPs Data. Measured vs. Calculated. XS Set 1.

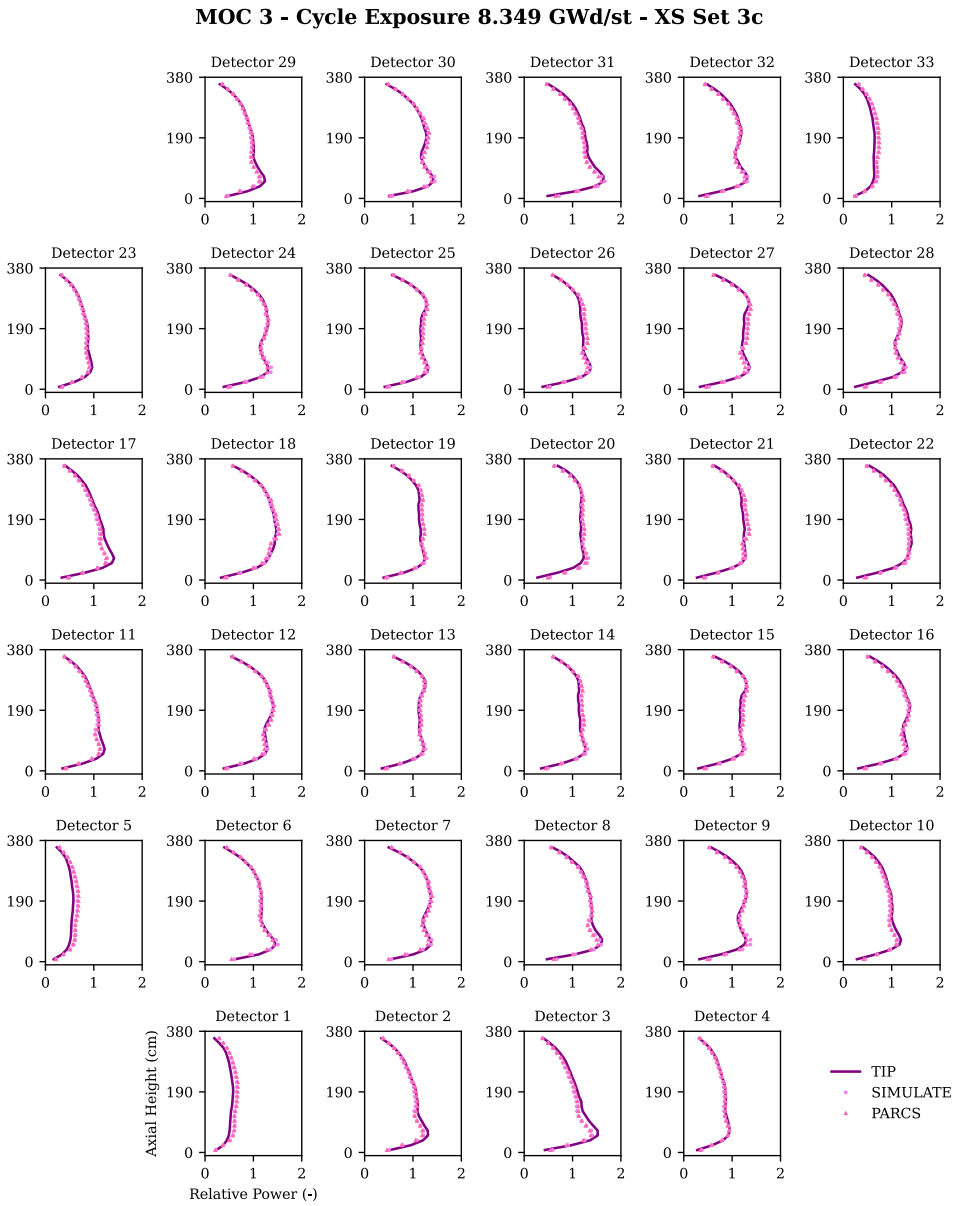

Figure 6.19. MOC #3 - TIPs Data. Measured vs. Calculated. XS Set 3c.

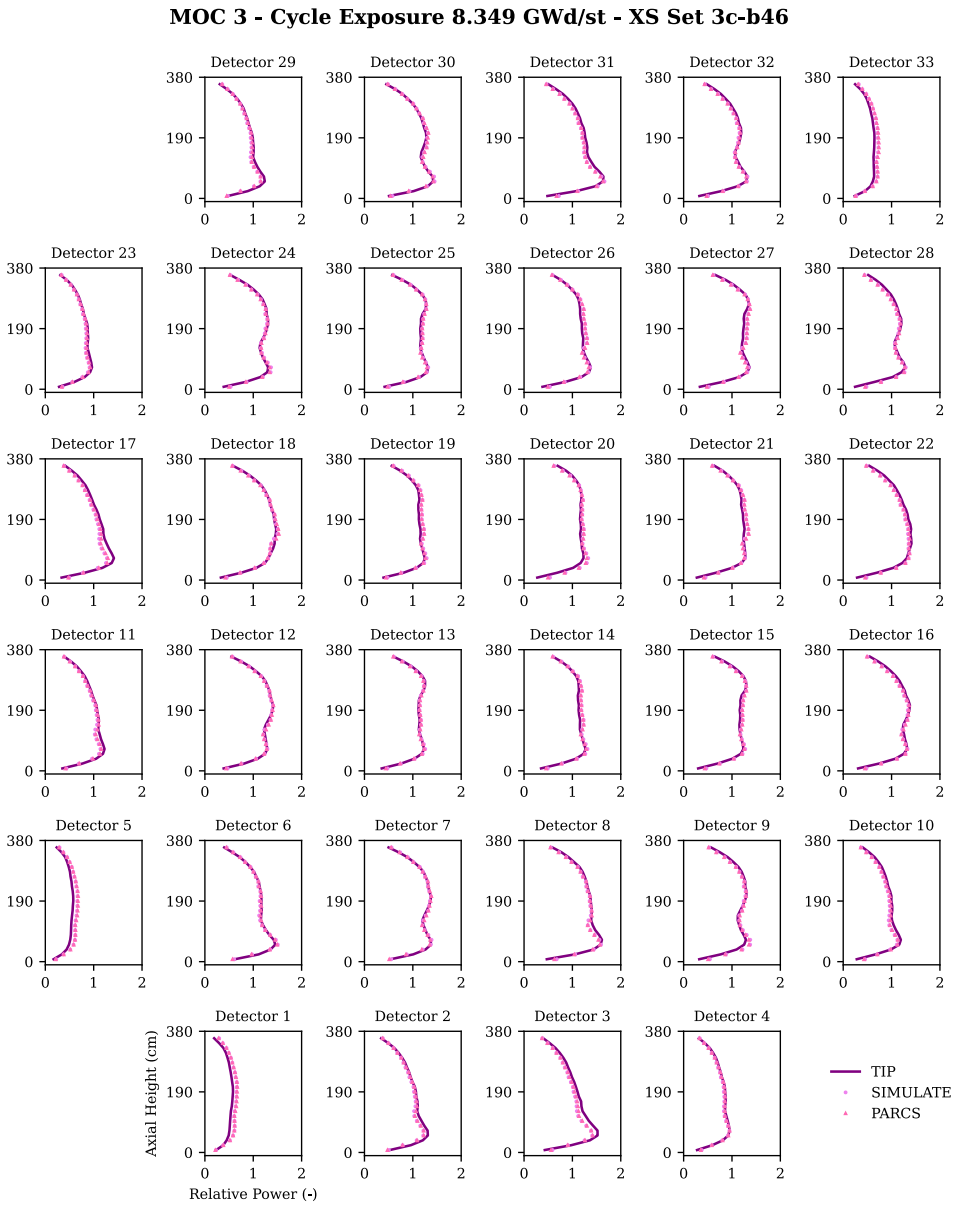

Figure 6.20. MOC #3 - TIPs Data. Measured vs. Calculated. XS Set 3c-b46.

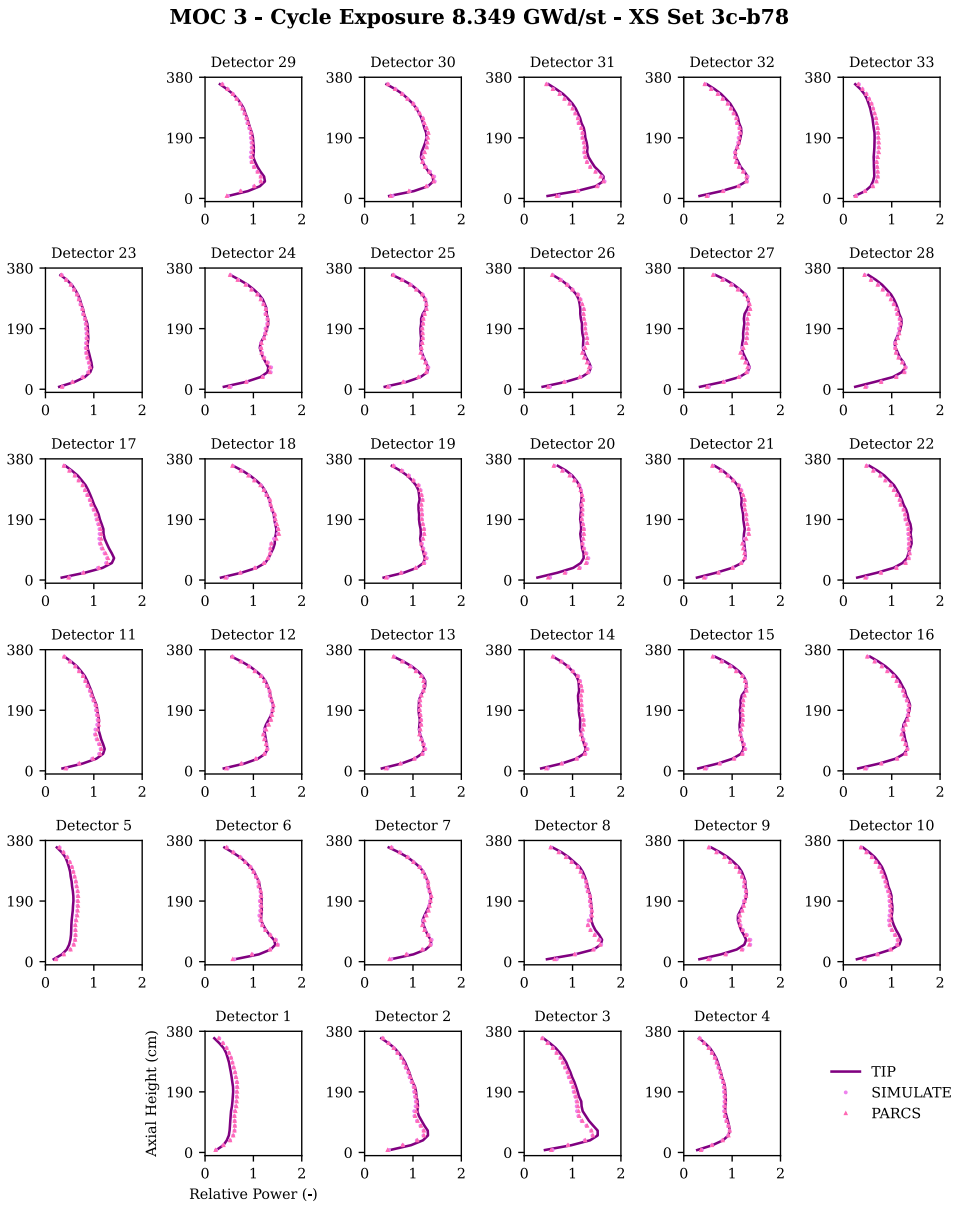

Figure 6.21. MOC #3 - TIPs Data. Measured vs. Calculated. XS Set 3c-b78.

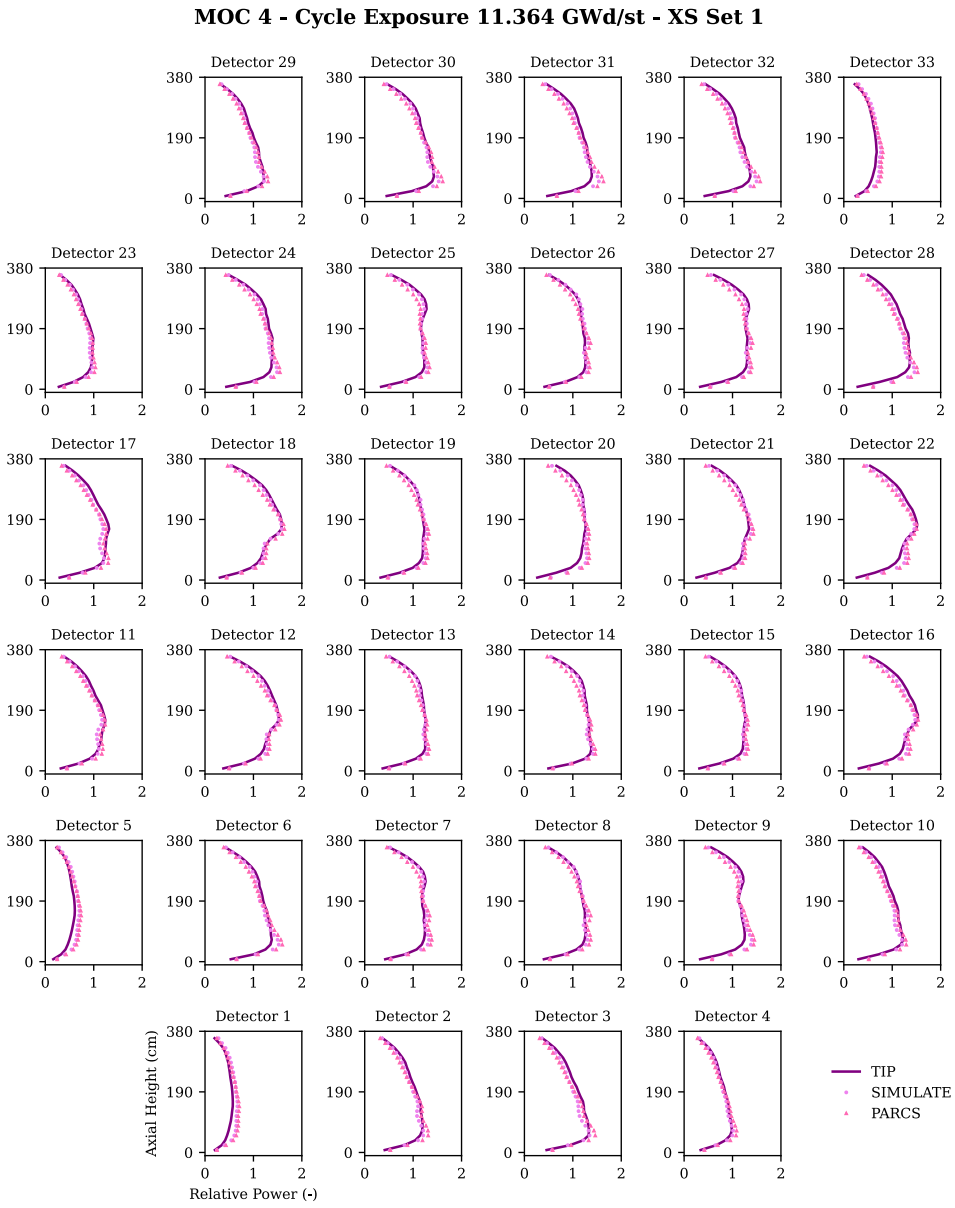

Figure 6.22. MOC #4 - TIPs Data. Measured vs. Calculated. XS Set 1.

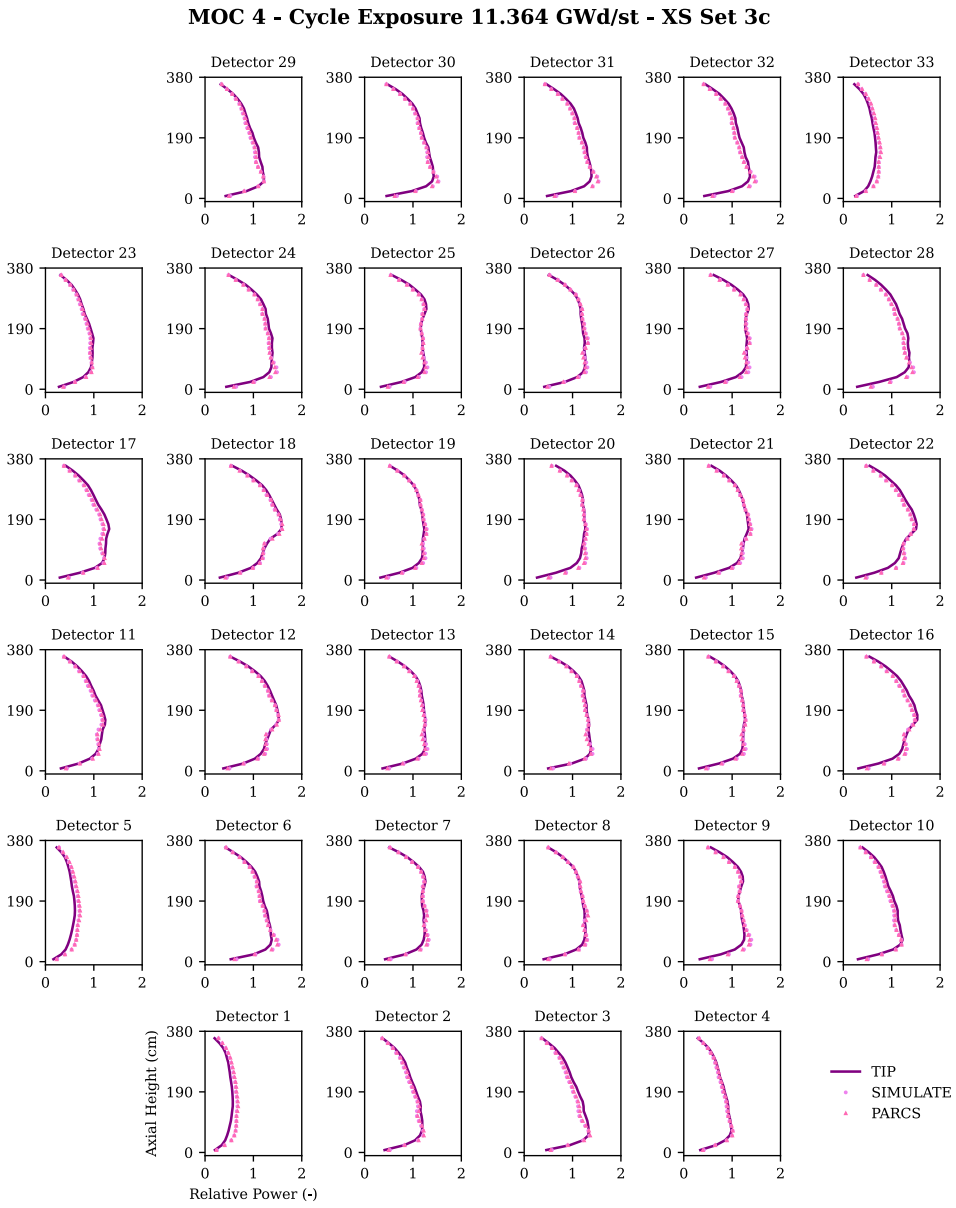

Figure 6.23. MOC #4 - TIPs Data. Measured vs. Calculated. XS Set 3c.

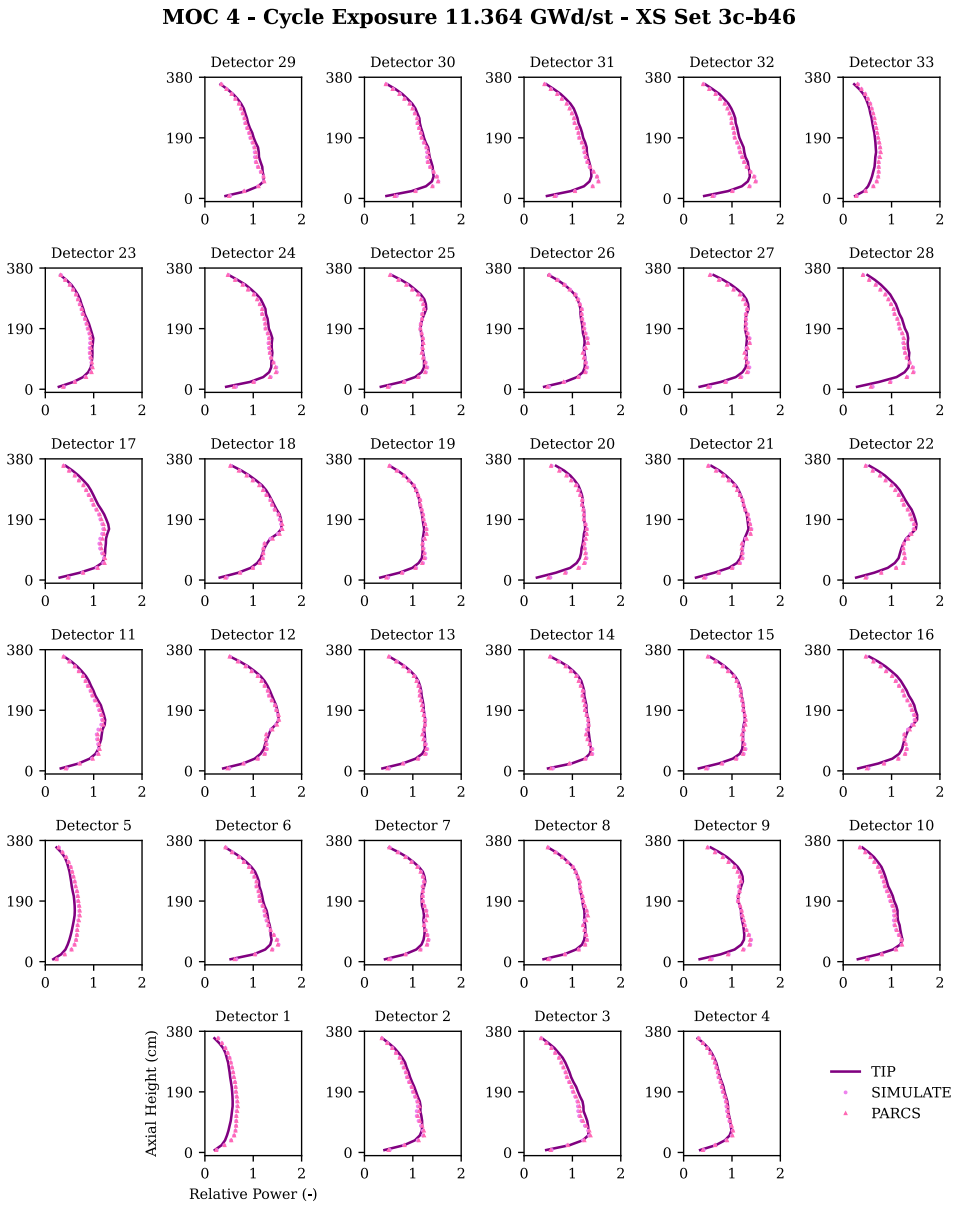

Figure 6.24. MOC #4 - TIPs Data. Measured vs. Calculated. XS Set 3c-b46.

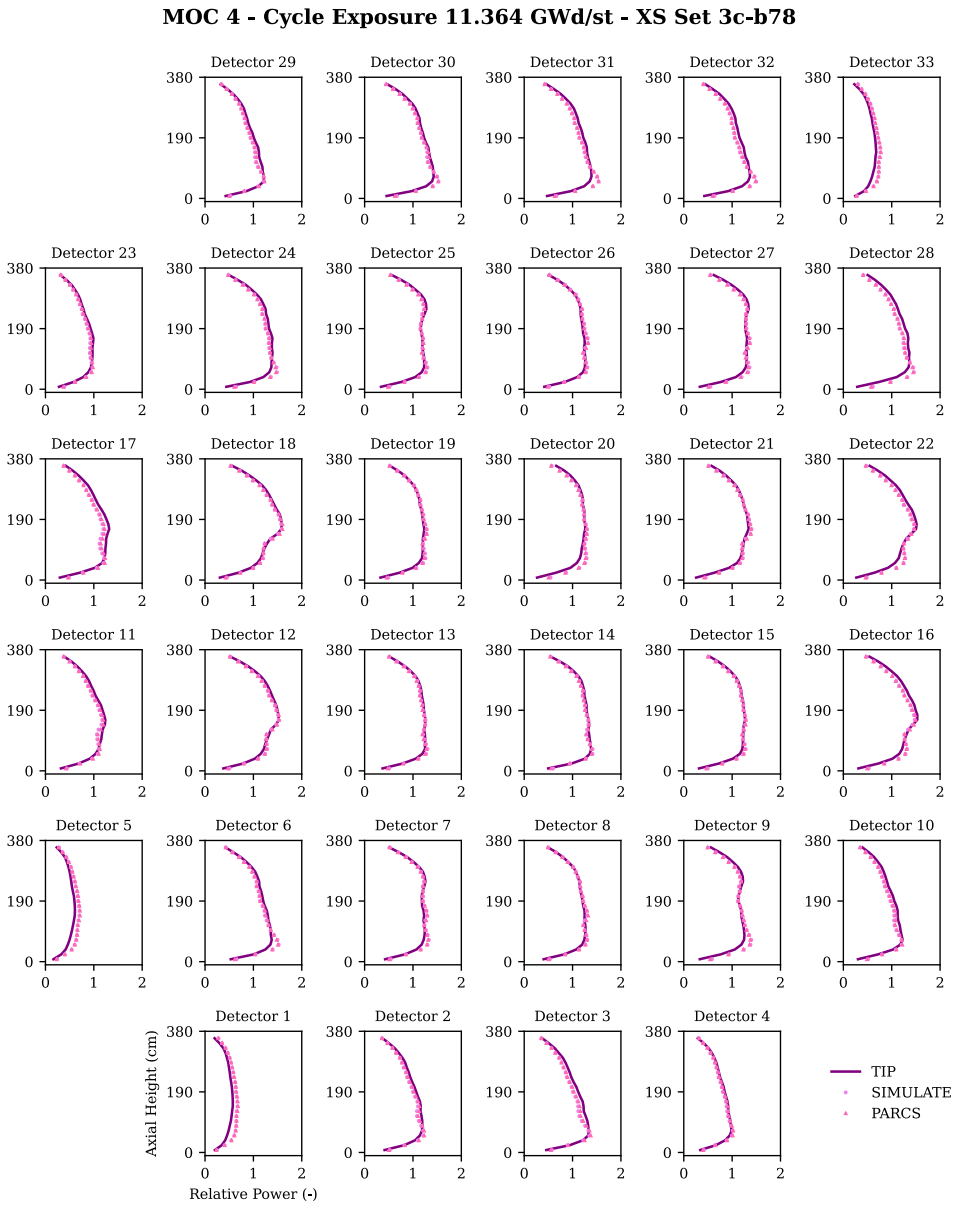

Figure 6.25. MOC #4 - TIPs Data. Measured vs. Calculated. XS Set 3c-b78.

6.4.3 EOC Condition Results.

A comprehensive summary of the calculated TIP responses at EOC is provided in Table 6.4. As the cycle progresses and the axial power distribution shifts towards the top of the fuel bundle, the impact of partial-length rods on the TIP gamma field becomes more evident.

Once again, SIMULATE-3 exhibits the best agreement with TIPs for nodal and axial power estimations.

Table 6.4. Comparison of Nodal and Axial RMSEs (%). EOC Condition. All XS Libraries.

RMSE (%)	SIMULATE-3	Set 1	Set 3C	Set 3c-b46	Set 3c-b78
Nodal	4.89	11.987	6.460	5.513	5.431
Axial	4.28	4.636	6.433	5.198	5.088

The nodal discrepancies between PARCS and TIPs are significantly reduced for Set 1 and Set 3c-b46 libraries in terms of nodal RMS from approximately 12% to 5.5% representing a reduction in error of over 50%. This reduction is attributed to the broader history ranges (70% to 90%) and finer depletion points in the cross-section library, which have a noticeable impact.

Likewise, the axial and nodal root mean square errors at EOC gradually decrease as the nuclear data library contains more burnup points. However, there is an exception with the axial RMS error obtained for the case using the Set 1 library. This result is somewhat surprising considering that the Set 1 library does not adequately capture the treatment of certain history variables crucial for end-of-cycle calculations, mainly due to the 70% upper boundary limitation in the nominal calculation.

It should be noted that 244 data points out of a total population of 792 have been excluded from the statistics for both SIMULATE-3 and PARCS at EOC conditions, as they exceeded the 10% error acceptance criterion. This represents the highest number of rejected points among all the analyzed cases. While inconclusive, this issue may be related to rejecting four consecutive full TIP measurements following this particular measurement.

Figure 6.26 to Figure 6.29 present a detailed comparison of the average axial power distributions calculated by SIMULATE-3 and PARCS for each detector at EOC conditions.

Generally, as the depletion of ^{235}U and the production of ^{239}Pu and other fission products occur with burnup, capturing all the neutronic phenomena within the reactor core becomes more challenging for two-group diffusion solvers due to the homogenization of the core.

As a result, the axial deviations observed in the peripheral detectors become more apparent towards the EOC conditions compared to the deviations observed throughout

the entire cycle. Similarly, the discrepancies in the axial reflectors become more evident as the cycle progresses due to the leakage in the boundaries is larger with a two-group diffusion solver.

Nevertheless, the agreement between PARCS and TIPs remains reasonably good. This indicates that PARCS, despite the inherent complexities associated with depletion and production of nuclides, is able to provide accurate predictions of the axial power distribution within the core, maintaining a satisfactory level of agreement with the measured TIPs.

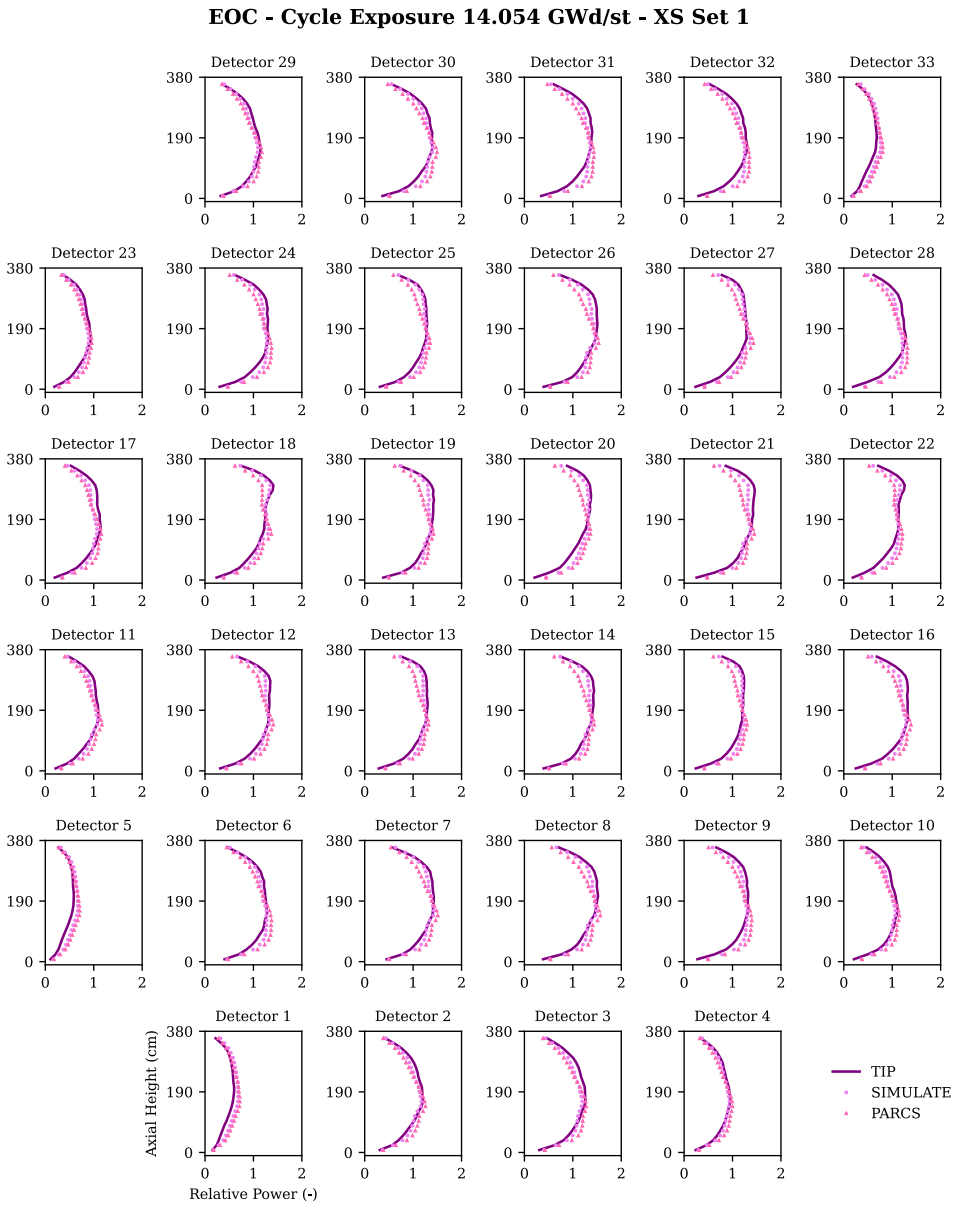

Figure 6.26. EOC - TIPs Data. Measured vs. Calculated. XS Set 1.

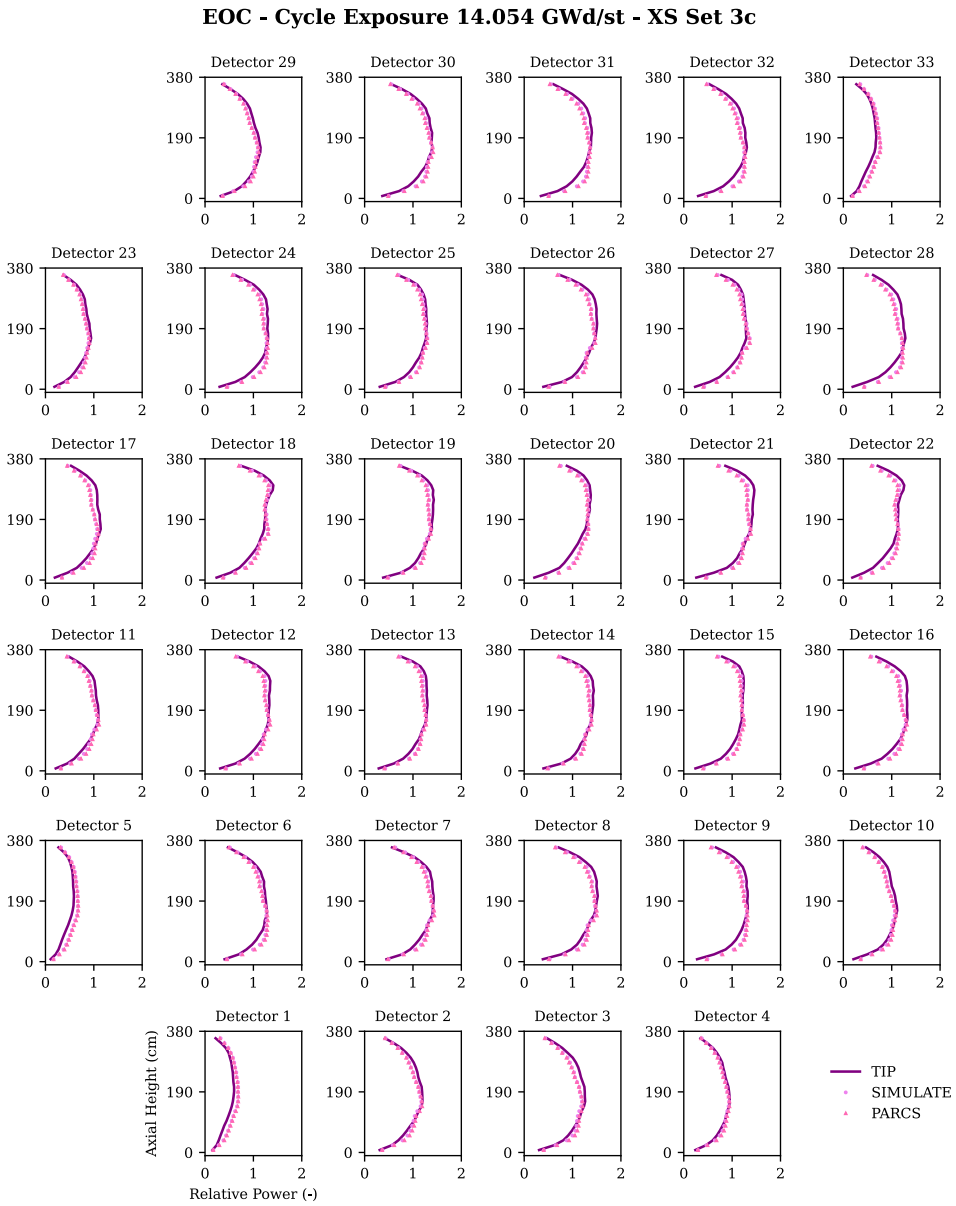

Figure 6.27. EOC - TIPs Data. Measured vs. Calculated. XS Set 3c.

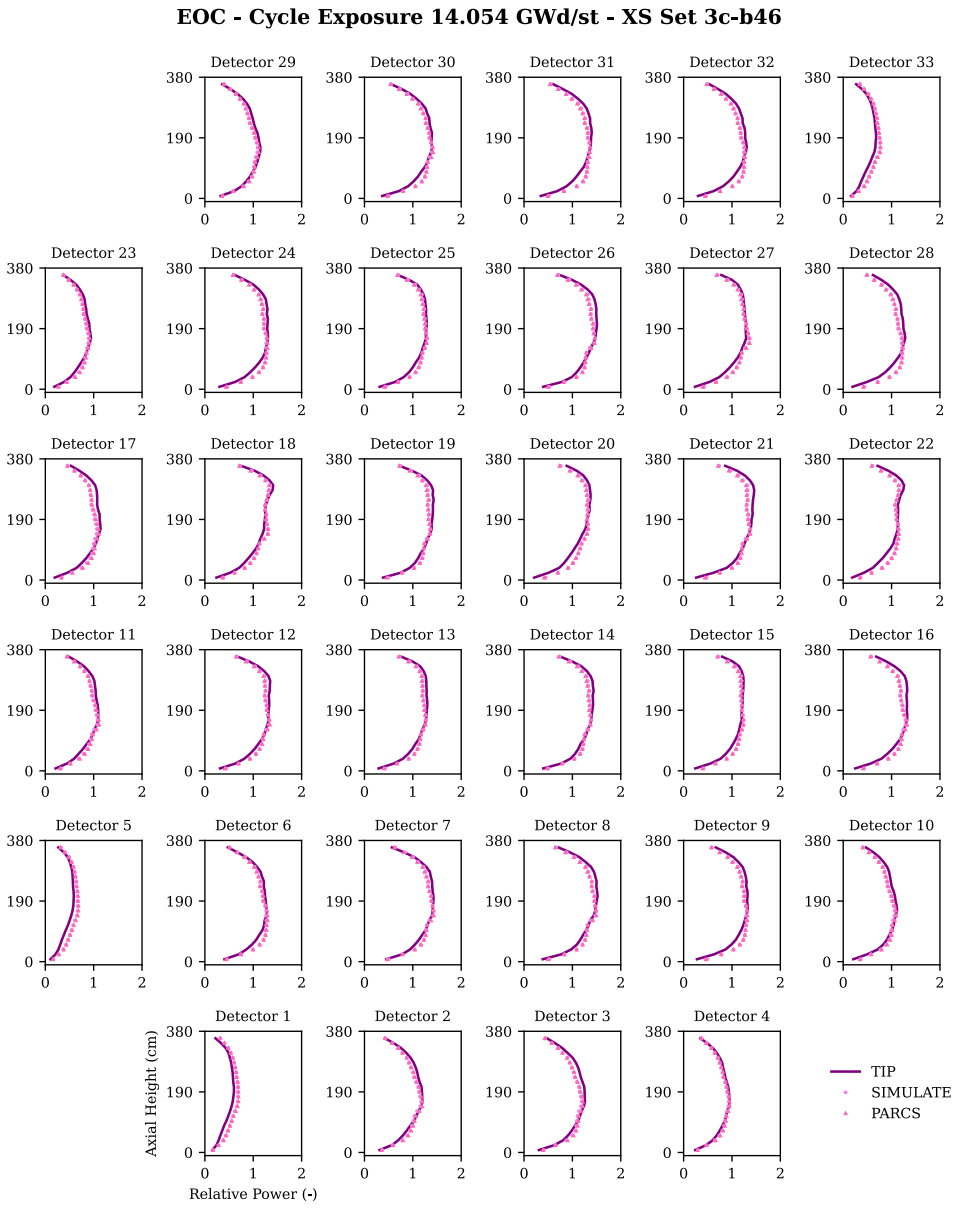

Figure 6.28. EOC - TIPs Data. Measured vs. Calculated. XS Set 3c-b46.

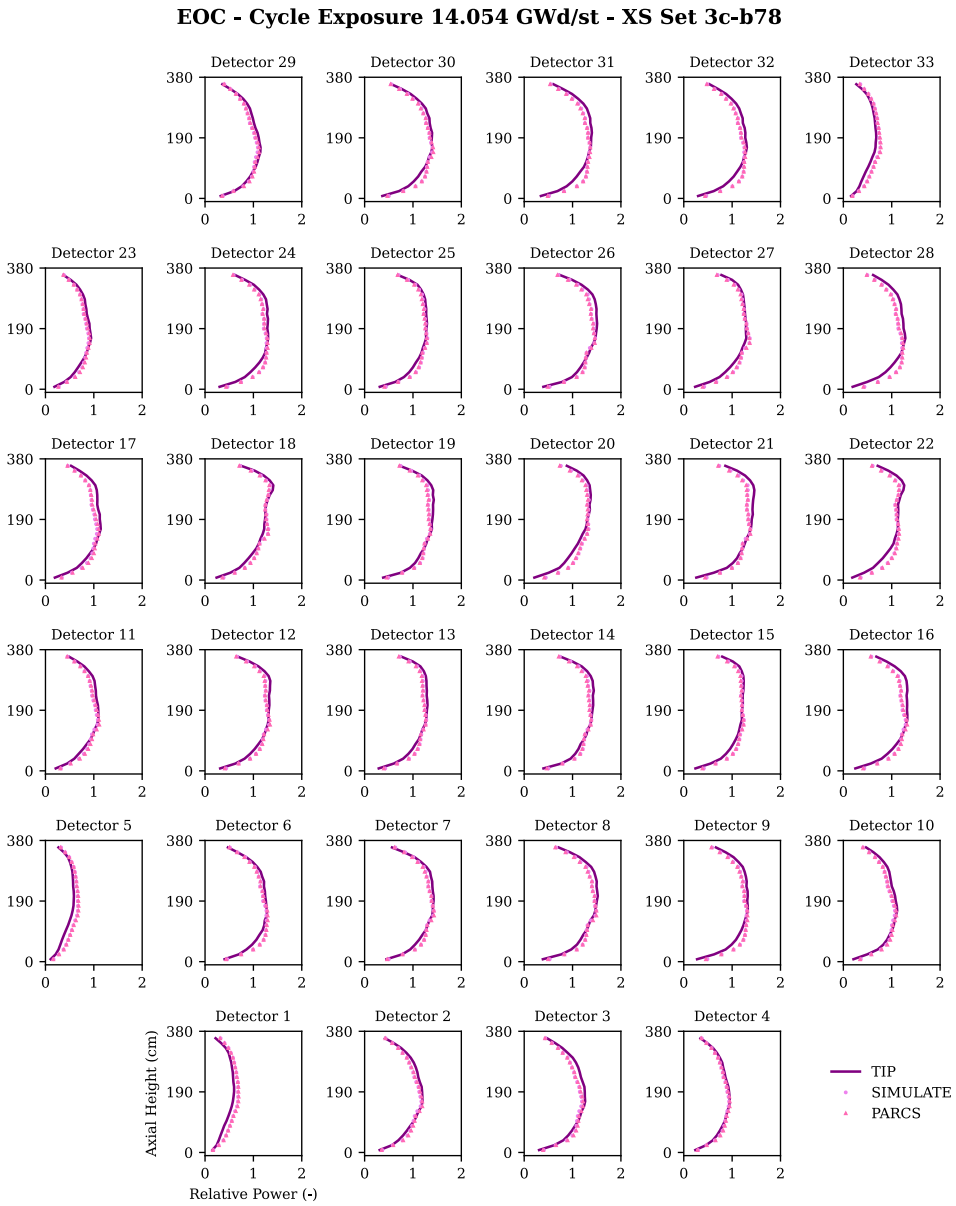

Figure 6.29. EOC - TIPs Data. Measured vs. Calculated. XS Set 3c-b78.

6.5 Summary & Conclusions.

Detector's responses estimated by PARCS have been rigorously assessed against measured Cycle B TIP data obtained from the plant. This process was carried out by utilizing the history files provided by SIMULATE-3, considering a range of plant operating conditions.

To gauge the effectiveness of the PARCS model, detailed comparisons of nodal and axial power levels at the TIPs' radial locations in the reactor between measured and calculated reaction rates were made for specific points. The aim was to thoroughly evaluate the accuracy of the PARCS model and its ability to predict power distributions within the reactor.

The findings of this analysis have been compiled and summarized in Table 6.5 and Table 6.6. These tables present a concise overview of the performance of the PARCS detector model and the different cross-section libraries under various scenarios.

Table 6.5. Summary of Nodal RMSEs (%) for All Calculated Detector Responses.

	SIMULATE-3	Set 1	Set 3c	Set 3c-b46	Set 3c-b78
BOC	4.831	7.946	5.114	5.580	5.517
MOC 1	3.969	7.196	4.290	4.461	4.455
MOC 2	4.541	7.047	4.527	4.465	4.455
MOC 3	4.132	7.196	4.469	3.947	3.947
MOC 4	4.845	8.699	4.102	4.519	4.547
EOC	4.89	11.987	6.46	5.513	5.431

Table 6.6. Summary of Axial RMSEs (%) for All Calculated Detector Responses.

	SIMULATE-3	Set 1	Set 3c	Set 3c-b46	Set 3c-b78
BOC	3.265	4.098	3.714	4.269	4.187
MOC 1	1.980	3.825	2.611	2.746	2.746
MOC 2	1.761	2.899	2.202	2.059	2.044
MOC 3	1.121	3.829	2.778	1.803	1.791
MOC 4	3.264	4.615	2.631	3.255	3.297
EOC	4.28	4.636	6.433	5.198	5.088

The comparison between the power distributions calculated by PARCS and the measured data from the plant yielded a high level of agreement throughout the entire cycle. Notably, the best performance was observed in the middle-of-cycle, while larger

discrepancies were found at the beginning and end-of-cycle. This trend is to be expected due to the dynamic changes in the core's behavior as burnup progresses.

In terms of power estimations, SIMULATE-3 consistently demonstrated the closest agreement with the TIP measurements, both in terms of nodal and axial power distribution. This aligns with expectations, as SIMULATE-3 is a well-established tool for reactor simulation.

The nodal and axial RMSEs consistently demonstrated high consistency across all nuclear data libraries. The predictions obtained from libraries Set 3c, b46, and b78 aligned with the conclusions drawn during the plant core follow computer benchmark, further validating their reliability. As anticipated, the Set 1 library produces the poorest power predictions overall, reaffirming the findings already presented in Chapter 5.

However, it is interesting to observe that the utilization of libraries with higher burnup points, such as libraries b46 and b78, did not lead to an improvement in power distribution estimations.

Despite these libraries behaving as expected in qualitative terms, the unexpected and counterintuitive outcome in terms of RMSEs suggested that there may be a limitation to the enhancements achievable, depending on the specific characteristics of the analyzed case. To gain a deeper understanding of this phenomenon, further investigations will be necessary in order to provide conclusive evidence.

The comparison of the calculated power distributions by PARCS with the measured data revealed significant differences near the locations of inserted control rods, regardless of the cross-section libraries used in the study. These discrepancies indicate potential inaccuracies in the control rod model employed by PARCS, particularly when multiple control rod definitions are utilized. This finding highlights the need for further investigation and improvement in the representation of the instantaneous and history cross-section values for multiple control rod compositions within PARCS.

Additionally, the omission of considering the variation of cross-sections and neutron kinetic parameters in the reflector region due to the instantaneous moderator density was evident in the larger discrepancy observed near the top and bottom of the active core. This suggests that the current approximation used by PARCS in this aspect may lead to inaccuracies in predicting the axial leakage of neutrons through the reflector region. These results confirmed the findings already documented in previous studies.

Lastly, slight deviations were observed in the peripheral detectors, where PARCS generally yields higher overall channel power levels compared to the TIP data throughout the whole cycle. This discrepancy becomes more apparent at EOC conditions.

For a more comprehensive and visually engaging representation of the results, Figure 6.30 has also been included, allowing for a clearer understanding of the comparison between actual measurements and calculated values.

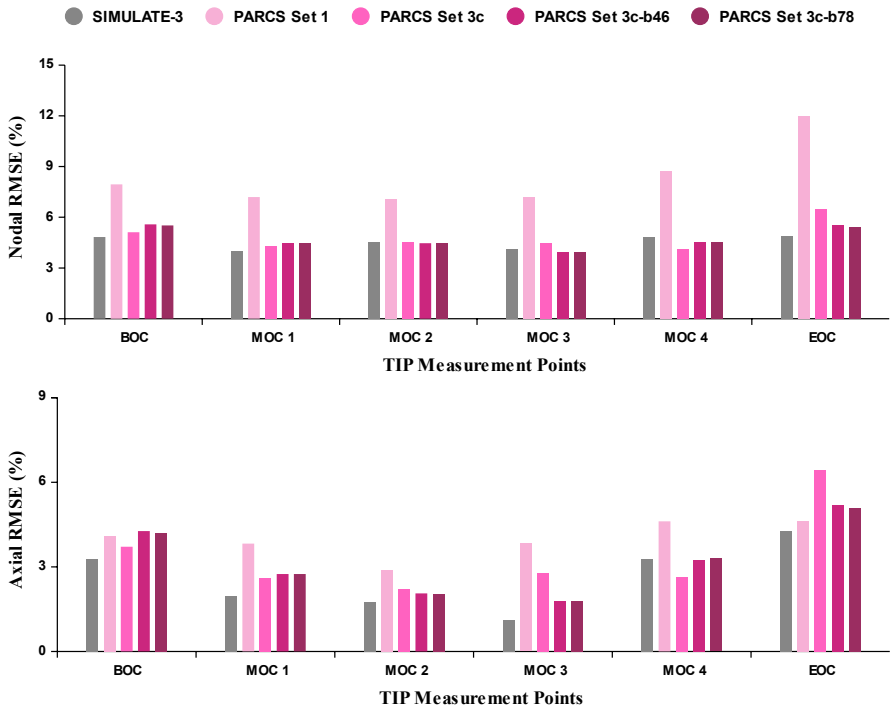

Figure 6.30. Summary of Nodal & Axial RMSEs (%) for All Calculated TIP Responses.

Examining the nodal average value of the relative differences between PARCS and the measured relative power fraction, it is reassuring to note the absence of any significant bias. In fact, the minimum and maximum values of the relative differences computed over all the nodes in which the core was discretized underlined that the PARCS calculations were completely satisfactory.

The accuracy of the comparison between PARCS calculations and TIP measurements is slightly compromised towards the end-of-cycle. This could be attributed to the axial power peaking at the top of the bundle and the limitations of part-length rods on the bundled-power averaging approximation, which does not account for self-shielding effects caused by missing rods. Also, due to the spectrum hardening, capturing all the neutronic phenomena within the reactor core becomes more challenging.

A summary of the rejected points due to discrepancies higher than 10% is shown in Figure 6.31.

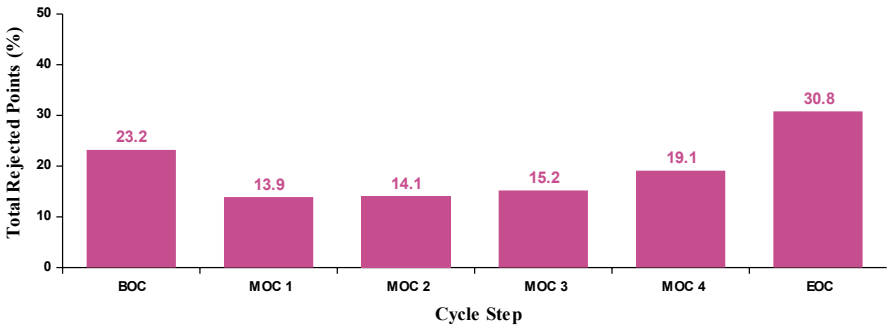

Figure 6.31. Number of Points Rejected for each calculated TIP Measurement Point.

It is important to note that the TIPs were modeled using the PARCS built-in detector model, which calculates the average thermal power of the surrounding bundles. However, it should be acknowledged that TIPs are gamma detectors in the BWR/6 reactor model, and this simple approximation may result in slight deviations.

To achieve a more accurate representation of TIP responses, a gamma transport model that considers the pin geometry at the detector corner would be necessary. Nonetheless, the results indicate that the bundle power average provides a reasonably good comparison for most of the cycle.

Furthermore, it is crucial to understand that discrepancies observed with a specific nuclear data library during a particular case do not automatically imply poor accuracy or the need to discard the entire library. Differences between detectors and calculated values are often attributed to variations in detector response modeling, which depletion models might not capture accurately, rather than inaccuracies in bundle power calculations.

Overall, considering the approximations involved, the results of PARCS calculations demonstrate a level of accuracy comparable to SIMULATE-3 calculations. Excellent agreement is achieved between the measured TIP data and the power distributions calculated by PARCS for all selected points throughout Cycle B.

Chapter 7
Cross-section Impact on DEC-A ATWS Analysis

7.1 Introduction.

During an Anticipated Transient Without Scram (ATWS) event, reactor system conditions undergo significant changes, leading to substantial alterations in core power and flow conditions. Typically, overpressurization transients, such as Main Steam Isolation Valve Closure (MSIVC), are limiting transients concerning peak vessel pressure and thermal-hydraulic performance.

In an MSIVC ATWS event, core responses are influenced by the interplay between void reactivity feedback, driven by void collapse, and negative Doppler reactivity feedback, reference (Hsiang-Shou, C. & Diamond, D. J., 1978). Consequently, the severity of the transient depends on both system behavior and the accuracy of cross-section libraries in predicting nuclear parameters.

Given these considerations, the MSIVC ATWS serves as an excellent transient scenario:

1) to assess the efficacy of cross-section libraries in predicting the evolution of critical parameters under demanding transient scenarios,

2) to enhance the capability of modeling such events using the TRAC-BF1/PARCS coupled code, with a focus on adequately covering the expected range of independent variables, and
3) to simulate complex thermal-hydraulic and feedback phenomena over an extended duration, enabling comprehensive understanding of critical component responses and, particularly, core behavior.

All ATWS simulations discussed in this chapter utilize the TRAC-BF1/PARCS coupled code system in the time domain, adhering to the cross-section modeling guidelines established in Chapter 5.

7.2 Description of the Simulated ATWS Scenarios.

ATWS-type sequences are anticipated operational events (defined as likely to happen at least once during the life of the facility) in which there is a total or partial failure of the Reactor Protection System (RPS) so that the rapid insertion of the control rods either does not occur or only partially occurs.

An MSIVC ATWS event has traditionally been considered one of the sequences that determines the most severe conditions in containment, i.e., suppression pool temperature and pressure, as all the steam generated in the reactor since the start of the event is discharged into the suppression pool. Likewise, it can also determine the highest initial peak of the vessel's neutron flux, calorific flux, and pressure.

As first order approximation, a critical core requires that the average void fraction remain constant; thus, the power required to maintain criticality is a function of recirculation flow. With higher flows, the same average void fraction results in increased steam mass leaving the core, which requires higher thermal power.

The large amount of steam produced in the core can only be relieved through safety relief valves to the containment wet well. As a consequence, the wet well suppression pool temperature increases, and the containment may eventually be heated and pressurized.

A safety concern associated with ATWS sequences is the incidence of re-criticality and return to power. Re-criticality may occur due to two identified mechanisms: (1) re-pressurization of the reactor (i.e., collapsing voids) or (2) boron dilution due to unborated water injection to maintain the water level.

The main strategy in the Emergency Procedure Guidelines (EPGs) actions for ATWS conditions is to reduce the supply of coolant to the vessel in order to lower the downcomer water level, which in turn reduces the recirculation flow and limits the energy produced by the system. Under most conditions, this strategy minimizes the total energy transferred to the containment wet well via safety relief valves and maintains containment pressure within acceptable limits.

The Emergency Procedure Guidelines (EPGs) are developed by the US BWR Owner's Group and then tailored to meet the specific requirements of each BWR plant

(Harter, R. & González-Cuesta, M., 2017). They are symptom based and do not require the operators to diagnose the root cause of the failure. For example, if a scram has been initiated but the power is still elevated, the operator does not to have to immediately identify the reason the rods didn't go in. Instead, the EPGs instruct the operator to inject boron to provide alternative means to reduce power. As such, the EPGs are not designed to provide optimal operational actions in all scenarios, but to maximize the probability that operators will maintain safety goals without introducing additional failures by performing incorrect actions.

In summary, EPGs offer comprehensive but straightforward technical directions for managing BWR nuclear power plants during emergency conditions. Structurally, the EPGs consist of four primary guideline branches and six associated contingencies. This framework ensures thorough and effective responses to a wide range of emergency situations, aligning with best practices for nuclear plant safety and operations.

In the context of an ATWS event, entry to the EPGs is generally through the Reactor Control guideline branch, which is initiated when the operator recognizes that the reactor power remains high after the scram demand. Once the branch is "entered," the EPGs define a generic set of operator actions for bringing the reactor to safe shutdown conditions.

Regarding the operator actions, our study assumes them to be consistent with the EPGs extensive training on plant simulators and periodic qualification testing ensures this assumption is very likely to be accurate. According to NUREG-0899, (Nuclear Regulatory Commission., 1982), Emergency Operating Procedures (EOPs) are plant procedures that direct operators' actions necessary to mitigate the consequences of transients and accidents that have caused plant parameters to exceed reactor protection system set points or engineered safety feature set points, or other established limits. EOPs are the plant-specific implementation of the generic EPGs.

Current EOPs require emergency depressurization before the heat capacity of the containment wet well suppression pool is exhausted, reference (Cheng, L. et al., 2013a). However, the manual activation of emergency depressurization raises several concerns, including:

1) the reactor undergoes a beyond-design basis event, and fuel damage may occur,
2) the pressure suppression capacity of the containment is exhausted, and
3) the reactor coolant pressure boundary is bypassed by manually opening the Automatic Depressurization System (ADS) valves.

Under these conditions, two of the three primary fission product barriers, i.e., the fuel and the primary system, might have been compromised, as stated in (Yarsky, P., 2011). Additionally, the local temperatures and pressures influence the fuel and core structures. Thus, the operating conditions must have certain margins to the imminent phenomena associated with the behavior of fuel and core materials (Silvennoinen, P., 1976). The rationale provided in the EPGs for this emergency depressurization is that while the depressurization occurs, the reactor power is essentially shutdown by

flashing (void creation). When the pressure equilibrates at a very low level, the power is significantly lower than at full pressure (because of the change in steam density). Thus, the integrated heat load to containment is reduced.

Two different postulated ATWS scenarios, initiated by the closure of the MSIVs with the reactor operating in the Maximum Extended Load Line Limit (MELLL) expanded operating domain, are simulated in this work to exercise more thoroughly the thermal hydraulics, core physics, and the impact of cross section libraries. These scenarios are almost certain to occur over a plant's lifetime, making it crucial to understand how the plant will behave and perform under such conditions.

The first scenario, **Scenario 1**, is a postulated ATWS that leads to an Emergency Depressurization (ED), as standard EOP indicates. In contrast, the second scenario, **Scenario 2**, is a postulated ATWS giving credit to High-Pressure Core Spray (HPCS) injection without ED activation to analyze the impact on the core response of the unborated subcooled water injection.

Both sequences, which share the same initiating event, include several manual operator actions, such as water level control or injection of boron via the Stand-by Liquid Control System (SLCS).

Event Tree (ET) headers for each simulated scenario are arranged following the expected actuation order of the corresponding safety systems depending on the postulated EPGs and the assumed EOPs.

7.2.1 ATWS Scenario 1.

In this scenario, an emergency depressurization will occur following the standard EOPs before the available pressure suppression capacity of the containment wet well is exhausted. Emergency depressurization is referred to the manual actuation of the ADS.

In generating the EOPs, each licensee evaluates how much heat capacity is required in the suppression pool to absorb all the steam energy that would be deposited during an emergency depressurization. This is known as the Heat Capacity Temperature Limit (HCTL). The EOPs then require the operator to initiate ADS if the HCTL temperature is reached; thus, guaranteeing that ADS will not increase the containment pressure from excess steam that cannot be condensed in the suppression pool.

The expected actions carried out by the operator under the premises of Scenario 1 are defined in EOPs and can be summarized as follows:

1) ADS & Feedwater runback logic inhibitions.
2) Water injection to the vessel is inhibited except for those from SLCS, Control Rod Drive System (CRDS), and Reactor Core Isolation Cooling System (RCIC).
3) Water level reduction. According to the EPGs, the water level is intended to be kept above the Minimum Steam Cooling Water Level (MSCWL). Above the MSCWL, enough steam is generated in the core and flows at sufficient speed through the upper, uncovered part of the fuel to maintain

it at a safe temperature (typically the 1477.6 K (2200 ºF) rapid oxidation limit). The MSCWL is calculated on a cycle specific basis and incorporated in the plant-specific EOPs.

4) Boron injection. Boron is manually injected when the suppression pool temperature reaches 316.5 K (110 ºF), or the operator determines that reaching it cannot be avoided with the current accident configuration. This 316.48 K limit is enforced to prevent boron injection actuation when it is not required by the scenario.
5) Emergency depressurization. According to EOP, it will be triggered whether:
   - The water level decreases below the minimum water level for steam cooling, or
   - Suppression pool temperature and vessel pressure exceed the HCTL.
6) Water injection to the vessel. Water injection with preferent systems is slowly performed through the feedwater line after Minimum Steam Cooling Pressure (MSCP) is reached.
7) Recovery of water level to the normal level.

According to NUREG-CR7181 (Cheng, L. et al., 2014a), for ATWS calculations, operator actions are assumed to be consistent with the existing EPGs and are taken as conditions warrant reducing reactor power without producing any core damage.

Figure 7.1 illustrates the ATWS event tree following the expected actuation order of the safety systems implemented for simulated Scenario 1. In consonance with Figure 7.1, the prescribed operator actions drive the ATWS event to *Sequence Number 1*. The actions are designed to cope successfully with the event by preventing core damage. The event tree headers are listed in Table 7.1.

Table 7.1. Event Tree Headers for Scenario 1.

Header	Description	Action	Main Function
ATWS	**MSIVC**	**--**	**Initial Event**
RPT	Recirculation Pump Trip	Auto	Reactivity Control
SRV	Safety Relief Valves	Auto	Pressure Control
CSRV	Close SRV	Auto	Pressure Control
INH	Inhibit (ADS + HPCS)	Manual	Reactivity Control
SLC	Stand-by Liquid Control	Manual	Reactivity Control
M-DEP	Manual Depressurization	Manual	Inventory Make-up
CBP + Control	Condenser + Booster Pumps + Level Control	Manual	Inventory Make-up
Low-Pressure Systems	LPCS or LPCI + Level Control	Manual	Inventory Make-up

By the nature of the sequence of events, it is expected that, in Scenario 1, the emergency depressurization will provoke a significant decrease in vessel pressure, which will lead to an abrupt change to the moderator temperature (because of the change in saturation temperature). The reduction in pressure will result in flashing (conversion from liquid to steam), generating a large core-average void fraction that will make the core subcritical.

As discussed in Chapter 5, drastic moderator temperature variations along with high voids may not be accurately modeled by PARCS with the designed cross-section libraries, so all predictions following automatic depressurization can be called into question if the proper moderator temperature branches are not used.

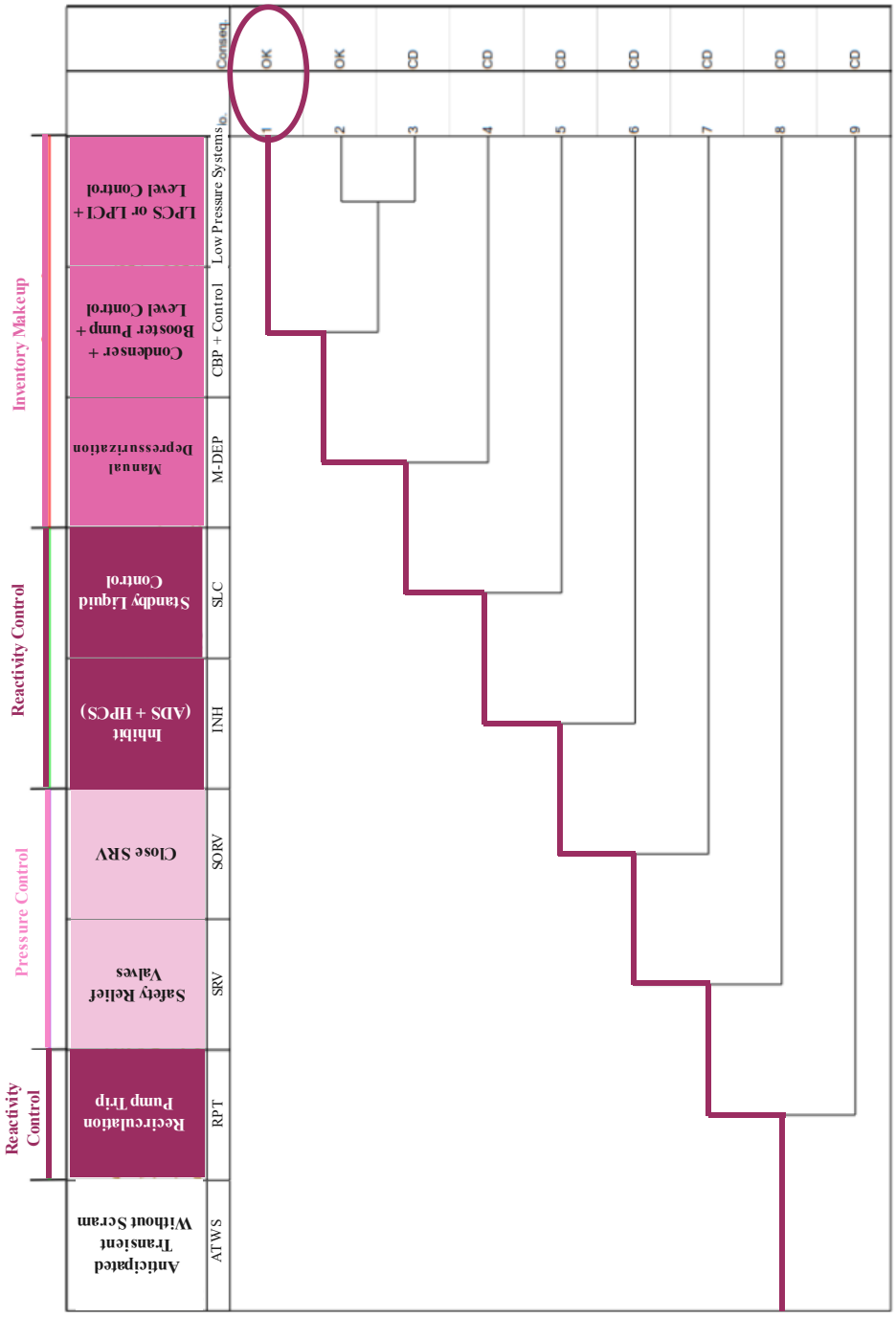

Figure 7.1. Simulated Event Tree for Scenario 1.

7.2.2 ATWS Scenario 2.

In contrast to the EOP guidance of Scenario 1, Scenario 2 entails the introduction of make-up inventory via the High-Pressure Core Spray (HPCS).

Scenario 2's simulation involves emulating some of the actions outlined in the Advanced Boiling Water Reactor (ABWR) guidance for ATWS conditions, as detailed in (Yarsky, P., 2013). This diverges from the current EPGs for BWRs, which instruct operators to deactivate the HPCS injection during ATWS and manually trigger emergency depressurization.

In essence, the actions simulated by the operator under Scenario 2's conditions mirror those of Scenario 1 with the exception of substituting ED activation with HPCS injection. The HPCS constitutes a crucial part of the plant's engineering safeguards, serving to provide core cooling and avoid potential fuel cladding damage. Its activation relies on manual intervention by the operator upon sensing a low-level indication (Level 2). The injected flow by the HPCS system is function of core pressure, decreasing as core pressure rises and vice versa.

Figure 7.2 illustrates the ATWS event tree following the expected actuation order of the safety systems implemented for simulated Scenario 2. According to Figure 7.2, the prescribed operator actions drive the ATWS event to *Sequence Number 1*. The actions are designed to cope successfully with the event by preventing core damage. The event tree headers are listed in Table 7.2.

Table 7.2. Event Tree Headers for Scenario 2.

Header	Description	Action	Main Function
ATWS	**MSIVC**	**--**	**Initial Event**
RPT	Recirculation Pump Trip	Auto	Reactivity Control
SRV	Safety Relief Valves	Auto	Pressure Control
SCRV	Close SRV	Auto	Pressure Control
INH	Inhibit (ADS + HPCS)	Manual	Reactivity Control
SLC	Standby Liquid Control	Manual	Reactivity Control
HPCS	High-Pressure Control System	Manual	Inventory Make-up
M-DEP	Manual Depressurization	Manual	Inventory Make-up
Low-Pressure Systems	LPCS or LPCI + Level Control	Manual	Inventory Make-up

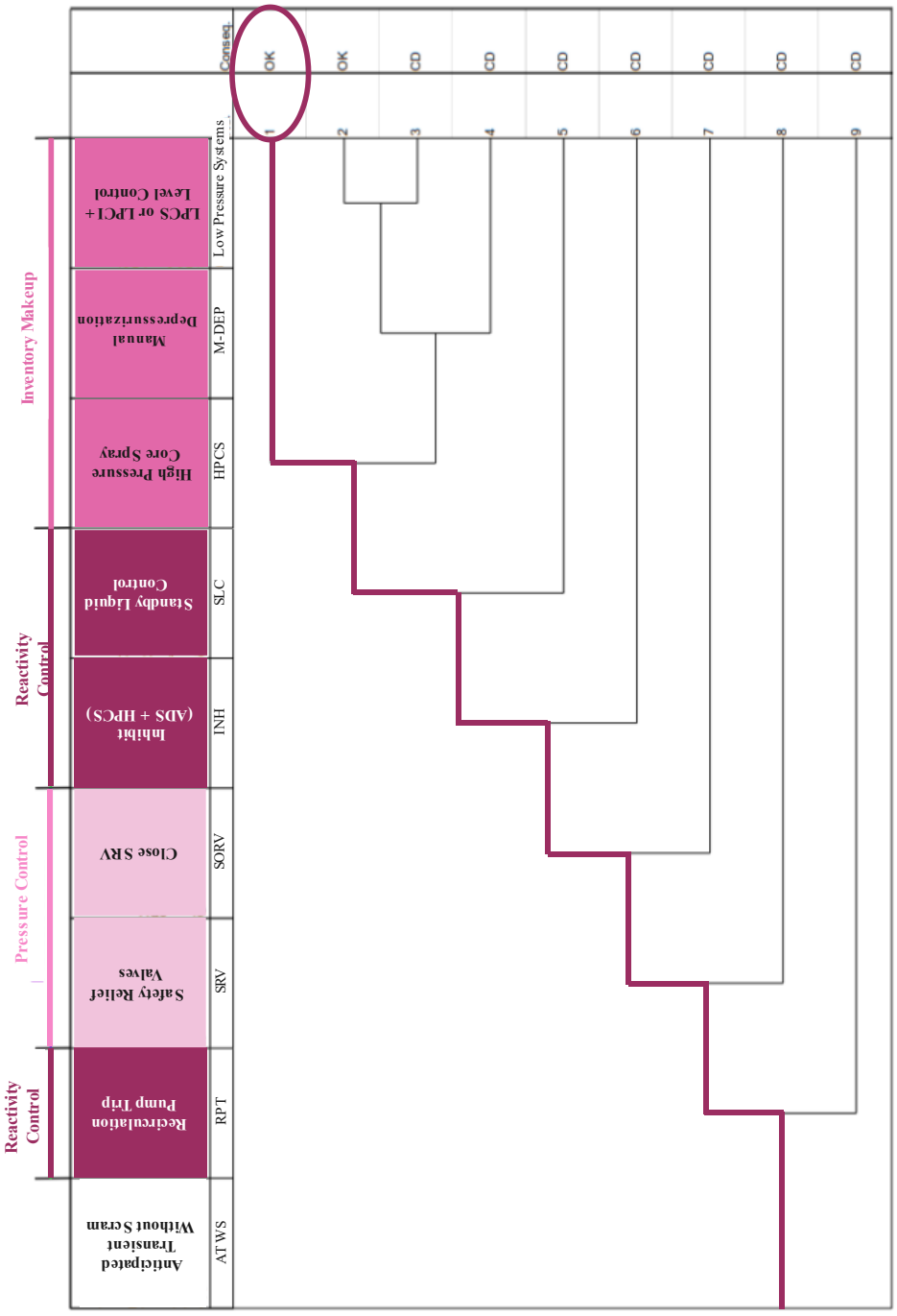

Figure 7.2. Simulated Event Tree for Scenario 2.

In Scenario 2, the vessel pressure variation is not expected to decrease significantly, leading to a saturation temperature change of up to 50 K. Consequently, the variation in moderator temperature falls within an acceptable extrapolation range from the moderator temperature branches covered by the cross-section library. This observation suggests that coupled codes, along with the conventional cross-section branching schemes, are likely to provide reliable predictions of core behavior and the evolution of key system parameters throughout the transient under consideration.

7.2.3 Figures-of-Merit.

The relevant Figures-of-Merit (FoM) for forecasting the severity of the consequences of an ATWS event are described in NUREG-CR7181 (Cheng, L. et al., 2014a), and include:

- Peak Cladding Temperature (PCT) as a surrogate of fuel damage.
- Suppression Pool Temperature (SPT).
- Reactor vessel & containment pressures.
- Recriticalities if shown.

Limits for these parameters are reported in the Standard Review Plan NUREG-0800, Chapter 15, Section 15.8 (US NRC, 2007): Anticipated Transients Without Scram, with the goal of maintaining core coolability. Table 7.3 shows the acceptable limits.

Table 7.3. ATWS Acceptance Limit Criteria.

Acceptance Criteria		
Max. Vessel Pressure	10.45 MPa	1500 psia
Containment Pressure	0.205 MPa	29.7 psia
Suppression Pool Temperature	358 K	185ºF
Peak Cladding Temperature	1478 K	2200ºF

7.3 Model Features.

The implementation of higher burnup, extended cycles, and novel fuel assembly designs in LWRs has introduced distinct safety analysis requirements. To address these needs effectively, precise 3D coupled neutronics/thermal-hydraulic calculations are imperative, as discussed in (Ivanov, K. & Avramova, M., 2007).

Thermal-hydraulic system codes such as TRAC-BF1, TRACE, or RELAP5 are capable of modeling a broad spectrum of systems and phenomena. Typically, system components such as pipes, valves, or channels are represented in 1D, while the vessel and/or the core are modeled in 3D.

Each transient scenario follows a specific sequence of events, encompassing diverse phenomena as the plant undergoes temporal evolution. During simulation, the thermal-hydraulic system code employs various time-varying models and correlations tailored to the progression of the transient.

In this study, the TRAC-BF1 and PARCS coupled systems are employed to analyze the two predefined postulated ATWS scenarios. Given the criticality of the coupled solution, it is imperative that the core kinetics model accurately captures the feedback between evolving moderator conditions and core power generation.

Based on previous studies, the TRAC-BF1 and PARCS models, along with the cross-section library, are sufficiently robust for predicting parameters such as reactor pressure vessel evolution, reactor core response, and core kinetics parameters, among others.

7.3.1 TRAC-BF1/BE Model.

The developed TRAC-BF1 model incorporates features that facilitate the simulation of ATWS events in a BWR/6 housed in a Mark III containment.

The reactor is represented by a 3D vessel with two radial rings, 11 axial levels, and one azimuthal segment. The core and the steam separators are located in the innermost ring (ring 1), while the downcomer is in the outermost ring (ring 2). The core comprises parallel channels with a common pressure boundary condition and without significant cross-flow among the channels.

Because of the large number of fuel assemblies (usually around 700), BWR cores require significant computational resources to fulfill the detailed coupled thermal-hydraulic and neutronics modeling (Ivanov, K. & Avramova, M., 2007). Depending on the code capabilities, BWR core models use channel grouping techniques to reduce the model's size by allowing a single channel component to represent several channels in the reactor core while keeping the detailed neutronics modeling.

One of the known constraints of TRAC-BF1 is its inability to model the entire core channel-by-channel; therefore, a collapsing grouping technique was performed. Determining the optimal number of thermal-hydraulic channels to represent the whole core is crucial for a proper simulation while balancing accuracy and computational cost.

Typically, the core representation is done by collapsing the channels into a sufficiently representative number of "grouped channels" so that the thermal-hydraulics of the system is well reproduced. In TRAC-BF1, these channel groups are modeled using CHAN components which represent the BWR fuel bundle model as described in the code user's manual (Borkowski, J. et al., 1992).

According to reference (Cheng, L. et al., 2014b), the grouping in an EPU core, where the reload fractions are high to achieve a radial power shape as flat as achievable, could be done based on geometrical and fuel cycle considerations because position-based grouping is similar to power grouping.

Nonetheless, for this specific analysis, the channel grouping has been performed under geometrical, position-based, and power-based conditions where no channel group represents more than 20% of the total power. In addition, for each mechanical fuel type, the bundle closest to its thermal limits is modeled independently as a hot channel.

As a result, in our model, 15 CHAN components model the 624 physical fuel assemblies for the core model. Modeling a core with 15 channels is sufficient for a general ATWS event because the core response is expected to be reasonably uniform, allowing a coarser TRAC-BF1 representation. However, a finer thermal-hydraulic-wise core collapsing model would be required when modeling instability events during ATWS, as outlined in (Baek, J. et al., 2013a; Cheng, L. et al., 2016).

Each CHAN component contains 25 axial nodes (15.24 cm in height each) for modeling the corresponding active core.

The TRAC-BF1 plant model also includes the following:

- Two independent recirculation loops.
- The Feedwater system.
- ECCS systems.
- Reactor Core Isolation Cooling (RCIC) system.
- Stand-by Liquid Control system (SLCS). Boron injection in upper plenum.
- Steam line (4 steam lines collapsed), including:
    - Five Safety/Relief Valves lines,
    - Turbine, and
    - Turbine bypass of 35% of nominal power.
- Automatic Depressurization System (ADS).
- Mark III Containment.
- Control systems including signal variables, control blocks, and trips.

The Mark III containment consists of a drywell and a wetwell (suppression pool) and relies on the principle of pressure suppression for accidents. The containment is designed to condense steam in the pool, to contain fission products released from accidents, and to provide a heat sink and water source for particular safety-related equipment.

The containment model is connected to the vessel, and the steam generated in the reactor is discharged into the suppression pool through the safety/relief valves without loss of fidelity.

Safety/Relief Valves (SRVs) are dual-function valves discharging directly to the suppression pool. The safety function includes protection against the overpressure of the primary reactor system. The relief function provides power-actuated valve opening to relieve steam during transients resulting in high system pressure or during postulated accident conditions to depressurize the primary reactor system.

The TRAC-BF1 model control system attempts to model the control system in the plant, with every plant component represented with real settings. It also includes control log actions to be initiated whether several trips are activated to mitigate the ATWS events, such as boron injection through the SLCS, water level control, and water injection through HPCS or condensate and booster pumps.

A three-element feedwater controller is modeled to maintain the reactor water level at a desired level setpoint based on the following controller inputs: feedwater flow, steam flow, and reactor water level. Adjusting the reactor water level input to the controller allows the simulation of operator actions to control the level according to different strategies.

Finally, the main characteristics for modeling the water injection initiation systems and their characteristics, e.g., shut-off pressure pumps and maximum injection flow rates, are summarized in Table 7.4.

Table 7.4 Shut-off Pressure Pumps & Maximum Injection Flow Rates of the Preferent Systems.

System	Pressure (kg/cm^2)	Pressure (MPa)	Mass Flow (kg/s)
HPCS	100	9.807	345
LPCS	30	2.942	434
LPCI	20	1.961	349
CB & CBP	50	4.903	612
RCIC	90	8.826	38
SLC	80	7.845	5

By design, the boron injection system (SLCS) is equipped with a relatively small capacity (~ 5 kg/s corresponding to 86 gpm), which requires several minutes to achieve subcritical boron concentration in the core. Consequently, a system with a larger capacity, such as CP & CBP or HPCS, would be required to offset heat generation adequately before the core remains uncovered for an extended period on ATWS scenarios, as outlined in NUREG-0460 (NRC, 1978).

7.3.2 PARCS Model.

The neutronic part of the core model was developed for the neutronics code PARCS. Overall, the PARCS model is expected to follow similar model guidelines to those described in Section 5.3 from Chapter 5.

The corresponding fuel bundle core loading pattern in Figure 7.3 contains 624 fuel assemblies with a one-to-one correspondence between radial neutronic nodes and fuel assemblies.

Those assemblies are of three different fuel types corresponding to 33 different lattice segments depending on the following:

- Enrichment (pin enrichments from 2.6% to 4.9%).
- 10 x 10 pins per bundle designs.
- Multiple-length part-length rods.
- Gadolinium content – axially non-uniform.

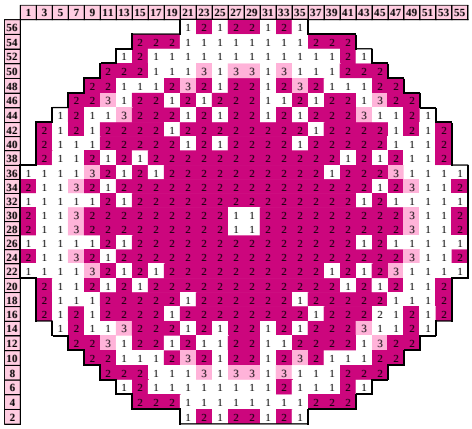

Figure 7.3. Simulated Case - Core Fuel Loading Pattern.

The model includes multiple planar regions with unique materials, representing several distinct axial segments in the active fuel region and accounting for the asymmetry of the gadolinium content. 25 axial neutronic nodes represent each fuel bundle.

The core nodalization provides a detailed representation of both radial and axial reflectors, each configured with a width of 30.48 cm. Radial reflector cross-sections have been incorporated, featuring the same 8 orientations - N, E, W, S, NE, NW, SW, and SE - as discussed in the methodology outlined in Chapter 5 for generating cross-section libraries.

The nuclear model needs to be coupled to the thermal-hydraulic model. The mapping scheme defines the correspondence between the neutronic nodes and the hydraulic volumes/heat structures (Cuadra, A. et al., 2013).

Developing appropriate nodalization and mapping schemes between thermal-hydraulics and neutronics models is challenging because one spatial coupling might be suitable for a specific transient but fails to capture essential physics for another transient (Ivanov, K. & Avramova, M., 2007). Usually, the coupling is done through the same radial and axial nodalization because the exact detailed mapping provides better spatial resolution in coupled calculations.

Each bundle is mapped to a characteristic hydraulic channel, from which vapor fraction distributions and fuel temperatures are taken as input to the neutronics calculation. Power feedback to the thermal-hydraulics uses the average power distribution from all neutronic channels mapped to a given thermal-hydraulic channel.

The mapping scheme between PARCS and the 15 TRAC-BF1 channels is delineated through an external file, called *Maptab*, illustrated schematically in Figure 7.4.

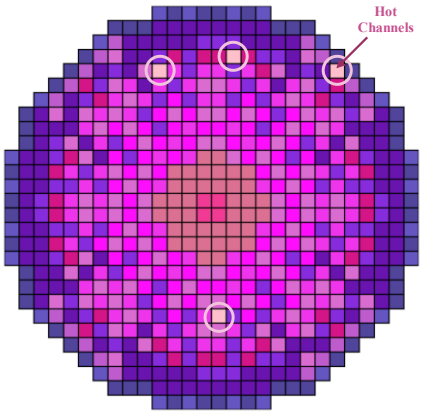

Figure 7.4. TRAC-BF1/PARCS Mapping Scheme Designed for the Simulated ATWS Case.

As illustrated in Figure 7.4, the bundles exhibiting the Maximum Average Planar Linear Heat Generation Rate (MAPLHGR) for each of the four distinct mechanical types incorporated into the core have been individually modeled as hot channels. The MAPLHGR, together with the Maximum Linear Heat Generation Rate (MLHGR), provides a comprehensive characterization of the thermo-mechanical behavior of the fuel rods.

Additionally, this mapping file includes fixed properties associated with the radial reflectors, which are not mapped into any thermal-hydraulic volume, as detailed by (Cuadra, A. et al., 2013).

The internal coupling approach between TRAC-BF1 and PARCS, as depicted in Figure 7.5, has been implemented. In this approach, the TRAC-BF1 model encompasses the entire BWR system, including the core. Consequently, core power distributions are calculated by PARCS, utilizing thermal-hydraulic feedback from TRAC-BF1, which is typical in such coupled calculations (Perin & Escalante, 2017).

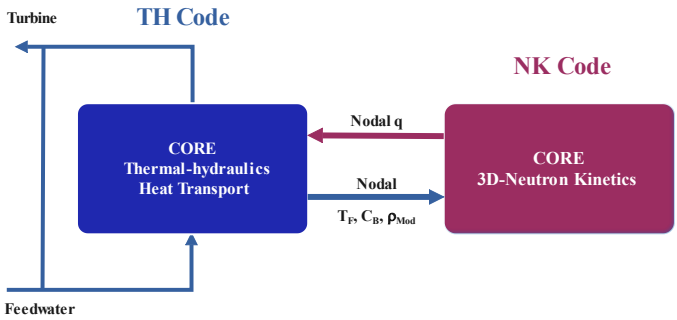

Source: (Perin & Escalante, 2017).

Figure 7.5. Internal Thermal-hydraulic/Neutron Kinetics Coupling Approach.

An accurate analysis of transients with a strong neutron flux distribution dependence requires calculations based on 3D kinetic models, which implies a particular cross- section set. Changes in the core kinetics reactivity parameters strongly influence the core response, so the cross-sections must be accurately calculated.

Figure 7.6 illustrates the moderator density and the fuel temperature histograms for the initial state right before the simulated ATWS transient.

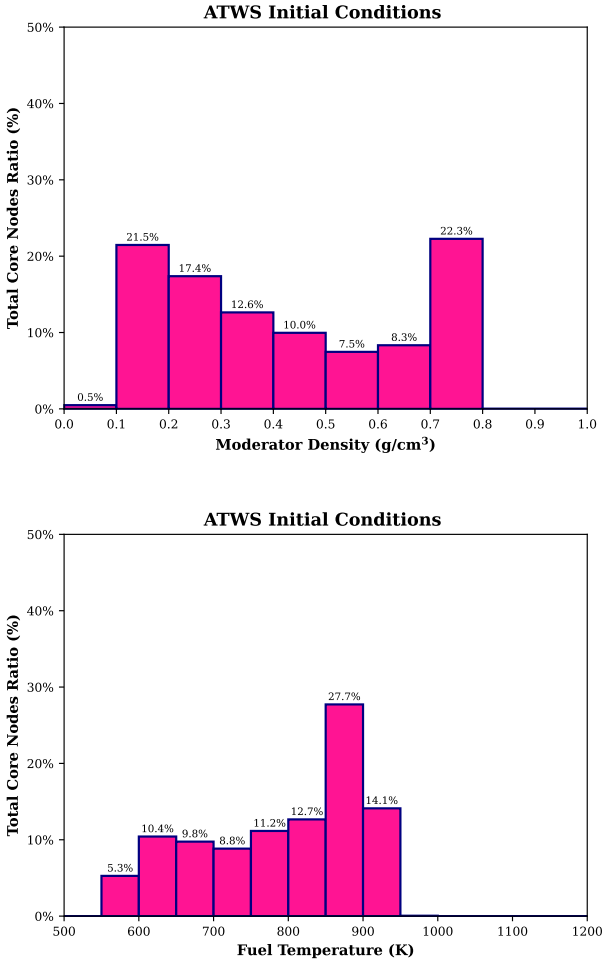

Figure 7.6. Instantaneous Moderator Density (top) and Fuel Temperature (bottom) Distributions.

The nodal moderator density distribution through the core is consistent with the void distributions and burnup at EOC conditions. Thus, the cross-section library must include different moderator density and fuel temperature conditions to cover the expected range of both steady-state and transient conditions.

The state variable range for the branch calculations is shown in Table 7.5.

Table 7.5. Range of State Variables for the ATWS Cross-section Libraries.

Variable	Range of Variation	Units
Fuel Temperature (T_f)	562-1500	K
Moderator Temperature (T_m)	293-562	K
Moderator Density (ρ)	107-999	kg/m^3
Boron Concentration (C_b)	0-5000	ppm
Control Rods (CR)	In/Out	--

The cross-section library created for these transients, labeled as **Set Atws**, has been developed based on the library Set 3c-b46 described in Chapter 5. The two-group bundle homogenized cross-sections set library for ATWS purposes is generated using the lattice physics code CASMO-4 and afterward converted to PMAXS format in accordance with the GenPMAXS guideline's procedure.

Figure 7.7 illustrates the distributions of history nodal moderator densities and fuel temperatures on the left and the instantaneous nodal distributions on the right. Following the same criteria as in Chapter 5, the solid blue line represents the boundaries of the cross-section history/branch matrix library. In contrast, the dashed blue lines represent the selected intermediate void fraction branches.

The history matrix consists of three moderator density histories at 0%, 45%, and 90% voids, considered suitable for most BWR applications. Conversely, six instantaneous moderator density variables have been selected, corresponding to 0%, 20%, 45%, 65%, 90%, and 100% void branches, each tailored to control rod states both in and out.

To adequately model boron injection for transient analysis, boron branches were integrated into the cross-sections. Typically, three to four branches prove ample for capturing any non-linear effects on neutron absorption, with additional branches added to simulate cold conditions for depressurization scenarios.

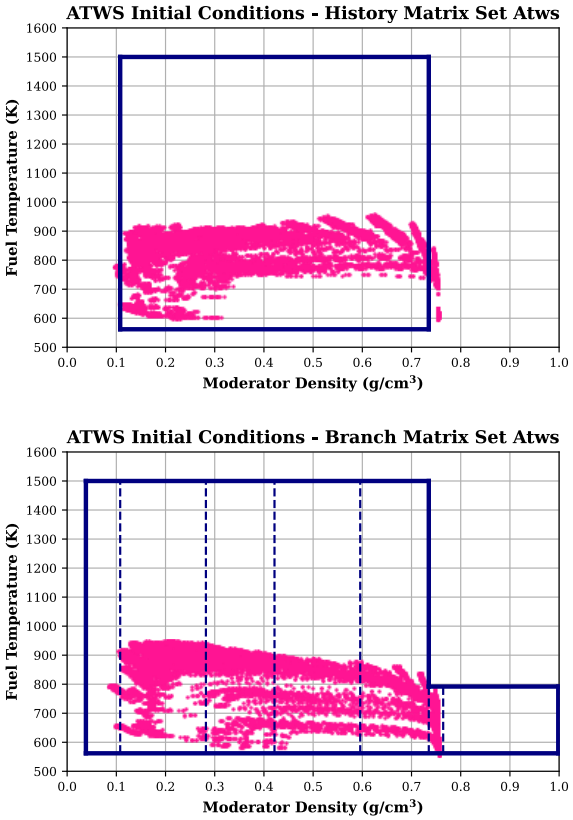

Figure 7.7. History (top) and Instantaneous (bottom) Moderator Density Boundaries for Set Atws Cross-section Library.

Table 7.6 and Table 7.7 contain the grid points that should cover the expected transient range. The chosen histories/branches aim to accurately represent system responses across a spectrum of conditions, reflecting the intricate and dynamic nature of reactor behavior during simulated transients.

Thus, the cross-section library includes 46 burnup steps up to a maximum exposure of 70 GWd/st, 10 different histories (rodded/unrodded three void histories, rodded/unrodded high fuel temperature history, and rodded/unrodded low fuel temperature history) and a selection of branches combining six moderator densities, three fuel temperatures, three moderator temperatures, four boron concentrations, and two control states (rodded/unrodded).

In total, 111 branch calculations are performed for each assembly type. Overall, the Set Atws library covers almost all nodes, so a very accurate nodal power distribution prediction for the initial steady-state is expected using this library.

Table 7.6. Cross-Section History Matrix Structure Set Atws Library.

Library History Matrix – Set Atws						
Fuel Temperature (K)	562	792.4	1500			
Moderator Temperature (K)	561.4					
Boron Concentration (ppm)	0.01					
Void Fraction (%)	0	45	90			
Control Rod	In	Out				

Table 7.7. Cross-Section Branch Matrix Structure Set Atws Library.

Library Branch Matrix – Set Atws						
Fuel Temperature (K)	561.4	792.4	1500			
Moderator Temperature (K)	293	545	561.4			
Boron Concentration (ppm)	0.01	400	1000	5000		
Void Fraction (%)	0	20	45	65	90	100
Control Rod	In	Out				

Regarding the numerics used in PARCS, Table 7.8 summarizes some of the options employed to improve the convergence of the calculations as well as to prevent possible code failure.

Table 7.8. Numerical Options in PARCS.

Numerical Option	ATWS Simulation
PARCS Coarse-mesh Finite-differences Method	CMFD (Option 2)
PARCS Nodal Kernel	HYBRID
PARCS Linear Solver	biCGSTAB
PARCS Exponential Extrapolation Option	Expo_opt=F F
PARCS Implicitness (THETA)	0.5 0.5 0.5

7.4 Methodology & Calculational Basis.

The MSIV closure ATWS transient will be simulated by a sequence of four consecutive runs as:

1) TRAC-BF1 steady-state stand-alone (SSA) to initialize the BWR model. This step sets appropriate plant boundary conditions for the reactor core before the coupling calculation.
2) PARCS steady-state stand-alone (SSA) to check the model and the validity of the cross-section library.
3) TRAC-BF1/PARCS coupled steady-state (CSS) calculation to initialize an integrated run and to set the initial conditions for the following transient.
4) TRAC-BF1/PARCS coupled transient (CTR) runs for the MSIV closure ATWS, Scenarios 1 & 2.

This methodology employs a collapsed core for thermal-hydraulic calculations and a 3D full-core for neutronics calculations as in the general process for performing a BWR coupled transient analysis.

Initial conditions, i.e., core flow, system pressure, pump speed, feedwater enthalpy, and core power, must be carefully calculated and confirmed with a steady-state TRAC-BF1 calculation before any transient analyses. The accuracy of coupled-code transient calculations strongly depends on an accurate and well-converged steady-state simulation.

7.4.1 Initial Conditions.

Proper initial conditions are essential for the analysis of a given event. Initial conditions are defined by rated core power, a top-peaked axial power distribution (the most limiting condition in pressurization transients), and the minimum allowed core flow within constraints of meeting the licensed thermal limits.

For pressurization and other transients where moderator density increases, the reactor period and Doppler coefficient trends are opposite to void coefficient and scram reactivity trends. Typically, the most severe combination of scram, void, and Doppler reactivity occurs at EOC; therefore, transient design and safety analysis are generally performed with the values of nuclear parameters representative of EOC conditions.

Both ATWS transient scenarios of interest are initiated, as aforementioned, based on a case with the reactor at MELLL operating condition, i.e., 111.85 % of originally licensed thermal power and 89% of core flow rate, with an average exposure of 15.90 GWd/st (EOC) at All Rods Out (ARO). Both scenarios include several system trips and operator actions.

Initial inlet feedwater temperature is consistent with the rated reactor steam flow. This condition will maximize the core power at natural circulation core flow following recirculation pump trip, which will also tend to maximize core inlet subcooling.

The radial and axial relative power fraction predicted by SIMULATE-3 at the given cycle exposure condition for the operating point to be analyzed is shown in Figure 7.8.

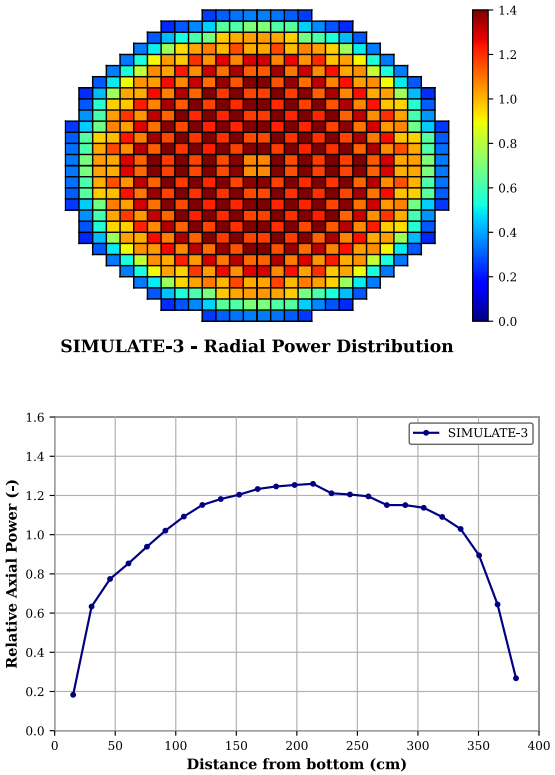

Figure 7.8. Radial and Axial Power Distributions predicted by SIMULATE-3. EOC conditions.

As seen, radial power distribution is relatively flat and symmetrical. Regarding the axial power distribution, the profile is consistent with axial void and burnup distribution for EOC conditions.

Reactor and plant system trip setpoints are set to nominal conditions with selected best-estimate parameters, and the transient response characteristics are assumed to behave as expected for ATWS analyses.

The initial and boundary conditions used as a reference for the steady-state calculation are obtained with the SIMULATE-3 code and shown in Table 7.9.

Table 7.9. Summary of Initial Conditions.

Parameter	Units	SIMULATE-3
Steam Dome Pressure	MPa	7.377
Total Core Flow	kg/s	9475.7
Core Power	MW	3237
Main Steam Flow	kg/s	1784.1
Feedwater Flow	kg/s	1781.6
Downcomer Level	m	0.884
Core Inlet Temperature	K	551.4
Feedwater Temperature	K	495.1
Core Inlet Pressure	MPa	7.574
Core Pressure Drop	--	0.140

7.5 Steady-State Results.

This section summarizes the results of the steady-state calculations and their comparison with the nodal power information provided by the reference SIMULATE-3.

As outlined in Section 7.4, the steady-state calculations are conducted in two steps. Table 7.10 presents key thermal hydraulic parameter results from the TRAC-BF1 Steady-State Stand-Alone (SSA) run, while Table 7.11 displays results from the TRAC-BF1/PARCS Coupled Steady-State (CSS) calculations.

The comparison of plant parameters between the reference and the calculations is favorable, indicating excellent agreement. The errors for all compared parameters are below 0.5% for both SSA and CSS calculations, demonstrating the accuracy and reliability of the simulation results.

Table 7.10. Summary of TRAC-BF1 Results for SSA.

Parameter	Units	Reference	TRAC-BF1	Error (%)
Steam Dome Pressure	MPa	7.3774	7.3467	-0.42
Total Core Flow	kg/s	9475.7	9470.3	-0.06
Core Power	MW	3237	3237	0.00
Main Steam Flow	kg/s	1784.1	1779.2	-0.28
Feedwater Flow	kg/s	1781.6	1773.9	-0.43
Downcomer Level	m	0.884	0.884	0.00
Core Inlet Temperature	K	551.4	551.1	-0.05
Feedwater Temperature	K	495.1	495.1	0.00
Core Inlet Pressure	MPa	7.574	7.609	0.46
Core Pressure Drop	--	0.140	0.140	0.33

Table 7.11. Summary of TRAC-BF1 Results for CSS.

Parameter	Units	Reference	TRAC-BF1	Error (%)
Steam Dome Pressure	MPa	7.3774	7.3466	-0.42
Total Core Flow	kg/s	9475.7	9482.7	0.07
Core Power	MW	3237	3237	0.00
Main Steam Flow	kg/s	1784.1	1779.0	-0.29
Feedwater Flow	kg/s	1781.6	1773.7	-0.45
Downcomer Level	m	0.884	0.884	0.00
Core Inlet Temperature	K	551.4	551.1	-0.05
Feedwater Temperature	K	495.1	495.1	0.00
Core Inlet Pressure	MPa	7.574	7.608	0.45
Core Pressure Drop	--	0.140	0.140	-0.06

The steady-state core-average axial power profiles for stand-alone and coupled cases estimated by PARCS are shown in Figure 7.9, while the relative radial power differences between SIMULATE-3 and PARCS predictions are illustrated in Figure 7.10.

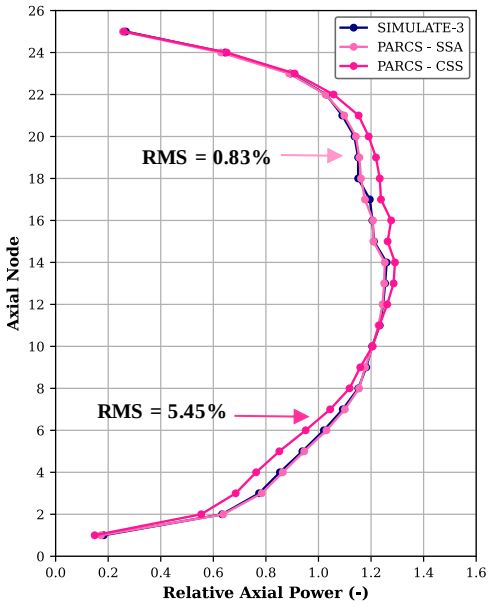

Figure 7.9. Axial Power Profile Predictions. PARCS vs. SIMULATE-3. SSA and CSS.

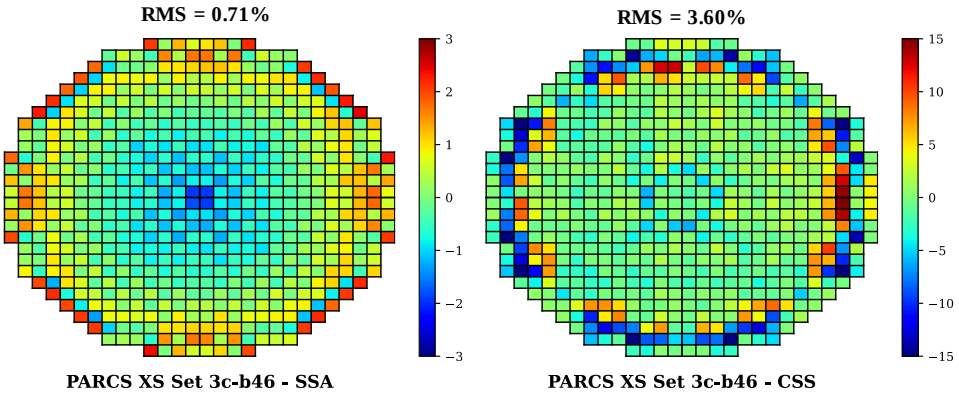

Figure 7.10. Relative Radial Power Errors (%). PARCS vs. SIMULATE-3. SSA and CSS.

The power distribution analysis yielded excellent agreement, with calculated root mean square differences of 0.83% axially and 0.71% radially for SSA PARCS calculations, confirming robust validation of the initial conditions. Notably, both SIMULATE-3 and SSA PARCS demonstrate the capability to model individual bundles.

In the CSS TRAC-BF1/PARCS calculation, the axial and radial power distributions exhibit slightly lower accuracy, which is expected in coupled simulations, as discussed in (Hursin et al., 2017). The CSS-predicted axial power shape tends to be more top-peaked, potentially leading to conservative results during pressurization transients. This observation is consistent with previous ATWS analysis studies using TRACE, detailed in (Yarsky, P., 2013). Despite this, given the core channel grouping strategy and the average thermal-hydraulic conditions employed to predict individual bundle power, the results remain reasonable and within acceptable limits.

Figure 7.10 illustrates that relative radial power errors are five times higher for the coupled steady-state than for the stand-alone case, highlighting the impact of core-channel grouping and advocating for its avoidance in coupled transients whenever feasible.

Furthermore, in the SSA case, PARCS consistently underpredicts power in the center of the core while overpredicting power at the periphery, as discussed in Chapter 5. Conversely, when thermal-hydraulic conditions originate from the TRAC-BF1 channel grouping for the CSS case, a pronounced power underprediction is observed at peripheral channels, with slight overprediction for inner channels.

A comprehensive summary of steady-state comparison results between PARCS and SIMULATE-3 is provided in Table 7.12.

Table 7.12. Summary of Steady-State Results for PARCS SSA and CSS.

	k_{eff}	Δk_{eff} (pcm)	RMS Axial (%)	RMS Radial (%)	MAX. Radial Peak (%)
SIMULATE-3	1.000172				
Parcs - SSA	0.999286	-89	0.83	0.71	2.53
Parcs - CSS	1.003734	356	5.45	3.60	17.83

Overall, the results prove that the initial conditions are well-established and validated; therefore, the given transient scenarios' analysis are ready to be performed.

7.6 MSIVC ATWS Scenario 1.

After completing the coupled steady-state case, the next phase entails conducting transient analysis using the TRAC-BF1/PARCS Coupled Transient (CTR).

The initializing event, the MISVs closure, begins at time zero. The valve closure isolates the RPV, causes a decrease in steam flow, and leads to rapid vessel pressurization, as shown in Figure 7.11. For ATWS simulation purposes, the expected SCRAM demand is initiated by the MSIV closure because high flux does not occur.

The transient could be divided into two stages, i.e., the initial short-term and the long-term. The former would focus on the pressure peak period, while the latter would focus on the nuclear reactor response after the operator's actions.

When the pressure increases in the RPV, there is an increase in power due to void collapsing with an increase in core flow rate, as seen in Figure 7.12 and Figure 7.13, respectively. For overpressurization transients, such as an MSIVC event, core responses are sensitive to Doppler and void feedbacks which are the driving mechanism as stated in (Hsiang-Shou, C. & Diamond, D. J., 1978). The severity of the power excursion is determined by the increase in reactivity due to collapse of voids.

Shortly after the MSIVs are fully closed, the closure triggers a Feedwater (FW) runback at 1.7 seconds, followed closely by a Recirculation Pump Trip (RPT) at 1.9 seconds due to high pressure. These simultaneous events result in a reduction in core flow rate and power, consequently leading to a decrease in water level. This sequence is clearly depicted in Figure 7.14.

Meanwhile, at 2 seconds, the SRVs open (with our analysis considering 11 valves in relief mode), mitigating the rate of pressure increase. Reactor pressure fluctuates around the SRVs' opening and closing setpoints during this phase. For the first five valves, the analysis adopts Low-Low set relief logic. The cycling of SRVs induces pressure oscillation, as observed in Figure 7.11, consequently altering the void fraction in the core and affecting the flow rate, as depicted in Figure 7.13.

As the core flow transitions to natural circulation, maintaining a constant core void is imperative to sustain reactor criticality. However, the decrease in flow necessitates a corresponding reduction in power to match the diminished core exit steam flow. This power reduction is necessary to ensure the availability of the primary heat sink (suppression pool).

Despite the reactor power remaining relatively high, i.e., around 50% of its initial level, due to the reduced core flow rate, the operator's adjustments to water level control, as illustrated in the Alternative Top of Active Fuel (TAF) level shown in Figure 7.14, effectively reduce reactor power. This new water level control strategy leads to a decrease in steam production until it reaches a point where the Steam Relief Valve (SRV) capacity surpasses the steam generation rate. As a result, vessel pressure begins to drop because the SRVs are expelling more steam than is being produced within the core.

Upon reaching 316.5 K (110°F) at 28.5 seconds, the suppression pool triggers the operator to initiate boron injection via the Standby Liquid Control System (SLCS),

ensuring eventual reactor shutdown across all scenarios. Boron injection, a crucial operator action, is intended to bring the reactor to subcritical conditions. To closely mirror actual plant operations, the ATWS analysis model includes a 220-second delay, accounting for the time it takes for the boron to travel from injection to the reactor core. Consequently, the boron is projected to reach the core approximately 250 seconds after its initiation, reflecting a realistic timeline for this critical safety measure.

Depending on core flow conditions, boron injected through the SLCS may undergo mixing or stratification in the lower plenum. When fully mixed, the boron introduced into the vessel becomes entirely entrained in the core flow, readily available to circulate throughout the core. Another notable phenomenon affecting boron transport within the reactor vessel is remixing, occurring when the core flow rate is sufficient to entrain stratified borated solution at the bottom of the lower plenum.

Previous analyses of ATWS for BWR/5 models simulated boron injection beneath the jet pump nozzle, near the lower plenum, as referenced in (Baek, J. et al., 2013b; Cheng et al., 2010). In this configuration, under low flow rates, boron tended to stratify. However, in the BWR/6 model developed for this study, boron is introduced into the upper plenum via the HPCS, resulting in mixing instead of stratification, despite the necessity to traverse one loop through the recirculation circuit (or descend through the core bypass, depending on conditions).

When the water level reaches Level 2 at 42.6 seconds, HPCS and RCIC systems should be automatically activated. However, in Scenario 1, the automatic HPCS action is inhibited; thus, the automatic injection system available providing additional inventory is the RCIC, as shown in Figure 7.15. Although the RCIC is a high-pressure emergency injection system, it is not anticipated to be deactivated during the transient. This is because the system's cutoff pressure, set at 0.05 MPa, is not expected to be reached.

In this scenario, the downcomer level reaches the minimum water level for steam cooling (i.e., -475 cm) resulting in emergency depressurization that is initiated at 80 seconds by manually actuating the ADS system (7 valves) to reduce vessel pressure, and eventually allowing preferential systems, e.g., Condensate Pumps (CP) and Condensate Booster Pumps (CBP), to inject through the feedwater line.

As a response to depressurization, flashing occurs, leading to an excess void fraction that drives reactor power reduction to decay heat levels. However, shortly after manual emergency depressurization activation, minor re-criticalities are observed, as depicted in Figure 7.12. It is worth mentioning that previously reported TRACE studies, referenced in (Cheng, L. et al., 2014b), have not documented instances of re-criticalities during water density increase resulting from depressurization and boron-diluted feedwater addition.

Furthermore, the impact of the emergency depressurization is prominently evident in the rapid decrease in reactor pressure around 100 seconds, resulting in a momentary swell in the downcomer water level, as illustrated in Figure 7.14. This is followed shortly after by a steady increase in peak cladding temperatures, Figure 7.16.

The rod temperature increases steadily after ADS activation because the core is uncovered (where the level drops below the TAF level for approximately 200 seconds, as shown in Figure 7.14 in the early stages of the transient. This heating trend persists until cooling water is injected because the upper portion of the core remains voided, despite the reactor power being at decay heat levels.

The periodic voiding and refilling of the lower plenum induce water level and core flow perturbations, as in Figure 7.13 and Figure 7.14. However, the negative reactivity introduced by boron entrained in the core flow at 250 seconds sustains the reactor at low power, Figure 7.12, a phenomenon well-documented in previous MSIVC ATWS analyses as noted in (Cheng, L. et al., 2013a).

As illustrated in Figure 7.17, the core's net reactivity remains negative following boron injection, indicating a sufficient accumulation of negative boron reactivity to sustain reactor shutdown. Fuel temperature, moderator density, and boron core reactivity components calculated by PARCS are shown in Figure 7.18. The impact of boron dilution is evident between 250s and 520s.

According to EOPs, water injection with preferential systems into the vessel is deferred until the pressure falls below the Minimum Steam Cooling Pressure (MSCP). Moreover, injection must be gradually conducted through the feedwater line.

The MSCP threshold is reached at approximately 322 seconds, as evidenced in Figure 7.19, prompting water injection through the CP and CBP. At this point, the PCT registers around 858.7 K.

The injection of CP+CBP flow through the feedwater line does not halt immediately the cladding temperatures increase because some time is needed to fill the partially empty downcomer and vessel lower plenum. The maximum PCT of 914.2 K is attained at 357 seconds, as depicted in Figure 7.16. Nonetheless, these injection systems deliver a significant volume of water, rapidly replenishing the lower plenum. After water injection at 322 seconds, the vessel water level starts to recover as depicted in Figure 7.14.

In addition, the CP+CBP water injection raises the moderator density reactivity, resulting in a positive moderator density reactivity around 540 seconds, as depicted in Figure 7.18. However, the impact of moderator density reactivity on the total core reactivity is overshadowed by the increased boron delivery to the core.

The progression of the main figures of merit throughout the transient is delineated in Figure 7.11 to Figure 7.19.

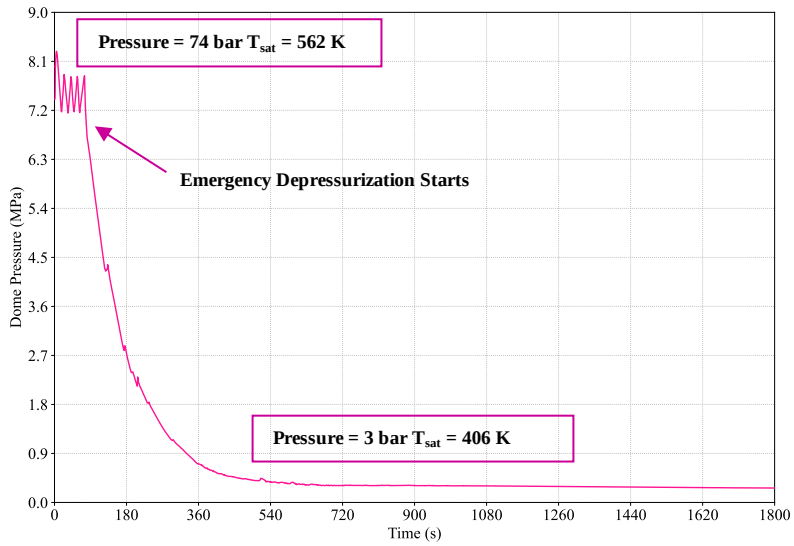

Figure 7.11. Vessel Dome Pressure.

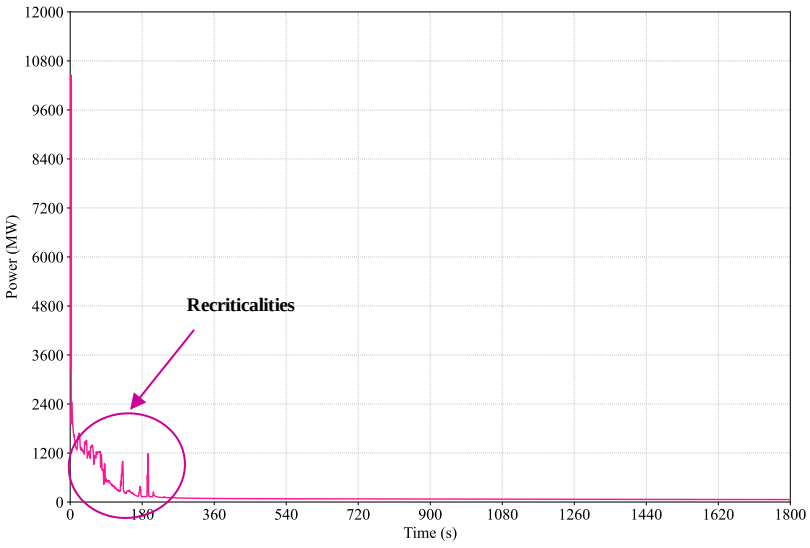

Figure 7.12. Total Reactor Power.

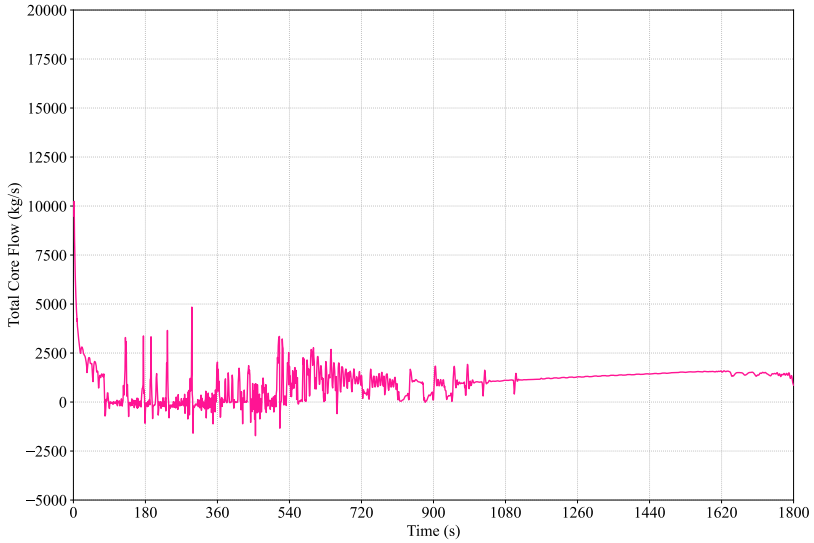

Figure 7.13. Total Core Mass Flow Rate.

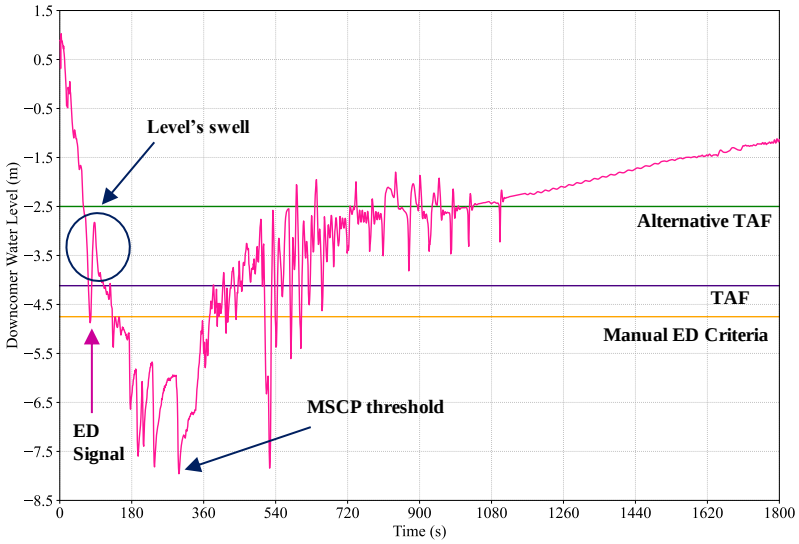

Figure 7.14. Downcomer Level.

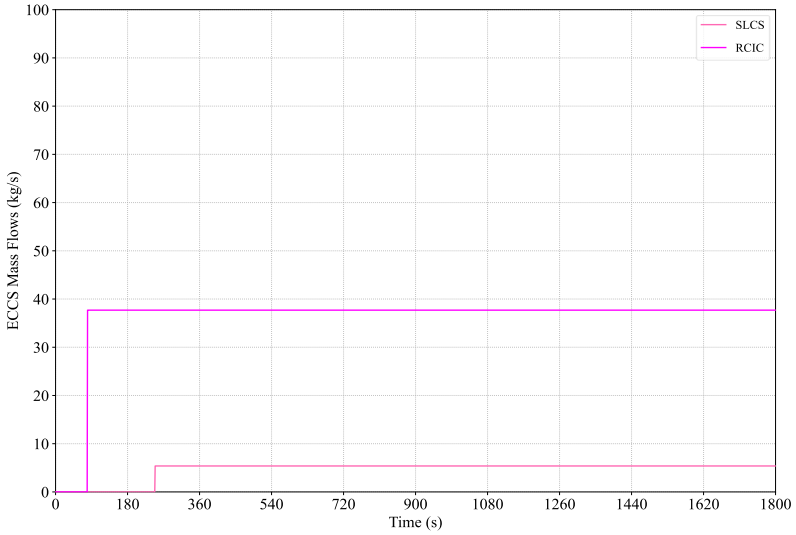

Figure 7.15. ECCS Mass Flow Rates.

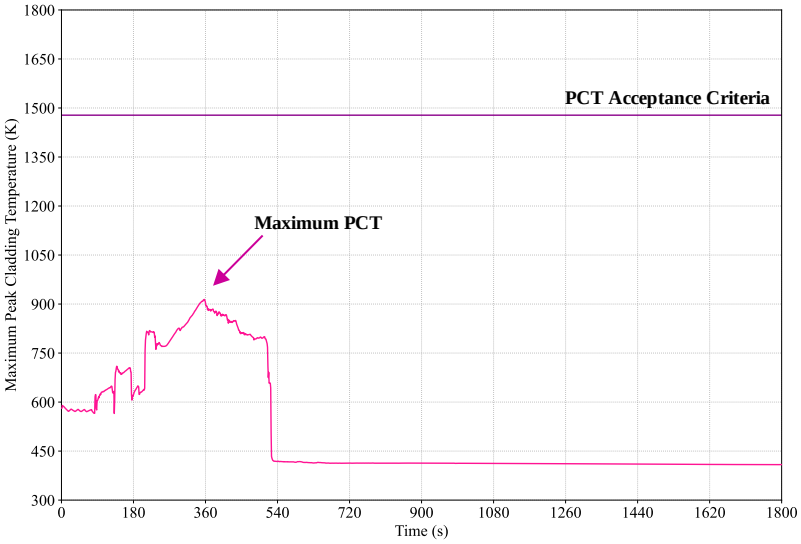

Figure 7.16. Maximum Peak Cladding Temperature.

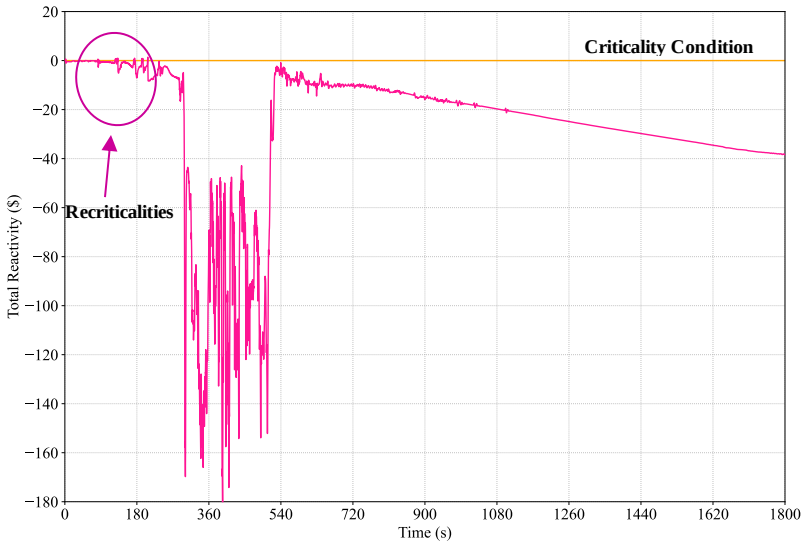

Figure 7.17. Total Core Reactivity.

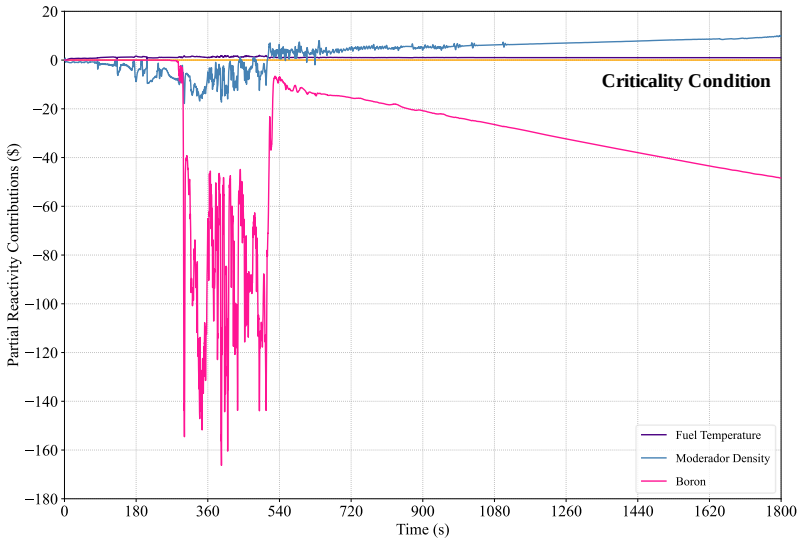

Figure 7.18. Partial Core Reactivities.

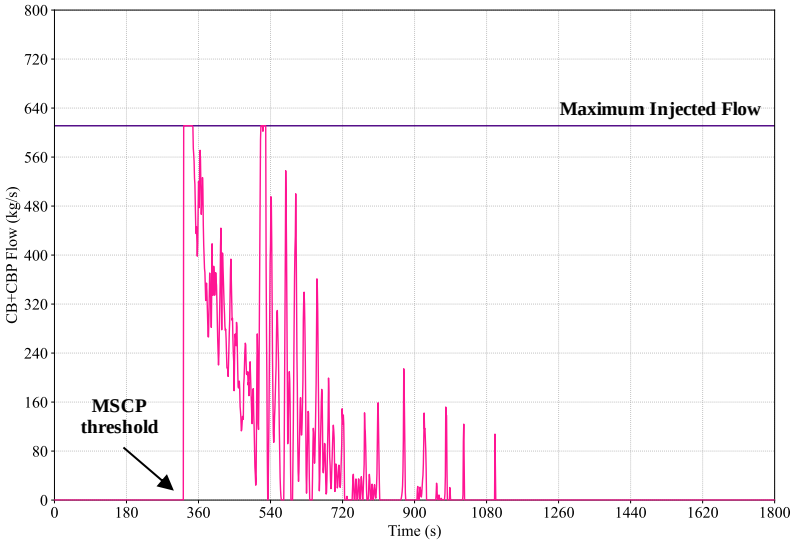

Figure 7.19. CP+CBP Mass Flows.

In a BWR, a significant quantity of high-temperature steam produced within the reactor is vented into the containment pressure suppression pool via SRVs. If the temperature of the suppression pool rises, it can lead to the heating and pressurization of the containment, as already discussed in the document NUREG/IA-0178 (Castrillo, F., 2000). Consequently, one of the most critical safety parameters for an MSIVC ATWS is the Suppression Pool Temperature (SPT) (Muñoz-Cobo et al., 2013).

Figure 7.20 illustrates how the temperature evolves with three different slopes during the transient, which presents distinct phases characterized by a series of phenomena in each one:

1) Phase 1: from MSIV valve closure at t=0.0 s to the manual activation of the emergency depressurization at t=80s.
2) Phase 2: from emergency depressurization to the start of boron safety injection in ~250s.
3) Phase 3: from the boron safety injection to the drop of the PCT at ~540s.
4) Phase 4: from the drop of the PCT at ~540s to the end of the transient.

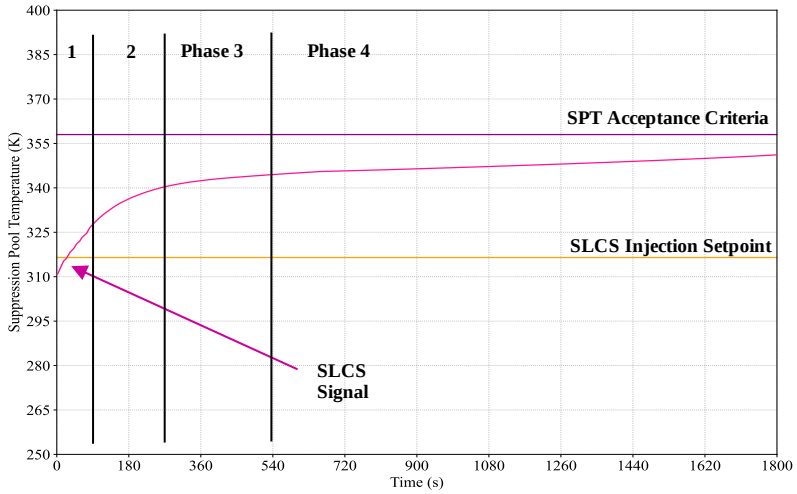

Figure 7.20. Suppression Pool Temperature.

The long-term behavior of the suppression pool temperature, as illustrated in Figure 7.20, shows a continuous increase that has not leveled off by the end of our TRAC-BF1 calculation. This trend correlates with the continuous steam discharge into the suppression pool from the Safety Relief Valves (SRVs) in Groups 1, 4, and 5, as shown in Figure 7.21. These groups represent the Automatic Depressurization System (ADS), which must remain open throughout the event once the ADS signal is activated.

The suppression pool temperature is expected to continue rising until the core decay heat is reduced below the capacity of the Residual Heat Removal (RHR) system, at which point the temperature will gradually begin to decrease. However, considering the slow rate of temperature increase and the continuous reduction of decay heat over time post-scram, combined with the capacity of the RHR system, it is unlikely that the temperature will rise enough to exceed the acceptance criteria. These conclusions align with previously reported studies (Cheng, L. et al., 2013a).

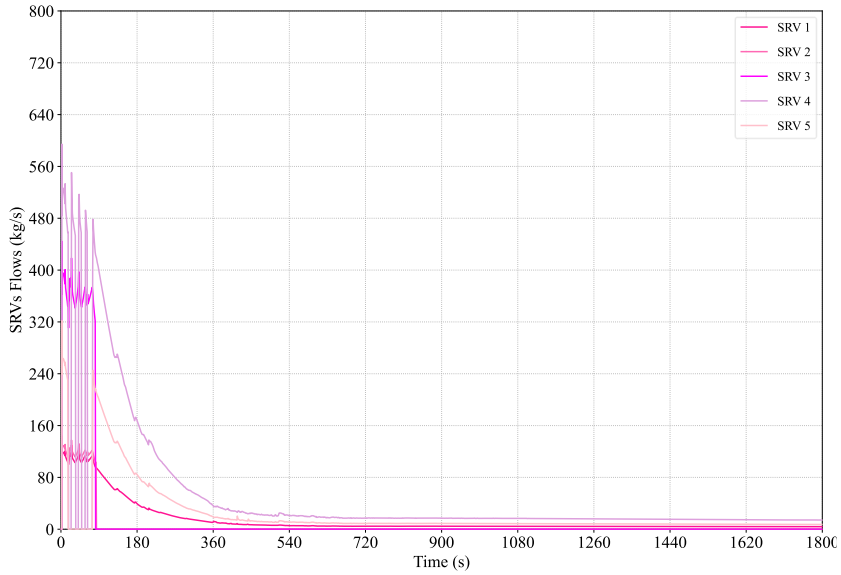

Figure 7.21. SRVs Mass Flows.

The transient finishes after 30 minutes (1800 seconds). The total transient simulation time should be sufficiently long to capture the water level recovery phase to the point where re-criticality becomes highly unlikely.

The plant response indicates that the reactor is stable and has achieved hot shutdown conditions. The event is mitigated successfully by a combination of automatic and manual operator actions that depressurize the reactor and reduce power by water level control and injection of boron.

The sequence of events to illustrate the general progression of the Scenario 1 transient is given in Table 7.13.

Table 7.14 summarizes the figures-of-merit values for the acceptance criteria.

Table 7.13. Sequence of Events for Scenario 1.

Problem Time (s)	Event/Action
0.0	Begin transient simulation
0.0	MSIV closure starts
0.0	Reactor trip due to MSIV closure fails
1.7	Feedwater trip
1.8	High-pressure signal
1.9	Recirculation pump tripped for high pressure
2.0	First lift of SRVs
3.0	MSIV fully closed
5.0	Peak vessel pressure
6.8	Feedwater stops
13.9	Level 3
28.5	Suppression pool temperature reaches 316.5 K (110 ºF). SLCS signal activated. Manual
42.6	Level 2
79.6	RCIC injection starts (Level 2 + delay)
79.6	HPCS injection starts (Level 2 + delay). Operator's manual inhibition
80.0	Manual emergency depressurization occurs (ADS activation)
82.0	Drywell reaches maximum pressure of 0.102 MPa
90.0	SRVs Groups 2 & 3 close
248.5	Boron starts accumulating in the core (SLCS signal + 220 s delay)
277.0	Power < 3%
322.9	CP+CBP injection starts. PCT at this time = 859 K
357.0	Maximum peak clad temperature of 914 K
660.0	RHR activation (11 minutes)
1800.0	Suppression pool reaches a maximum temperature of 351 K
1800.0	End of simulation

Table 7.14. Scenario 1. Comparison to Applicable Limits.

	Acceptance Criteria	TRAC-BF1/PARCS 3D Set Atws Library
Max. Vessel Pressure (MPa)	10.45	8.284
Contaiment Pressure (MPa)	0.205	0.102
Suppression Pool Temperature (K)	358	351
Peak Cladding Temperature (K)	1478	914

Results indicate that applicable regulatory limits are met with margin. As shown in Table 7.14, the predicted PCT is below 1478 K (2200°F) and does not challenge the fuel integrity.

However, the emergency depressurization has provoked a significant drop in pressure within the vessel, which has led to an abrupt change to the moderator temperature with still high void fractions' core distributions.

In this scenario, 3D kinetics PARCS estimations might be less accurate than desirable or influenced by a broad extrapolation due to the vast moderator temperature drop. Thus, it sounds plausible that multi-level tables might be needed to adequately capture reactor physics phenomena related to severe depressurization conditions, as already concluded in Chapter 5, when predicting the power profiles during the coast-down phase modeling.

A comparison with a 1D kinetics model using multi-level NEMTAB format, which employs a generalized tabular cross-section representation instead of the PMAXS files functionalization, has been considered convenient to test the validity of the 3D kinetics PARCS estimations.

7.6.1 Comparison 1D Kinetics vs. 3D Kinetics.

The use of the 1D kinetics TRAC-BF1 model compared to 3D kinetics when coupled to PARCS will allow for a more detailed and comprehensive analysis of the impact of the cross-section libraries.

All the 1D needed nuclear parameters were generated by CASMO-4 and collapsed into 1D neutronic information through the SIMTAB methodology, which allows representing the core in a much simpler way by using a reduced number of neutronic compositions. The SIMTAB methodology, (Roselló, 2004), was developed at the Universitat Politècnica de València (UPV), and it has been extensively used in many previous research works (Barrachina Celda, 2020; Hidalga García-Bermejo, 2020).

The predicted pressure by the 3D model presents hiccups while depressurization happens, which will cause a positive pressure derivative, leading to void collapsing and fuel cooling. The dome pressure evolution from 1D calculation generally agrees well with 3D estimation.

Regarding power prediction, the 3D kinetics model has enabled the identification of criticalities and unstable flow oscillations that were not observable with the 1D

kinetics model. Yet, as mentioned in Chapter 5, the moderator temperature functionalization in GenPMAXS might not be as accurate with the 3D model as expected. Consequently, while some criticalities are predicted, their magnitudes might vary once the moderator temperature functionalization in GenPMAXS is reviewed.

Table 7.15 shows the comparison results between the two kinetic models to the applicable limits.

Table 7.15. Scenario 1. Comparison to Applicable Limits. 1D vs. 3D Predictions.

	Acceptance Criteria	TRAC-BF1/PARCS 1D	TRAC-BF1/PARCS 3D
Max. Vessel Pressure (MPa)	10.450	8.282	8.284
Containment Pressure (MPa)	0.205	0.102	0.102
Suppression Pool Temperature (K)	358	343	351
Peak Cladding Temperature (K)	1478	957	914

The results using the TRAC code's 3D and 1D nodal kinetics model for the given transient scenario are depicted next from Figure 7.22 to Figure 7.26. The comparison of the evolution of the main figures of merit using both kinetics is only shown up to 1500 seconds because 1D kinetics simulation was originally run for 25 minutes.

The predicted pressure by the 3D model presents hiccups while depressurization happens, which will cause a positive pressure derivative, leading to void collapsing and fuel cooling. The dome pressure evolution from 1D calculation generally agrees well with 3D estimation.

The implementation of a 3D kinetics model has significantly enhanced the identification of criticalities and unstable flow oscillations that were previously undetectable with the 1D kinetics model. However, as discussed in Chapter 5, the moderator temperature functionalization in GenPMAXS may not achieve the expected accuracy with the 3D model. This discrepancy suggests that while criticalities can be predicted, their magnitudes might differ upon reevaluation of the moderator temperature functionalization in GenPMAXS.

The 3D neutron kinetics model offers a more comprehensive characterization of reactor phenomena during transients compared to its predecessors. These results align with the findings from the NUREG/IA-0178 analysis of the Main Steam Isolation Valve Closure (MSIVC) event (Castrillo, F., 2000), which compared the responses of point kinetics models and 1D kinetics models. The study indicated that the point kinetics model fails to adequately capture all the reactor phenomena due to the event's severity, especially when boron injection commences.

Based on these insights, it is recommended to utilize the highest order kinetic model available. Specifically, the 1D kinetics model should be preferred over the point

kinetics model, and the 3D model should be employed instead of the 1D model, to more accurately capture reactor behavior during transients.

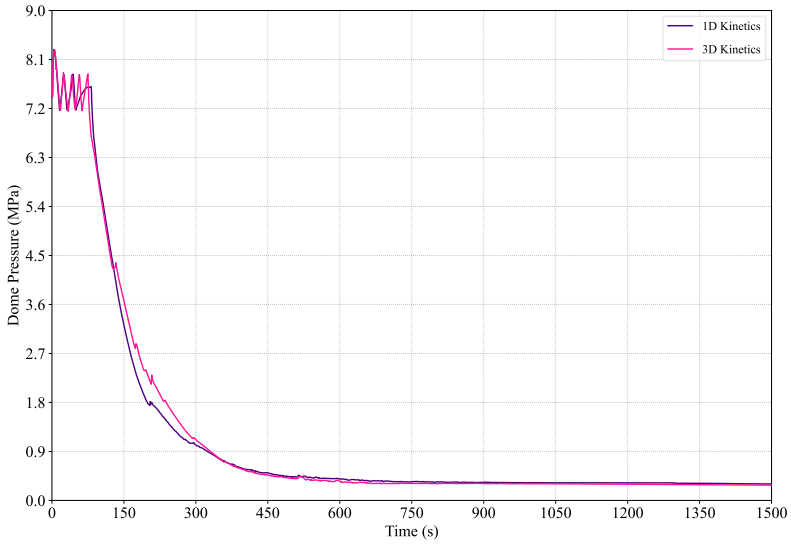

Figure 7.22. Vessel Dome Pressure. 1D vs. 3D Predictions.

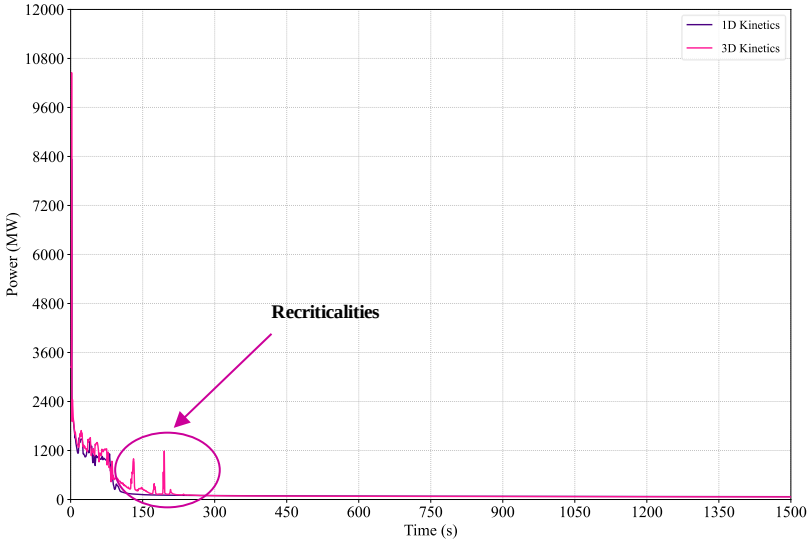

Figure 7.23. Total Reactor Power. 1D vs. 3D Predictions.

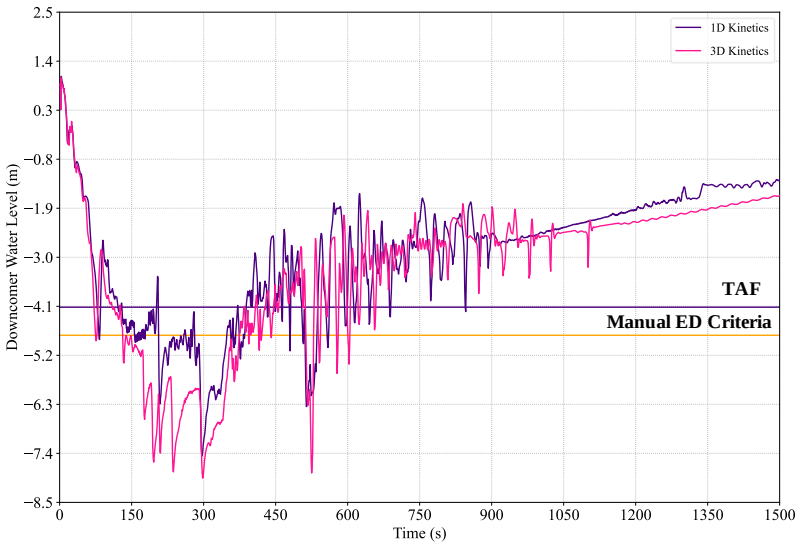

Figure 7.24. Downcomer Level. 1D vs. 3D Predictions.

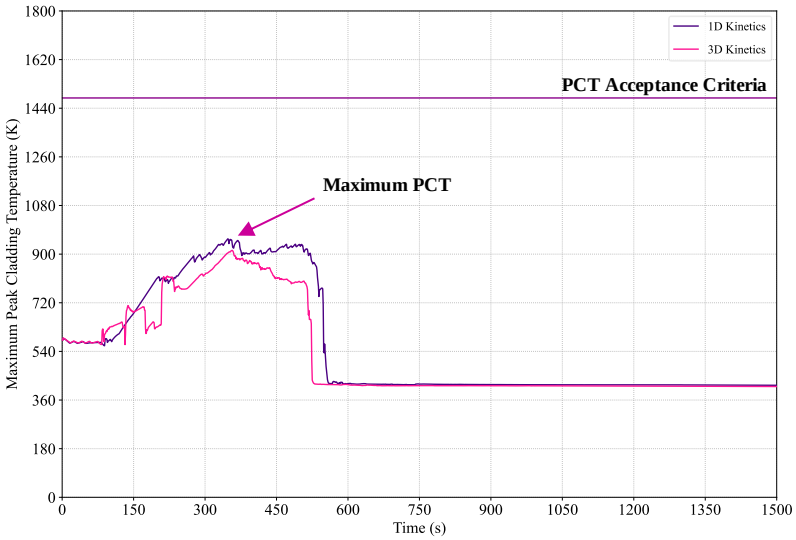

Figure 7.25. Maximum Peak Cladding Temperature. 1D vs. 3D Predictions.

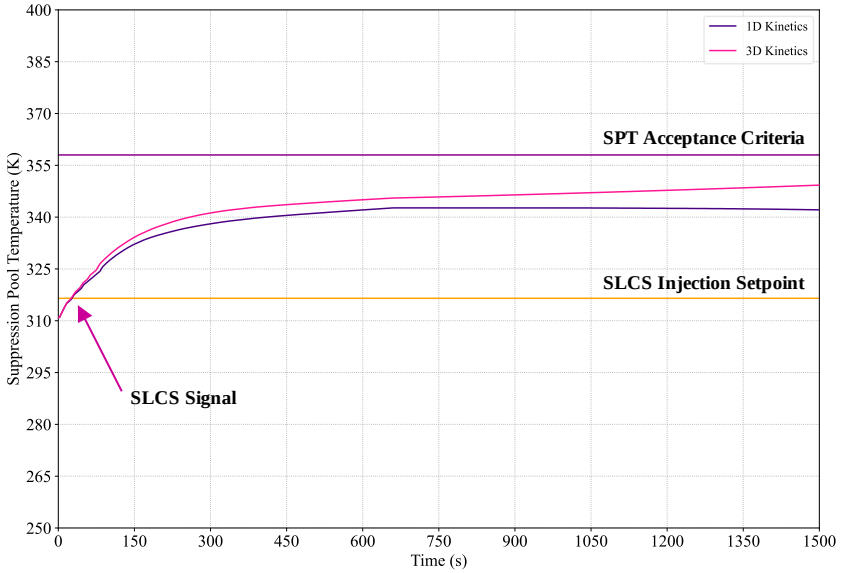

Figure 7.26. Suppression Pool Temperature. 1D vs. 3D Predictions.

7.7 MSIVC ATWS Scenario 2.

The progression of the ATWS event closely mirrors that of Scenario 1 until the activation of high-pressure safety injection systems in the core.

Upon the water level in the downcomer reaching Level 2, Figure 7.27, HPCS and RCIC systems are initiated with a certain delay, Figure 7.28. The HPCS system injects coolant into the upper plenum, while the RCIC system supplies coolant through the feedwater line, with both systems drawing suction water from the suppression pool.

Despite the additional coolant inventories provided by the RCIC and HPCS systems, the water level continues to decline as the steam exhaust through the SRVs exceeds the injection flow rates. The combined effect of water injection and SRV flow results in a drop in dome pressure, Figure 7.29. However, a sharp re-pressurization occurs around 160 seconds due to attained recriticalities, Figure 7.30.

Following HPCS injection, steam condensation reduces the dome pressure, leading to a steady decline without further SRV cycling, Figure 7.28. As reactor vessel pressure declines, HPCS flow increases, further decreasing vessel pressure and raising the water level. These effects contribute to the steady decrease in dome pressure and the cessation of downcomer level reduction after 350 seconds, Figure 7.27.

Power reduction is achieved through the combined effects of decreased pressure from the High-Pressure Core Spray (HPCS) system and the introduction of boron. A

delay of 220 seconds is employed once again, reflecting the time from the activation of the boron injection signal until the boron begins to be injected into the reactor core.

Reactor power falls below 3% around 342 seconds. TRAC-BF1/PARCS results also display recriticalities during the transient response, with average power increasing due to subcooled water HPCS injection and the rising core flow rate. The simulated thermal power response is illustrated in Figure 7.30.

The RCIC and HPCS systems maintain long-term RPV inventory and water level, ensuring the core remains covered. The maximum water level is attained around 865 seconds, corresponding to the peak core flow rate due to the driving head. At this point, the level reaches Level 8, triggering the cessation of high-pressure injection, Figure 7.27. Figure 7.31 shows that the reactor recirculation core flow rate remains low throughout the transient but exhibits long-term oscillations.

The evolution of the main figures of merit, i.e., downcomer water level, ECCS injections, dome pressure, total reactor power, total core mass flow, and PCT evolution are shown from Figure 7.27 to Figure 7.32.

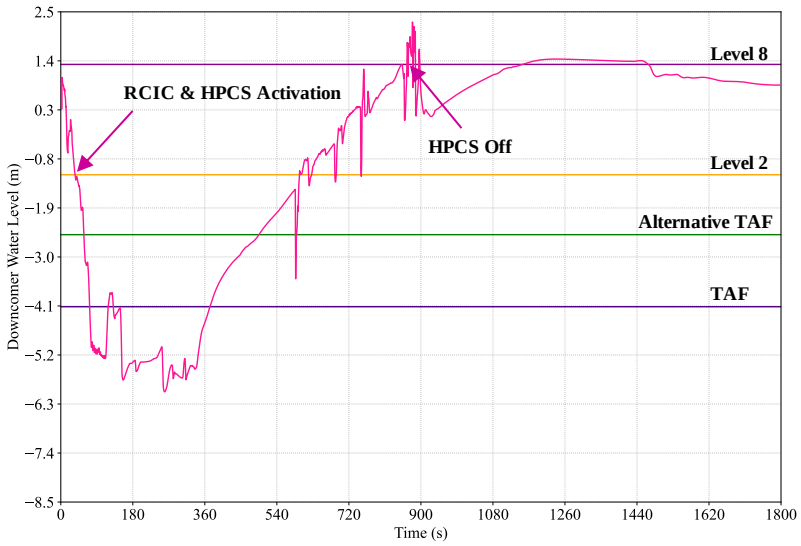

Figure 7.27. Downcomer Level.

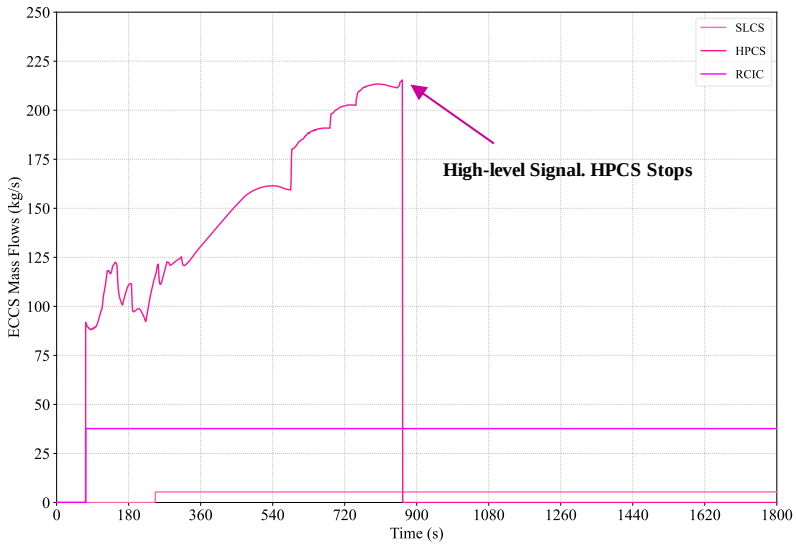

Figure 7.28. Preferent ECCS Mass Flow Rates.

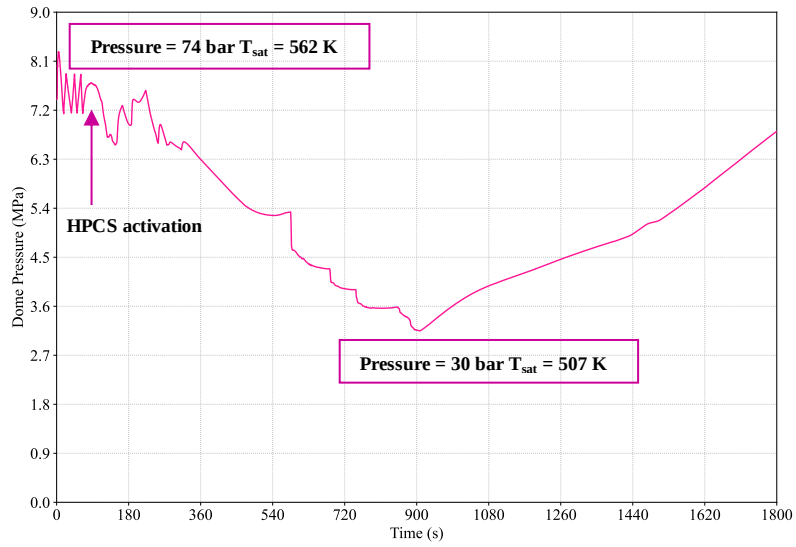

Figure 7.29. Vessel Dome Pressure.

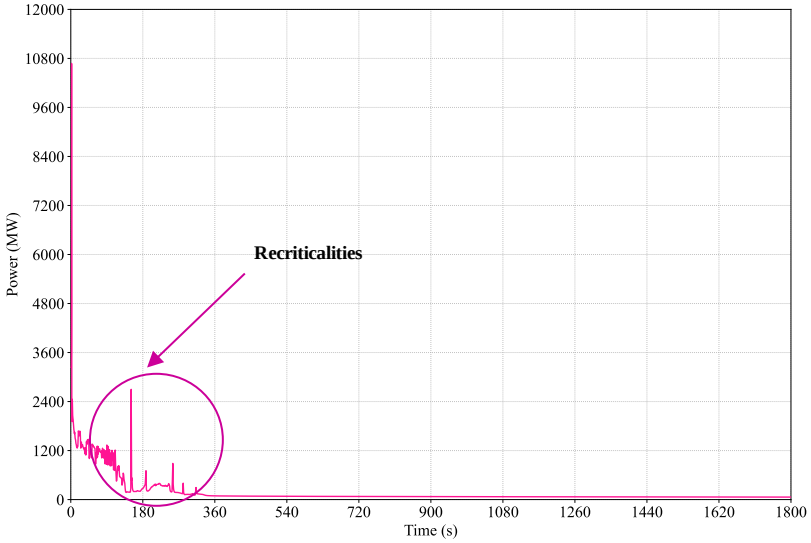

Figure 7.30. Total Reactor Power.

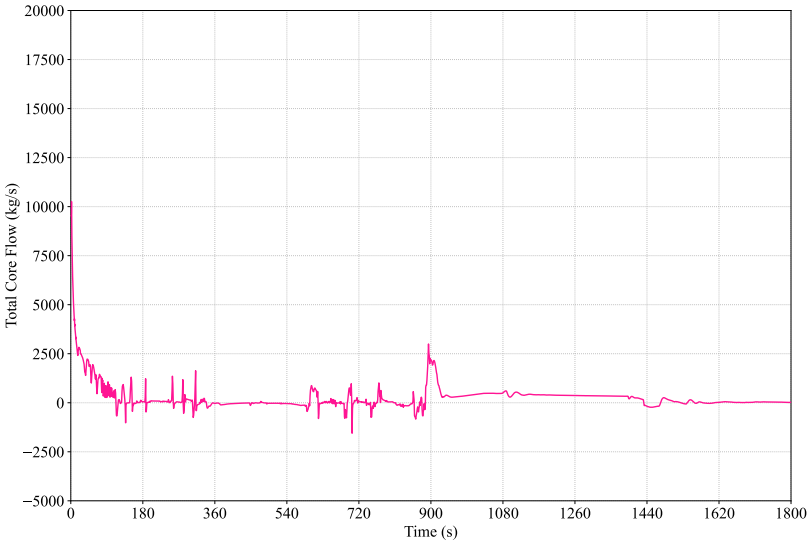

Figure 7.31. Total Core Flow.

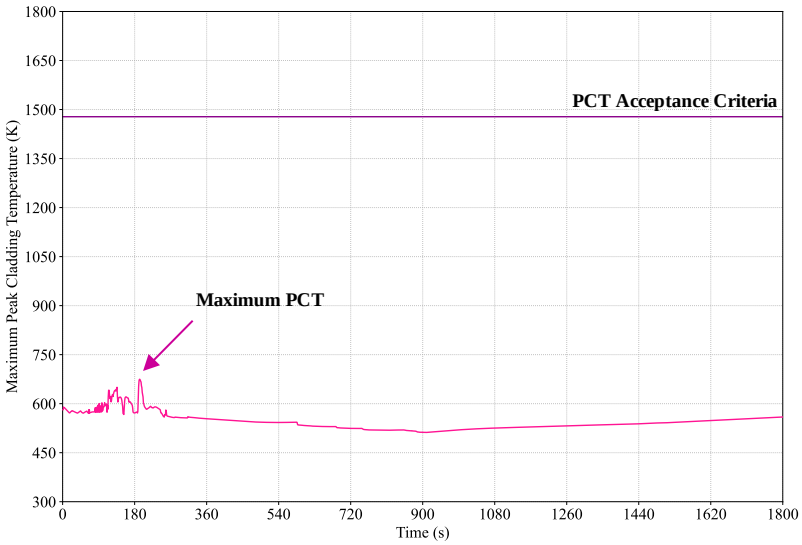

Figure 7.32. Maximum Peak Cladding Temperature.

As illustrated in Figure 7.32, the PCT maintains a consistently low profile throughout the entire transient period. This observation might indicate that the Minimum Critical Power Ratio (MCPR) remains above unity, even during the transient phase when reactor power is sufficiently high to induce a cladding temperature excursion.

Note that MCPR serves as the primary parameter for delineating the thermal limits of BWRs, representing the safety margin of the assembly closest to dryout which is directly associated with changes in flow pattern during evaporation in the high-quality region. The design of a BWR core aims to ensure MCPR values exceed 1.0 under various operational and transient conditions, encompassing all conceivable uncertainties (Nikitin et al., 2022).

The minor fluctuations in cladding temperature at the initial stages of the transient might result from overall reactor power level oscillations, as previously observed in Figure 7.29. Furthermore, oscillations in PCT may signify periodic incidents of dryout promptly followed by rewetting. This phenomenon strongly correlates with low-flow conditions. Since prolonged dryout is not observed, the TRAC-BF1/PARCS predicted PCT remains slightly higher than the saturation temperature at the operating pressure.

As illustrated in Figure 7.33, the core's net reactivity remains negative following boron injection, signifying an adequate accumulation of negative reactivity to maintain reactor shutdown. This outcome aligns with the observations from Scenario 1.

Figure 7.34 presents the fuel temperature, moderator density, and boron reactivity components calculated by PARCS. At 200 seconds post-initiation, the HPCS water injection induces a positive reactivity in the moderator density, persisting for most of

the transient duration. However, the positive reactivity contribution from moderator density does not exceed the negative reactivity introduced by boron injection, ensuring the overall core reactivity remains negative.

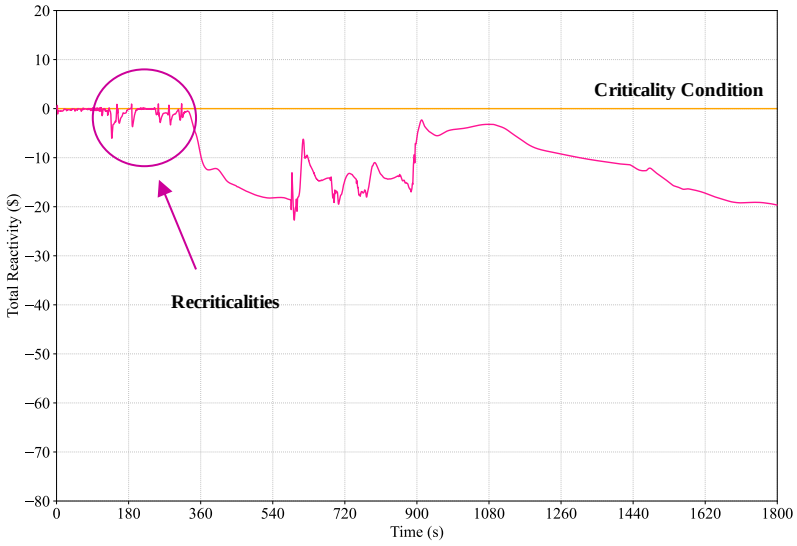

Figure 7.33. Total Core Reactivity.

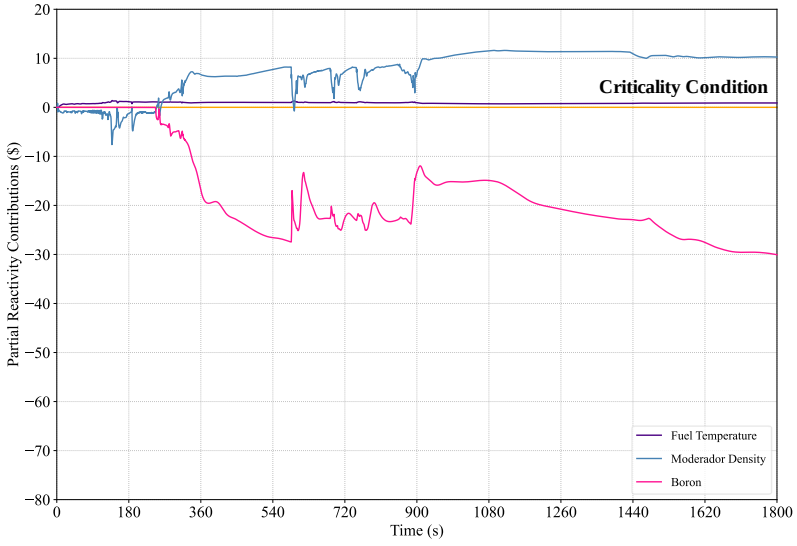

Figure 7.34. Partial Core Reactivities.

Concerning the dynamic behavior of the suppression pool throughout the Scenario 2 transient, Figure 7.35 delineates four distinct phases characterized by varying slopes:

1) Phase 1: Commencing from the MSIV closure at t=0.0 s until the initiation of the ECCS system for safety injection at t=80 s.
2) Phase 2: Extending from the activation of the ECCS system to the commencement of boron safety injection at t=248.5 s.
3) Phase 3: Encompassing the period from the initiation of boron water safety injection to the attainment of Level 8 and the cessation of HPCS injection at t= 865 s.
4) Phase 4: Spanning from the disconnection of the HPCS to the conclusion of the transient.

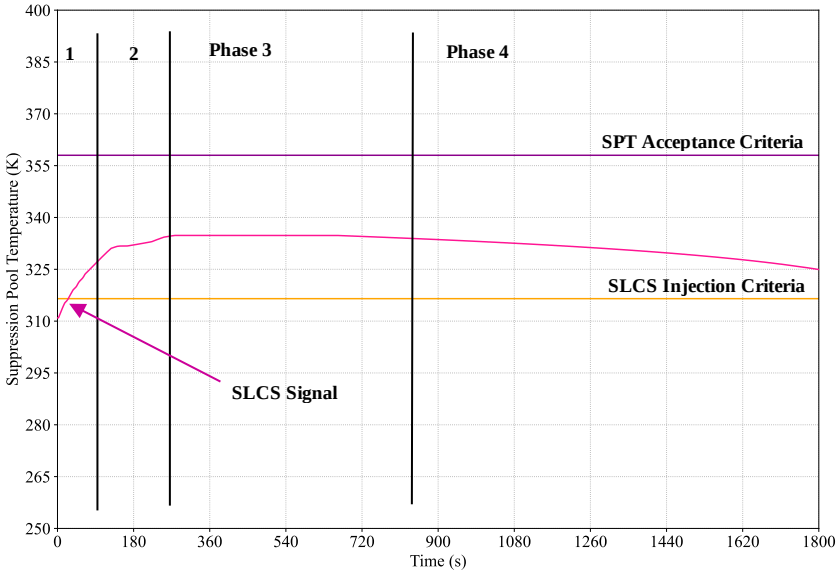

Figure 7.35. Suppression Pool Temperature.

The initial increase in suppression pool temperature is driven by reactor steam vented through the Safety Relief Valves (SRVs). As the High-Pressure Core Spray (HPCS) system activates, it begins to cool the suppression pool, initiating a steady decrease in temperature that continues throughout the transient. This cooling trend is further supported by the closure of all SRV groups around 280 seconds, as illustrated in Figure 7.36, which ceases the steam introduction into the containment.

The scenario results confirm that the suppression pool temperature remains well within safe limits throughout the event, ensuring that containment integrity is effectively maintained.

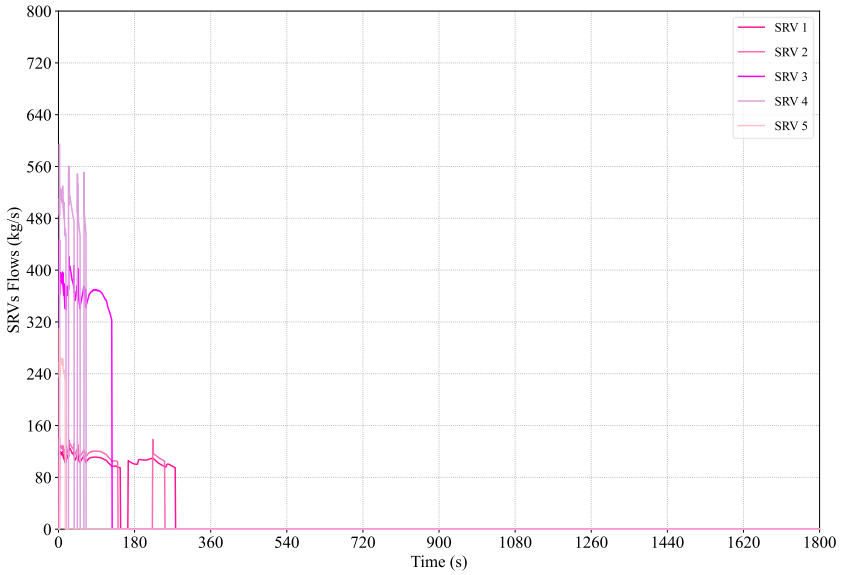

Figure 7.36. SRVs Mass Flows.

Our transient simulation finishes after 30 minutes. A detailed sequence of events outlining the overall progression of the transient is presented in Table 7.16. Additionally, Table 7.17 provides a concise summary of the margins concerning acceptance criteria limits.

Table 7.16. Sequence of Events for Scenario 2.

Problem Time (s)	Event/Action
0.0	Begin transient simulation
0.0	MSIV closure starts
0.0	Reactor trip due to MSIV closure fails
1.7	Feedwater trip
1.8	High-pressure signal
1.9	Recirculation pump tripped for high pressure
2.0	First lift of SRVs
3.0	MSIV fully closed
5.0	Peak vessel pressure
6.8	Feedwater flow equals 0
13.9	Level 3
28.5	Suppression pool temperature reaches 316.5 K (110 ºF). SLCS signal activated. Manual
42.6	Level 2
79.6	RCIC injection starts (Level 2 + delay)
79.6	HPCS injection starts (Level 2 + delay)
82.0	Drywell reaches maximum pressure of 0.102 MPa
192.0	Maximum peak clad temperature of 675 K
248.5	Boron starts accumulating in the core (SLCS signal + 220s delay)
276.0	Suppression pool reaches a maximum temperature of 335 K
277.0	All SRVs Groups are closed
342.0	Power < 3%
660.0	RHR activation (11 minutes)
864.9	Level 8. HPCS injection stops
1800.0	End of simulation

Table 7.17. Scenario 2. Comparison to Applicable Limits.

	Acceptance Criteria	TRAC-BF1/PARCS 3D Set Atws Library
Max. Vessel Pressure (MPa)	10.45	8.28
Contaiment Pressure (MPa)	0.205	0.102
Suppression Pool Temperature (K)	358	335
Peak Cladding Temperature (K)	1478	675

The plant response indicates that the reactor is stable and has achieved hot shutdown conditions. The event is mitigated successfully by a combination of automatic and manual operator actions that depressurize the reactor by HPCS injection and reduce power by water level control and injection of boron.

In Scenario 2, the drop of the pressure vessel is smaller than the one from Scenario 1. The cross-section library sufficiently covers the saturation temperature variation, i.e., 50 K vs. 150 K. Therefore, the overall predictions by the coupled-code could be regarded as adequate.

7.7.1 Comparison Set 1 vs. Set Atws Libraries.

Effects related to the modeled cross-section libraries are also of interest when the objective is to predict the core response under transient conditions. Hence, Scenario 2 was simulated using two distinct cross-section libraries; *Set 1* and *Set Atws*.

As previously discussed, Set 1, designed following NUREG/CR-7164 guidance (Wang, D. et al., 2013), proved inadequate for characterizing reactor conditions in steady-state and core-follow calculations using PARCS in stand-alone mode, primarily due to significant errors in power distribution estimation. Consequently, it was suggested to reconsider the branch/history matrix structure to identify appropriate cross-section sets.

Figure 7.37 showcases the lower and upper history boundaries of cross-section library Set 1, alongside the branch ranges designed to cover the distributions of history nodal moderator densities.

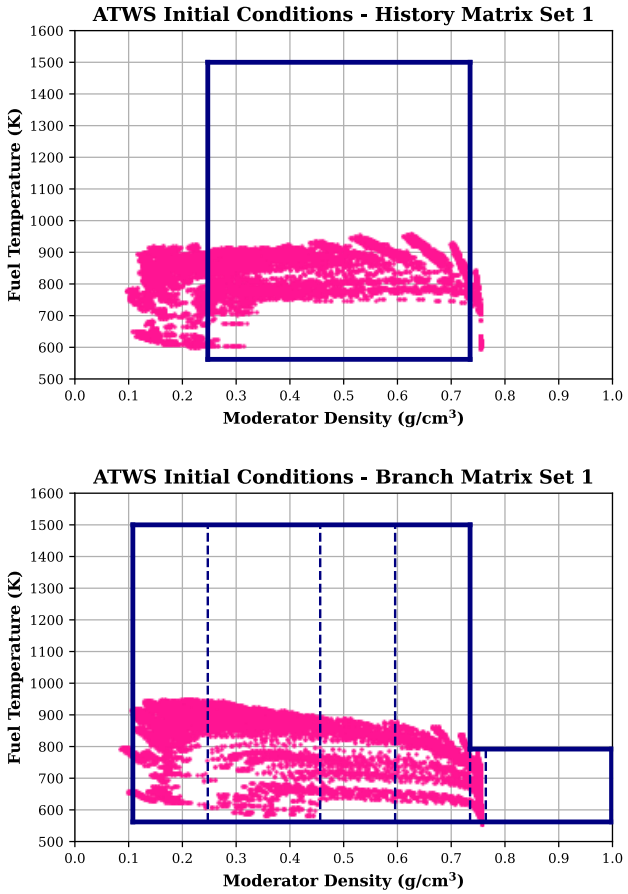

Figure 7.37. Moderator Density Boundaries History (top) and Instantaneous (bottom) for Set 1 Cross-section Library.

Figure 7.38 illustrates the structure conditions of the instantaneous moderator density matrix for both libraries under consideration: Set 1 and Set Atws. Due to the significant heterogeneity of BWR assemblies and the presence of two-phase flow in the reactor core during the transient, it was prudent to encompass the full 0-100% void fraction range with Set Atws.

In contrast, Set 1 only covers the void fraction range from 0 to 90%. This comprehensive approach with Set Atws ensures a more accurate representation of the reactor conditions during the transient.

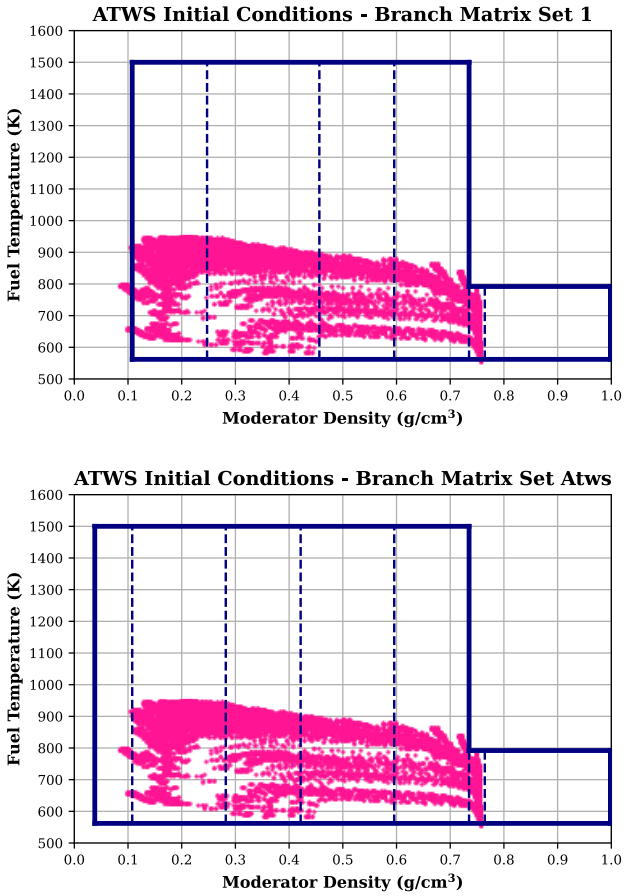

Figure 7.38. Moderator Density Branches Matrix for Set 1 Library (top) and Set Atws Library (bottom).

Figure 7.39 illustrates the boundary conditions of the void fraction histories for the two libraries used: Set 1 and Set Atws. As shown, the maximum historical value for the Set 1 library corresponds to a 70% void fraction, whereas for Set Atws, it reaches 90%. The 70% boundary condition for Set 1 leaves a significant number of reactor nodes outside the control area, suggesting that extrapolation will likely be necessary in the PARCS calculations when using Set 1.

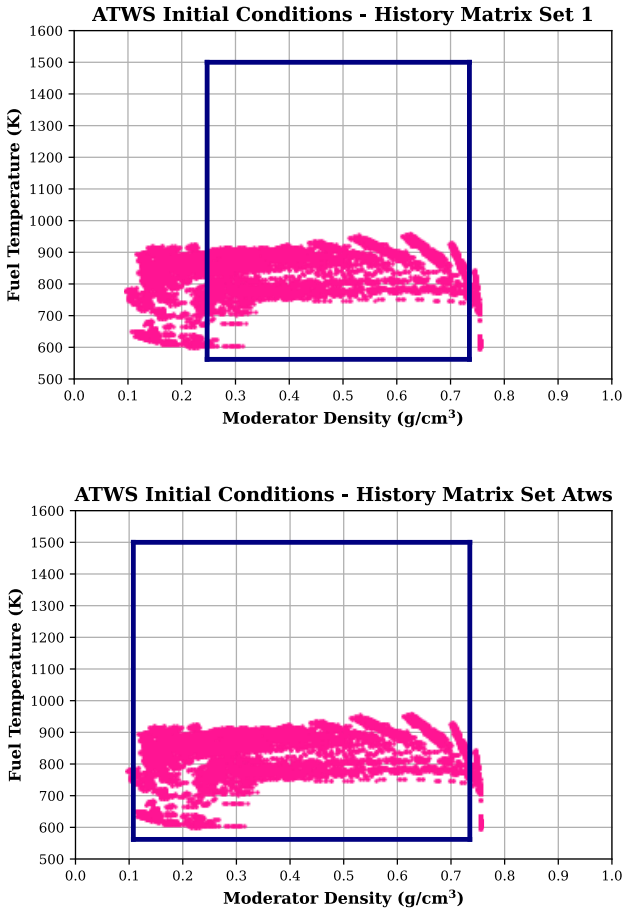

Figure 7.39. Moderator Density History Matrix for Set 1 Library (top) and Set Atws Library (bottom).

The results for the given simulated transient scenario using both cross-section sets, with Set Atws as the reference, are depicted next from Figure 7.40 to Figure 7.44. Table 7.18 summarizes the margins to the acceptance criteria limits from both used libraries.

Table 7.18. Scenario 2. Comparison to Applicable Limits. Set 1 vs. Set Atws Predictions.

	Acceptance Criteria	Set 1	Set Atws
Max. Vessel Pressure (MPa)	10.45	8.27	8.284
Contaiment Pressure (MPa)	0.205	0.102	0.102
Suppression Pool Temperature (K)	358	335	335
Peak Cladding Temperature (K)	1478	713	675

As shown in Table 7.18, the most significant discrepancy among the accepted criteria variables lies in the predicted Peak Cladding Temperature (PCT), i.e., when using the Set 1 library, there is a roughly 40 K disparity compared to the Set Atws library.

Figure 7.40 reveals a more pronounced discrepancy in the pressure evolution within the reactor dome. An increase in pressure occurs around 800 seconds when employing the Set 1 library, whereas a similar increase is observed around 900 seconds with the Set Atws library. This deviation stems from the modeling of the High-Pressure Core Spray (HPCS) system, where the inventory contribution ceases upon reaching the high-level L8 signal.

Figure 7.41 illustrates that the high-level L8 signal is triggered 100 seconds earlier with the Set 1 library compared to the Set Atws library. This earlier triggering is due to a spurious signal rather than an actual reactor issue. Despite this discrepancy, the observed pressure variations do not impact the overall system response computation significantly.

In the broader context, the trend in the evolution of main parameters throughout the transient is effectively captured by both modeled libraries. This consistency is depicted in Figure 7.42, Figure 7.43, and Figure 7.44. These figures demonstrate that despite the discrepancies in specific variables such as PCT and pressure timing, the overall behavior and response of the reactor system are accurately modeled by both the Set 1 and Set Atws libraries.

The analysis underscores the robustness of both cross-section libraries in capturing the essential dynamics of the reactor during transient conditions. This reinforces the importance of thorough validation and comparison of different modeling approaches to ensure precise and reliable reactor simulations.

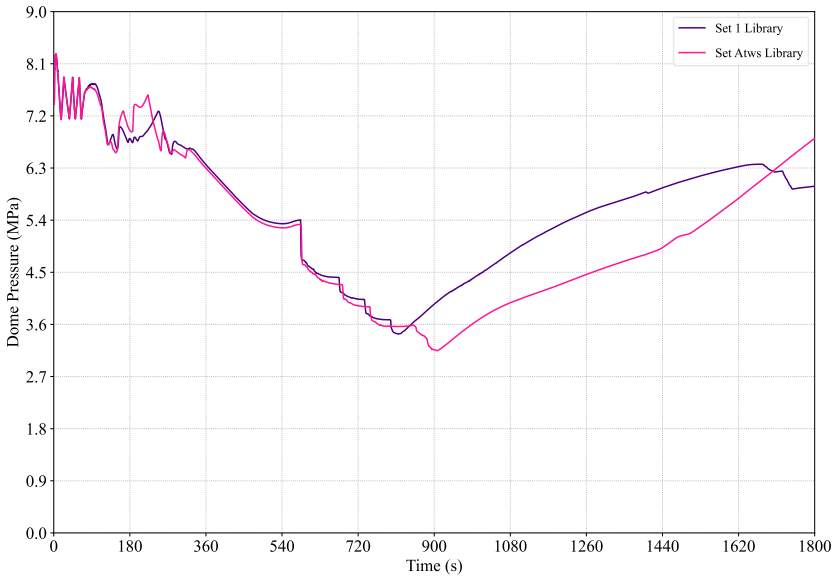

Figure 7.40. Vessel Dome Pressure. Set 1 vs. Set Atws Predictions.

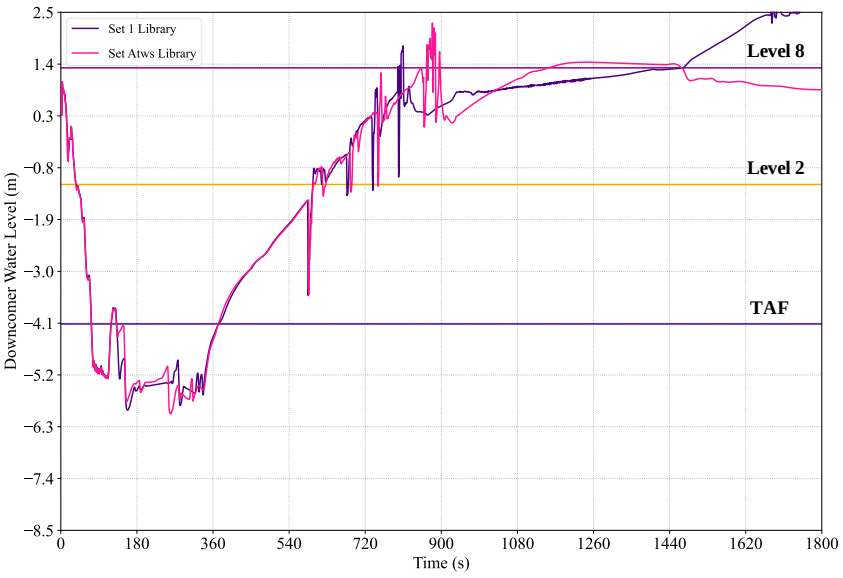

Figure 7.41. Downcomer Level. Set 1 vs. Set Atws Predictions.

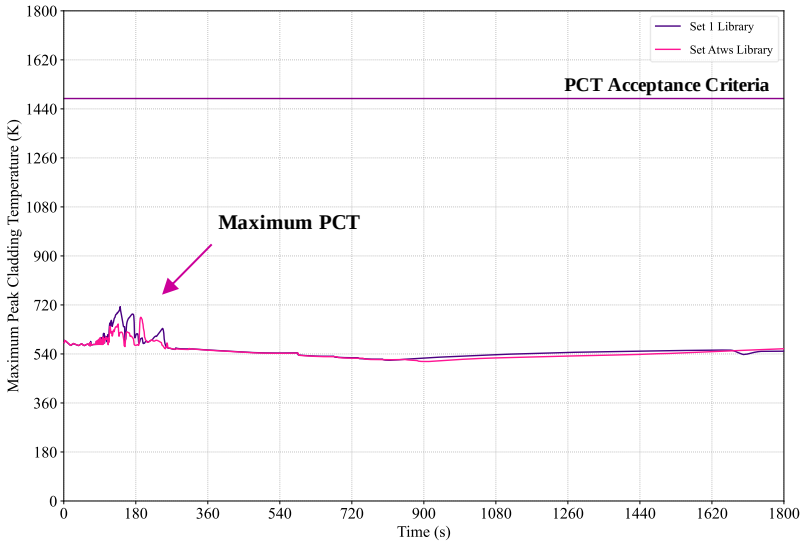

Figure 7.42. Maximum Peak Cladding Temperature. Set 1 vs. Set Atws Predictions.

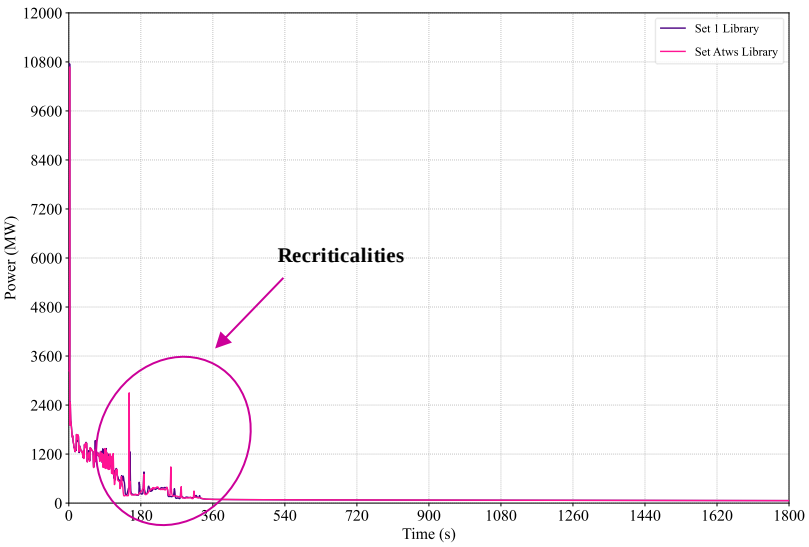

Figure 7.43. Total Reactor Power. Set 1 vs. Set Atws Predictions.

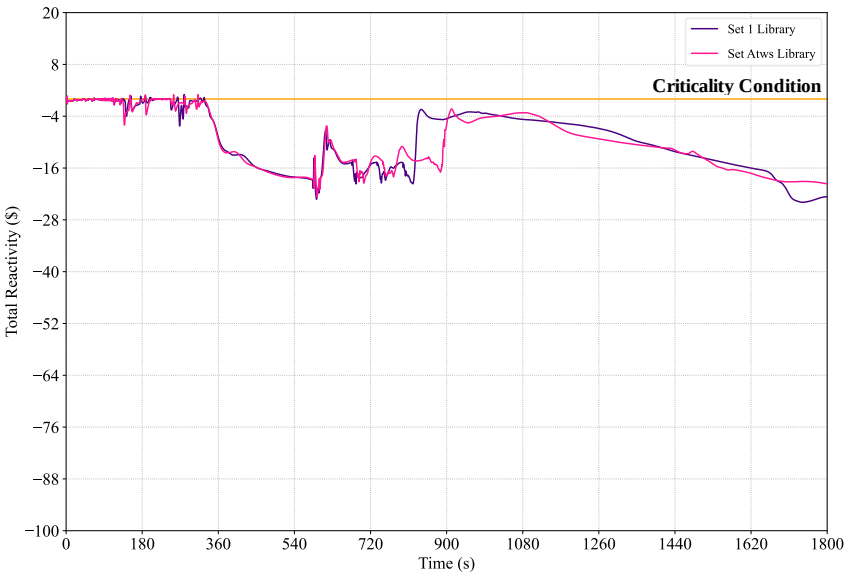

Figure 7.44. Total Core Reactivity. Set 1 vs. Set Atws Predictions.

The outcomes of this work suggest that in reproducing transients, the significance of the historical aspect of cross-sections diminishes, while the modeling of system branches gains prominence. As long as the number of branches ensures adequate interpolation and sufficiently covers the anticipated application range for the transient, all predicted values from the cross-section sets could be regarded as valid.

This is why cross-section libraries unsuitable for predicting core power distributions in purely neutronic calculations might be used in transient analyses using coupled codes with reasonable validity, as long as the thermal-hydraulic conditions of the transient remain within the cross-section domain.

Therefore, when employing coupled codes for simulating certain transients, the effect of cross-section libraries on the evolution of the main figures-of-merit may not be discernible due to the thermal-hydraulics and neutronics feedback, especially with collapsed cores, which conceal the neutronic response of the reactor. This emphasizes the importance and relevance of this work in advancing our understanding and improving the accuracy of transient simulations in nuclear reactors.

This conclusion offers intriguing insights into the design, modeling, and utilization of cross-section libraries in coupled-code calculations, emphasizing the evolving importance of modeling branches in transient reproduction.

7.8 Summary.

Coupled-code TRAC-BF1/PARCS was employed to simulate a postulated Anticipated Transient Without Scram (ATWS) initiated by Main Steam Line Isolation Valve Closure (MSIVC), exploring two operator action scenarios. This aimed to examine transient plant behavior and gauge the impact of cross-section library variations on the overall core response. The selection of the MSIVC ATWS event was drive by its potentially limiting nature due to the severity of the initial pressurization.

Scenario 1 led to an emergency depressurization following standard EOPs, while Scenario 2 represented a postulated ATWS with High-Pressure Cooling System (HPCS) injection, excluding Emergency Depressurization (ED) activation, to assess the core response to subcooled water injection.

The calculations of both scenarios have been performed with a detailed plant and core model utilizing 15 TRAC-BF1 channel components and 3D neutron kinetics via PARCS. A mapping scheme condensed 624 assemblies to 15 TRAC-BF1 hydraulic channels, derived from the core-simulator code SIMULATE-3.

Furthermore, Scenario 2 was utilized to evaluate the impact of the cross-section libraries on core response. Neutronics calculations utilized cross-section libraries sourced from the lattice code CASMO-4, comprising two sets: *Set Atws* and *Set 1*. The history/branch matrix design for Set Atws library aligned with conclusions from Chapter 5, while Set 1 library followed guidance from NUREG/CR-7164.

After MSIVc, the short-term response of the reactor was driven by three effects: Recirculation Pump Trip (RPT), Safety Relief Valve (SRV) operation, and loss of feedwater. At longer times, the behavior of the reactor was primarily influenced by the boron injection, the water injection, and the actuation of the emergency depressurization or the HPCS injection, depending on whether Scenario 1 or Scenario 2 was being analyzed.

In both simulated scenarios, the initial event was mitigated successfully by preventing damage to the fuel and assuring the ability of the containment to fulfill its function.

Short-term, low power re-criticalities were observed due to choking in the Automatic Depressurization System (ADS) valves or increased coolant density reactivity due to the subcooled water injection through HPCS. However, no sustained power oscillations related to density wave oscillations (and core instability) were observed.

In Scenario 1, as expected by the sequence of the events, a moderator saturation temperature variation of around 150 K associated with the abrupt drop in the pressure vessel was observed together with sufficiently high void fraction distribution in the core. As pointed out, drastic moderator temperature variations along with high voids might not be well simulated by PARCS. Therefore, it was suggested that the core response estimations following the automatic depressurization action be called into question.

In Scenario 2, the drop in the pressure vessel entailed a moderator saturation temperature variation of roughly 50 K which was sufficiently covered by the moderator

temperature parameterization by GenPMAXS for the cross-section set used. Consequently, the overall predictions by the coupled-code could be regarded as adequate.

In general, the trend of the evolution of the main parameters during the transient was equally well captured by the cross-section libraries.

The results of this work indicate that in reproducing transients, the instantaneous parameters gain importance in the core response when the feedback between the thermal-hydraulics and the neutronics is present. As long as the branch matrix reasonably covers the state variables' domain without the need for very large interpolations, the cross-section libraries are less sensitive to history effects during transient predictions with coupled codes compared to standalone neutronics applications such as core follow calculations, depletion modeling, or coast-down predictions.

This highlights the significance of this work in demonstrating that cross-section libraries can be effectively used in transient analyses, provided the state variables are adequately covered. The findings emphasize the critical role of this research in enhancing the accuracy and reliability of transient simulations in nuclear reactors, particularly when utilizing coupled codes.

In summary, TRAC-BF1/PARCS represented all fundamental phenomena with either reasonable or excellent agreement over the range of interest for MSIVC ATWS at MELLL conditions. Thus, the performance of the system model confirms the applicability of the TRAC-BF1 and PARCS codes to analyze such ATWS events and reinforces the importance of cross-section modeling.

Chapter 8
Conclusions & Future Work

8.1 Conclusions.

The findings and conclusions detailed in this chapter arise from a comprehensive analysis undertaken to support this thesis, employing advanced methodologies as outlined in previous chapters.

The key conclusions drawn from the **code-to-code benchmark** chapter are as follows:

1) PARCS has been rigorously benchmarked against SIMULATE-3, demonstrating accurate predictions for eigenvalue calculations and power distributions in modern BWR operations. This confirmation establishes PARCS's reliability and adherence to contemporary software quality standards, making it a robust tool for analyzing current BWR fuels.

2) The study reveals significant limitations in the current NUREG/CR-7164 guidelines for cross-section library modeling. The discrepancies observed, particularly in axial power distributions, suggest that these guidelines need revision to better accommodate modern fuel designs and reactor operating conditions.

3) History effects, particularly those associated with variations in moderator density and control rod positions, are pivotal in determining the precision

of power distribution predictions. This underscores the need for enhanced modeling techniques to accurately capture these effects. Traditionally, history effects were considered less significant compared to branch effects, but these findings challenge this notion, revealing their substantial influence on simulation accuracy.

4) Sensitivity analysis has demonstrated that BWR steady-state results exhibit generally lower sensitivity to variations in moderator density branch effects compared to history effects. However, this trend may not apply universally across all transient scenarios. Consequently, it is crucial to revisit and refine cross-section branches and histories, particularly for transient analyses, to ensure their accuracy and relevance. This nuanced understanding highlights the importance of tailored approaches for different operational conditions and reinforces the need for ongoing refinement in modeling practice.

5) The meticulous analysis of cross-section libraries with varying burnup points revealed that smaller time step sizes, around 0.5 GWd/st, are crucial for accurately modeling gadolinium depletion. This fine granularity is essential because gadolinium, used as a burnable poison, significantly influences reactor behavior in the early stages of the fuel cycle. Additionally, incorporating a finer depletion step between 0 and 0.5 GWd/st, specifically at 0.1 GWd/st, markedly enhances power predictions at the Beginning of Cycle (BOC) by effectively mitigating the Xenon effect, which can otherwise skew power distribution predictions.

6) The study also indicates that merely increasing the number of burnup points beyond a certain threshold, such as the 46 points evaluated in this thesis, does not necessarily lead to improved accuracy in power distribution predictions. Contrary to the intuitive notion that more data points will always enhance simulation fidelity, this analysis reveals diminishing returns with an increase in burnup points. The variability in power errors and the additional computational overhead for libraries with an excessive number of burnup points highlight practical limitations. This suggests a need for a strategic approach to library development, balancing the benefits of detailed data against computational efficiency.

7) Traditional nodal analysis methods encounter significant challenges when modeling coast-down conditions, primarily due to fluctuations in moderator density and saturation pressure. The study underscores the necessity for refined void branching and more precise parameterization of moderator temperature in GenPMAXS to better predict three-dimensional power distributions. This improvement is essential for accurately capturing the dynamic behavior of the reactor core during coast-down scenarios, where conventional models may fall short.

8) A notable observation is the significant shift in nodal distribution of void fractions from high to low void branches at End of Cycle (EOC) conditions. Specifically, nodes with a 90% void fraction decreased from 23% at BOC to 4.5% at EOC, while nodes with a 0% void fraction increased from less than 20% at BOC to around 40% at EOC. This dramatic shift highlights the critical need for accurate modeling of void branching to reflect changes in moderator density and reactor conditions throughout the fuel cycle. Understanding and predicting these shifts are vital for maintaining reactor efficiency and safety.

Overall, the comparison between power distributions calculated by PARCS and SIMULATE-3 shows a high level of agreement throughout the entire cycle.

These findings underscore the importance of rigorous software assessment, precise cross-section library modeling, and continuous improvement in simulation capabilities for the effective analysis and modeling of modern BWR operations.

Library Set 3c-b46 has shown excellent agreement between power distributions calculated by PARCS and those calculated by the plant computer for model core designs. These results demonstrate PARCS' ability to accurately model reactor data with modern fuel designs, including large water rods, part-length rods, and significant gadolinium loading.

Conclusions regarding **the code-to-TIPs benchmark** are as follows:

1) The meticulous comparison of detector responses estimated by PARCS with measured Cycle B TIP data from the plant reveals insightful trends and performance metrics. PARCS consistently demonstrated a high level of agreement with the measured data throughout the cycle, performing optimally in the middle of the cycle while exhibiting larger discrepancies at the beginning and end. These variations align with the anticipated dynamic behavior of the reactor core as burnup progresses, highlighting the challenges of accurately modeling these phases.

2) SIMULATE-3 consistently matched the TIP measurements most closely in both nodal and axial power distributions, confirming its reliability as a reactor simulation tool.

3) The study also examined the consistency of nodal and axial Root Mean Square Errors (RMSEs) across various nuclear data libraries. Libraries **Sets 3c**, **b46**, and **b78** exhibited strong alignment with plant core follow benchmarks, validating their reliability. In contrast, the Set 1 library continued to produce the least accurate power predictions, as previously observed.

4) An intriguing finding is that libraries with higher burnup points, such as **b46** and **b78**, did not yield improved power distribution predictions

compared to the Set 3c library. This unexpected result suggests inherent limitations in the advantages offered by higher burnup points, depending on the specific case characteristics. Further investigation is necessary to unravel these complexities.

5) Significant discrepancies were found near control rod locations, indicating potential issues with PARCS's control rod modeling, especially when multiple control rod definitions are used. This highlights the need for better modeling of control rod effects in PARCS.

6) The analysis highlighted that insufficient consideration for variations in moderator density in the reflector region led to larger discrepancies near the core's top and bottom. This finding suggests that PARCS's current approach might not accurately predict neutron leakage in these areas, corroborating previous studies.

7) Peripheral detectors exhibited slight deviations, with PARCS generally predicting higher power levels compared to TIP data, particularly toward the cycle's end. Despite this, the results displayed no significant overall bias.

8) The accuracy of PARCS calculations was slightly reduced toward the end of the cycle, influenced by factors such as axial power peaking, limitations in part-length rod modeling, and spectrum hardening. These challenges underscore the difficulty in capturing the reactor's complex neutronic phenomena during this phase. The summary of rejected points due to discrepancies greater than 10% was 23% for BOC, averaging 15% for MOC, and 31% for EOC.

9) It is important to note that TIPs were modeled using PARCS's built-n detector model, which averages the thermal power of surrounding bundles. Given that TIPs are gamma detectors, this approximation might introduce minor deviations. A more accurate representation would necessitate a gamma transport model that incorporates pin geometry. Despite this, the bundle power average provided a reasonably good comparison for most of the cycle.

10) It is important to note that discrepancies with specific nuclear data libraries do not inherently indicate poor accuracy or the need to discard those libraries. Often, these differences stem from variations in detector response modeling rather than inaccuracies in power calculations.

Overall, PARCS calculations demonstrated an accuracy comparable to SIMULATE 3, achieving excellent agreement with TIP data throughout Cycle B. These findings underscore the robustness and reliability of PARCS in modeling

modern BWR operations, emphasizing the importance of continuous refinement in modeling practices and strategic development of cross-section libraries for enhanced predictive accuracy.

Finally, conclusions regarding **the impact of the cross-section libraries on DEC-A ATWS transient** analysis are as follows:

1) The coupled-code TRAC-BF1/PARCS successfully simulated postulated Anticipated Transient Without SCRAM (ATWS) scenarios initiated by main steam line isolation valve closure (MSIVC), representing emergency depressurization (Scenario 1) and ATWS with High-Pressure Core Spray (HPCS) injection (Scenario 2). The MSIV closure ATWS event was selected due to its potential severity in terms of initial pressurization.

2) The calculations were performed using a detailed plant and core model, including 15 TRAC-BF1 channel components and 3D neutron kinetics with PARCS. A mapping scheme collapsed the 624 assemblies to 15 TRAC-BF1 hydraulic channels, and cross-section libraries from CASMO-4 were used in the neutronics calculations.

3) In both scenarios, the initial event was successfully mitigated, preventing severe fuel damage and ensuring the containment's functionality.

4) Short-term, low-power recriticality events occurred due to choking in the Automatic Depressurization System (ADS) valves or increased coolant density reactivity from subcooled water injection through HPCS. However, no sustained power oscillations related to density wave oscillations or core instability were observed.

5) In **Scenario 1**, a significant moderator temperature variation and high void fraction distribution in the core was observed. However, the PARCS model faced challenges in accurately simulating these drastic moderator temperature variations and high void conditions. This limitation raises concerns about the precision of core response estimations following automatic depressurization. The difficulty in modeling these variations was previously highlighted during the coast-down analysis, further emphasizing the need for enhanced GenPMAXS capabilities.

6) Moreover, a comparative analysis with a 1D kinetics model utilizing the multi-level NEMTAB format was conducted for Scenario 1. NEMTAB approach uses a generalized tabular cross-section representation instead of the PMAXS files functionalization. By comparing the 1D kinetics TRAC BF1 model to the 3D kinetics model coupled with PARCS, a more detailed and comprehensive understanding of the impact of cross-section libraries on the reactor's response can be achieved. The comparison between 1D and 3D kinetics models underscores the superiority of the 3D neutron kinetics model in capturing the complex phenomena within the reactor

during severe transients. These insights reinforce the necessity for continuous enhancement of simulation tools like PARCS to ensure precise core response estimations and robust safety analysis.

7) In **Scenario 2**, the moderator temperature variation was adequately covered by the parameterization in GenPMAXS, indicating the overall adequacy of the coupled code's predictions.

8) The impact of cross-section libraries on core response was analyzed in Scenario 2 using two libraries, Set ATWS and Set 1. Both libraries captured the trend of the transient's main parameters equally well. Instantaneous parameters gain importance in core response when there is feedback between thermal-hydraulics and neutronics.

9) Cross-section libraries are less sensitive to history effects during transient predictions with coupled codes compared to other stand-alone applications like core follow calculations, depletion modeling, or coast-down predictions, as long as the branch matrix reasonably covers the state variables' domain without the need for extensive interpolations.

Overall, the TRAC-BF1/PARCS coupled code represented all fundamental phenomena with reasonable or excellent agreement during the ATWS transient, confirming its applicability to analyze such events and reinforcing the importance of cross-section modeling in ensuring accurate simulations.

8.2 Future Work.

The following additional recommendations for future work are provided to further extend the understanding of modeling cross-section libraries for BWRs:

1) **Evaluation of PARCS for Transient Applications**: Although PARCS has been successfully benchmarked against steady-state data, its performance during transient scenarios needs thorough evaluation. Future research should focus on validating the accuracy and relevance of computed cross-section branches and histories during transients. This will ensure that PARCS provides reliable predictions across a range of operating conditions.

2) Analysis of Moderator Density Branch Effects: While the study found BWR steady-state results to be relatively insensitive to moderator density branch effects, it is crucial to investigate these effects during transient conditions. Future work should specifically assess how variations in moderator density impact core response during transients to confirm the consistency and significance of these effects.

3) **Assessment of Sensitivity to History Effects:** Although cross-section libraries appear less sensitive to history effects during transient predictions with coupled codes compared to standalone applications, further investigation is needed. Future studies should explore additional transient scenarios and conduct sensitivity analyses to better understand the impact of history effects on core response and refine prediction methodologies accordingly.

4) **Detailed Comparative Analysis of Dynamic Core Behavior:** Although PARCS has shown high agreement with measured data throughout the cycle, discrepancies are notable at BOC and EOC conditions due to dynamic core changes. Future work should investigate these dynamic behaviors in greater detail and develop strategies to improve prediction accuracy during these critical periods.

5) **Enhancing PARCS' Coast-Down Modeling Accuracy**: To improve PARCS' predictions of 3D power distributions during coast-down scenarios, further research is needed to refine GenPMAXS' parameterization of moderator temperature. This will better account for changes in moderator density and saturation pressure, leading to more accurate predictions of power distributions in this critical phase.

6) **Examination of Additional Factors Influencing Accuracy:** The study has highlighted several factors, such as the number of burnup points and the weighting of linear/non-linear state variables and histories, that may affect prediction accuracy. Future research should conduct an in-depth analysis of these factors to understand their individual and combined impacts. Developing strategies to address any discrepancies will enhance the overall accuracy of predictions.

7) **Ongoing Applicability Analysis of TRAC-BF1/PARCS:** The TRAC-BF1/PARCS coupled code has demonstrated effectiveness in representing fundamental phenomena during ATWS transients. Future efforts should extend this analysis to a broader range of transient scenarios to validate the code's performance further and ensure its robustness in various challenging situations, including stability analyses. This will provide a deeper understanding of the code's capabilities and limitations.

8) **Comprehensive Sensitivity Analysis of Cross-Section Libraries: A** thorough sensitivity analysis of various cross-section libraries is essential. Future research should evaluate a broader range of libraries and assess their impact on core response in different ATWS scenarios. This analysis will help identify the influence of different libraries on instantaneous parameters and determine the need for updates to ensure accurate predictions.

9) **Investigation of Sustained Power Oscillations:** The absence of sustained power oscillations in the ATWS scenarios modeled is noted, but further research is needed to explore the potential for such oscillations under different conditions. Future studies should identify conditions that could lead to sustained power oscillations and develop strategies to mitigate or manage these occurrences.

Chapter 9
References

Alcouffe, R. E., et al. (1991). *PARAGON: A Code for Multidimensional Neutron Transport and Reactor Physics Analysis*. Idaho National Laboratory.

Allison, C. et al. (1990). *RELAP5/MOD3 code manual. NUREG/CR-5535*.

Baek, J., Cuadra, A., Aronson, A., Diamond, D., & Yarsky, P. (2013a). *BWR Anticipated Transients Without Scram Leading to Instability* (No. BNL-101129-2013-CP). Brookhaven National Lab. (BNL), Upton, NY (United States).

Baek, J., Cuadra, A., Aronson, A., Diamond, D., & Yarsky, P. (2013b). *TRACE Model for Simulation of Anticipated Transients Without Scram in a BWR* (No. BNL-101130-2013-CP). Brookhaven National Lab. (BNL), Upton, NY (United States).

Bahadir, T. (2015). *IMPROVED PWR RADIAL REFLECTOR MODELING WITH SIMULATE-5*. Proc. in Advances in Nuclear Fuel Management V, Hilton Head Island, South Carolina, USA.

Barrachina Celda, T. (2020). *Aportaciones y Mejoras en los Códigos Termohidráulicos y Neutrónicos de Estimación Óptima RELAP5, TRAC-BF1, TRACE y PARCS*, [PhD Thesis, Universitat Politècnica de València].

Barrachina, T., Jambrina, A., Miro, R., Verdu, G., Soler, A., & Concejal, A. (2013). *High order boron transport scheme in TRAC-BF1*.

Barrachina, T., Soler, A., Olmo-Juan, N., Miró. R., Verdú. G. (2015), *Development of a High Order Boron Transport Scheme in TRAC-BF1*. ANS MC2015, Nashville, Tn, USA, April 19-23.

Bokov, P. M. (2009). *Automated few-group cross-section parameterization based on quasi-regression*. Annals of Nuclear Energy, 36(8), 1215–1223.

Bolger, F. T., Holmes, M. A., & Klapproth, J. F. (2003). *TRACG Application for Anticipated Transient Without SCRAM Overpressure Transient Analyses*.

Borkowski, J. et al. (1992). *TRAC-BF1: An advanced best-estimate computer program for BWR accident analysis. NUREG/CR-4356*.

Bozzola, S. (1982). *Fundamentals of boiling water reactor (BWR)*. (No. IAEA-SMR--68/2).

Cacuci, D. G. (Ed.). (2010). *Handbook of Nuclear Engineering: Vol. 1: Nuclear Engineering Fundamentals; Vol. 2: Reactor Design; Vol. 3: Reactor Analysis; Vol. 4: Reactors of Generations III and IV; Vol. 5: Fuel Cycles,*

Decommissioning, Waste Disposal and Safeguards (Vol. 1). Springer Science & Business Media.

Castrillo, F. (2000). *Cofrentes NPP (BWR/6) ATWS (MSIVC) Analysis with TRAC-BF1. NUREG/IA-0178.*

CEA (Ed.). (2015). *Neutronics*. Editions Le Moniteur.

Cheng, L., Baek, J., Cuadra, A., Aronson, A., Diamond, D., & Yarsky, P. (2014b). *TRACE Simulation of BWR Anticipated Transient Without SCRAM leading to Emergency Depressurization* (BNL-103756-2014-CP). Brookhaven National Lab. (BNL), Upton, NY (United States).

Cheng, L., Baek, J., Cuadra, A., Aronson, A., Diamond, D., & Yarsky, P. (2013b). *TRACE/PARCS Core Modeling of a BWR/5 for Accident Analysis of ATWS Events*. Transactions of the American Nuclear Society, 109.

Cheng, L., Baek, J., Cuadra, A., Aronson, A., Diamond, D., & Yarsky, P. (2014a). *BWR Anticipated Transients Without Scram in the MELLLA+ Expanded Operating Domain. NUREG/CR-7181. Part 3.* (BNL-NUREG-105328-2014).

Cheng, L., Baek, J., Cuadra, A., Aronson, A., Diamond, D., & Yarsky, P. (2014b). *TRACE SIMULATION OF BWR ANTICIPATED TRANSIENT WITHOUT SCRAM LEADING TO EMERGENCY DEPRESSURIZATION* (BNL-103756-2014-CP). Brookhaven National Lab. (BNL), Upton, NY (United States).

Cheng, L., Baek, J., Cuadra, A., Aronson, A., Diamond, D., & Yarsky, P. (2015). *BWR Anticipated Transients Without Scram in the MELLLA+ Expanded Operating Domain. NUREG/CR-7179. Part 1.* (BNL-NUREG-105325-2014).

Cheng, L., Baek, J. S., Cuadra, A., Aronson, A., Diamond, D., & Yarsky, P. (2016). *TRACE/PARCS Analysis of ATWS with Instability for a MELLLA+ BWR/5*. Nuclear Technology, 196(BNL-111742-2016-JA; BNL-112141-2016-JA).

Cheng, L. Y., Diamond, D., & Arantxa Cuadra, G. R., Arnold Aronson. (2010). *Trace Assessment for BWR ATWS Analysis* (BNL--91311-2010-IR, 1013471; p. BNL--91311-2010-IR, 1013471).

Choi, S., Ward, A., Graham, A., Collins, B., Kochunas, B., & Asgari, M. (2022). Preliminary Simulation Results of Peach Bottom Unit 2 Cycles 1 and 2 with MPACT. *International Conference on Physics of Reactors 2022 (PHYSOR 2022)*, 2316–2325.

Cochran, R. G. & Tsoulfanidis, N. (1999). *The nuclear fuel cycle: Analysis and management*.

Covington, L.J., Cronin, J.T., & Umbarger, J.A. (1995). *SIMULATE-3: Advanced Three-dimensional Two-group Reactor Analysis Code*. Studsvik Scandpower, Studsvik/SOA-95/15 Rev 2.

Crank, J. & Nicolson, P. (1947). A practical method for numerical evaluation of solutions of partial differential equations of the heat-conduction type. *Mathematical Proceedings of the Cambridge Philosophical Society*, *43*, 50–67.

Cuadra, A., Baek, J., Cheng, L., Aronson, A., Diamond, D., & Yarsky, P. (2013). *TRACE/PARCS Core Modeling of a BWR/5 for Accident Analysis of ATWS Events* (No. BNL-101128-2013-CP). Brookhaven National Lab. (BNL), Upton, NY (United States).

D'Auria, F., Bousbia-Salah, A., Petruzzi, A., & Del Nevo, A. (2006). *State of the Art in using Best-estimate Calculation Tools in Nuclear Technology*. Nuclear Engineering and Design, 38(1).

Demazière, C., Stålek, M., & Vinai, P. (2012). *Comparison of the US NRC PARCS Core Neutronics Simulator Against In-Core Detector Measurements for LWR Applications. NUREG/IA-0414*. US Nuclear Regulatory Commission.

Downar, T., Joo, H. G., & Jiang, G. (1997). *A hybrid ANM/NEM interface current technique for the nonlinear nodal calculation*. Proc. Joint Int. Conf. Math. Comp, 124–133.

Downar, T. & Xu, Y. (2004). *GenPMAXS Code for generating the PARCS cross-section interface file PMAXS (draft).* Purdue University, School of Nuclear Engineering, West Lafayette, USA.

Downar, T., Xu, Y., Seker, Y., & Hudson, N. (2012). *Theory Manual for the PARCS Kinetics Core Simulator Module*.

Duderstadt, J. J. & Hamilton, L. J. (1976). *Nuclear reactor analysis.* Wiley.

Edenius, M., Ekberg, K., Forssén, B., & Knott, D. (1995). *CASMO-4, A Fuel Assembly Burnup Program, User's Manual. Technical report*. Studsvik0SOA-9501, Studsvik of America, Inc.

Eisenhart, L.D., Dias, A.F., Westacott, J.L., Downar, T.J., & Joo, H.G. (2000). *CORETRAN- 01: A Three-Dimensional Program for Core Physics and Thermal-Hydraulic Analysis* (Report WO-3574, Revision 3). EPRI.

Ferroukhi, H., Zezkak, O., & Chawla, R. (2009). *Cross-section modelling effects on pressurized water reactor main steam line break analyses*. Annals of Nuclear Energy, 36, 1184–1200.

Fisher, J. R. (1977). *Review of in-core power distribution measurements: Technical status and problems* (EPRI-NP-337, 7331326; p. EPRI-NP-337, 7331326).

Fridström, R. (2010). *Response of the Gamma TIP Detectors in a Nuclear Boiling Water Reactor*. [PhD Thesis, Uppsala Universitet].

Fujita, T. (2015). *Study on Cross-Section Generation for BWR Pin-by-Pin Core Analysis.* [PhD Thesis, Nagoya University].

Fujita, T., Endo, T., & Yamamoto, A. (2014). *A macroscopic cross-section model for BWR pin-by-pin core analysis*. Journal of Nuclear Science and Technology, 51(3), 282–304.

General Electric Company. (2001). *CONTROL BLADE SEQUENCE PATTERNS FOR OPTIMIZATION OF BWR POWER* (Patent US 6,259,756 B1).

Giust, F., Greiner, D., & Vidal, C. (2004). *BWR CORE MONITORING WITHOUT LPRM ADAPTION*. Forth American Nuclear Society International Topical Meeting on Nuclear Plant Instrumentation, Controls and Human Machine Interface Technologies (NPIC&HMIT 2004), Columbus, Ohio.

Grandi, G. M. (2005). *SIMULATE-3K: Theory and Methodology Report*.

Gruel, J., et al. (2011). *APOLLO2: A Transport Theory Code System for Reactor Physics Analysis*. CEA.

Grundmann, U., Kliem, S., & Rohde, U. (2005). DYN3D: Three-Dimensional Core Simulation Program for Steady-State and Transient Analysis of Thermal Reactors. *Proceedings of the 13th Symposium of AER.*

Harfst, W. (1985). *Neutron monitoring system for BWR's. Experience and developments* (No. IWG-NPPCI--84/1).

Harter, R. & González-Cuesta, M. (2017). *Technical Support Guidelines for BWR-SAMGs.* International Atomic Energy Agency (IAEA).

Hidalga García-Bermejo, P. (2020). *Development and validation of a multi-scale and multi-physics methodology for the safety analysis of fast transients in Light Water Reactors.* [PhD Thesis, Universitat Politècnica de València].

Hsiang-Shou, C. & Diamond, D. J. (1978). *Void Effects on BWR Doppler and Void Reactivity Feedback.* International Atomic Energy Agency (IAEA).

Hursin, M., Bogetic, S., Dohkane, A., Canepa, S., Zerkak, O., Ferroukhi, H., & Pautz, A. (2017). *Development and validation of a TRACE/PARCS core model of Leibstadt Kernkraftwerk cycle 19*. Annals of Nuclear Energy, 101, 559–575.

IAEA. (2016). *Safety of Nuclear Power Plants: Specific Safety Requirements*. IAEA.

Ivanov, K., & Avramova, M. (2007). *Challenges in coupled thermal–hydraulics and neutronics simulations for LWR safety analysis*. Annals of Nuclear Energy, 34(6), 501–513.

Ivanov, K., Todorova, N., & Sartori, E. (2001). *Using the OECD/NRC PWR MSLB benchmark to study current numerical and computational issues of coupled calculations* ((No. ISSN 0003-018X; CODEN TANSAO)). OECD-NEA Data Bank, Issy-les-Moulineaux (FR).

Ivanov, K.N., Beam, T.M., & Baratta, A.J. (1999). *PWR Main Steam Line Break (MSLB) Benchmark, Volume I: Final Specifications* (NEA/NSC/DOC(99)8).

Iwamoto, T. & Yamamoto, M. (1999). *Advanced nodal methods of the few-group BWR core simulator NEREUS*. Journal of Nuclear Science and Technology, 36(11), 996–1008.

Jambrina, A., Barrachina, T., Miró, R., Verdú, G., Concejal, A., & Melara, J. (2012). *PROCEDIMIENTO DE ACOPLAMIENTO DE LOS CÓDIGOS TRAC-BF1 Y PARCSv2.7*. Reunión Anual Sociedad Nuclear Española, Cáceres, Spain.

Jambrina, A. et al. (2013). *Peach Bottom Turbine Trip Benchmark Analysis with TRAC-BF1/PARCS and TRACE/PARCS Coupled Codes*. The 15th International Topical Meeting on Nuclear Reactor Thermal-Hydraulics (NURETH-15), Pisa, Italy.

Knott, D., Forssén, B. H., & Edenius, M. (1995). *CASMO-4. A Fuel Assembly Burn-up Program Methodology*. STUDSVIK/SOA-95/2, 1995.

Knott, D. & Yamamoto, A. (2010). *Lattice physics computations. In Handbook of Nuclear Engineering*. Springer Science& Business Media.

Kok, K. D. (Ed.). (2016). *Nuclear engineering handbook*. CRC Press.

Kozlowski, T. & Downar, T.J. (2003). *OECD/NEA and US NRC PWR MOX/UO2 Core Transient Benchmark. Final Specifications, Rev. 2* (NEA/NSC/DOC (2003) 20).

Kulikowska, T. (2001). *Reactor Lattice Codes: Vol. (No. INIS-XA--858)*.

Lautard, J. J., Fauchet, G., & Henry, J. Y. (1990). *CRONOS: A Modular Computational System for Neutronics*. Proceedings of the International Conference on the Physics of Reactors: Operation, Design and Computation.

Lee, C. H., Zhong, Z., Taiwo, T. A., Yang, W. S., Smith, M. A., & Palmiotti, G. (2006). *Status of reactor physics activities on cross section generation andfunctionalization for the prismatic very high temperature reactor, and development of spatially-heterogenerous codes.* ((No. ANL-GENIV-075)). Argonne National Lab.(ANL), Argonne, IL (United States).

Leppänen, J., et al. (2014). *SERPENT 2: A Continuous-energy Monte Carlo Reactor Physics Burnup Calculation Code*. VTT Technical Research Centre of Finland.

Lewis, E. E. & Miller, W. F. (1984). *Computational methods of neutron transport*. La Grange Park, IL: American Nuclear Society, Inc.

Lobo, L. G. (1980). *COASTDOWN IN LIGHT WATER REACTORS AS A FUEL MANAGEMENT STRATEGY*.

Lucius, R. (1980). *CPM-3: The Comprehensive Physics Model for Nuclear Reactors*. Argonne National Laboratory.

Mesado, C. (2017). *Uncertainty Quantification and Sensitivity Analysis for Cross Sections and Thermohydraulic Parameters in Lattice and Core Physics Codes. Methodology for Cross Section Library Generation and Application to PWR and BWR*. [PhD Thesis, Universitat Politècnica de València].

Milošević, M. J. (2001). *A PROCEDURE FOR EFFECTIVE DANCOFF FACTOR CALCULATION*. International Yugoslav Nuclear Society Conference (YUNSC-2000), Belgrade (Yugoslavia), 2-5 Oct.

Muir, D., et al. (1982). *WIMS: A Neutron Transport Code for Reactor Core Analysis*. UKAEA.

Muñoz-Cobo, J. L., Escrivá, A., Mendizabal, R., Pelayo, F., & Melara, J. (2013). *Desarrollo y Aplicación de una Metodología CSAU para el Caso de un ATWS en un BWR utilizando Métodos de Teoría de la Información*. Reunión Anual Sociedad Nuclear Española, Reus, Spain.

Mylonakis, A. G., Varvayanni, M., Catsaros, N., Savva, P., & Grigoriadis, D. G. E. (2014). *Multi-physics and multi-scale methods used in nuclear reactor analysis*. Annals of Nuclear Energy, 72, 104–119.

Nikitin, K., Clifford, I., Dokhane, A., & Ferroukhi, H. (2022). *Methodology for CPR estimations of BWR cycle specific transient reload analyses using CTF sub-channel code*. Nuclear Engineering and Design, 389, 111649.

Nuclear Regulatory Commission. (1978). *ANTICIPATED TRANSIENTS WITHOUT SCRAM FOR LIGHT WATER REACTORS. NUREG-0460*.

Nuclear Regulatory Commission. (1982). *Guidelines for the preparation of emergency operating procedures. Resolution of comments on NUREG-0799 (No. NUREG--0899).* Nuclear Regulatory Commission.

Nuclear Regulatory Commission. (1984). *Regulatory Guide 1.157: Instrumentation for Light-Water-Cooled Nuclear Power Plants to Assess Plant Conditions During and Following an Accident*. U.S. Nuclear Regulatory Commission.

Nuclear Regulatory Commission. (1993). *TRACE: The Transient Reactor Analysis Code*. U.S. Nuclear Regulatory Commission.

Nuclear Regulatory Commission. (2005). *Regulatory Guide 1.203: Transient and Accident Analysis Methods.* US Nuclear Regulatory Commission.

Oblozinsky, P., & Schwerer, O. (1998). *Nuclear data libraries and online services. An introduction to the data types and services available from the IAEA Nuclear Data Section.* IAEA.

Odar, F., Murray, C., Shumway, R., Bolander, B., Barber, D., & Mahaffy, J. (2003). *Volume II: User manual for the PARCS spatial kinetics core simulator (draft).* US Nuclear Regulatory Commission.

Ott, K. O. & Neuhold, R. J. (1985). *Introductory nuclear reactor dynamics*. American Nuclear Society.

Perin, Y. (2016). *Development of a Multi-Physics, Multi-Scale simulation tool for LWR safety analysis*. [PhD Thesis, Technishen Universitüt München].

Perin, Y., & Escalante, J. J. (2017). *Application of the best-estimate plus uncertainty approach on a BWR ATWS transient using the NURESIM European code platform*. Nuclear Engineering and Design, 321, 48–56.

Perin, Y., Soler, A., & Velkov, K. (2012). *Coupling of the System Code ATHLET-QUABOX/CUBBOX with the Sub-Channel Code COBRA-TF*. The 9th International Topical Meeting on Nuclear Thermal-Hydraulics, Operation and Safety (NUTHOS-9), Kaosiung, Taiwan.

Peterson, L. (2003). *HELIOS: A Modular Neutronics Code System for Reactor Core Analysis*. Studsvik Scandpower.

Ragusa, J., Santandrea, S., & Sanchez, R. (2005). *A TECHNIQUE FOR REFLECTOR HOMOGENIZATION*. Mathematics and Computation, Supercomputing, Reactor Physics and Nuclear and Biological Applications, Palais des Papes, Avignon, France.

Rearden, B. T. (2018). *SCALE 6.1: A Comprehensive Software Package for Nuclear Criticality Safety Analysis and Reactor Physics*. Oak Ridge National Laboratory.

Rhodes, J. & Edenius, M. (2004). *CASMO-4, A Fuel Assembly Burnup Program: User's Manual. Studsvik Scandpower Inc. SSP-01/400 Rev 4.*

Roselló, Ó. (2004). *Desarrollo de una metodología de generación de secciones eficaces para la simplificación del núcleo de reactores de agua ligera y aplicación en códigos acoplados neutrónicos termohidráulicos* [PhD Thesis, Universitat Politècnica de València].

Sánchez-Cervera, S., García-Herranz, N., Herrero, J. J., & Cuervo, D. (2014a). *Effects of cross sections tables generation and optimization on rod ejection transient analyses*. Annals of Nuclear Energy, 73, 387–391.

Sánchez-Cervera, S., García-Herranz, N., Herrero, J. J., & Cabellos, O. (2014b). *Optimization of multidimensional cross-section tables for few-group core calculations*. Annals of Nuclear Energy, 69, 226–237.

Schnurr, N.M. et al. (1992). *TRAC-PF1/MOD2: Volume 1. Theory Manual* (Report LA-12031-M, Vol. I, NUREG/CR-5673). Los Alamos National Laboratory.

Shim, C. B., Lee, K. H., & Cho, J. Y. (2016). *Improvement of Axial Reflector Cross Section Generation Model for PWR Core Analysis*. Transactions of the Korean Nuclear Society Autumn Meeting, Gyeongju, Korea.

Silvennoinen, P. (1976). *Reactor core fuel management*. PERGAMON INTERNATIONAL LIBRARY of Science, Technology, Engineering and Social Studies.

Smith, K. & Forget, B. (2013). *Challenges in the Development of High-Fidelity LWR Core Neutronics Tools*. Proc. M&C 2013, Sun Valley, Idaho, May 5–9, 2013, American Nuclear Society.

Smith, K. S. (1986). Assembly homogenization techniques for light water reactor analysis. *Progress in Nuclear Energy*, *17*(3), 303–335.

Stacey, W. M. (2018). *Nuclear reactor physics.* (3rd ed.). John Wiley & Sons.

Stålek, M., & Demazière, C. (2008). *Development and validation of a cross-section interface for PARCS*. Annals of Nuclear Energy, 35(12), 2397–2409.

Stamm'ler, R.J. & Abbate, M.J. (1983). *Methods of Steady-State Reactor Physics in Nuclear Design*. Academic Press London, 111.

Studsvik Scandpower. (2008). *HELIOS Methods (Version 1.10)*. Studsvik Scandpower.

Todorova, N. & Ivanov, K. (2001, April). *PWR REA sensitivity analysis using TRAC-PF1/NEM*. Proceedings of ICONE-9 Conference, CD-Rom (Electronic Publication).

Trkov, A., et al. (2010). *TransLAT: A Code for Generating Cross Sections and Covariance Data for Reactor Physics*. JRC.

US NRC. (2007). *Standard Review Plan for the Review of Safety Analysis Reports for Nuclear Power Plants: LWR Edition—Transient and Accident Analysis (NUREG-0800, Chapter 15). Section 15.8. Rev 2.*

US NRC. (2011). *General Electric Systems Technology Manual, Chapter 5.6, Traversing Incore Probe System* (NRC Accession Number ML11258A311.).

US-NRC Library—Glosary. (2021). U.S. NRC. https://www.nrc.gov/reading-rm.html

Ver Planck, D.M., Smith, K.S., & Umbarger, J.A. (1995). *TABLES-3 users's manual, Studsvik Scandpower/SOA-95/16*.

Vondy, D. R., et al. (1973). *PHOENIX-3: A Multigroup Cross Section Generation Code*. Los Alamos National Laboratory.

Wang, D., Ade, B. J., & Ward, A. (2013). *Cross Section Generation Guidelines for TRACE-PARCS. NUREG/CR-7164* ((No. ORNL/TM-2012/518)). Oak Ridge National Lab. (ORNL), Oak Ridge, TN (United States).

Watson, J. K., & Ivanov, K. N. (2002). *Improved cross-section modeling methodology for coupled three-dimensional transient simulations*. Annals of Nuclear Energy, 29(8), 937–966.

Yarsky, P. (2011). *MELLLA+ BWR ATWS Analyses – Revision 1* (ML113350073). US Nuclear Regulatory Commission, Office of Nuclear Regulatory Research.

Yarsky, P. (2013). *TRACE/PARCS ANALYSIS OF ABWR FOR MSIV CLOSURE ATWS EVENT*. The 15th International Topical Meeting on Nuclear Reactor Thermal - Hydraulics, NURETH-15, Pisa, Italy.

Yarsky, P., Ward, A., Xu, Y., Downar, T., & Hudson, N. (2013). *THE APPLICATION OF PARCS/PATHS TO DEPLETION OF HATCH CYCLES 1-3*. The 15th International Topical Meeting on Nuclear Reactor Thermal - Hydraulics, NURETH-15, Pisa, Italy.

Yee, B. C., Larsen, E. W., Kochunas, B., & Xu, Y. (2016). *Space-Dependent Wielandt Shift Methods for Multigroup Diffusion Eigenvalue Problems*. Transactions of the American Nuclear Society, 114(1).

Zimin, V. G. & Semenov, A. A. (2005). *Building neutron cross-section dependencies for few-group reactor calculations using stepwise regression*. Annals of Nuclear Energy, 32(1), 119–136.